Development of a Low Power Reactive Wireless Chemical Sensing Network

by

Stephen Beirne, BEng

A thesis submitted in part fulfilment of the requirement for the degree of

Doctor of Philosophy

Supervisors: **Dr. Brian Corcoran,** School of Mechanical and Manufacturing Engineering, Dublin City University

Prof. Dermot Diamond, National Centre for Sensor Research (NCSR), Dublin City University

Dr. Roderick Shepherd, National Centre for Sensor Research (NCSR), Dublin City University

September 2008

DECLARATION

I hereby certify that this material, which I now submit for assessment on the programme of study leading to the award of Doctor of Philosophy is entirely my own work and has not been taken from the work of others save and to the extent that such work has been cited and acknowledged within the text of my work.

Signed: _____

Stephen Beirne

ID No.: 99006154

Date: September 2008

ACKNOWLEDGEMENTS

I would like to take this opportunity to express my sincere thanks and appreciation to all those who have helped guide and motivate me during the course of this research.

I would like to thank my family, friends and colleagues who I have always been able to rely upon, especially my parents whose love and encouragement have made this all possible. Special thanks to those close to me who have provided constant support, encouragement and in particular during the final few months of this research, understanding; it is deeply appreciated.

I am indebted to my supervisors, Brian Corcoran, Roderick Shepherd and Dermot Diamond. Thank you all for giving me the opportunity to further my studies to the point where I am now able to present this thesis. The support, guidance and direction that were always on offer have been invaluable. It is unquestionable that this work would not have been possible without the inspired direction provided, sometimes at a moments notice, by Roderick Shepherd. Additionally, I would especially like to extend my greatest thanks to Breda Kiernan for her assistance in the final assembly of this thesis.

I would also like to acknowledge the work of the skilled and professional technical staff of the Mechanical and Manufacturing Engineering Department of DCU. Any requests for parts, component manufacture or computer assistance were addressed as quickly as possible. Their expertise and constructive practical suggestions have helped greatly during my undergraduate studies and throughout this research project.

This research has been supported by Science Foundation Ireland (SFI) under the Adaptive Information Cluster Award (SFI 03/IN3/1361).

This thesis is dedicated to the memory of,
Felim O'Raghallaigh
A man of many musical talents and mechanical skills,
who never hesitated in passing his knowledge and abilities
to those who were willing to learn.

ABSTRACT

Development of a Low Power Reactive Wireless Chemical Sensing Network

By

Stephen Beirne BEng

The development and recent advances in commercially available wireless communications platforms commonly referred to as motes has led to research in the area of deployable wireless sensor networks (WSNs) that monitor changing parameters of indoor and outdoor environments. Most published research in the area of WSNs focuses on the passive monitoring of physical parameters such as temperature, humidity and light, with the main research concerns being scale of deployment, data communication protocols and node operating longevity. The research presented in this thesis addresses the integration of novel light emitting diode (LED) based chemical sensing techniques with an available wireless communications platform, to allow for active real-time monitoring of changing chemical parameters over a distributed area.

In this thesis, the design, development and construction of a custom Environmental Sensing Chamber (ESC) test-bed within which the operation of low-power WSNs can be tested and analysed is discussed. Initial trials using the wireless sensing platform utilise temperature as the target parameter so that the platform's operation and communications methods can be refined to suit the requirements of this laboratory based research. Following this, the construction, development and testing of a low power wireless colorimetric chemical sensing node is investigated. The process results in a reliable, reproducible and calibrated sensor which has been replicated to achieve a test-scale network of five similar deployable chemical sensing nodes.

An integrated sensing and control system for the purpose of demonstrating low-cost wireless chemical vapour monitoring and automatic real-time reaction to sensed chemical events using, the developed sensor node, is described. Data returned by the sensor network successfully track plumes of acetic acid vapour as they move through the ESC. Collected data are used as an input to a real-time management system so that with the detection of a chemical event, the contaminant is removed from the sensor network environment through controlled purging of the chamber. This demonstrated system is referred to as a low power reactive wireless chemical sensing network.

TABLE OF CONTENTS

LIST OF FIGURES

LIST OF TABLES

LIST OF ACRONYMS

ADC	Analogue to Digital Converter
AI	Artificial Inteligence
BAN	Body Area Network
BPB	Bromophenol Blue
BSP	British Standard Pipe
CAD	Computer Aided Design
CDA	Clean Dry Air
CFD	Computational Fluid Dynamiccs
CO	Control Output
DLL	Dynamic Link Library
DPCO	Double Pole Change Over
DSP	Digital Signal Processing
ESC	Environemntal Sensing Chamber
FID	Flame Ionisation Detection
FPGA	Field Programmable Gate Array
GC	Gas Chromatography
GC/MS	Gas Chromatography Mass Spectroscipy
GPL	General Public License
GUI	Graphical User Interface
IC	Integrated Circuit
IDT	Interdigital Transducer
IMU	Inertial Measurement Unit
LED	Light Emitting Diode
LOD	Limit of Detection
LPWN	Low Power Wireless Network
MEMS	Micro Electro-Mechanical Systems
NTC	Negative Thermal Coefficient
PC	Personal Computer
PDA	Personal Digital Assistant
PID	Photoionisation Detection
PMMA	Polymethyl Methacrylate
ppb	parts per billion
ppm	parts per million
PV	Process Variable
RF	Radio Frequency
RSD	Relative Standard Deviation
SAW	Surface Acoustic Wave
SP	Set Point
VB	Visual Basic
VOC	Volitile Organic Compound
WCSAN	Wireless Chemical Sensor Actuator Network
WCSN	Wireless Chemical Sensor Network
WSAN	Wireless Sensor Actuator Network
WSN	Wireless Sensor Network

PUBLICATIONS ARISING

Journal publication

- R. Shepherd, S. Beirne, K. T. Lau, B. Corcoran and D. Diamond, "Monitoring chemical plumes in an environmental sensing chamber with a wireless chemical sensor network", *Sensors and Actuators B: Chemical*, 2007, *121(1)*, 142-149

Conference papers

- Breda M. Kiernan, Cormac Fay, Stephen Beirne and Dermot Diamond, "Development of an Autonomous Greenhouse Gas Monitoring System", Proceedings of the 5th International Conference on Environmental Sciences and Engineering, Venice, Italy, October 29-31, 2008 (Accepted)
- Jer Hayes, Stephen Beirne, Conor Slater, Breda M. Kiernan, King-Tong. Lau and Dermot Diamond, "Chemical species concentration measurement via wireless sensors", Proceedings of the 5th International Conference on Environmental Sciences and Engineering, Venice, Italy, October 29-31, 2008 (Accepted)
- S. Beirne, B. Corcoran, K.T. Lau and D. Diamond, "Chemical event tracking using a low cost wireless chemical sensing network", *IEEE Sensor 2008*, Oct, 26-29, 2008, Lecce Italy. (Accepted)
- B. Kiernan, S. Beirne, C. Fay and D. Diamond, "Landfill gas monitoring at borehole wells using an autonomous environmental monitoring system" Accepted for the *5th International Conference on Climate Change and Global Warming*, Sept. 24-26, 2008, Heidleberg, Germany
- D. Diamond, N. E. O'Connor, A. F. Smeaton, S. Beirne, B. Corcoran, P. Kelly, K. T. Lau and R. Shepherd, "Sensor node localisation using a stereo camera rig" In *Proceedings of the 4th workshop on Embedded networked sensors*, 2007, 43-47
- D. Marsh, R. Tynan, S. Beirne, R. Shephard, G.M.P. O'Hare, D. Diamond, B. Corcoran, "Microcosm: a low cost 3-D wireless sensor test-bed within a controllable environment", In *Proceedings of International Conference on Mobile Ad-hoc and Sensor Networks*, 13-15 December, Hong Kong, China, 2006.
- E. Cooke, N. O'Connor, A.F. Smeaton, D. Diamond, R. Shepherd, S. Beirne and B. Corcoran, "Video analysis of events within chemical sensor networks", *ICOB 2005 - 2nd Workshop on Immersive Communication and Broadcast Systems*, Oct 2005.

Poster presentations

- J. Hayes, S. Beirne, K.T. Lau and D. Diamond, "Evaluation of a low cost Wireless Chemical Sensor Network for Environmental Monitoring", Accepted for *IEEE Sensor 2008*, Oct. 26-29, 2008, Lecce Italy
- S. Beirne, B. Corcoran, R. Shepherd, K.T. Lau and D. Diamond, "Control and modelling of an environmental chamber", *3rd International Symposium on Sensor Sciences (I3S 2005)*, 18-JUL-05 - 21-JUL-05, Juelich, Germany
- S. Beirne, R. Shepherd, K.T. Lau, B. Corcoran and D. Diamond, "Control and modelling of chemical plumes in an environmental chamber" *AIC Annual Conference*, Crowne Plaza Hotel, Dublin, Ireland, 12 November 2004

1 Introduction

The principle of wireless data communication is not in its infancy. Neither is the idea of sensing parameters of interest from our surrounding environment. The merging of these two concepts into operational wireless sensing systems is at present an ever-expanding area of research interest for both academic and commercial development laboratories [1, 2]. The factors driving these research activities include the expected cost savings that may be obtained from Wireless Sensor Networks (WSNs) because of, the ease of component installation, the huge reduction in required hard wiring and the flexibility in positioning of small lightweight sensor nodes [3-5]. The wide range of applications resulting from the flexibility, high sensing fidelity, low-cost and rapid deployment characteristics of WSNs are envisaged to make them an integral part of everyday human life [6].

The objective goal of much of the on-going research is the deployment of efficient, low maintenance and effective WSNs capable of reliably monitoring changing parameters observed in their specific environment. Research groups in this field are now tending to use "off the shelf" wireless communications data processing platforms, with average computational functionality, commonly referred to as "motes" [7, 8], as research tools to form the equipment base of developmental wireless sensing systems. Deployments of WSNs undertaken by research groups are highlighting the present limitations in communications hardware, node power management and general communications protocols. Although, outside of the scope of this particular study, continued research in these areas is critical, as without efficient reliable hardware platforms it will not be possible to build effective WSNs.

Current and proposed WSNs collect information from their associated sensing nodes so that sensed data can be accessed via a human interface, such as, a PC or PDA. In some cases, this information is only processed and analysed after the monitoring period has been completed. More sophisticated networks have been developed where the information is not purely logged to file. In such networks, the user can remotely query nodes within a network for recent readings [4, 9-13]. This is suitable for some applications, especially where the purpose of the network is purely monitoring of changing variables over time. However, an additional step, which to this researcher's knowledge has only had limited attention, is the use of mote-based information to facilitate a real-time response to a change in a target parameter. This step transfers the

focus of a WSN to real-time reactive systems rather than purely data logging and visualisation. Changing the focus of a WSN so that it performs an active role, adds an important new dimension to this area of research, which opens up a vast range of parameter monitoring and management applications. For example, systems, referred to as Wireless Sensor Actuator Networks (WSAN), have been proposed with the objective of controlling heat and lighting in commercial building environments based on monitoring data supplied by a distributed WSN [3, 4, 14, 15]. While development in this area is ongoing, deployment of such systems is, thus far, limited.

It is not just physical parameters, such as, temperature, pressure and humidity that are of importance in our environmental surroundings. Chemical species monitoring capabilities, which exploit the characteristics posed by WSNs such as, their low cost and ease of deployment are also of interest. It is envisaged that low-cost devices would form the lowest level of a chemical contaminant sensor network hierarchy [16]. These devices will, therefore, have the responsibility of being the first line in detecting the presence of a chemical contaminant. They will also be tasked with reporting of a chemical event detection, to the next level of responsibility in their respective network hierarchy. Data supplied by a network of low-cost wireless chemical sensor nodes will provide trend information with regards to the contaminant dispersion pattern over the area of the network deployment that could be used to make an informed decision with regards to the source of the contaminant. The dynamic data could also be used to plot the movement of a contaminant vapour and assist in selection of the most appropriate response method by selecting evacuation routes that direct individuals away from the contaminant's location or by activation of systems to contain or remove the contaminant, i.e., a reactive Wireless Chemical Sensor Actuator Network (WCSAN).

The predominant research gap, that at present impedes the realisation of such a sensor network, is the development of low-cost low-power alternatives to conventional laboratory sensing methods. Research is underway in this area, with chemically sensitive devices being developed that show potential for integration with wireless sensing platforms. However, reported combination of low-cost chemical sensors with low-power wireless sensing platforms, let alone examination of their operation within a WSN are limited, as opposed to the more regularly investigated physical sensor networks.

The research focus of this body of work is to progress a recently developed low-cost optical chemical sensing method so that it can be integrated with a wireless sensing platform and deployed to form a distributed Wireless Chemical Sensing Network (WCSN) that allows for real-time reaction to a chemical event. Due to its reactive nature and the fact that it is used to influence the parameter being monitored, the system is referred to as a Wireless Chemical Sensor Actuator Network (WCSAN). Studies will be conducted on the developed wireless chemical sensor's response characteristics, to ascertain the device's response time, response reproducibility and limit of detection (LOD). The developed WCSN will be studied within a custom built Environmental Sensing Chamber (ESC) by exposure to varying contaminant sources. These trials will highlight the plume tracking and contaminant source identification capabilities presented by a distributed low-cost WCSN. The devices will subsequently be implemented so that they act as on/off indicators for the presence of a contaminant vapour. Automatic reaction to a chemical event by a WCSAN will only occur once the detection of a contaminant by a wireless chemical sensor node is confirmed by additional nodes within the network. The structure of this thesis will, therefore, be as described in the following outline.

- After this introduction, Chapter 2 presents a critical literature review where a range of WSN deployments are analysed to highlight the communications and power management challenges that face the future realisation of large scale WSNs. The analysed deployments also highlight the current and proposed sensing applications of WSNs. Conventional gas phase contaminant measuring techniques are discussed before the theory and two example cases of the low-cost optical chemical sensing method employed during this research are introduced.
- In Chapter 3, the examination will then focus on the establishment of a laboratory scale wireless sensor actuator network targeting a physical parameter and using an established sensor to verify the operation of the communications platform, data acquisition interface and system output controls.
- In Chapter 4, the research will subsequently concentrate on the integration of a low-cost component based optical chemical sensing technique with the wireless communications platform. The operation of the resultant wireless chemical sensor device will be examined, to determine its response characteristics, such as response time, response reproducibility and LOD.

- Finally, the results, presented in Chapter 5, will show how a deployed laboratory scale network of calibrated wireless chemical sensor nodes within the monitoring environment can be used to dynamically track a chemical plume development. Further to this, it will also be shown how retrieved sensor data can be used as an input to a reactive response system for the detection and removal of a gas phase chemical contaminant from a monitored environment.

2 Literature Review

This literature review will begin with a brief introduction into the history of wireless communication, showing the primary advances that have been made towards low power wireless networks since the late 19th century. An overview of a selection of low-power wireless communications nodes that have been developed for use in wireless sensor networks (WSNs) will then be presented. Additional information will be provided on devices available from three leading wireless node manufacturers.

The factors that currently affect the future realisation of large long-term deployable wireless sensor networks will be investigated. It will be shown that the current WSN research focuses on the areas of data communications methods and power management strategies to achieve the goal of long term reliable WSNs. Examples of deployed WSNs will be provided. This will identify the current applications where wireless sensor networks are being utilised and the emerging applications where sensor data will be collected in real time and used as an input to control systems.

Current applications and deployments have identified that the ability to detect chemical vapours, measure gas concentrations and pH would augment the measurement capabilities of currently available physical sensors. Conventional analytical chemical concentration measurement techniques will be described and will act as an introduction to low power electrochemical sensing devices. Subsequently, reported integrations of chemical sensors with wireless sensor nodes will be analysed.

Before the objectives of this research are stated, the emerging low-cost optical chemical sensing technique that is explored and implemented as part of a wireless chemical sensor actuator network in this body of work will be introduced.

2.1 Wireless Communication History

The development of wireless communications devices as we know them today began in the late 19th century with the early generation and detection of what we now call radio waves, by Heinrich Hertz. Hertz conducted experiments confirming the predictions of James Clerk Maxwell that electromagnetic waves similar to light waves existed [17]. Still it is Guglielmo Marconi who is most associated with wireless transmissions. Building on early experiments carried out in his family home, Marconi first displayed wireless transmission in 1895 with a signal being transmitted a distance of one mile.

Marconi further developed the technology so that by 1899 transmission ranges of sixty miles were accomplished. At this point it became feasible to use this technology for short range ship-to-shore communications. By 1901 the first basic signals were being sent across the Atlantic Ocean [17]. Within a few short years, wireless had improved to the point where in 1909 few passenger ships left port without it [18]. Radio, although still in its infancy and only transmitting Morse code, allowed vessels to communicate with other ships beyond the distance of the horizon.

Naturally, the military and police forces saw many applications where radio communications would be of assistance to them and their operations. During the First World War however, radio communications did not play a large role, as wired telephone and telegraph were far more dependable [18]. In 1928, one-way broadcasts were being made to receiver units in mobile police cars of the Detroit police department. By 1934, over 5000 police cars were equipped with two-way radio communications [19]. At the outbreak of the Second World War, radio technology had been advanced to the point where radio transmissions were used by the warring forces to send heavily encrypted data between military stations and outposts [20].

The first transistor was invented at Bell Laboratories on 16th December 1947, and published in 1948 [21]. This device brought a dramatic reduction in the size of the components and the energy required for radio signal amplification. The possibility of grouping transistors together to develop integrated circuits (ICs) was recognised by a number of groups. Jack Kilby achieved this in 1958 while working for Texas Instruments, when he built the first crude IC [22]. This led to the birth of the vast electronics based industry that is prevalent in the world today. The same advances have

led to the arrival of small, low power processors that can be integrated with radio transmitters and receivers.

The recent coupling of low power processors with radio communications have spawned a great interest in the use of wireless data collection and communication technology in multi-point distributed parameter sensing and measurement applications, otherwise known as Low Power Wireless Networks (LPWN). The progression in development of wireless communication is presented in Fig. 2.1. It is this area of communication that is necessary for the work described in this thesis.

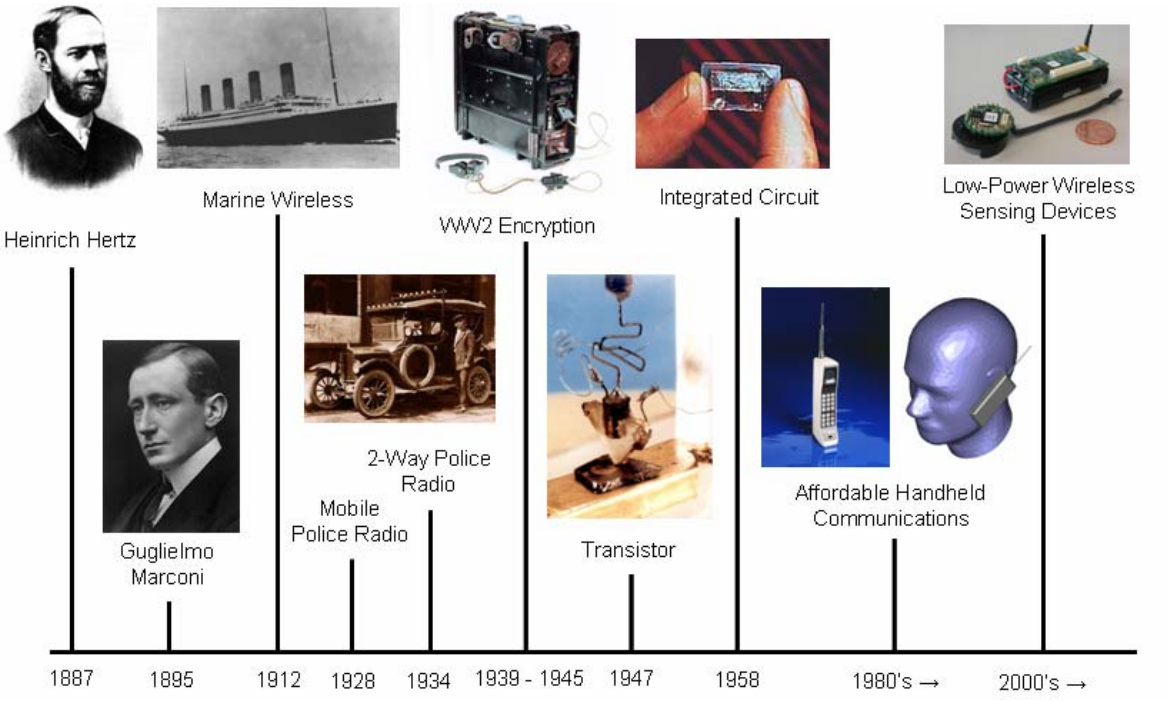

Fig. 2.1 Historical timeline of wireless communications development

2.2 Wireless Sensor Communication Platforms

LPWN are viewed by researchers as the potential gateway through which the world of sensed digital information and the real world will communicate [16]. It is envisaged that low cost sensing networks will furnish their users with useful distributed monitoring data, through web interfaces, giving them a better understanding of the environment being monitored. In fact, at the start of this century, the view of Akyildiz *et al*. was that in the future wireless sensor networks will be an integral part of our lives, even more-so than present-day personal computers [6].

These views and expectations of distributed monitoring systems have led researchers to develop, experiment with, and deploy small-scale wireless sensor networks. The growing research interest in LPWN has also led electronics manufacturers such as Crossbow [23], Tyndall [24], MoteIV [25], Art-of-Technology [26], Teco [27] and Ambient Systems [28] to develop "off the shelf" wireless sensing test kits. The devices that these kits are composed of are generally referred to as "motes". The term, "mote" was first introduced by the Intel-Berkeley research group to describe a node that incorporates sensing and communications capabilities in a single platform [16]. A node forms the lowest component part of a sensing network hierarchy and is responsible for performing sensor measurements and transmitting measurement data.

The general features of current development packages are the same. The sensing nodes are relatively small, lightweight devices consisting of a low-power processor and short-range radio transmitter (typical maximum transmission range is in the order of 100 m). They operate under small control programs that require little onboard memory. In general, the operation of a mote is autonomous and once activated it performs a structured sensing and communications routine, without human interaction for weeks or months at a time until it is manually stopped or exhausts its battery power supply [29].

The device is programmed before deployment to execute an operating routine so that information can be retrieved from a physical sensor, such as a thermistor or light dependent resistor, connected directly to the processor. It is usual for devices to be programmed to operate a fixed sample rate. However, more sophisticated programming can allow for adaptive sensing rates, meaning that, at a time where more valuable information can be gathered the sensing rate will be increased [30, 31]. The operating program converts sensor information, usually in an analogue form, to a digital

representation of the parameter being sensed. Collected information is transmitted at regular intervals, in a digital format unique to each device manufacturer, to a system basestation that is connected to a human interface such as a PC or PDA.

Received data is extracted from data packets and processed within software operating on the human interface, where it can then be displayed to the user or logged to file. In the main, the constructions of mote devices allow for the attachment and integration of a number of individual sensors via digital I/O connection points. This allows the user flexibility in the selection of a specific sensor to monitor a specific parameter of interest.

Sections 2.2.1 to 2.2.3 give an insight into the products available from three particular manufacturers, giving a brief description of their properties and qualities.

2.2.1 Crossbow Motes

Crossbow Technology is the leading end-to-end solutions supplier in wireless sensor networks. The company's ranges of mote devices are currently viewed as the industry standard for wireless sensor networks and are in use in many wireless sensing research groups. Crossbow's sensor networking platform enables powerful, wireless and automated data collection and monitoring systems [23]. As well as supplying devices for dedicated roles such as security, tracking and power monitoring, platforms are available with expansion boards that can be modified by the end user and thus, can be adapted for many specific sensing applications. Two of the commonly used device platforms produced by Crossbow are the Mica2 and Mica2Dot motes. A recent redesign of these devices that has not been as readily implemented in WSN research is called the Telos.

The Mica2 unit is the company's third generation wireless sensor platform. This small unit (58 x 32 x 7 mm excluding battery pack) is powered by two 1.5 V AA alkaline batteries, such as the Duracell MN1500 with a capacity of 2600 mAh [32]. The main components of the device are an ATmega128L low-power microcontroller and a Chipcon CC1000 transceiver radio, with a maximum transmission range of approximately 100 m. There are three variations of this unit available, differentiated by the radio operating frequency required by the customer to adhere to the radio transmission regulations in their country of use. The three available frequencies are

868/916 MHz, 433 MHz and 315 MHz. The transmitter can accommodate up to 4 channels of information allowing the user to place a total number of four individual sensors on each platform. The current unit cost of a single Mica2 node is in the order of $155 (€97.76) [33].

A small operating program in the TinyOS format controls the devices. TinyOS is an operating system designed for embedded devices and is written in the nesC programming language [34]. This language is a dialect of C and was designed for processing environments where there is limited memory, e.g., low-power wireless sensing and communications nodes [35]. The end user software developer is provided with control libraries from which they can control the devices communications and sensing routines. Before transmission, sensed data are assembled into a packet of digital information with the standard packet size being 26 bytes [36].

Assembled packets from each device are broadcast to a basestation of corresponding radio operating frequency that is connected to a PC via an RS232 serial cable. Raw sensor data received from the device can be extracted from the packet and displayed on screen or logged to file for later analysis. Crossbow can supply the user with sensor boards that they have developed themselves such as the Mica Weatherboard [13] and Fireboard [11], or development boards onto which the user can arrange their own sensors and components. The boards are placed on top of the Mica2 and connected via a 51-pin connector. Multiple boards for additional sensing capabilities can be added on top of each other giving a sandwich effect.

The Mica2Dot is an evolution of the Mica2. The main difference between the Mica2 and the Mica2Dot devices is their size; displayed in Fig. 2.2. The Mica2Dot has a much smaller footprint, with a diameter of 25 mm and a height of 6 mm, again excluding the battery pack. This device has been designed for applications where size is an important constraint. The power source is also different. Power is supplied from a 3 V lithium coin cell battery (CR 2354) with a capacity of 560 mAh [37].

The Mica2 and Mica2dot both utilise the same operating hardware, such as microprocessor and transceiver radio. They are interchangeable and can be used together within a network. The devices employ the same standard data packet structure and it is possible for both to communicate with the same network basestation. Apart

from the difference in physical size and standard battery power supplies, the units are differentiated by an onboard thermistor based temperature sensor that has been integrated into the construction of the Mica2Dot. Due to the different construction of the Mica2Dot, expansion boards connect via an 18-pin connecter that runs around the circumference of the unit. However, the same sandwiching method for attachment of additional sensor boards is still employed.

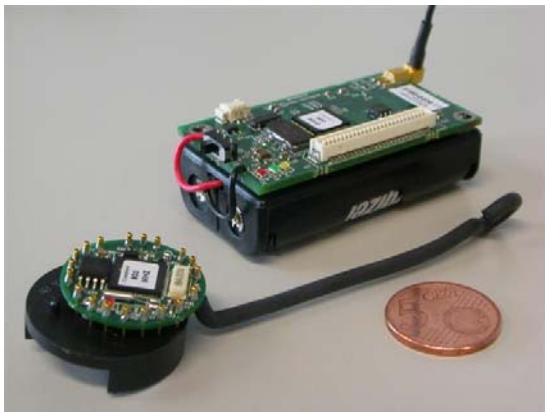

Fig. 2.2 Crossbow Mica2 & Mica2Dot motes

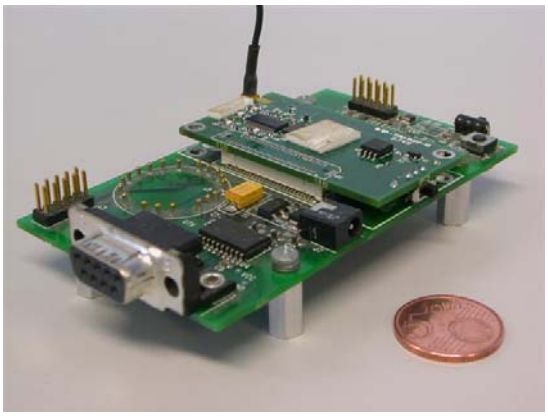

Fig. 2.3 Crossbow mote basestation

Programming of both the Mica2 and the Mica2Dot is performed via a serial interface board, which also acts as the interface between the basestation node and the host PC, pictured in Fig. 2.3. The device to be programmed, or indeed reprogrammed, is connected to the interface board via either the 51-pin or 18-pin connector. Operating programs are transferred from the TinyOS software environment running on the host PC to the interface board, and in turn to the node that is being programmed, via a standard RS232 connection. Successful installation of an updated operating program is visually confirmed by an onscreen confirmation on the host PC.

Telos is a complete redesign of the Mica2 and Mica2Dot motes and is shown in Fig. 2.4. It has been designed by researchers at UC Berkeley based on experience with the earlier mote generations [38]. Firstly, it was desired to make the device easier to use. To achieve this, the requirement of a programming station was removed. Each Telos mote is programmed directly from a

Fig. 2.4 Telos mote [39]

USB connection on the programming PC. The control architecture and programming functions have also been modified to give the user extra functionality. Since the development and experimental use of the Mica2 began there have been concerns with regard to the energy consumption of the motes. This will be explored in more detail in Section 3.2.2.

The designers of the Telos mote recognised a significant downfall of the Mica2 and Mica2Dot; its ATMega128L microcontroller would not operate with a power supply of less than 2.7 V [38]. The microcontroller was replaced with a Texas Instruments MSP430 which operates down to a voltage of 1.8 V and has a better start up time than the ATMega128L, while also using less current [40]. The cut off voltage for an AA battery cell is 0.9 V, therefore, when the Telos is powered by two AA 1.5 V batteries it will operate until the batteries are fully exhausted.

A further development was the introduction of a higher frequency (2.4 GHz) transceiver radio, which allows for a higher data transmission rate of 250 kbps [38]. The benefit here is that the radio does not need to be active for as long as previously required with the Mica2 series while sending a data packet of the same size. The transceiver radio antenna is no longer in the form of a wire antenna and has been incorporated into the body of the device. Although, this product has been on the market for in excess of two years it has not yet replaced the Mica2 series of motes as the standard sensor and communications platform used in WSN research [38].

2.2.2 Tyndall Mote

A highly modular, miniaturised wireless sensor platform has been developed at the Tyndall National Institute, Cork [41]. Hardware modules are assembled in a sandwich layer format similar to that employed by the Mica series of motes, as shown in Fig. 2.5. The stacking process employed by the Tyndall mote is, however, far more robust, and thus, more reliable than that used on the Crossbow Mica series. The robust stacking method provides its own structural support while also making it impossible to incorrectly interconnect stacked modules [42].

The platform has been designed to have a small form factor with a length of side of 25 mm, comparable in size to the Mica2Dot [42]. Further similarities between these two products include a common ATMega128L microcontroller, a 3 V coin cell power

source and the use of TinyOS. From a functionality perspective, the Tyndall mote is distinguished from the Mica2Dot by a higher level of processing power provided by an onboard field programmable gate array (FPGA). This allows for on-board high-speed digital signal processing (DSP) of sensor information [43]. The higher processing capabilities are mainly applicable to multi-hop sensor deployments, where it is necessary for a communications node to examine incoming data and determine if these data are relevant to the monitoring system before retransmission. This functionality allows for the quantity of information transmitted through a network to be managed.

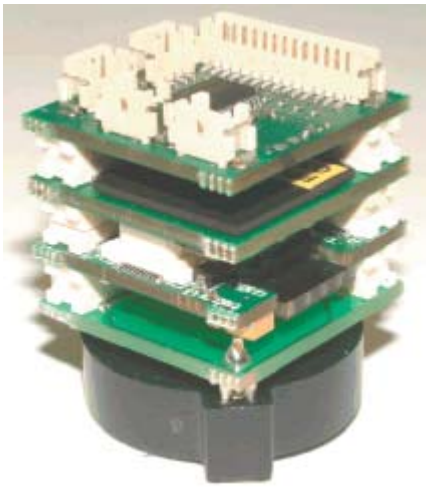

Fig. 2.5 Tyndall Mote with power, communications, FPGA and sensor modules [44]

The lowest module layer of the wireless sensor platform contains the power supply in the form of a 3 V coin cell. Options exist that can accommodate Ø 20 mm and Ø 24.5 mm cells with capacities ranging from 130 mAh to 560 mAh [43]. The next module layer of the nodes construction is dedicated to communications. The transceiver radio (Nordic Nrf2401) operates on the 2.4 GHz ISM band. A 50 Ω antenna is incorporated into the PCB module [43]. This allows for the small form factor of the platform to be maintained by eliminating the need for an external whip antenna similar to that used on the Mica2Dot.

A drawback, caused by the high operating frequency and the internal antenna construction is that the radio transmission range is limited to 10 m (in low power mode) [41, 42]. This equates to one tenth of the reported transmission range of the Chipcon CC1000 transceiver and whip antenna combination employed on the Mica2Dot [45]. The radio is however, able to operate in a “Shockburst” mode which allows for a high data transmission rate that reduces power consumption [43].

Sensor modules are stacked on top of communications and processing modules. Sensor layers that have been developed and tested by Tyndall include, an I2C temperature sensor, an Isfet based pH sensor, a six degree of freedom inertial measurement unit

(IMU), a battery power monitoring layer and a generic sensor interface layer that allows for access to the eight ADC channels on the microcontroller [24].

The robustness and high data processing functionality make this unit a strong test-bed platform for wireless sensor network research. The maximum communication range of 10 m is significantly less than that available from other devices and could possibly be seen as a limiting factor for outdoor sensor network deployments. The Tyndall National Institute is driving research, in the area of wireless sensor platforms, forward with the objective of dramatically reducing the physical size of deployable nodes. The 25 mm form factor node that is presently available is being used as a test bed in the development of 10 mm side and 5 mm side cube form factor nodes with an objective goal of a 1 mm^3 sensor node [44].

2.2.3 TecO µPart

Another range of wireless sensor platforms are the µPart produced by TecO, shown along with the TecO Bridge basestation in Fig. 2.6. The µPart is a very small and easy to use wireless sensor platform measuring just 20 x 17 x 7 mm. A 3 V CR1620 lithium coin cell, with a capacity of 78 mAh [46] is used as the battery power supply. The device is equipped with a PIC microcontroller operating at 4 MHz with 1.4 kb Flash ROM and 64 byte SRAM, an RF transmitter and integrated battery clip [47].

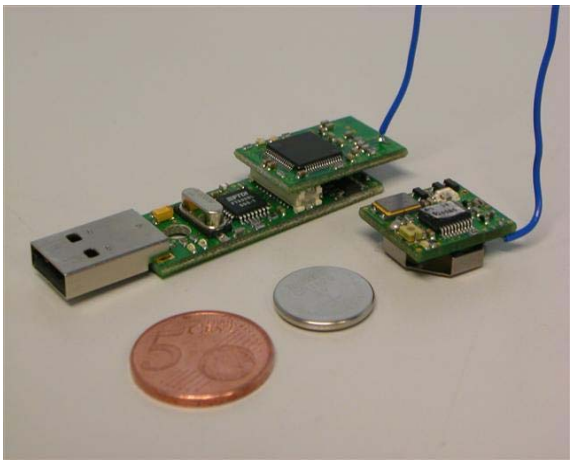

Fig. 2.6 TecO µPart, TecO Bridge basestation and 3 V coin cell battery

This device does not have the same functionality of either the Crossbow or Tyndall mote, but because of this, it is much less expensive (€30 approx per node) and therefore, may lend itself to large-scale deployments. There are two available transmission frequencies, 315 MHz for the US and Japan, and 868 MHz for Europe, having antenna lengths of 21.8 cm and 9 cm respectively. Transmissions are received by a TecO bridge basestation unit. Sensor data are transferred to the host PC via an integrated USB connection. Processed sensor information is then displayed in real-time on the PC screen using the supplied µPart Data Plotter program.

As standard, the µPart014xilmt is fitted with light, temperature and motion sensors. The light sensor is a TSL13T from Taos Inc. It is most effective when measuring light being shone directly onto the device. The sensitivity of the sensor reduces as the angular displacement between the sensor and the light beam falling on it increases. A TC1047A temperature to voltage converter is used as a temperature sensor with an accuracy of ±0.5 °C [47]. The digital motion sensor is a ball switch that is activated when the unit moves, returning basic information on whether the unit is moving or stationary.

The µPart is supplied with pre-loaded firmware so that as soon as it is activated it will start to operate as a sensing node, taking measurements and sending them to the basestation. This is different to the Crossbow and Tyndall devices, which require operating programs to be written and installed before they can operate. There are two methods for changing the parameters of the µPart. Firstly, using a web interface where the user can select and change the parameters via drop down menus. The new parameter values are then sent to the unit as a modulated light transmission via a flickering on-screen display. The onboard light sensor detects this reconfiguration information and stores it in memory. This programming method is only possible with certain types of screens and, because of the sensitivity of the light sensor, interference can occur as a result of ambient lighting conditions.

The alternative method requires a stand-alone programming unit. This method gives the user much more control over the device as they can completely change the PIC operation program instead of just changing some of the operating parameters. The drawbacks of this device are that the maximum transmission range is limited to approximately 30 m and that it is not possible to easily change the onboard sensors or add additional sensors. The device is catered towards network communications testing and research. It is not suitable for testing of novel component based chemical sensing devices due to the impracticality of reprogramming and sensor integration.

2.2.4 Wireless Sensor Communications Platforms Summary

Table 2.1 presents an overview and comparison of the different components and properties of the wireless sensing and communications platforms, which have been discussed in this section. Platform name, manufacturer, device microcontroller, onboard memory capacity, radio transmission frequency, available sensor interfaces and standard form of power supply are detailed.

Sensor Platform	Manufacturer	Processor	Memory	Radio	Interface	Power supply
Mica2	Crossbow	ATmega128L	Flash Memory 128K bytes, Measurement (Serial) Flash 512K bytes, Configuration EEPROM 4 K bytes	315, 433 or 868/916 MHz Multi-Channel Radio Transceiver	10 bit ADC Other Interfaces DIO,I2C,SPI	2 x AA batteries
Mica2Dot	Crossbow	ATmega128L	Flash Memory 128K bytes, Measurement (Serial) Flash 512K bytes, Configuration EEPROM 4 K bytes	868/916 MHz,433 MHz or 315 MHz multi-channel transceiver	10 bit ADC Other Interfaces DIO, 18 pin expansion board	3 V coin cell
Telos	Crossbow	8 MHz Texas Instruments MSP430	1 MB external flash for data logging	2.4 GHz IEEE 802.15.4	I/O,I2C,SPI, Onboard Sensors include light, temperature and humidity sensor, 6 and 10 pin expansion connectors	2 x AA batteries
Tyndall 25 mm mote	Tyndall	ATmega128L	Flash Memory 128K bytes, FPGA 512 K bytes, EEPROM 4 K bytes	2.4 GHz	8 channel 10 bit ADC Other Interfaces DIO, SPI 80 + 40 pin expansion connectors	3 V coin cell
µPart	TecO	PIC12F675 at 4 MHz	n/a	Transmitter in 868, 914 MHz band communication or 433, 310/315 MHz band	On board-sensors: movement, light sensor, temperature 1 LED, power regulation for unit	3 V coin cell

Table 2.1 Properties of reviewed Crossbow, Tyndall and TecO motes

The studies discussed in the forthcoming chapters used the Mica2Dot mote, because literature at the time of this body of work showed that Crossbow Motes were the industry standard for wireless sensor research.

2.3 Factors Affecting Wireless Sensor Network Deployments

Collective groups of wireless sensor nodes can be deployed as networks. Star or tree network configurations are most common. However, network configurations are also being developed where nodes can communicate with any other nodes that are within communication range allowing multiple data transport routes [48]. In both the star and tree configuration the sensing node performs its measurement operation and transmits collected data to a more senior node within the network.

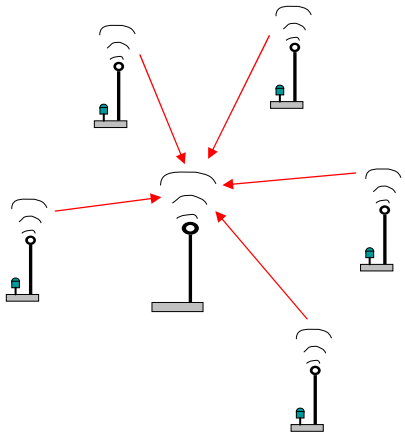

Fig. 2.7 Star network arrangement

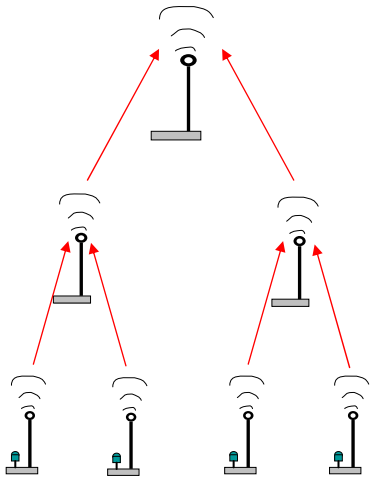

Fig. 2.8 Tree network arrangement

In the case of a simple star network each node communicates directly with a system basestation, as shown in Fig. 2.7. In a tree network, a group of nodes report to an intermediary node, which in turn reports the sensed information to a basestation, as shown in Fig. 2.8. This network arrangement is also referred to as multilevel network architecture [49] and the method of transporting sensor information to a basestation node is referred to as "multi-hopping" [48]. This technique can be used in instances where it is necessary to transport a packet of sensor data over a distance that exceeds a node's communications range.

The two most evident factors that affect WSN deployments presented in the literature are communications reliability and power management. The following subsections will examine these factors and show how they affect the vision of large scale long term deployable wireless sensor networks.

2.3.1 Communications Reliability

The most important factor in the success of a WSN deployment is reliable communication between distributed sensing nodes and the network basestation. A breakdown in communication between these two points results in lost data and thus, a reduction in the quality of data describing changing parameters of interest in the monitored environment. Present first-generation WSN deployments are largely continuous data acquisition systems where data from every sensor are collected at a central location [50]. Increasing the scale of WSNs will lead to increased volumes of sensor data that need to be processed through the network. The present challenge facing computer scientists is how to transfer these large volumes of data reliably and in an energy efficient manner.

However, before identifying the communication techniques that will be used in future large scale WSN deployments, it is first necessary to identify base level precautions that are critical to the success of a WSN. Outdoor deployments have highlighted that changing environmental factors can negatively affect node operation, resulting in unexpected node failure when inadequate protection is provided against changing parameters within the monitored environment [11, 13]. This challenge is not as prevalent within indoor environments, which are not subject to harsh weathering factors, such as, moisture and large temperature shifts. However, as a first course of action in ensuring reliable communications between sensing nodes and a network basestation, it is essential that the conditions within which a node will ultimately be deployed are taken into consideration during its design and development phase. Additionally, it is imperative that the method of protection from changing environmental factors should not impact on, or restrict the node's sensing capabilities.

Natural factors that affect communications reliability are physical obstacles in the communication path between nodes and the network basestation. The interference effect caused by these obstacles can be alleviated in small to medium scale manual node deployments by repositioning of nodes or basestations so that the communication range of the sensor node is maximised. However, non-stationary objects, such as wildlife [13], or humans and machinery [9, 51] in close proximity to sensor nodes can cause intermittent communications obstructions that are not possible to predict.

Rudimentary node hardware protection and suitable positioning with respect to the basestation location does not guarantee reliable communication. From the literature, intermittent transmission losses are inevitable in deployed WSN. Transmission successes achieved in laboratory trials do not correlate with results found when networks are subsequently deployed in real-world environments [9, 52]. This is especially true as the scale of network deployments increase in size. Initial methods used in WSN deployments for increasing communications reliability were to repeatedly transmit data packets from sensor nodes up to five times and so reduce the probability of "dropped packets", i.e., transmitted packets that are not received at the basestation [9].

This approach of arbitrarily transmitting a data packet multiple times to combat transmission losses is a misuse of a sensor node's already restricted power supply and also has the effect of increasing communications traffic within a network. More robust networks, but still small scale deployments in terms of what is expected from future WSN, incorporate a closed loop data packet transmission system to minimise packet loss effects [12, 53]. In these network deployments, nodes repeatedly transmitted a data packet until its reception at the basestation was acknowledged by a message returned to the transmitting node.

The issue of communication reliability in large scale deployments is of great concern. The main challenge is reliable routing of data through multilevel network architectures while also providing for careful resource management of sensor nodes that are tightly constrained in terms of energy, processing, and storage capacities [54]. The practicalities of deploying considerable numbers of sensing nodes over a large area will mean that devices will need to be self organising and capable of forming ad hoc networks that will facilitate "multi hop" communication paths from sensor to basestation.

An in depth analysis of the software based challenges that affect future large scale WSN deployments is outside of the scope of this review. However, a number of critical factors that will determine how routing protocols are implemented are discussed in the following paragraphs.

The methods of data extraction will depend on the specific applications of WSNs. There are three main categories for data reporting, they are, time-driven, query-driven and event-driven [54]. Time-driven protocols will be applicable where nodes are required to turn on, perform measurements and transmit sensed values at set time intervals before returning to sleep (i.e., a low power energy saving mode). Examples of such deployments will be long term environmental monitoring exercises. Query-driven reporting methods will see nodes being activated in response to a message sent from the system basestation requesting data from specific locations. This will allow network operators to ascertain the values of sensed parameters at particular points or over portions of monitored areas.

Of the three categories, event-driven reporting will be most applicable to wireless chemical sensor networks. A sensed change in the chemical properties at a nodes location will prompt the affected node to return updated chemical species concentration data at a predetermined rate to the basestation. Quality of service, i.e., the period of time taken to return the sensed value to the basestation, will be critical in event-driven network arrangements [54]. If data are not returned in a reasonable time period, it will cause a delay in initiating any reactive response to detected chemical events.

Sensor networks will have to be robust, i.e., sensor nodes must remain in communication with the basestation even if intermediary nodes fail. It will, therefore, be crucial for multiple communication paths to exist so that in the event of a node failure sensed values can be communicated to an alternative intermediary node and then subsequently to the basestation. The network will have to be able to adapt to these changes by possibly rerouting data from groups of sensor nodes to other intermediary nodes in their vicinity so that the energy consumption rate is balanced across intermediary transmission nodes.

It is inevitable that large quantities of generated data will be redundant, e.g., when there is no change in sensed parameters from previous measurements. A level of intelligence will have to be incorporated into sensor nodes so that sensed values can be compared to stored threshold levels. The node itself will then be able to determine if the sensed data are critical to the network. If a sensor records no change in its parameter of interest it would not report the value and, thus, reduce the quantity of data introduced into the communication path.

The one critical constraint currently faced by computer scientists in developing effective communications protocols for large-scale WSNs is energy consumption. Reliable communication has to be achieved over extensive periods of time but within the finite limits of small battery power supplies.

2.3.2 Power Management

As a result of the reducing costs of wireless sensor technology, it is expected that sensor nodes will be introduced into their monitoring environment in a "deploy and forget" scenario [55]. However, the challenge that this concept of future WSN deployment poses has been simply stated by Paradiso *et al*. in a recent review paper as,

> *"ubiquitous computing's dream of wireless sensors everywhere is accompanied by the nightmare of battery replacement and disposal"* [56]

An extreme case of power consumption within a WSN has been reported by Beckwith *et al*. The operating lifespan of nodes provided with 42 Ah battery supplies was found to be 6 weeks [9]. This, of course, is a completely impractical energy requirement for a long term WSN. Practical deployments implement node power management schemes. Although, energy savings are found by shutting down non-essential sensor node components when they are not required, the limiting factor of a node's lifespan is its power source [57]. Mainwaring *et al*. attempted to achieve a network lifetime of 9 months through restricting node power consumption to an average of 8.148 mAh per day [13].

Constraining the use of the power supply to achieve a practical deployment lifespan would limit the effectiveness of a device when a dynamic parameter of interest, such as a changing chemical species concentration, has to be monitored at a high rate and reported in real-time. In addition, current research questions the effectiveness of using conventional battery power sources for long term deployable WSNs, due to the impracticality and prohibitive cost of battery replacement [55]. Indeed it may be a fact that the cost of battery replacement would outweigh the cost of the node itself [58].

It would, therefore, be more cost effective to manufacture a new node and deploy it into the environment rather than incur the expense of changing the battery of the exhausted node. The question of what are the long term environmental effects of not disposing of

discharged battery cells correctly is then raised [55]. For these reasons, renewable forms of low power energy supplies, termed energy scavenging devices, are being investigated. Energy scavenging principles under investigation for integration with low power WSNs include vibration, thermoelectric effect and photovoltaic cells (solar). Each source is applicable to differing operating environments and it is, therefore, necessary to cater the energy source to the natural resources available at the node's intended location.

Vibration and oscillation energy scavengers harvest energy from movements occurring in their environment or induced upon them. These could be vibrations on building surfaces such as doors and windows, higher frequency vibrations in close proximity to mechanical equipment, or vibrations on the human body while in motion [59]. Proposed devices operate by means of converting kinetic energy of a moving mass to electrical energy. An example of this is where the energy in an environmental vibration causes a magnetic mass to move relative to a coil, generating a voltage and causing a current to flow through a connected electrical load [55]. Physical examples currently in use include the Seiko AGS (Automatic Generating System) generator for their Kinetic series of wrist watches and "shake-powered" LED flashlights [56].

The presence of temperature differentials in an environment allow for energy scavenging by means of heat transfer. Large scale examples of this include generation of electricity from the hot exhausts of internal combustion engines [55] and heat engines running in geothermal power stations [56]. In small scale devices, thermal gradients are converted to electrical energy using the Seebeck effect of voltage generation at a thermocouple [55, 59]. Examples of small scale devices are generally catered to wearable sensing applications where temperature gradients of 5 degrees Kelvin are achievable. Reported devices include a wristband thermoelectric Micro Electro-Mechanical Systems (MEMS) power supply [60]. The developed power supply has been coupled with a wireless sensor platform to form a fully autonomous node of a Body Area Network (BAN) for a wearable sensing application [61]. A commercially available product that uses a thermoelectric energy scavenging power source is the Seiko Thermic wristwatch. This device generates microwatts of power to operate the clock mechanism from the temperature difference between the wearer's body temperature and ambient air through ten thermoelectric modules [56].

Solar energy scavenging photovoltaic cells have been commonly used for decades in products such as calculators and wristwatches [55] and more recently in public illumination and parking meters [59]. This technology is now being investigated for use in both indoor and outdoor low power sensor applications. From the power density data presented in a number of low power energy scavenging review papers it is clear that at present this energy scavenging method provides more electrical energy for similar device size than previously mentioned harvesting techniques. This is especially applicable in the outdoor environment where it has been stated that solar energy harvesters are capable of achieving power densities of 7.5 mW/cm^2 to 15 mW/cm^2 depending on the environment's ambient conditions [55, 58].

The achievable power density in the outdoor environment is approximately 100 times greater than in the indoor environment under typical room lighting. One reported wireless communications node test bed scavenges energy based on room lighting conditions. Wireless routing nodes based on a Crossbow MICAz platform have been coupled with a group of photovoltaic cells and Maxwell PC5-5, 5 V ultracapacitors [58]. The ultracapacitors were connected in parallel with a group of twelve 3.75" x 2.5" monocrystaline solar panels to store harvested energy which would be provided to the node in times of low light. A group of twelve solar panels were necessary as each panel could source approximately 2 mA of current and the minimum requirement for the MICAz node under full load at 3 V was 25 mA [58]. Hande *et al*. anticipate that this arrangement would work well for outdoor environments where the solar energy source is not limited to standard overhead 34 W fluorescent lights.

It is unlikely that vibration or oscillation energy scavenging devices will be employed in distributed networks in outdoor environments because of a lack of easily accessible high frequency vibrations from which energy could be harvested. These devices would seem more suited to either indoor environments, where it would be more likely to find harvestable vibrations, or integration with human clothing/footwear, where energy can be extracted from motion of the body. Thermoelectric power scavenging approaches are also unlikely to be successfully implemented for outdoor environmental sensor nodes, as temperature gradients are relatively small and difficult to find [59].

Currently, the most promising prospect of sustainable renewable energy sources for small wireless sensor nodes would appear to be solar energy harvesting cells coupled

with storage capacitors to allow operation of a node during periods of low light intensity.

It is not a requirement of this particular research to investigate integration of energy scavenging devices with a wireless chemical sensing node. It has, however, been noted that this research is ongoing and will allow for future fully autonomous outdoor field deployable systems that will not have a significant cost overhead incurred as a consequence of the necessity of manual power supply changes. It has been similarly noted, that when considering large scale deployments it is essential to implement robust communications protocols to reliably retrieve good quality information from a WSN.

Small scale laboratory WSNs that focus on the operation of a sensing mechanism, rather than communications reliability or long term power management, and such as that under investigation in this body of work, are not constrained by these limiting factors. However, in the development of a laboratory scale wireless chemical sensor network it should be acknowledged that these limiting factors exist and are the basis for essential research by a number of other research groups and wireless platform manufacturers, such as Tyndall, that will facilitate the realisation of large-scale WSNs.

2.4 Current and Emerging Applications

Research into WSNs has been underway for some time, however, there is a belief that WSNs are currently at the same developmental stage as the Internet was in the 1970's, but that they possess the same or even greater potential [16]. For the most part, current WSN deployments focus on the monitoring of physical parameters in both indoor and outdoor environments. In this section, a sample of the current applications of WSNs that are being investigated and have been reported will be outlined and discussed.

Mainwaring *et al*. presented work on a 32 node WSN deployed on Great Duck Island, Maine, USA, to remotely monitor a Petrel seabird colony [13]. The method of monitoring the habitat using fixed sensor nodes as a WSN was expected to be less invasive and result in data that gave a better representation of the colonies actual behaviour than would be achieved through conventional monitoring methods.

Werner-Allen *et al*. presented a WSN using Mica2 motes equipped with low frequency microphone sensors for the monitoring of volcanic eruptions. The incentive for this particular WSN application was that current wired monitoring methods require human retrieval of collected data from monitoring stations located in potentially hazardous locations on the volcano being monitored [12]. An added advantage of using a wireless network was the possibility of deploying a greater volume of sensors over a wider ground area than had previously been possible with the conventional wired measurement technology in use.

In both of these cases, WSNs were implemented to gather reference data from which trend information could be extracted or logged for future reference. WSNs have also been developed to gather data from environments where the incentive is to use collected data to reduce the expenditure associated with the environments being monitored.

Beckwith *et al*. deployed a WSN for the purpose of temperature monitoring in a grape-producing vineyard [9]. Their goal was to investigate if dense monitoring of the varying temperature conditions in a vineyard could provide the proprietors with information allowing them to react to temperature changes or trends and in return increase their crop yield. Kintner-Meyer *et al.* investigated the deployment of wireless devices in building facilities [4, 62]. Temperature values were recorded over time, analysed and then used to improve the energy efficiency of a chiller unit and in turn

improve the energy efficiency of the building leading to a reduction in energy expenditure.

Systems are being developed where data collected from a number of dispersed locations are analysed in real-time to act as early warning systems. In early 2005, Doolin *et al*. presented research on the use of wireless sensors for wildfire monitoring [11]. It was the belief of Doolin *et al*. that real-time information retrieved from a network such as this would be used to identify when a fire has started so that fire-fighting authorities could be informed to the occurrence as soon as possible.

The use of real-time data collected from WSNs is also being explored in indoor environments. Introduction of wireless systems into indoor environments has been likened to the development of television [62]. Initial thoughts on the arrival of television were that it would completely replace radio. However, this did not happen, instead both media now co-exist. In the same vane, it would not be expected for wireless sensors to completely replace hardwired sensors. It is proposed that both systems will be used together with wireless sensors providing additional flexibility for system installations. Kintner-Meyer *et al*. suggest that wireless sensors will first be used solely for monitoring operations requiring only one-way data transmission. Their role is then expected to grow into simple control applications; however, this may be limited by the reliability and update frequency of control transmissions [62]. Integrated networks, where sensed data are used to influence parameters of interest have resulted in the development of Wireless Sensor Actuator Networks (WSAN).

Sandhu *et al*. proposed a WSN incorporating artificial intelligence (AI) for the control of office lighting [14]. From other research they stated that 40 % of the energy supplied to office buildings in the United States is used for lighting and that energy savings of 45 % are possible through the use of occupant and light sensors. The proposed system would take information from multiple wireless light sensors dispersed within an office space. Dimmable lighting would then be adjusted based on these sensor values so that a predetermined optimum lighting level would be obtained. The system would allow for the individual user's lighting preference by allowing them to manually adjust the lighting level about their workspace.

The monitoring capabilities of WSN deployments have predominantly focused on sensing of physical parameters using well established sensing techniques. However, current deployments have identified that the ability to sense chemical vapours, gas concentrations and pH would augment measurements of current physical sensors [13]. Thus, research into low-cost, low power alternatives to conventional laboratory chemical sensing methods is emerging.

The merits for using low-power wireless sensing devices as opposed to conventional laboratory equipment to perform a distributed sensing role are outlined in the chart displayed in Fig. 2.9. LPWNs would provide large density deployment and in turn, large volumes of data. It is inevitable that the reliability and quality of data produced by low cost sensors will be less than that of sophisticated measurement and analysis equipment. However, it may be possible to use collective data from a number of spatially distributed low cost sensors to identify and track events, rather than using one complex device to gather data from one single location. Before detailing new alternatives, the following section will provide an understanding of conventional chemical sensing methods and how their costs and power requirements are being reduced.

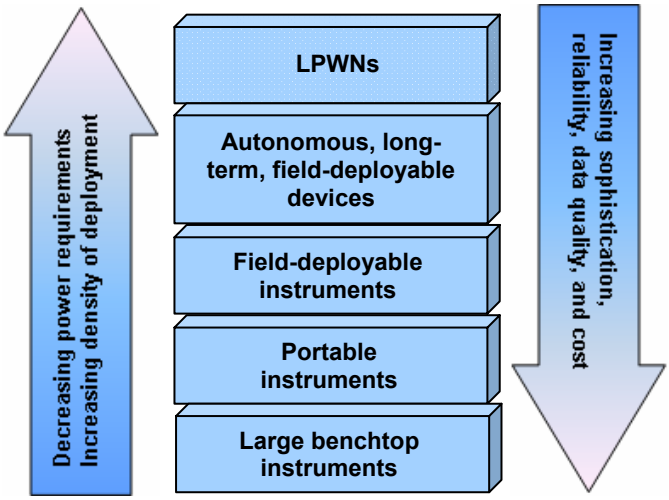

Fig. 2.9 Instrumentation hierarchy [16]

2.5 Chemical Sensing and Chemical Sensing Techniques

Chemical sensing and the techniques used to detect and quantify the presence of chemical species vary in sensitivity, power consumption, range, selectivity of targets, portability and, as always, significantly in price. It is the measurement of pH changes that is used as an application for the chemical sensor described in this thesis and, therefore, it is necessary to introduce this concept with some background in the area of pH and chemical species detection.

The following definition of a chemical sensor, its role and construction are given by Janata and Bezegh: "a chemical sensor is a device which furnishes the user with information about its environment; it consists of a physical transducer and a chemically selective layer" [63]. The most commonly measured chemical variable is pH [64] and is "a measure of the acidity or alkalinity of a solution equal to the common logarithm of the reciprocal of the hydrogen ions in moles per cubic decimetre of solution" [65]. In effect, this is a measure of the concentration of hydrogen ions in a sample. The pH scale in common use today ranges from 0 to 14 and was invented in 1909 by Soren Sorensen. The pH scale is numerically equal to 7 for neutral solutions, increasing with increasing alkalinity and decreasing with increasing acidity.

The pH scale is measured using an electrochemical measurement device known as a pH meter. The first commercial pH meters were built around 1936 by Dr. Arnold Orville Beckman in the United States [66] as a means to quickly and accurately measure the acidity of lemon juice for the California Fruit Growers Exchange. Electrochemical sensing is defined as the measurement of a change in an electrical property such as voltage, resistance or capacitance resulting from the presence of a chemical. The pH meter measures the potential difference between a pH-sensitive glass electrode and a reference electrode when both are placed in a liquid solution. The results given by a properly calibrated pH meter are very accurate.

Colorimetric sensing tends to be indicative of changes in the environment but quantification is more difficult to accurately measure using these techniques. A colorimetric chemical reaction occurs when the presence of a chemical species changes the colour of a substance, known as an indicator. This degree of colour change can be optically measured to further determine the presence and possibly the concentration of the chemical species. The commonly known indicator substance, litmus, can facilitate

this colorimetric chemical reaction. Litmus, when immobilised onto paper is used to perform coarse visual pH measurements. To conduct a measurement, litmus paper is brought into physical contact with a liquid solution. The colour of the litmus paper is dependent on the degree of acidity or alkalinity of the solution and termed a pH induced colour change. An approximate pH value is found by the individual performing the test through visually comparing the altered colour of the paper to a chart of corresponding colour changes.

Numerous indicator dyes whose colour change is dependent on certain chemical conditions are commercially available in both acidic and alkaline ranges. Introduction of a suitable indicator dye into a solution will result in a colour change if a target chemical species is present. Traditionally, the solution is further analysed using a UV-Visible spectrometer in the correct wavelength range to determine the light absorbance of the coloured solution. The obtained absorbance spectrum is then used to determine the concentration of the chemical species present in the sample.

The following subsection introduces a variety of chemical sensing techniques and compares them with respect to the criteria of sensitivity, power consumption, range, selectivity of targets, portability and cost. This analysis of conventional sensing techniques will act as an introduction into the emerging area of colorimetric sensing which has inspired the work described in this thesis.

2.5.1 Laboratory Sensing Techniques

Conventional laboratory chemical sensing methods of solutions rely heavily on electrochemical sensing and colorimetric sensing techniques as just described. Modern laboratory techniques for chemical sensing offer highly selective and sensitive methods in determining the chemical species present in a sample. In fact, some devices can detect and identify a number of different species present in a single sample during a single sensing operation. This statement is equally true for detection of chemical species in solution and in gaseous form. It is the detection of chemical species in the gas state which will be further discussed in this section.

There are a number of reliable standard bench-top techniques used in analytical laboratories for the detection and separation of chemical species in gas samples. Gas chromatography (GC) is the premier analytical technique for the separation of volatile

compounds [67]. However, GC alone cannot identify the particular volatiles present in a sample gas. Therefore, this technique is often coupled to other techniques which can further analyse the species present in the gas sample. Coupling a mass spectrometer to a GC system (GC-MS) allows for the identification of separate unknown compounds by calculating their molecular weight [68]. This technique can deliver quantitative analysis of chemical species concentrations down to the ppb (parts per billion) level [67], but this technique takes time.

Other techniques often used for identification and quantification of gas species include Flame Ionisation Detection (FID) and Photoionisation Detection (PID). The FID system works by burning the gas in a hydrogen flame. Any organic compounds present will produce ions (charged species) which are measured at the sensor electrodes. The resulting current is proportional to the concentration of the organic species present. The sensitivity is in the ppm (parts per million) range so it is not as sensitive as the GC-MS system. In terms of selectivity, it is able to distinguish between length of carbon chains but not functional groups, i.e., it can distinguish between ethane and butane but not ethane and ethanol, as indicated in Fig. 2.10.

Alternatively, PID systems are capable of distinguishing between functional groups but not chain length of the species present, as also described in Fig. 2.10. This system works by ionising the sample using an ultraviolet light source. Again, the current produced by the ions is measured, indicating the species present. The sensitivity of this technique is in the ppb range.

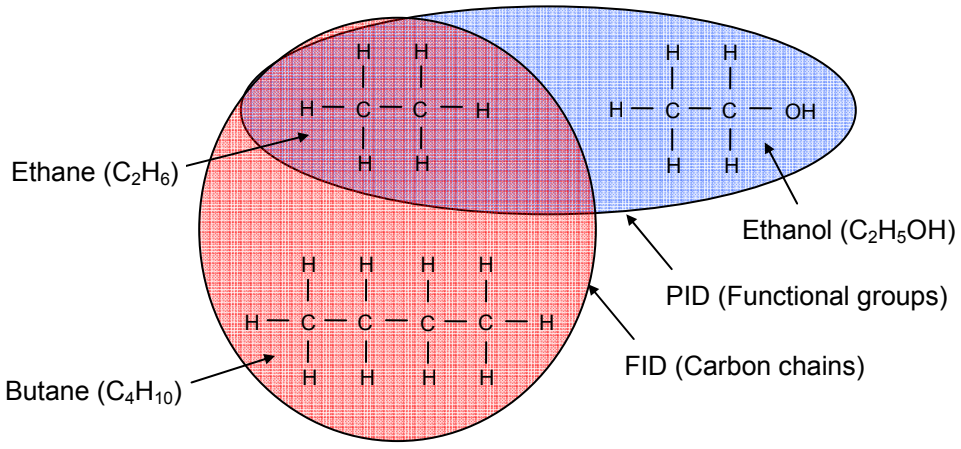

Fig. 2.10 Differentiation between functional groups and carbon chain length by PID and FID

The precision laboratory measurement equipment necessary for GC/MS, FID and, PID sensing techniques require regular maintenance and calibration to ensure their correct and reliable operation. The precise and versatile measurement capabilities of the equipment results in these devices being complex, expensive bench top units. However, systems that employ these sensing techniques have become commercially available as portable units and can be used at the site of an event or suspected release of an unwanted target gas.

An example of a portable GC/MS system is the HAPSITE smart chemical identification system. This unit has been developed to be field portable by one person and provide highly accurate identification of volatile organic compounds (VOCs) at concentration levels in the low ppb range [69]. Portable FID and PID systems are more common. The TVA1000B is an "over the shoulder" portable device that integrates both of these chemical species quantification techniques into one unit [70]. While these devices are portable they can only be placed into a monitoring area to perform measurements by a suitable trained operator.

More mobile versions, in the form of handheld devices are available that use the FID and PID techniques. The Photovac MicroFID Flame Ionization Detector is a handheld device that is catered towards landfill monitoring, emergency response, i.e., HAZMAT monitoring, and natural gas pipeline leak detection [71]. An example of a mobile PID gas detector is the GasAlertMicro [72]. This piece of equipment can be utilised in monitoring VOCs, oxygen and combustible gases.

To facilitate remote monitoring of an area, e.g., manually introducing a monitoring device into a hazardous area and moving outside of the hazard area to monitor measurements, FID and PID devices, such as the MiniRAE 3000 [63] and the AreaRAE Steel [74] have been equipped with wireless modems. However, the drawbacks to all of the above devices in terms of a large scale wireless chemical sensor network are that they are too expensive to deploy in large quantities (unit cost of MiniRAE 3000 is $3,825 [75]), and have a high power demand (AreaRAE Steel battery lifetime is 36 hrs in continuous stand-alone operation [74]).

At this stage, it is important to acknowledge that in the area of chemical sensing there is middle ground between the selectivity and sensitivity of bench-top instrumentation and

the low-cost, low-power colorimetric sensing techniques described in this work. Sensor systems and individual sensors, based on infrared technology are commercially available, field deployable and have a proven track record. These sensors provide gas detection with excellent selectivity and reliability. Infrared sensors are target specific as the wavelength of the sensor can be tuned to a specific band or bands of interest for target gases including hydrocarbons, carbon dioxide, carbon monoxide and ammonia. An example of a readily employed mobile gas monitoring system that employs the infrared gas sensing technique is the Geotech GA2000 [76]. This handheld device is primarily used in the monitoring of combustible gas in landfill sites. Infrared sensing technology is also being incorporated into an automated field deployable landfill gas monitoring device capable of measuring percentage volume of carbon dioxide and methane in extracted samples that will operate over a period of one month [77, 78].

Infrared sensors are, however, not low-cost compared with the sensors described in Section 2.5.2. Moreover, these sensors are not low-power, in comparison with the sensor system described in this work, needing time to "warm-up" and stabilise, drawing power before data acquisition is possible.

The hierarchy of analytical gas analysis devices has been presented. Alternative techniques which do not rely on complex measurement methods that will allow for the development of low-power, low-cost chemical sensors are described in the following section. The development of such sensors is a necessity that must be achieved before it will be possible to deploy large-scale low-power wireless chemical sensing networks.

2.5.2 Low Cost Chemical Sensing

Before the sensing system described in this thesis is discussed, it would be advantageous to compare and contrast commercially available low cost chemical sensor systems.

If we return to the definition of a chemical sensor, we see that to obtain a measurement the chemical of interest will have to interact with the surface of a chemically sensitive material. The makeup of the chemically selective layer is critical as it determines the effectiveness of the sensor, i.e., it affects the device's sensitivity, lifetime and response time [79]. Diamond points out that the "ideal" sensor does not exist [79]. A sensor that is suitable for one environment may be completely unsuitable for use in a different

environment due to changes in the physical properties of the second environment such as temperature or pressure. Therefore, low cost chemical sensors are constructed specifically for the parameter that they are used to sense, i.e., they are target specific. This is the trade off when using these less sophisticated and comparatively cheap devices compared to precise laboratory equipment.

Catalytic bead sensors, also known as pellistor sensors are used for the detection of combustible gases. They have been in use for the past 50 years and their first application was underground gas monitoring in the mines. This gas sensor exploits the phenomenon known as catalytic combustion whereby some catalysts such as platinum, palladium or thoria will cause gases to combust at lower temperatures than their ignition temperature. The sensor surface is coated in an appropriate metal oxide while the electrical circuit used to measure the output of the combustion of the gases is based on the design of a Wheatstone bridge. As the gas burns the catalyst on the sensor coating the resistance of the bridge changes relative to the reference sensor. This change is measured as a signal which is dependent on the concentration of the gas combusted. As the catalyst is combusted, the lifetime of these sensors is short, usually 1-2 years. Also, the sensor can be poisoned by silicon, sulfur compounds and chlorine.

Improvements to the pellistor sensors led to the development of semiconductor sensors, also called solid state sensors, which have been around since the 1970s. These sensors use metal oxides prepared from transition metals, e.g., tin or aluminium, to sense the target gas species. Examples of these are tin-oxide (SnO_2) for the detection of nitrous oxides and VOCs [80] and zinc-oxide (ZnO) for the detection of hydrocarbons [81]. In the presence of gas, the metal oxide film causes the gas to dissociate into charged ions producing a current. This change in conductivity produces a signal which indicates the concentration of the target species present. Semiconductor sensors are cheap, abundantly available, have a life expectancy of up to ten years and can be used to detect a wide variety of gases. The variation in target species measured is achieved through variation in the metal used in the metal oxide film or by changing the operating temperature of the sensor.

These sensors have many applications including, electronic nose devices, where detection of a number of target species is necessary. They can be used for measuring toxic, combustible and odorant gases displaying the versatility of these types of sensors.

The sensor is vulnerable to interference from other gases as it is not as specific as other sensor technologies discussed here.

The next step forward in chemical sensing comes in the form of commercially available electrochemical sensors. These sensors work by reaction of the target gas at the sensing electrode which produces an electrical signal proportional to the gas concentration present. The main components of an electrochemical sensor are the sensing electrode (target specific) and the counter electrode, separated by a layer of electrolyte. This sensor is minimally affected by pressure changes and is temperature compensated, to ensure that changes in temperature have little effect on the efficiency of the sensor. They are selective to the target species; the most selective being the sensor for oxygen detection. Other electrochemical sensors do have some interference from other gases. The life expectancy of this type of sensor is 1- 3 years. Electrochemical sensors require the least amount of power of all the gas sensors described in this review.

Categories of low cost electrochemical sensors include, chemiresistors, CHEMFET's, and SAW (Surface Acoustic Wave) sensors. Changing electrical parameters monitored by these devices include, dc resistance, field effect transistor threshold voltage, and phase change of a wave propagated across the sensor surface [82]. Chemiresistors operate based on a change in resistance of a conductive layer between two electrodes when it interacts with a chemical stimulus. Sensing materials include semi-conducting metal oxides [83, 84], and conducting polymer composites [85-89]. Recently, conducting polymers, resulting from their strong absorbance properties towards gases [90], have been combined with carbon nanotube technology for selective chemical sensing [91, 92]. Conducting polymer layers have been used for the sensing of ammonia (NH_3) and nitrogen dioxide (NO_2) [88, 89]. It is the view of Wilson *et al.* [82] that electrodes in devices such as these must be produced from materials such as gold or platinum to achieve sufficient inertness to chemical contaminants and minimise signal noise. This requirement increases the complexity and cost of these devices. In the rest of this subsection, these sensors will be described in more detail.

CHEMFET's, which can also be referred to as potentiometric sensors operate by measuring the voltage between a measurement and reference electrode in a field-effect transistor architecture [82]. The voltage output of a CHEMFET is affected by a change in the conductive chemically sensitive layer on the measurement electrode.

CHEMFETS have been applied to the detection of many gases including, hydrogen [93], oxygen [94] and the measurement of pH [95-100]. A disadvantage of this form of sensor is that the power of the measured signal is very low and requires significant amplification [82].

SAW devices typically consist of a piezoelectric substrate with interdigital transducers (IDTs) as an electrode structure on a single plane [101]. A wave is produced on the substrate by applying an alternating voltage to the IDTs [101]. Chemical reactions are identified by measured changes in the wave's velocity due to mass absorption or viscosity changes in a chemically sensitive layer on the substrate surface [102-105]. Acoustic wave devices are required to operate at a high frequency which complicates their operating circuitry and necessitates stringent noise management [82].

The integration of a limited number of chemical sensor devices, including low power electrochemical sensors, with wireless communication nodes has been reported in the literature. The following section will discuss these devices and the means in which they have been implemented, prior to the introduction of the optical sensing technique that is utilised in this body of work in Section 2.6.

2.5.3 Current Wireless Chemical Sensors

Recently, Han *et al*. have reported the coupling of 6 Telos motes with a total of 10 conductivity probes to monitor chemical changes in subsurface environments [106]. Fixed voltage power supplies for the devices were provided via USB connections. Initial trial results, in response to the introduction of a tracer solution of known concentration have been presented for a single device. No comparison or trend data between the individual sensor devices was presented.

Yang *et al*. have published results for a single RF wireless chemical sensor node which used a magnetoelastic sensor array to measure pH in an aquatic environment [107]. The device was tested in a small volume of water through exposure to varying pH levels. The device was shown to provide reproducible results to 5 consecutive pH step changes from pH 2.0 to pH 7.5. Yang *et al*. suggest that a sensor device such as this could be deployed as a network to monitor drinking water reservoirs.

Chavali *et al.* presented research on the development of a wireless sensor node for the purpose of monitoring a volatile anaesthetic agent [91]. A Mica2dot mote was coupled with an electrochemical gas sensor. The electrochemical sensor comprised of an aluminium substrate, onto which two comb-like gold electrodes were screen printed. A thin sensing film of a synthesised composite of multi-walled carbon nanotubes and the conducting polymer polypyrrole was applied to the surface by dip coating. The gold electrodes were connected to the sensing platform via platinum electrodes. A change in response of the sensor due to interaction of a gas contaminant with the conducting polymer was determined from a measured change in resistance between the two electrodes.

The responses of a number of constructed sensors were individually examined within a controlled flow chamber environment. Temperature, humidity, gas concentration, and gas flow rate were managed during conducted experiments. The results found that the sensor was responsive to the target gas, displayed an approximate response time of 75 s and was reproducible over a number of exposure periods. Chavali *et al*. believe that this sensor platform paves the way towards sensor networks monitoring hazardous environments in real-time. However, they have not yet progressed to examine the operation of a network of such chemical sensing nodes.

2.6 Emerging Low-cost Low-power Chemical Sensing Techniques

Colorimetric sensing techniques are also being explored to achieve low-cost chemical sensing devices. The properties of many indicator dyes are such that their induced colour changes are reversible. In typical laboratory testing, an indicator introduced into a solution to conduct a measurement cannot be easily removed, i.e., the dye cannot be extracted so that it can perform another test. To perform a measurement in a gaseous environment, it is possible to immobilise a dye into a membrane structure [108 - 112].

Immobilisation of an indicator dye into a polymer allows for the indicator to be deployed as a thin film of chemically sensitive material that can repeatedly react to changes in pH by a measurable colour change. In the present research, a chemical reaction between the sensing layer and a chemical stimulus has been facilitated by matching the indicator component to the particular gas being detected. For example, thymol blue and metacresol purple have been used in the detection of carbon dioxide gas [108, 109] and 2,6-dichloroindophenol (2,6-DCIP) has been used in testing for oxygen gas [110]. The response, i.e., colour change, of the developed sensing films has been examined in controlled laboratory settings using spectroscopic equipment [108, 110].

The simplicity of pH sensitive indicator dye films makes them attractive for use in low-cost, large-scale chemical sensing networks. The fact that induced colour changes are reversible increases the functionality of any developed sensors so that they can be used to monitor a number of separate events. A low-power method to measure chemically induced colour changes in reactive sensing layers is necessary so that colorimetric chemical sensing can be integrated onto small low-power wireless sensing platforms and possibly provide a less complex alternative to electrochemical sensing techniques. A potential technique to perform these measurements is the use of LEDs as light detectors. The underlying principle is discussed in the following subsection and it is this principle for light detection that is the basis for the low-cost chemical sensors considered in this body of work.

2.6.1 LEDs as Light Sensors

Light Emitting Diodes (LEDs) are generally regarded as devices for emitting a small light and today are commonly used as status indicators for devices such as computer equipment, numeric displays and televisions. Recently the use of LEDs in home

lighting has begun as an alternative to conventional filament bulbs. However, an LED is fundamentally a photodiode and is therefore, also a light detector. Although LEDs are not optimised for light detection, they do operate very successfully in that role [113]. During the 1970's, Mims began investigating the use of LEDs for light detection and in switching between light emission and detection [114, 115]. Dietz *et al.* further investigated the use of an LED for ambient illumination sensing and the principle of this measurement method is discussed in the following paragraphs [113].

An LED is connected in series with a resistor between two digital I/O (Input/Output) pins on a microprocessor device. This arrangement is shown in Fig. 2.11 and the sequence of the sensing cycle is then shown in Fig. 2.12. Fig. 2.12a shows the normal arrangement for a LED with a voltage being supplied via the LEDs anode through a resistor and towards ground. This results in the LED lighting up. When a LED is connected in reverse bias, (see Fig. 2.12b), i.e., when the LEDs cathode is connected to a pin in a logic high state (output mode), the LEDs internal capacitance is charged.

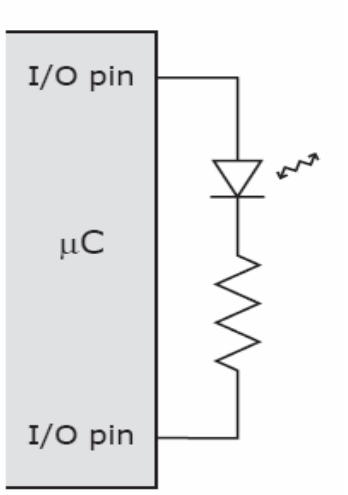

Fig. 2.11 LED detector I/0 pin arrangement [113]

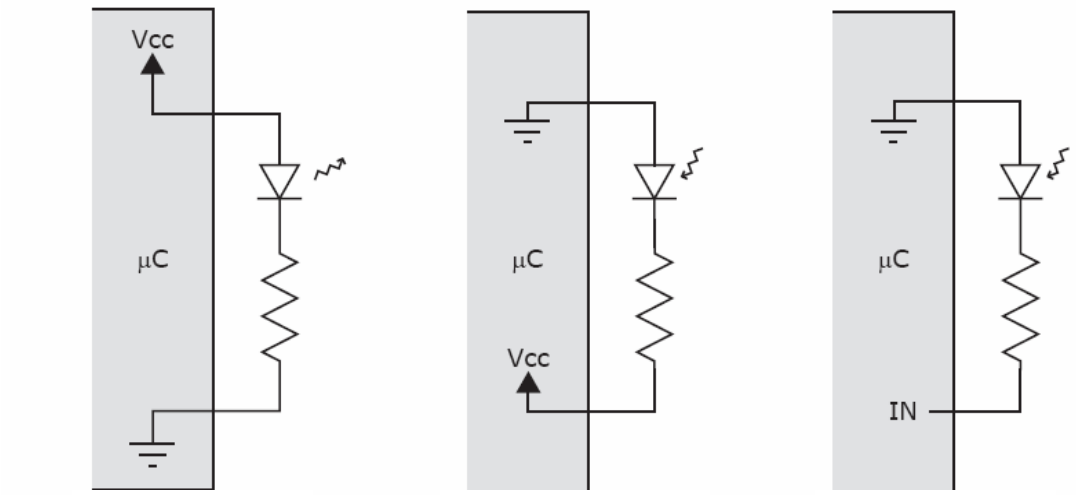

a) "Emitting" **b) "Reverse Bias"** **c) "Discharge"**

Fig. 2.12 LED Sequencing [113]

Switching the state of the I/O pin connected to the LED cathode to input mode, as shown in Fig. 2.12c, allows the capacitance to discharge into the microcontroller I/O pin at a rate dependent on the light falling on the LED [114]. A light intensity measurement is performed by repeatedly checking the logic status (1 or 0) of the I/O pin as the internal capacitance of the reverses biased detector LED is discharged into it. The status of the pin is checked the same quantity of times and over the same time period for each subsequent measurement. Each increment during the measurement routine that the status of the pin is checked is referred to as a count. The status of the I/O pin is checked 4000 times in each measurement routine, i.e. 4000 counts. The data output range is, therefore, 0-4000 processor counts. The status of the I/O pin is determined by the voltage at the pin at the time of sampling. The status of the pin will be logic high, i.e., 1, when to voltage at the pin is greater than the logic zero threshold (≈ 1.7 V). The measured response of the sensor is the quantity of counts over the 4000 unit measurement period where the logic state of the I/O pin was in a logic high state. For example, in the illustrative decay curve, shown in Fig. 2.13, the quantity of counts where the logic zero threshold was exceeded within the fixed sampling period of 4000 counts was 2138 counts.

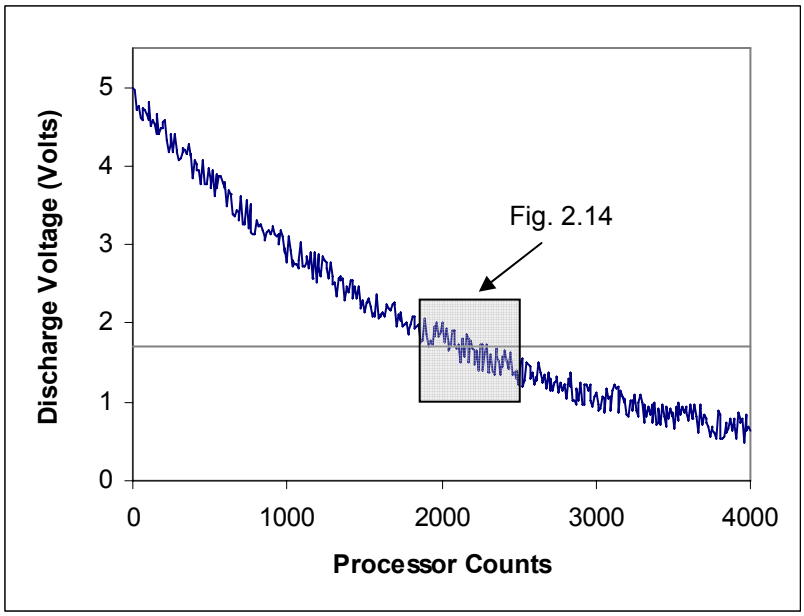

Fig. 2.13 Illustrative example of LED capacitance discharge

An element of noise in the discharging voltage of the detector LED is depicted in the illustrative example of Fig. 2.13. The effect of this noise around the threshold level is highlighted in Fig. 2.14. Here, it can be seen that noise fluctuations do not allow a

distinct point at which the voltage has decreased to a level less than the logic zero threshold to exist. Therefore, at a constant incident light level, there will be variation, i.e., noise, in the output signal of the sensor over successive light measurement periods. However, regardless of the inherent element of noise present in the sensor output, by comparing an obtained measurement value to previous readings it can be determined if the incident light falling on the LED is changing.

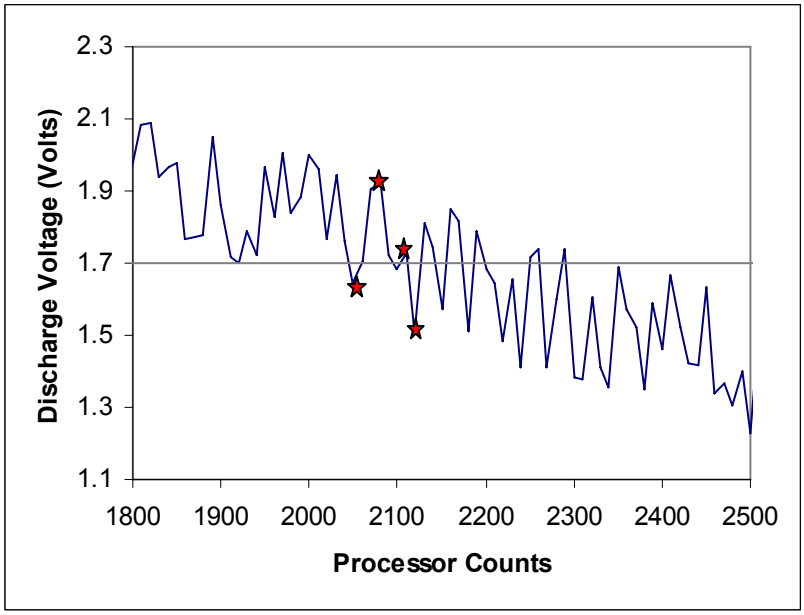

Fig. 2.14 Noise in decay signal around logic zero threshold

2.6.2 Low-cost Optical Chemical Sensors

It is not sufficient to restrict wireless monitoring systems to their current roles when the technology to advance their sensing capabilities is in development. Recent advances in the use of simple electronic components such as LEDs for optical sensing, as outlined in the previous section, provide the ability to cost effectively gather important real-time data with regards to our surrounding environments in a way and at a density that was not possible before.

The construction and operation of chemical sensors using LEDs is being explored, with the ultimate goal of developing low-cost component based chemical sensors that provide analytical performance at a significantly lower cost relative to conventional instrumentation. The initial basis of the sensor platforms currently being developed at DCU came from the development of a system for communication using bidirectional LEDs [113]. On-going research has shown that LEDs can be effectively used in

chemical sensing applications [116, 117]. Additional information, which will be discussed in following paragraphs, highlights the research carried out to date in this area on the construction, sensing regime and implementation of LED based chemical sensors [118, 119]. Much of the research conducted into these devices has led to the wireless chemical sensing device that is examined and implemented as a component of a wireless chemical sensing network within this thesis.

Lau *et al.* constructed a fused-LEDs light sensor, which was used to measure the colour of liquids into which it was immersed [118]. Fabrication of the fused-LEDs sensor's basic structure involved the epoxy encasings of two identical LEDs being shaped and polished so that they could be bonded together using UV curable epoxy glue in a 90° angle, as shown in Fig. 2.15. While based on the light sensing method of Dietz *et al.* [113] the sensing method differed slightly with the inclusion of an "Emitter LED" which provided a constant light source for successive measurements. Light emitted from this LED was reflected onto the "Detecting LED". A change in the colour at the fused-LEDs immersed surface affected the reflected light and so the discharge of the "Detecting LED". A PIC based microcontroller circuit was used to operate the developed sensor and monitor the LED discharge rate over consecutive measurements.

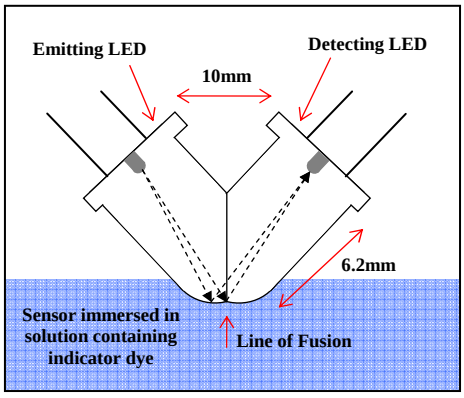

Fig. 2.15 Schematic of fused-LEDs [118]

The device was trialled through immersion in a solution containing an indicator dye. Adjusting the pH value of the solution through addition of acids and alkalis changed the solution colour and thus induced a response change in the sensor output. The findings of Lau *et al.* proposed that the surface of the developed sensor could be modified with a colorimetric reagent to allow the device to operate as a selective chemical sensor.

Shepherd *et al.* [119] expanded on this work through the development of a selective optical chemical sensor with a target chemical species of gas phase ammonia. Similar PIC based control circuitry to that used by Lau *et al.* was used to control the sensor's operation and perform measurements. Unlike the colour change in solution studies of Lau *et al.*, the light transmission path between the emitter (referred to as "Exciter LED"

by Shepherd *et al*.) and detector LED was not inhibited by the medium within which measurements were to be taken. Thus, an alternative and somewhat less complicated sensor arrangement was developed. The simplified sensor configuration used two rectangular, surface-mount LEDs with dimensions of 3.2 x 1.6 mm placed opposite each other, as displayed in Fig. 2.16.

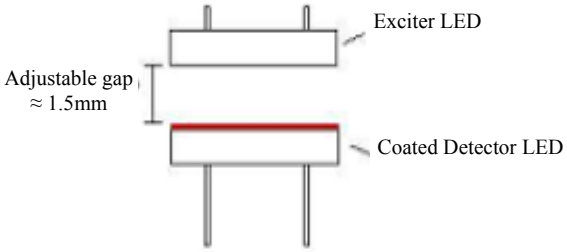

Fig. 2.16 Configuration of LED based ammonia sensor [119]

Chemical selectivity was achieved through addition of a chemically selective reagent coating on the surface of the detector LED, as also indicated in Fig. 2.16. This was achieved by manually applying a small volume of reagent (<5 µl) to the LED surface in a droplet form using a small volume pipette.

Reported trial results stated that the developed LED based chemical sensor provided reproducible results for ammonia detection in the 5 – 15 ppm range with a LOD (limit of detection) of approximately 5 ppm. A response graph resulting from the sensor being repeatedly exposed to the target stimulus over a 35 minute time period, as shown in Fig. 2.17, indicated the characteristic response of the sensing device.

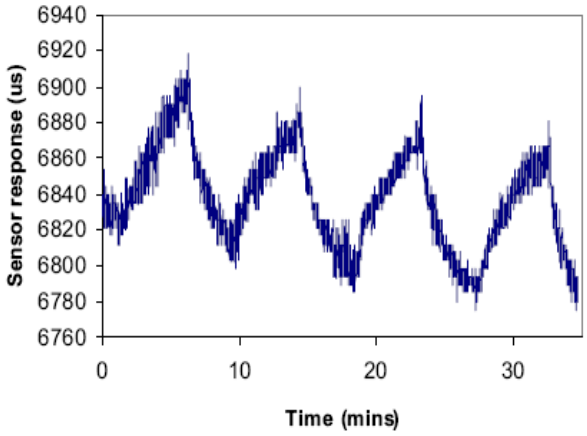

Fig. 2.17 Response of ammonia sensor to repeated chemical stimulus exposures [119]

While response of the sensor to the chemical species can be distinguished in Fig. 2.17, a number of issues arise from this reported sensor output that are important to the further development of a low cost chemical sensor using this configuration.

Firstly, the output signal contains significant noise. It will be essential to examine the factors leading to noise in the output of a low-cost optical chemical sensor. The effect that noise has on the overall signal quality will then have to be accounted for through a

form of signal conditioning. In addition, there is drift in the baseline response of the signal over the 35 minute trial period. If instability such as this is a feature in the developed wireless chemical sensor node, the causes that lead to this effect will have to be identified and addressed. However, the response magnitude to each exposure appears to be similar. This indicates that the sensor can generate reproducible results to common concentration exposures. Finally, the unit of response measure (μs) employed by Shepherd *et al*., which was a conversion related to the discharge rate of the detector LED is not a standard measure of chemical species concentration. So that data retrieved from a wireless chemical sensor can be readily used in determining chemical events in its environment it will be crucial to present data in a standard form.

2.7 Literature Review Conclusions and Research Objectives

In this thesis, a number of areas of research, namely, chemical sensing, electronic engineering, mechanical engineering and communications have been married together in an effort to produce a wireless chemical sensor actuator network. This chapter has highlighted and critically reviewed publications and available commercial technologies in these research areas which have inspired, or impacted upon, the rest of the research described as part of this thesis. Because a major component of the research undertaken here lies in the realm of wireless communications, the initial development of wireless communications from the initial generation of radio waves in the late 19th century to the present age of small low-power mote devices was presented. Following on from this, current and common features from three separate mote manufacturers were also highlighted.

WSN deployments, reported in the literature, were examined to provide an understanding of existing operational issues. The challenges that face researchers in the future development of large scale long-term networks, i.e., communications reliability and power management, were highlighted. Further research and development is necessary in both of these fields, however, this will be outside the scope of this body of work. Published WSN deployments were also studied to show a sample of application areas within which WSNs have, thus far, been employed. It has been shown that these applications are varied and require different approaches for effective data collection and transmission, i.e., long term monitoring systems will operate at relatively low sampling rates, while systems that will be used in control loops or to initiate a reactive response to a changing parameter will require high sampling rates and will need to be able to return data to the system basestation as quickly as possible.

Detection of chemical vapours and measurement of gas concentrations and pH will complement physical sensor data currently being examined by WSN deployments. Conventional sensing methods have been outlined to introduce the need for low cost chemical sensing in large scale network deployments. The impracticalities of deploying large numbers of expensive, high-power sensing systems to perform distributed monitoring has led to investigations into the development of inexpensive, low-cost alternatives. In the literature, a limited number of electrochemical sensors have been integrated with wireless sensing platforms, in the past. However, the use of these devices in collective network deployments or further still in real-time monitoring and

reaction applications has not been reported. Low-power, optical based alternatives to conventional sensing methods are also in development.

The gas phase sensing method developed by Shepherd *et al*. shows great potential for integration into wireless sensor networks, as it requires very little computational and physical power to operate. The advantages of this have been implemented in this thesis as the principles of the sensing method can be maintained when trying to identify other chemical species. However, it is necessary to tune the emitter and the chemically sensitive reagent layer to the chemical species of interest. To date, the author has found no significant research into WCSANs, but is confident that, with validation, the scope of their applications in real world deployments is vast. The desire to develop and successfully validate a WCSAN, which can achieve one of the envisaged applications, i.e., chemical contaminant plume tracking, prompts the statement of the primary objective of this thesis.

The primary objective is thus, the development and subsequent validation of a Wireless Chemical Sensor Actuator Network for the application of chemical contaminant plume tracking. In achieving this primary objective, a number of secondary objectives must be outlined. These are:

- development of a controllable WSN simulation environment,
- development of a stable platform for data acquisition and wireless data communication,
- design of a data acquisition interface to facilitate real time control of a monitored parameter,
- validation of the WSN using a physical sensor measurement, i.e., temperature,
- integration and validation of an optical chemical sensor with the wireless communications platform,
- comparison of the less proven chemical sensing method with established commercially available monitoring technologies.

3 Studies Developing a Wireless Sensor Actuator Network

An Environmental Sensing Chamber (ESC) where parameters of interest for the wireless sensor network trials discussed in this body of work could be varied was developed. For further information on the design, development and control of the constructed test chamber refer to Appendix 1.

Before testing of a chemical sensing network could commence, it was necessary to select a platform on which to test be-spoke sensing devices. A decision was taken to use the Mica2Dot platform because as found during the literature review, publications at the time of the project showed that Crossbow Motes were the industry standard for wireless sensor research [125].

To allow for familiarisation with the device, its communications protocols, power requirements and data acquisition methods, the platform was fitted with a temperature sensor. Preliminary testing was carried out and the results are outlined in this chapter. Inefficiencies in the selected platform's initial operation are also addressed in this chapter so that the platform operates reliably and allows for laboratory scale testing of a network of similarly constructed wireless sensing devices.

Data acquisition software that would allow for real-time processing and display of received data was developed as an alternative to software supplied by the wireless sensing platform's manufacturer. An additional benefit provided by the developed interface was the functionality of PC output control signal generation based on received sensor data in a common interface. This is shown to facilitate the control of parameters during sensor network trials within the ESC. Integration of output control functionality with sensor data acquisition software has paved the way towards a Wireless Sensor Actuator Network (WSAN). Studies are conducted on the operation of the developed system based on the temperature response of a single device in comparison to the collective responses of a network of wireless temperature sensors.

These developmental steps allow for the later integration of an LED based chemical sensor with the wireless sensing platform for the development of a real-time reactive Wireless Chemical Sensor Actuator Network (WCSAN) with event detection and plume monitoring capabilities.

3.1 Mica2Dot Wireless Temperature Sensor

This section examines the development of a wireless temperature sensor for preliminary testing of the Mica2Dot sensing platform.

The MPR500 Mica2Dot mote, from Crossbow with a transceiver radio operating at 868 MHz was used as the sensing and wireless communications platform. The interface between the component based sensors and the Mica2Dot mote was a MTS510A prototyping board connected to the mote via the 18-pin expansion connector. It would have been possible to use the temperature sensor that is incorporated on the Mica2Dot mote, however, the fabrication and testing of a separate sensor mounted on a prototyping board allowed for sensors developed later in the research to be interchangeable using the same board interface and arrangement.

The Mica2Dot mote used was modified because of initial concerns with regards to the suitability of the standard power supply. The modified sensing platform used in the following sections to monitor varying temperatures within the ESC is presented in Fig. 3.1.

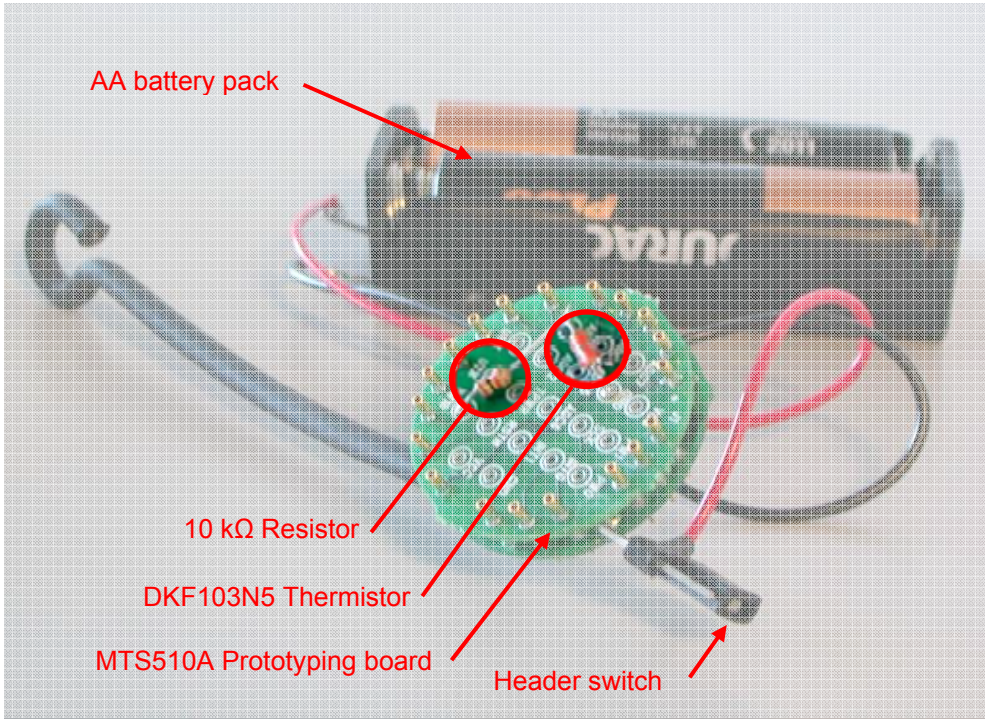

Fig. 3.1 Modified Mica2Dot mote equipped with thermistor sensor board

The Mica2Dot and Mica2 mote wireless communications platforms share many common components, such as the main processor (Atmel ATmega 128L) and radio chip (Chipcon CC1000). The Mica2 device was supplied with a standard battery pack (2 x AA), yet the Mica2Dot device was supplied with a coin cell battery clip. The capacity of the recommended coin cell battery was approximately 33 % that of two standard AA batteries.

Published research examined and discussed in Chapter 2 of this thesis has shown that energy consumption levels can have limitations on the effectiveness of deployed networks, and was especially evident in the research of Beckwith *et al*. [9]. For this reason, the device was adapted by replacing the coin cell battery pack with an AA battery pack as a simple means of increasing the power supply capacity.

The Mica2Dot mote was programmed in TinyOS, a component-based event driven operating system designed for memory constrained wireless sensor platforms. Code was written in nesC, a C-based component language used to develop TinyOS applications. In general, the sensing routine of the platforms involves the sampling of specified input channels at set time intervals. Analogue sensed values are converted into a two-byte digital representation and placed within a structured data packet. Once a packet is completed, the program routine instructs that the sensed information, as well as information relating to the identity of the particular sensing device and the destination device, be sent to the transceiver radio for transmission to a basestation.

The packet structure employed by Crossbow motes is the standard type used in TinyOS, with a data payload of 26 bytes. The payload includes the mote ID (2 bytes), packet count (2 bytes), ADC channel (2 bytes) and 10 x ADC values (20 bytes) in what is known as Little Endian format, with the least-significant-byte (LSB) followed by the most-significant-byte (MSB). In addition to the data payload, a series of header bytes are incorporated in each packet. These include the destination address of the receiving basestation and the length of the payload data being sent. An example of a typical series of received packets of information is shown in Fig. 3.2. Table 3.1 shows the second data packet from Fig. 3.2 separated into the information segments that it represents.

```
7e 00 0a 7d 1a 01 00 13 00 01 00 94 03 94 03 95 03 94 03 94 03 95 03 97 03 96 03 95 03 96 03
7e 00 0a 7d 1a 01 00 14 00 01 00 96 03 97 03 97 03 98 03 97 03 96 03 97 03 96 03 96 03 96 03
7e 00 0a 7d 1a 01 00 15 00 01 00 95 03 95 03 94 03 95 03 94 03 96 03 97 03 97 03 98 03 98 03
```

Fig. 3.2 Series of incoming data packets

				Payload							
Destination Address	Active Message Handler ID	Group ID	Message Length	Source Mote ID	Sample Counter	ADC Channel	ADC Data Readings				
7e 00	0a	7d	1a	01 00	14 00	01 00	96 03	97 03	97 03	98 03	97 03
							96 03	97 03	96 03	96 03	96 03

Table 3.1 Standard mote data packet

3.1.1 Thermistor Sensor

Monitoring of a well known physical parameter such as temperature validated the operation of a network of similar devices before the later introduction of a less established component optical chemical sensor, in Chapter 4.

A physical temperature sensor specified to have ±5 % accuracy (10 kΩ thermistor manufactured by Thermometrics) and a thermal time constant of 7 s [126], was incorporated onto the sensing platform using a potential divider circuit, as displayed in Fig. 3.3. The thermistor in this case was a Negative Thermal Coefficient (NTC) type. This means that, as the surrounding temperature increases the component's resistance decreases. The fixed component in the potential divider circuit was a 10 kΩ resistor, (Radionics no, 135-910) also manufactured to a tolerance of ±5 %. The output voltage, with reference to the voltage applied to the potential divider, was proportional to the temperature surrounding the

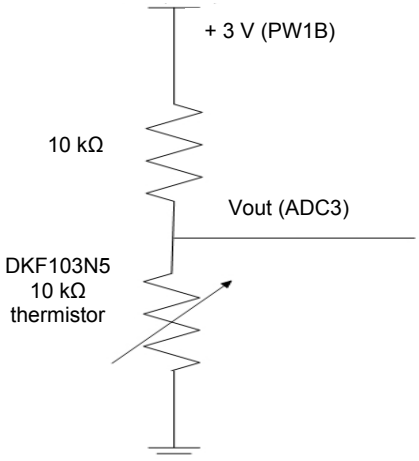

Fig. 3.3 Thermistor arrangement

thermistor. The circuit was constructed on the MTS510A prototyping board supplied by Crossbow, and then stacked on top of a Mica2Dot mote, as shown earlier in Fig. 3.1.

The conversion equation to calculate the actual thermistor temperature as a function of the thermistor resistance provided by Thermometrics is shown in Equation 3.1 [127]. This equation is known as the Steinhart-Hart calibration equation for thermistors. Thermometrics have provided constants for the variables, "a", "b", "c" and "d", to be used within specified operating temperature ranges. Of the temperature range variables supplied, the range most applicable to this application was -40 °C to 155 °C. The conversion constants provided for this range are shown in Table 3.2.

$$\frac{1}{T} = a + b\left(Ln\left(\frac{R_T}{R_{25}}\right)\right) + c\left(Ln\left(\frac{R_T}{R_{25}}\right)\right)^2 + d\left(Ln\left(\frac{R_T}{R_{25}}\right)\right)^3 \qquad (3.1)$$

a	b	c	d
3.3539908E-03	2.5788772E-04	2.5364809E-06	5.3216393E-08

Table 3.2 Thermistor conversion constants

In Equation 3.1, R_{25} is the nominal resistance of the thermistor at 25 °C and was stated as having a value of 10 kΩ [126]. R_T, the resistance of the thermistor relative to the temperature of its surroundings was determined from the digital representation of voltage at the sensing ADC (Analogue to Digital Converter) channel.

The particular ADC in use on the Mica2Dot mote has a 10-bit resolution [45]. There were, therefore, 1024 (2^{10}) possible output values from the ADC. The voltage represented by each ADC unit, with a voltage of 3 V (V_{IN}) applied to the potential divider, equalled 2.9296875 mV. An ADC value, multiplied by the milli-volt value per ADC division and then divided by 1000 gave the original voltage level, V_{ADC}, applied to the ADC pin, as shown in Equation 3.2. The obtained voltage value, along with the resistance of the fixed resistor, R, and the voltage applied to the potential divider, was then used to calculate the resistance of the thermistor, R_T, as shown in Equation 3.3. An example of the conversion for an ADC reading of 550 is provided in Appendix 3.

$$V_{ADC} = \frac{ADC \times 2.9296875}{1000} \tag{3.2}$$

$$R_T = \left(\frac{R}{V_{IN}} \times V_{ADC} \right) \Big/ \left(1 - \frac{V_{ADC}}{V_{IN}} \right) \tag{3.3}$$

3.1.2 Temperature Sensing Routine and Operation Concerns

When the Mica2Dot node was active, the sensing circuit was driven from a digital output line on the mote processor, PW1B, giving a 3 V supply. The output of the potential divider was interfaced to an input channel, ADC3, of the motes onboard ADC. To take a temperature measurement, the 3 V supply was activated and the ADC pin then sampled. The value was recorded and the 3 V supply turned off. This meant that the supply to the potential divider was only active for the very short time while a temperature measurement was being taken. The 10-bit ADC converted the voltage applied to channel 3 to a 2-byte hexadecimal digital representation of that voltage. The digital value was packaged in the standard format along with nine other measurements and transmitted to the system basestation so that temperature conversion could be performed on the host PC. It would have been possible to perform the temperature conversion onboard; however, this was considered to be a waste of limited energy resources through unnecessary processor usage.

For initial testing of the temperature sensor a sample rate of 1 Hz was used. This would result in a completed standard packet of ten data readings being transmitted to the basestation once every ten seconds. While this would be suitable in a purely temperature monitoring role, it would not be sufficient in this application of real-time control as the only real-time data value within the packet would be the last temperature measurement, with the first temperature measurement within the packet being ten seconds “out of date”. It was, therefore, considered necessary to receive an updated temperature value once per second. The conventional packet structure of the Mica2Dot mote determined that to achieve this the ADC channel would need to be sampled at a frequency of 10 Hz so that a completed packet would be received once every second. By operating the mote in this manner only one of the ADC values would require conversion to its corresponding temperature value. This raised concerns as to the effective use of the device. To achieve the required data acquisition rate it would be necessary to use the device in an inefficient manner.

The management of the sensing routine and the resultant power consumption was analysed based on the premise of having a wireless sensing platform that would be suitable for laboratory scale testing routines. It was, therefore, deemed necessary to have a device which could operate for a continuous period in excess of 1 week. It is noted that the concept of wireless sensor networks require that deployed nodes should operate for a significantly longer time. However, this body of work focuses on the sensing mechanism and resultant plume tracking and source identification capabilities of a wireless chemical sensor network. As highlighted in the literature review, Section 2.3.2, long term power management is a broader issue in WSN research. The following section presents the implementation of a power management scheme suitable for the research objectives for this thesis.

3.2 Node Power Management

The effectiveness of a wireless sensor is not solely dependent on the accuracy of its measured values. Other factors influence the use of a wireless sensor in a practical application. The most important of these factors is the device's rate of power consumption, which is directly related to the routines that are executed in the process of collecting and transmitting data. A wireless sensor that requires regular preventative maintenance, such as battery change, is not a viable consumer product or test device, because of the recurring expense of technical labour and consumables, i.e., batteries. The operating monetary costs of the device are minimised by managing its power requirement, while maintaining a suitable sensing resolution. Research has shown that wireless sensing technology will only be employed where absolutely necessary or when its installation and operating costs are competitive with an alternative wired option [3].

This section highlights the excessive power consumption rate of the initial node operating program. The structure of the data packet generated by the operating program is modified to eliminate the transmission of data that are discarded upon reception at the basestation. Two ADC values, battery voltage level, and thermistor temperature level, are sampled at a frequency of 1 Hz. In the period where sample measurements are not being taken or transmitted, the node is instructed to enter a "sleep" mode to conserve the power source. The current consumption of the revised operating program is compared to the consumption rate of the initial operating program. A node lifetime prediction is made based on the revised current consumption rate and confirmed through a node longevity trial.

3.2.1 Identified Inefficiencies and Resultant Modifications to Sensor Node

In the case of the temperature sensing platform developed as part of this research the initial operation lifespan was found to be of the order of 48 hrs. While sufficient for short term trial studies, this was inadequate for prolonged laboratory testing applications. To reduce the power consumption of the unit and, in turn, increase the operational lifetime, inefficiencies in the sensing and communication program code have been isolated and improved upon. The specific sensing requirements were defined and implemented such that the available power source was used in a more efficient manner.

To achieve the desired temperature sensing rate of 1 Hz, the standard data packet arrangement dictated that the thermistor sensor was sampled at a frequency of 10 Hz. This would have resulted in data transmitted to the host PC being discarded. The data packet structure was modified so that it would accommodate a single 2 byte hexadecimal temperature value.

With the objective of improving the lifetime of the power supply it was critical to know the actual voltage level of the device's battery power source. The battery voltage level affects the operation of the device as it is this voltage (V_{batt}) that determines the full scale reference level for the 10-bit ADC such that V_{batt} is equal to 1024 ADC divisions (ADC_FS). As the battery level decreases during the operational lifespan of the device the voltage level corresponding to each ADC division also decreases. This, in turn, would affect any measurements taken by sampling the thermistor connected to the ADC.

The device manufacturers have accounted for this effect of decreasing voltage of the power supply within the operating circuitry. A Schottky reference diode, acting as an external reference point, allows for the calculation of the power source voltage so that the micro-controller can compensate for power supply changes during operation. The diode is connected to channel 1 of the ADC, providing a constant and stable 0.6 V reference level (V_{ref}). By sampling channel 1, an ADC value (ADC_count) corresponding to 0.6 V was obtained and included in each transmitted data packet. This voltage reference to a specific point on the ADC scale was used to calculate the battery voltage using Equation 3.4 [45].

$$V_{batt} = V_{ref} \times \left(\frac{ADC\_FS}{ADC\_count} \right) \tag{3.4}$$

Revising the packet payload so that it consisted of only 2 ADC values, one corresponding to a thermistor temperature measurement and the other to the battery voltage level reduced the size of each transmitted packet data payload from 26 bytes to 10 bytes. This marginally reduced the time taken to transmit data packets and in turn the energy required to do so. The minimised packet structure also reduced the possibility of data packet collisions when using a number of sensing devices, reducing the possibility of loss or corruption of data at the basestation.

Alternative data acquisition software was necessary to process data packets that did not conform to the Crossbow standard. The developed data acquisition interface will be discussed further in Section 3.4

The basic TinyOS firmware for the Mica2Dot mote, operated in a way which the ATMega128L processor was in continuous operation and power to the transceiver radio was constantly on. The reason for this is to facilitate the "hopping" of data packets between nodes in deployed networks. This allows nodes outside of direct communications range with the basestation to report their sensor measurements by transferring data to a node located in closer proximity to the basestation. Although, this is the simplest "listening" method employed by these devices it should be noted that there are more complex listening modes that consume less power.

There was no necessity for a "multi-hop" function in this particular sensing application as sensor nodes would always be within communications range of the network basestation. It was, therefore, unnecessary to implement a listening function on sensor nodes.

The device was only required to take and transmit two ADC measurements per second. The actual time required for the device to perform this function was much less than this, therefore, having the device in an operational state while it was not sampling or transmitting was an inefficient use of the power resource. The mote operating program was modified to incorporate a "sleep" function that allowed the device to "wake" once per second, perform its sensing routine, transmit the collected data and then return to "sleep".

The benefit of instructing the device to enter the sleep mode was that each of the device's components required much less power. Implementation of a "sleep" mode for the majority of the device's sensing duty cycle increased the node's operating lifespan by reducing the energy being consumed.

3.2.2 Evaluation of Initial and Modified Device Energy Consumption

With the improvements in payload size and duty cycle implemented, the current consumption of the wireless temperature sensor was analysed and compared to that of the initial sensing routine. Two Mica2Dot devices were programmed, one with the

initial operating code and the other with the revised code. Both were individually connected to an electrochemical analyser (CHI630B) manufactured by CH Instruments [128]. A potentiostat incorporated with this piece of equipment allowed for measurement of the current drawn by the devices while in operation, with accuracy of the order of tens of picoamperes.

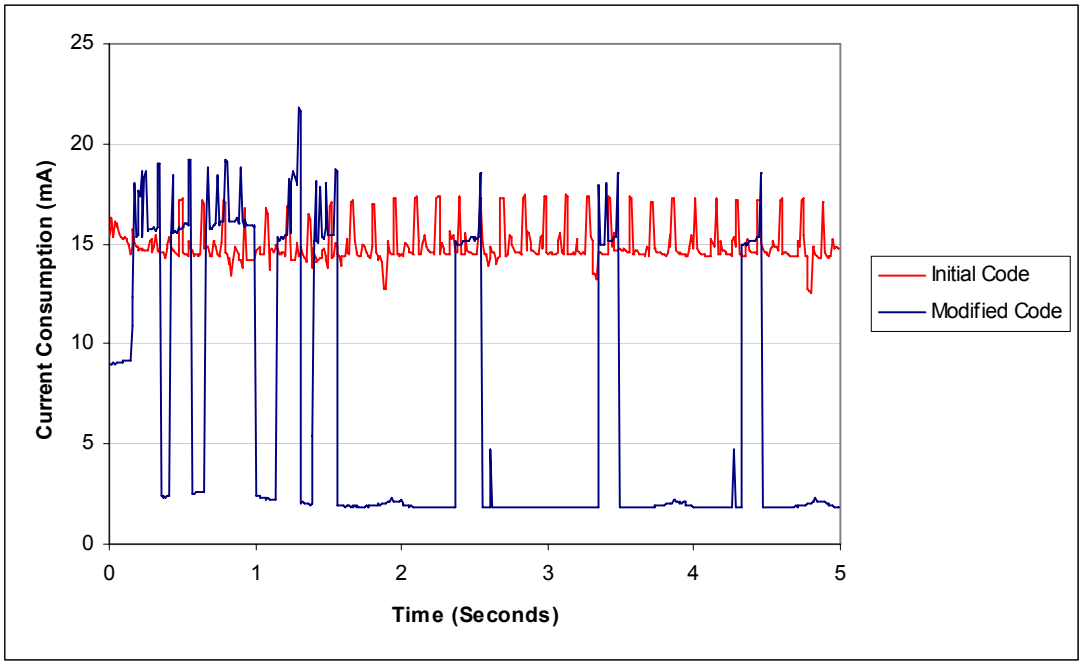

Fig. 3.4 Current consumption of initial and modified temperature sensing code

The results shown in Fig. 3.4 indicate significant differences in the energy usage of the two operating programs. The average current draw required by the initial sensing program of 15.04 mA, was much greater than that of the revised temperature sensing operating program. After the initial start up period of the revised sensing routine (approximately 1.5 s), it was observed that the current consumption level dropped to a value of 2 mA. This value was maintained for the majority of the operating duty cycle. Sharp increases in the current consumption were observed at intervals of 1 s, where the device's processor and transceiver radio had been powered up to perform the program's measurement and data transmission routine.

The data were subsequently analysed over a period of 1 s, the duty cycle of the modified temperature sensing code, and shown in Fig. 3.5. A summary of the measured current consumption levels is presented in Table 3.3. The modified operating code resulted in the wireless temperature sensing node being in "sleep" mode for 85 % of the operating

duty cycle. The remaining 150 ms of the duty cycle was dedicated to powering up the device, performing the measurements and transmitting the collected data, as shown in Fig. 3.6.

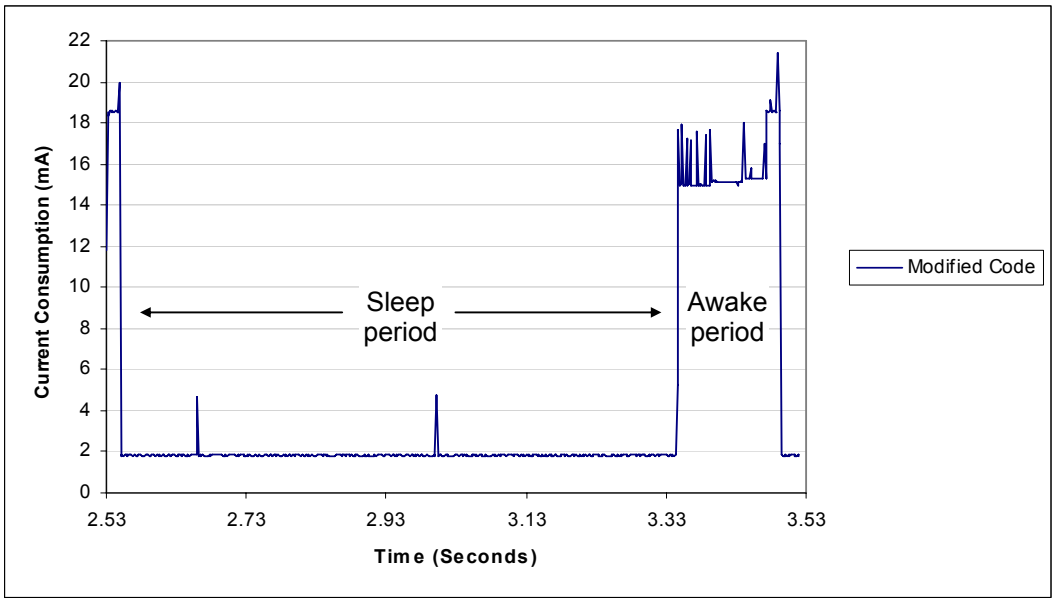

Fig. 3.5 Current consumption over 1 s duty cycle

Properties	Initial Code	Modified Code
Average Current Draw (mA)	15.04	4.05
Maximum Current Draw (mA)	17.43	21.81
Minimum Current Draw (mA)	12.81	1.79
Processor sleep time (%)	n/a	85

Table 3.3 Current consumption rates

While in the "awake" state, there were two distinct periods of current draw activity, as seen in Fig. 3.6. The first period (12.5 % of the duty cycle) was dedicated to microcontroller power up and sensor measurement. The average current draw over this time was approximately 15 mA. The second period (2.5 % of the duty cycle) saw an increase in current draw, peaking at 21.8 mA, where the data packet was transmitted.

It would have been possible to marginally reduce this current spike by reducing the transmission power of the radio. This would further conserve the power supply and increase node operating lifespan but was not implemented because a medium radio

power setting allowed for versatility in basestation positioning with reference to the ESC location during laboratory testing.

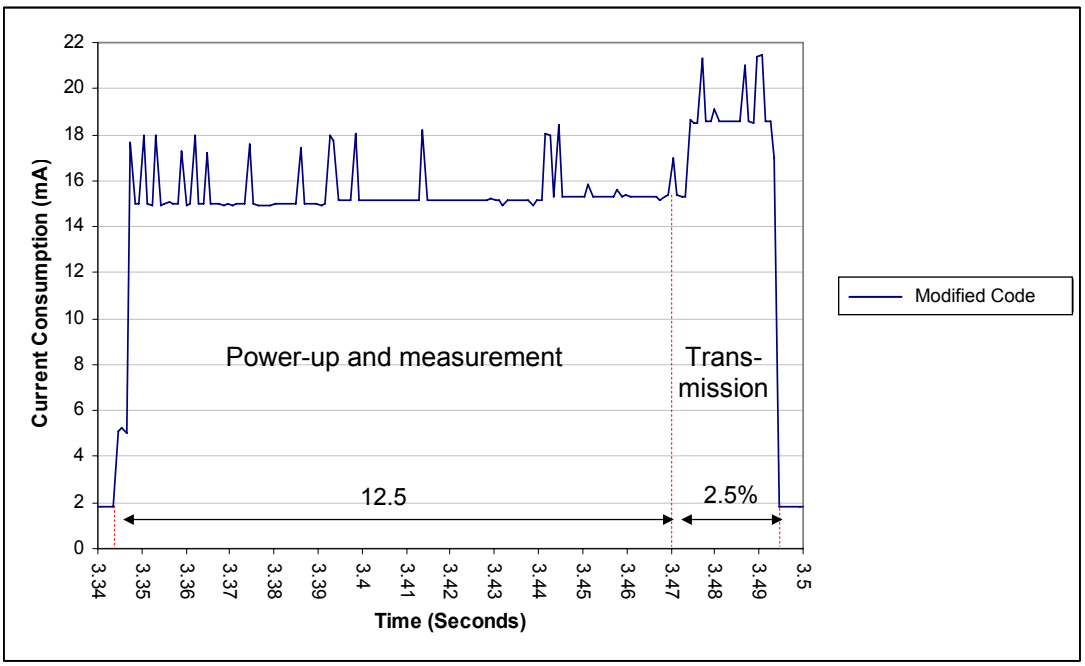

Fig. 3.6 Current consumption during active mode of revised sensing program

The average current consumption over the 1 s duty cycle was calculated as 4.05 mA. This value was used to predict the operating lifespan from a power source using Equation 3.5. The power source used during testing was two Duracell Plus AA batteries [32]. The 2600 mAh capacity of these batteries results in a predicted node operating lifespan of 26.75 days. Increasing the duty cycle to a practical room or environmental monitoring level of one sample measurement every 5 minutes results in an increased predicted lifespan of 53.99 days.

$$Lifespan(Days) = \left(\frac{Battery\_Capacity}{Calculated\_Current}\right) \times \left(\frac{1}{24}\right) \tag{3.5}$$

The underlying limiting factor in the lifespan predictions is the high current draw of 2 mA while in "sleep" mode. Reducing this value further would greatly increase the node operating lifespan, by decreasing the average current consumption of the node and using the available power supply more efficiently. As will be shown in the subsequent node operating longevity trial, further reduction of power consumption was not necessary for

this particular laboratory based wireless sensor testing platform, but would be essential in a real-world deployment.

A trial was conducted to confirm the predicted operating lifespan of the temperature sensing node. Examination of the manufacturer's datasheet provided the minimum supply voltage needed to operate the device (2.7 V), which is the minimum voltage requirement of the ATMega128L processor [45]. Other components on the platform, such as the radio, can operate at a lower voltage level of 2.1 V. New batteries were installed and the device was allowed to operate continuously with a 1 s duty cycle. The decay in voltage level was recorded over the testing period and is presented in Fig. 3.7. The expected shut down voltage of 2.7 V was reached after a period of 6 days. The device continued to operate below this level.

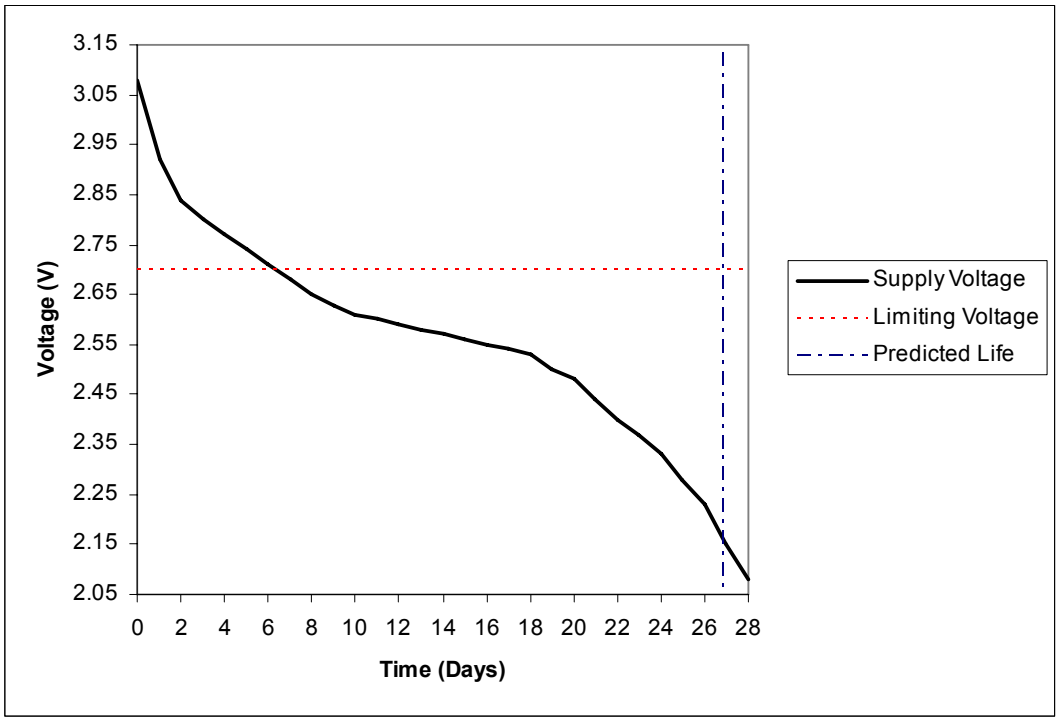

Fig. 3.7 Voltage decay over node operating lifespan

The device operated without interruption for 28 days, comparing well with the predicted operating lifespan of 26.75 days. The final transmitted node voltage measurement was 2.08 V and does not correlate with the minimum operating voltage of the ATMega128L microcontroller of 2.7 V. It is likely that the voltage measurement taken by the device was distorted because the power supply was under load during the brief period of node

activity. The voltage measurement was, therefore, considered unreliable and only used as an indication of battery power.

Node longevity is of major concern in long-term deployments. However, the node operating lifespan that has been acquired by implementation of a range of energy saving methods, including programming of a sleep function, was found to be more than adequate for the laboratory based wireless chemical sensor network studies under investigation in this body of work.

3.3 Thermistor Validation

The accuracy of the thermistor sensor operating on a Mica2Dot wireless platform was examined. Measured sensor values were compared against those of a known temperature measuring device to determine whether or not the thermistor sensor was working within its defined tolerance values. If necessary, calibration or adjustment of the sensor would be carried out. A t-type welded tip thermocouple (range -270 ºC to 400 ºC) was used during the validation process.

3.3.1 T-type Thermocouple Validation

To confirm the correct operation of the thermocouple used in this validation test, its temperature response was checked against two controlled temperature points, that of boiling water (100 °C) and ice water (0 °C). The thermocouple was connected to a Pico TC-08 8 channel thermocouple data logger, as shown in Fig. 3.8.

Fig. 3.8 Welded tip t-type thermocouple and TC-08 data logger

The temperature data taken at 1 s intervals was transferred from the data logger to PicoLog data acquisition software operating on a laptop PC over a standard RS232 connection. To obtain the response for the first temperature point, the thermocouple was positioned so that it was located in the centre of a volume of boiling water. To get the second point, the thermocouple was placed into a Pyrex™ measuring jug with a volume of ice water which was continually stirred. The accuracy limits of the TC-08 unit are given by the sum of ±0.3 % of the measured value ±0.5 °C [129]. For operation within this specification, the measured temperature of boiling water would be 100 ±0.8 °C and, similarly, for ice water the measured temperature would be 0 ±0.5 °C. The

respective recorded temperature values of 99.29 ºC and -0.15 ºC fall within these specification limits, verifying correct operation of the thermocouple as seen in Fig. 3.9.

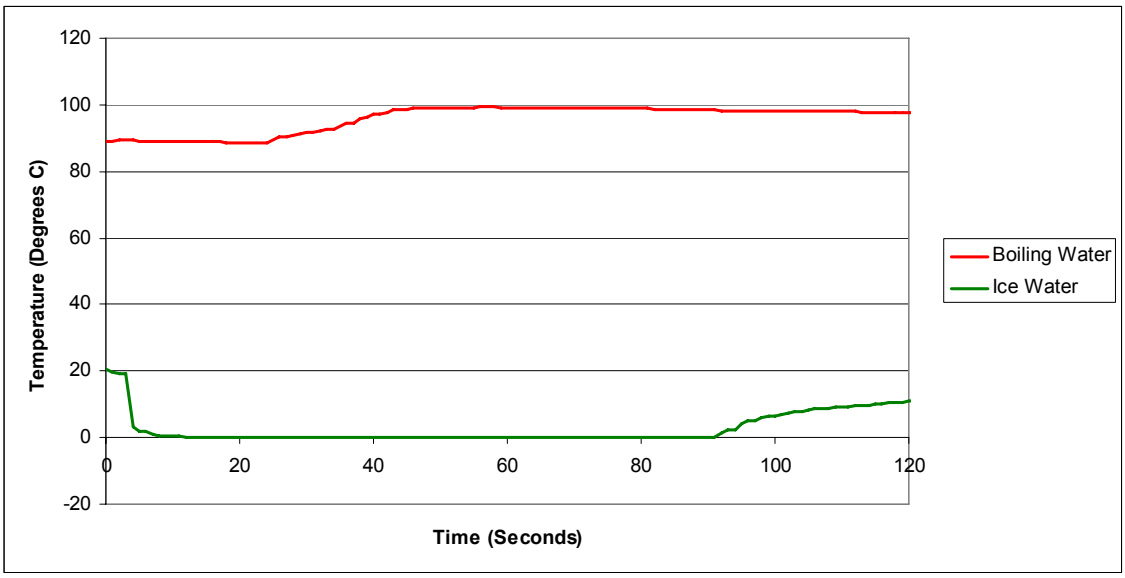

Fig. 3.9 Temperature response of t-type thermocouple

3.3.2 Comparison of Thermistor Sensor against Thermocouple Reference

The thermocouple was placed beside the thermistor equipped sensing node at the outlet port of the chamber, as shown in the cross-sectional representation, Fig. 3.10. The devices were positioned so that the tip of the thermocouple was in close proximity to the thermistor, approximately 2 mm apart from each other. The orientation of the devices was checked so that they were both unobstructed and facing the heat source.

Before the test commenced, the temperature sensors were allowed to stabilise for a period after positioning in the chamber's outlet had taken place. Logging of the incoming data began when both devices had reached a steady state. Updated temperature values were received from the two devices at a frequency of one temperature measurement per second. After a period of 100 s the heat source was activated. The test was run in total for 1200 s, and the resultant temperature responses are shown in Fig. 3.11.

It can be clearly seen that there was a difference in the two recorded data sets. The temperature logged from the thermocouple always exceeded the temperature recorded from the thermistor at the corresponding time interval. The initial temperature

difference between the two devices was approximately 2 °C. A similar temperature difference was maintained over the test period.

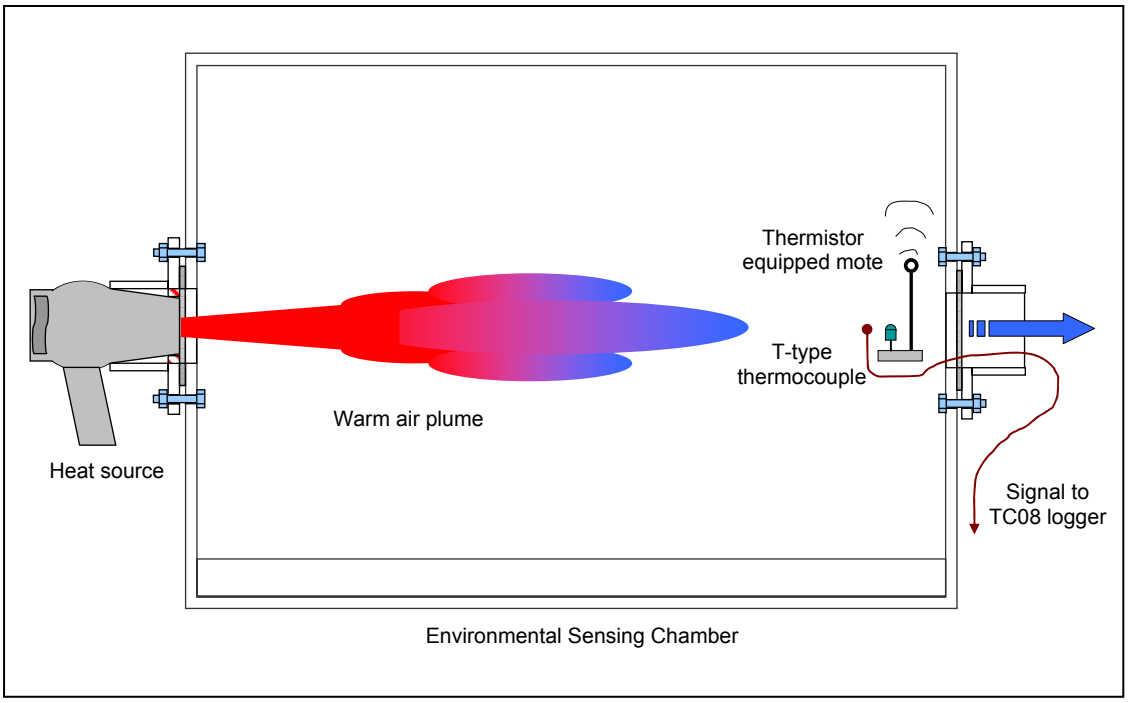

Fig. 3.10 Temperature comparison arrangement

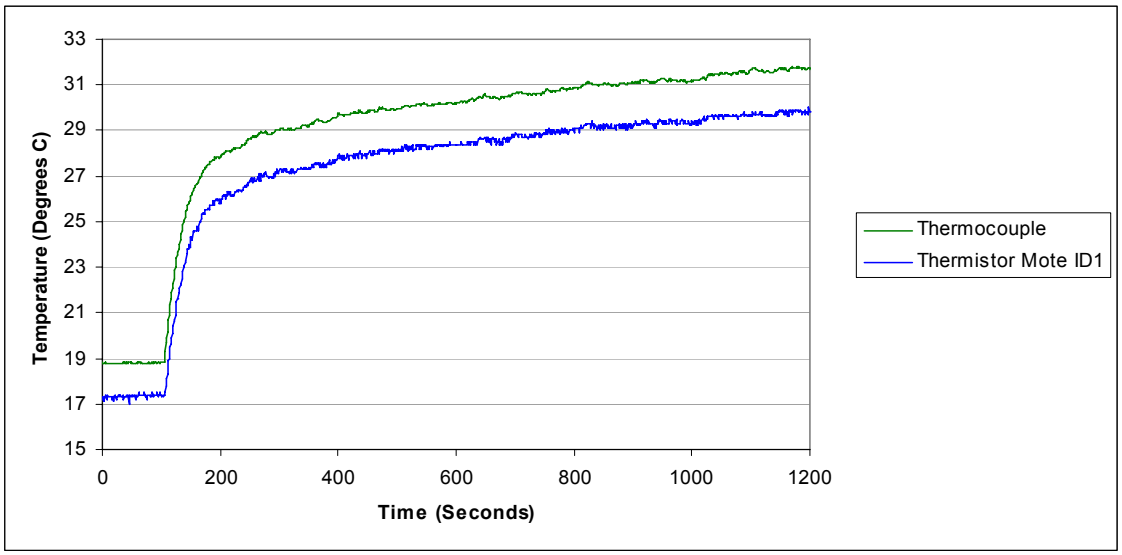

Fig. 3.11 Thermocouple and thermistor sensor responses to heat source over 1200 s

The appropriate error limits for both devices were applied to the collected data. Data including the error limits, over the time interval between 50 s and 300 s of the test is

displayed in Fig. 3.12. The red line shows the lower error limit of the thermocouple. The thick blue line indicates the positive error limit of the thermistor sensor of 5 %.

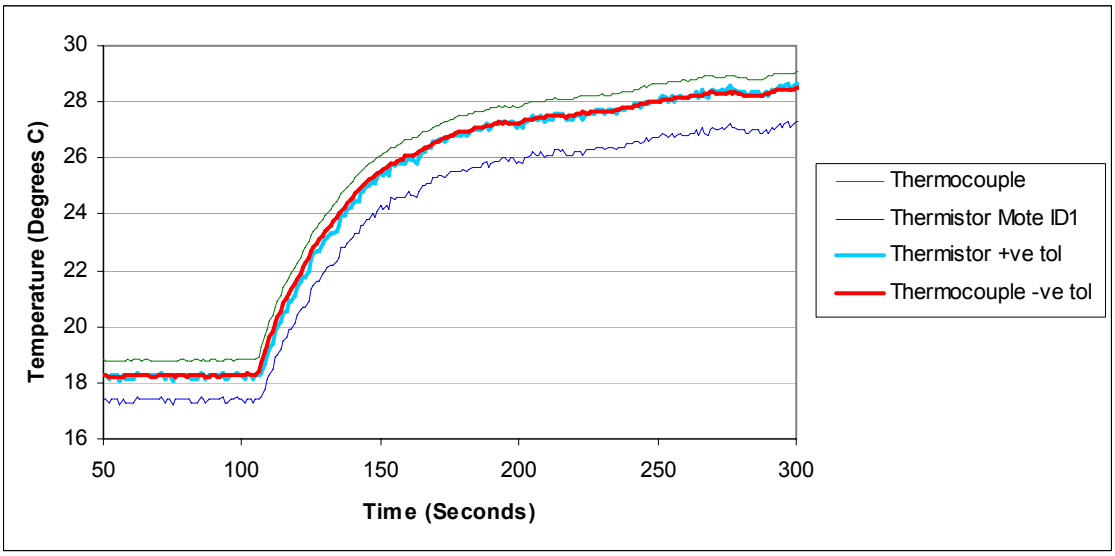

Fig. 3.12 Temperature responses including device error limits

The devices appear to have operated on the thresholds of their tolerance limits. To account for the offset present in the thermistor sensors response, and to facilitate continuity between additional wireless temperature sensor nodes, the response of this sensor was normalised against that of the thermocouple. This required the inclusion of an additional component, added to received temperature values after conversion from hexadecimal ADC data.

As temperature was not the critical target parameter of this research, a simple two point normalisation equation was generated based on the percentage difference in temperature observed between the thermistor sensor and the thermocouple at the start and finish of the comparison test. The equation of this linear approximation (displayed in Fig. 3.13) describes a percentage part of the incoming temperature value (T_I) to be added to itself so that the resultant normalised temperature value (T_N) is comparable to the value recorded by the thermocouple. The normalisation equation is presented as Equation 3.6. Further simplification (Equation 3.7) yielded an equation which was easily incorporated into a routine for data packet processing associated with this node on the host PC.

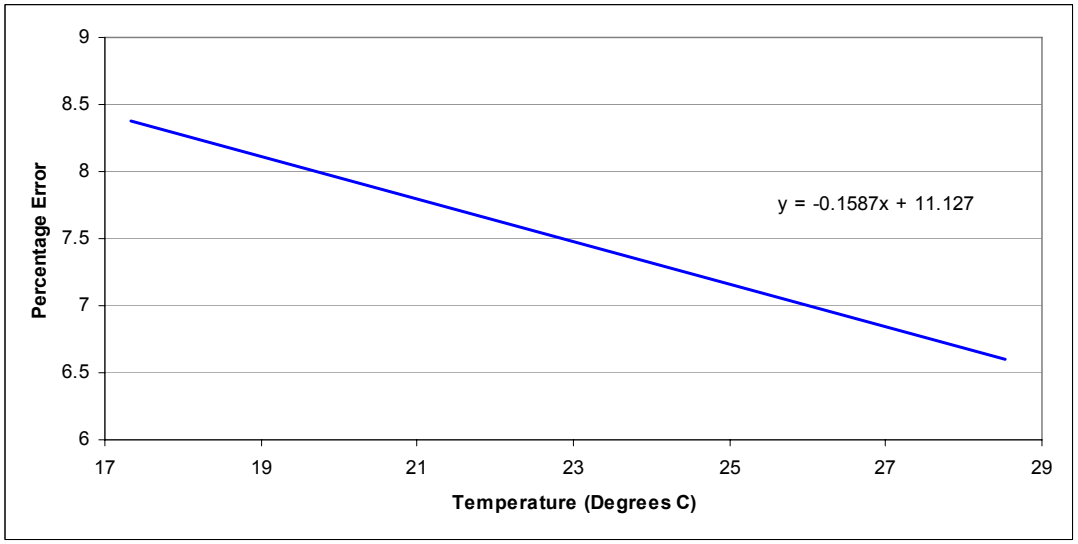

Fig. 3.13 Linear percentage error with corresponding line equation

$$T_N = T_I + \left(\left((-0.1587 \times T_I) + 11.127 \right) \times \frac{T_I}{100} \right) \tag{3.6}$$

$$T_N = 1.11127 T_I - 0.001587 T_I^2 \tag{3.7}$$

Equation 3.7 was applied to the thermistor temperature data set and plotted along with the original thermistor and thermocouple values. A shorter time set of the data, 400 seconds, has been presented in Fig. 3.14 to show the close correlation between the normalised thermistor values and the thermocouple values.

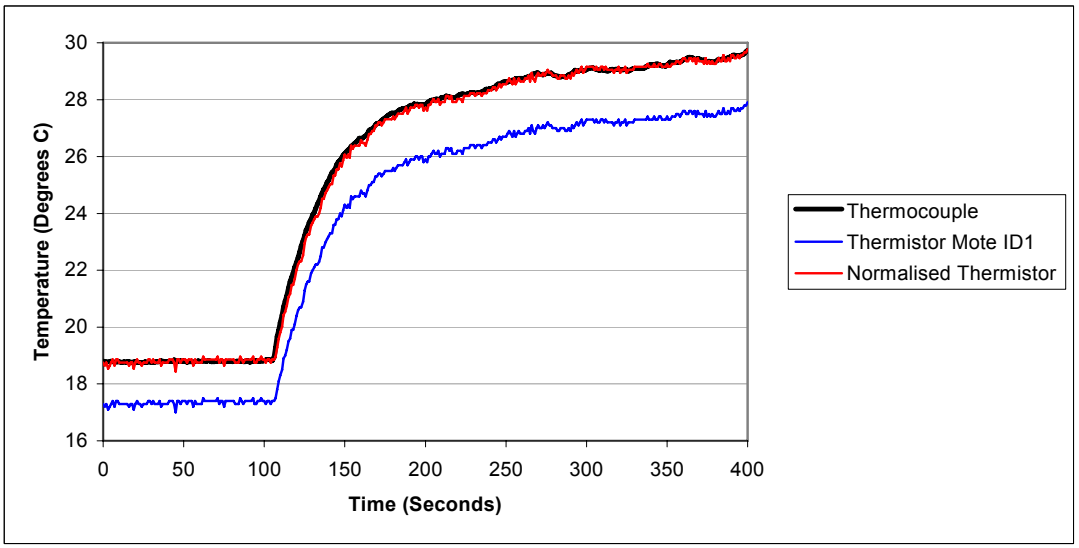

Fig. 3.14 Normalised thermistor values

3.3.3 Comparison of Multiple Temperature Sensor Nodes

The operations of two additional temperature sensing nodes, assigned mote IDs of 2 and 3 respectively, and the existing sensor were examined by placing them in close proximity with the validated thermocouple and observing their response to a stable temperature environment. The normalisation equation was not applied to the existing temperature sensing node. Temperature data was collected concurrently from the devices for a period of 1000 s. Analysis of this data, as seen in Fig. 3.15, showed that there was a large error between the temperatures recorded by individual sensors.

Alternating the prototyping sensor boards between the mote platforms and repeating the same test would identify whether or not the error between the thermistor sensors and the thermocouple was due in part to the mote devices themselves. It would also identify if the sensing inaccuracies were consistent across each of the mote platforms.

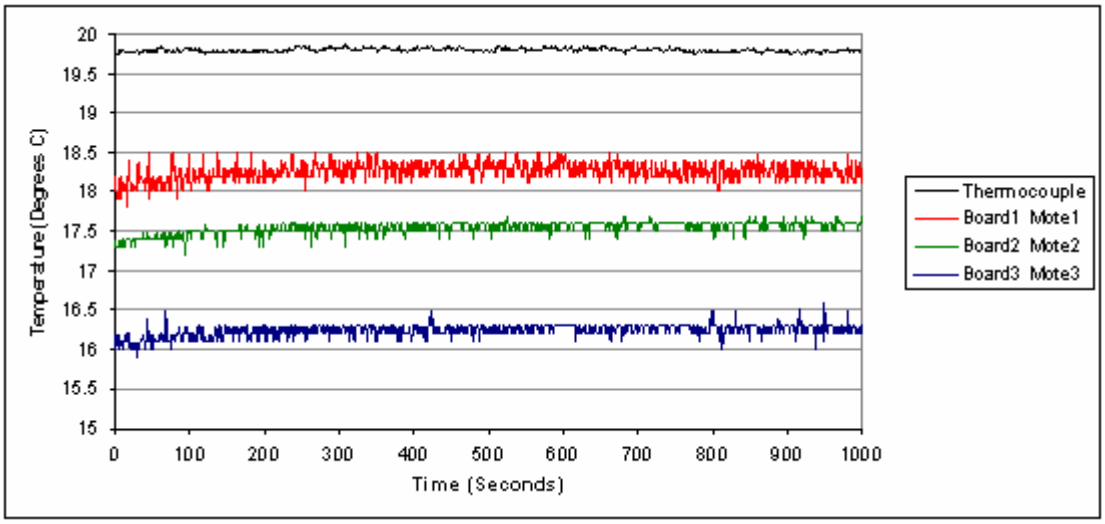

Fig. 3.15 Sensor board rotation study 1

The results obtained for the two additional studies that were conducted are shown in Fig. 3.16 and Fig. 3.17 respectively. The series of studies indicated that most of the error resulted from the individual sensor boards. This can be seen where the mote on which Board 3 was placed (indicated in each of the data graphs by the blue line), consistently recorded the lowest temperatures.

Comparison of Board 1 and Board 2 indicates that the error value for each of the boards when operating on different motes was not constant. The observed error was, therefore,

a result of the combined tolerance errors of the electronic components used in the wireless platforms and the potential divider thermistor sensor arrangement.

This was a very important consideration when moving to a wireless chemical sensor network. It can not be guaranteed that the properties of sensor platforms and the component based sensors would be consistent between each fabricated sensing node. Therefore, calibration of each produced device to determine measured chemical concentrations would be necessary.

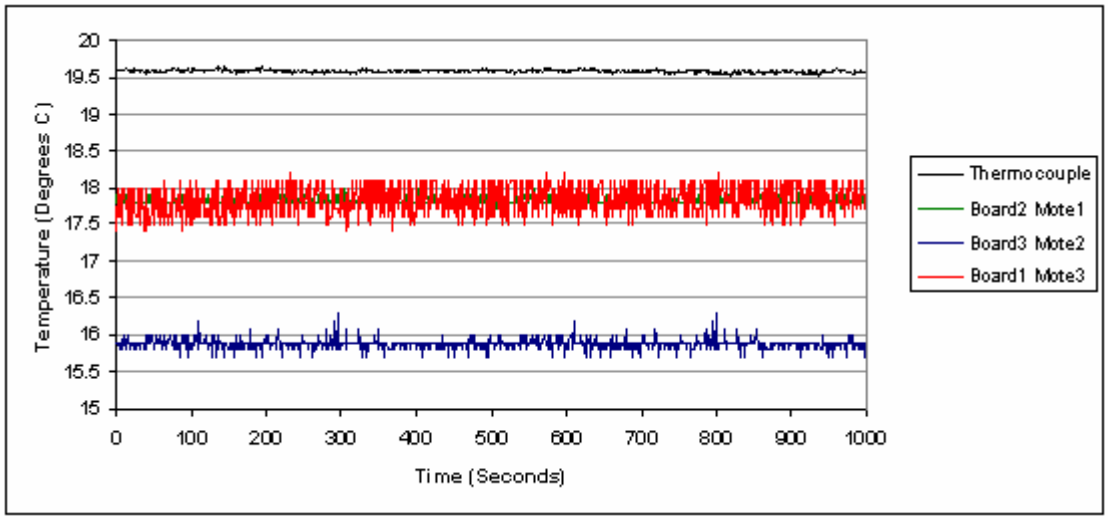

Fig. 3.16 Sensor board rotation study 2

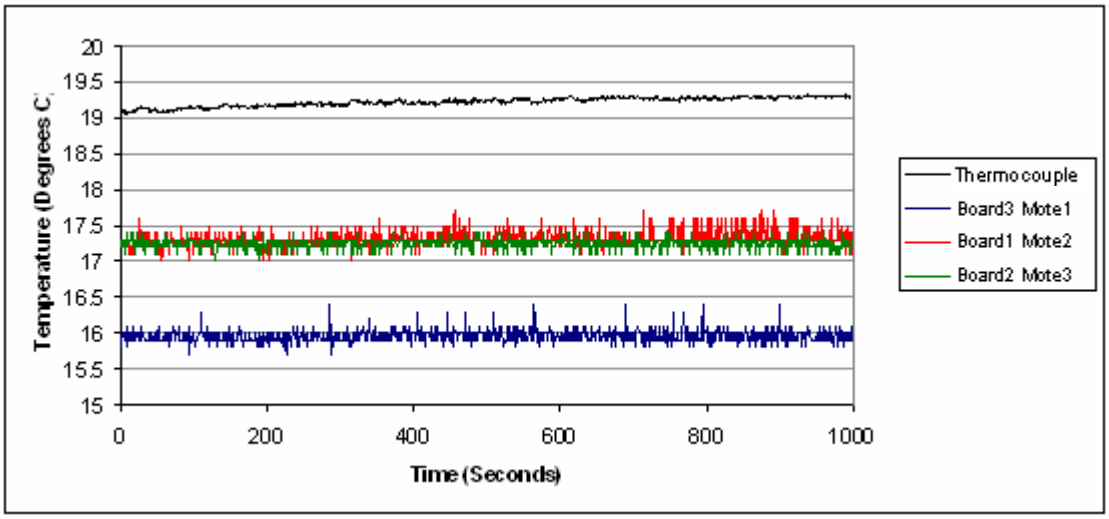

Fig. 3.17 Sensor board rotation study 3

The sensor boards were returned to their original wireless platform so that the tolerance errors could be accounted for using the same normalisation method that was applied in

Section 3.3.2. The responses of the three sensor nodes were normalised against the response of the validated thermocouple for convenience in later temperature trials. As anticipated, small differences in the sensor platforms and the sensor component parts resulted in a unique normalisation equation for each device. The normalisation equations developed for motes 2 and 3 are shown in Equation 3.8 and Equation 3.9, respectively.

$$T_N Mote2 = 1.20071T_I - 0.004616T_I^2 \tag{3.8}$$

$$T_N Mote3 = 1.30951T_I - 0.006172T_I^2 \tag{3.9}$$

Individual sensor responses were simultaneously tested against the verified thermocouple. Temperature results from this test with the sensing devices positioned at the chamber outlet are presented in Fig 4.18. Temperature values from each device, after application of the appropriate normalisation equation, compare well with those from the thermocouple and each of the other wireless temperature sensors in the network. The small deviation between recorded values at higher temperatures is attributed to the slightly different location of each of the devices at the chamber outlet.

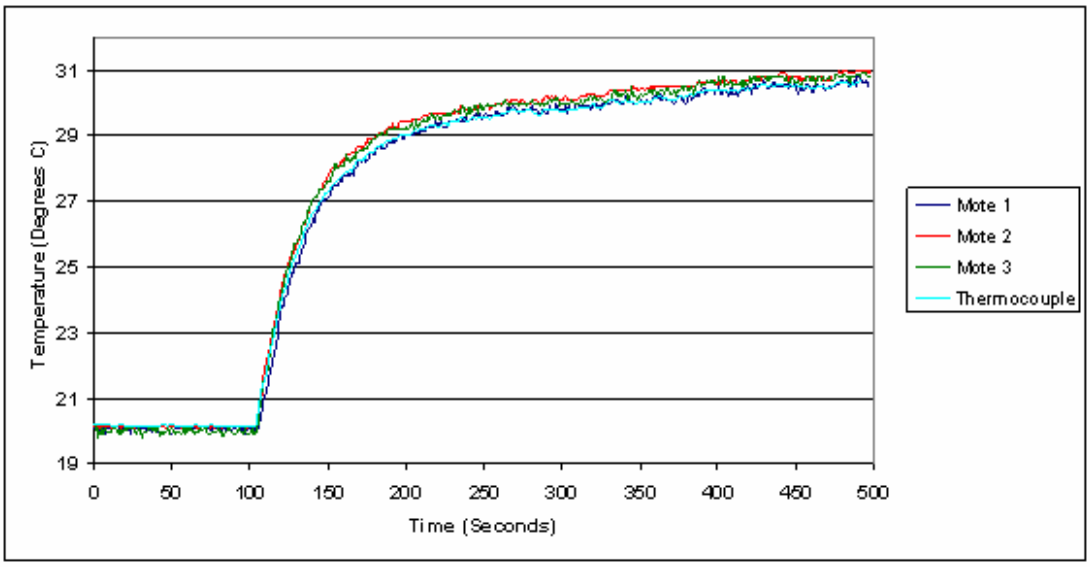

Fig. 3.18 Normalised temperature sensor responses

Based on these trials it was concluded that the implemented wireless temperature sensors were deemed suitable for preliminary feedback control trials of a Wireless Sensor Actuator Network (WSAN).

3.4 Data Acquisition Interface and Requirements

Crossbow supplied Java based visualisation and data logging software, known as Scope, which accessed received data packets at the host PC's serial port, as part of their Mica2Dot development kit. Examination of and basic testing with this software, raised concerns in terms of its suitability for the sensing applications being investigated in this research.

Without an in-depth knowledge of Java programming it was not possible to modify this software for the specific requirements of this research. Only packets that were assembled in the correct Crossbow packet structure would be accepted by the Scope software operating on the host PC. Data packets with a modified structure, such as those utilised in this research, would be rejected at the basestation and consequently lost. An alternative software interface for data collection and manipulation was required.

To have full control over the information being received at the host PC it was necessary to programme a user interface that would receive and accept all packets transmitted by nodes within range of the basestation. The interface would then process the incoming data accordingly, by selecting those packets that conformed to the structure being looked for.

Computational conversions on data contained within received packets, e.g., temperature conversion from the recorded voltage output of a potential divider circuit or chemical concentration conversion from the responses of low-cost chemical sensors, could be performed on the host PC. A custom data acquisition interface would also accommodate the incorporation of normalisation equations, specific to individual sensor nodes. The processed data could then be presented to the user on screen, in real-time and in the format of their choice. To achieve this, VB Mote Gateway data acquisition software was used.

3.4.1 VB Mote Gateway

VB Mote Gateway was developed by Ian Lesnet in 2005 as a Windows alternative to Java based programs for receiving, decoding and logging of mote data packets. The Visual Basic 6 source code is available under a General Public License (GPL) from

SourceForge under the TinyOS project [130]. This piece of software allows for simple data collection, retransmission and presentation.

Although this program did not possess all of the functionality required by the application described in this thesis, it served as a highly suitable starting point from which to build upon. The advantage in using the Visual Basic (VB) program rather than the Java based option available from the supplier is that VB is an easier programming environment to work within. Using C programming principles it allows for the construction of a versatile user interface using pre-defined command blocks.

The VB Mote Gateway program was significantly modified in order to meet the needs of the intended application. A lot of specific functionality was incorporated into the program structure that was not required, an example being the option of data transfer to a web based database. This was systematically removed until only the program code responsible for the reception, basic parsing, and packet logging remained. A new program was then built around these basic functions so that the incoming data would be processed and displayed in the required manner.

One factor for implementing mote data acquisition via a VB interface was that it allowed for access to the PC parallel port. This made it possible to control peripheral components of the ESC via control signals sent to available digital I/O pins of the host PC's parallel port.

Parallel port access is not supported under VB 6, but dynamic link library (DLL) files for this purpose can be written in VC++ and the exported functions accessed from VB 6. A freeware DLL providing both parallel input and output functions to VB 6 was obtained and incorporated into the software interface [131]. The logic state of the port pins can be easily manipulated via commands within the program.

Incorporation of sensor data acquisition, processing and output signal generation in one common graphical user interface (GUI) allowed preliminary feedback control trials of a Wireless Sensor Actuator Network (WSAN) to commence.

3.5 Wireless Sensor Actuator Network System

The test conducted for the initial sensor calibration (Section 3.3.2) gave an indication of the typical temperature increase provided by the heat source at the chamber outlet. Data presented in Fig. 3.12 and Fig. 3.18 showed that the external heat source, in normal uninterrupted operation, induced a positive temperature change at the outlet of the chamber of approximately 10 °C over a period of 200 s. By developing a feedback control loop using the temperature data collected from a thermistor equipped Mica2Dot mote to influence the parallel port output from a PC, it was possible to control the measured temperature parameter at a point in space within the ESC.

Coarse control of a process variable (PV) using updating data obtained from a single wireless sensor within a control loop was first examined. This demonstrated how data obtained from the constructed Mica2Dot wireless temperature sensor can be integrated with a temperature process controller and used in real-time to react to changes in the monitored parameter.

Once the capability of using a wireless sensor to fulfil this role had been demonstrated additional sensors were introduced into the network so that reactions to changes in the temperature parameter could be based on the collective responses of a multi-node temperature sensing network.

3.5.1 Single Sensor Control System Implementation and Testing

An On/Off control strategy of the heat source and extraction fan was developed based on the temperature state of a single wireless temperature sensor positioned at the outlet of the ESC. This approach to system control is used to keep PV between two set points.

If the temperature variable under consideration exceeds a user defined maximum set point (SP), an operation is invoked to bring the variable down to a system minimum SP. When the system variable passes below the minimum point another operation commences to bring the variable back to the maximum SP. The limitations of this control method are obvious in that the system is only marginally stable, i.e., it never settles at a constant value. However, this method has the advantage of achieving moderate control with great simplicity [132]. It was, therefore, an appropriate starting point for real-time temperature control depending on the response of a wireless sensor.

Hot air, used to increase the temperature within the chamber environment was provided by the heat source while the extractor fan placed at the outlet provided a means of reducing the chamber temperature by drawing air from the chamber interior. The location of the wireless sensor was fixed at the chamber outlet to allow for easy access, if periodic maintenance of the node was required during the course of testing. The system components and their layout relative to the ESC are detailed in Fig. 3.19.

The operation of the system required that the data acquisition interface would incorporate an output control program. Output commands were generated to actively manage the chamber temperature based on input data from the wireless temperature sensor.

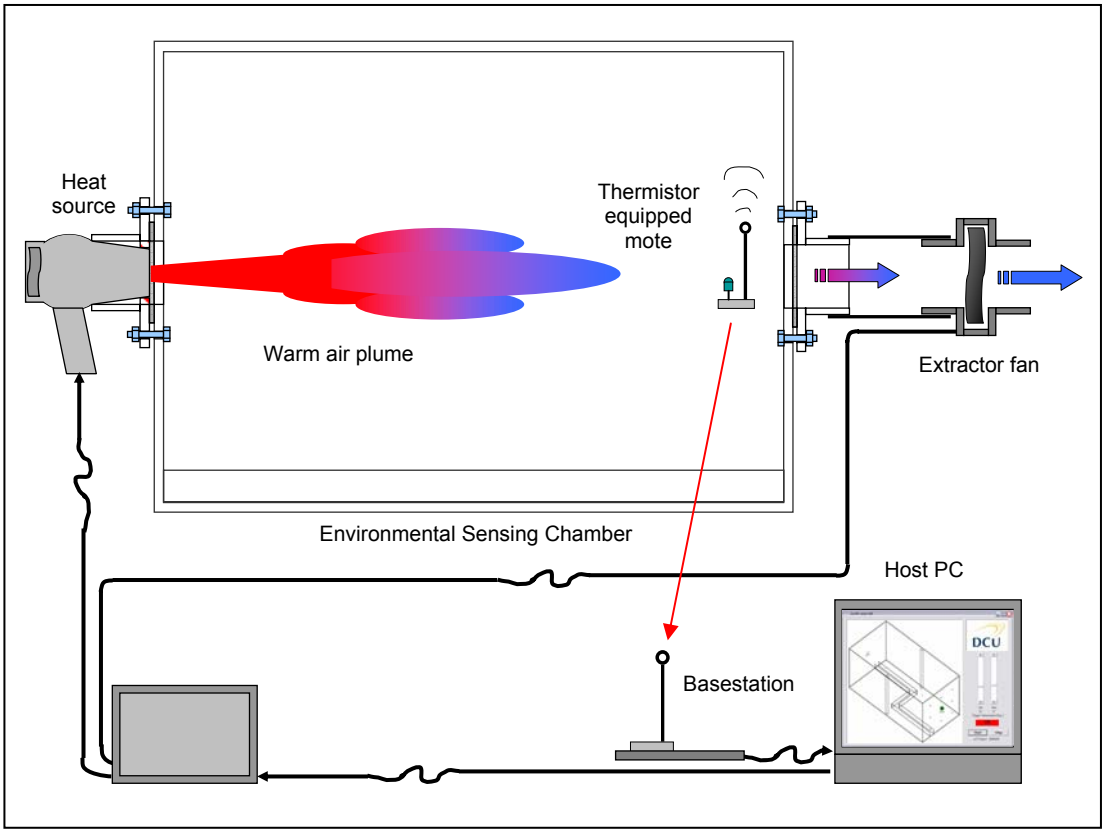

Fig. 3.19 On/Off control component layout

A screenshot of the control interface window, with additional overlaying identification tags, is shown in Fig. 3.20. The interface consisted of a number of components that supplied the user information regarding the current state of the system and allowed them to alter parameter settings while the system is in operation.

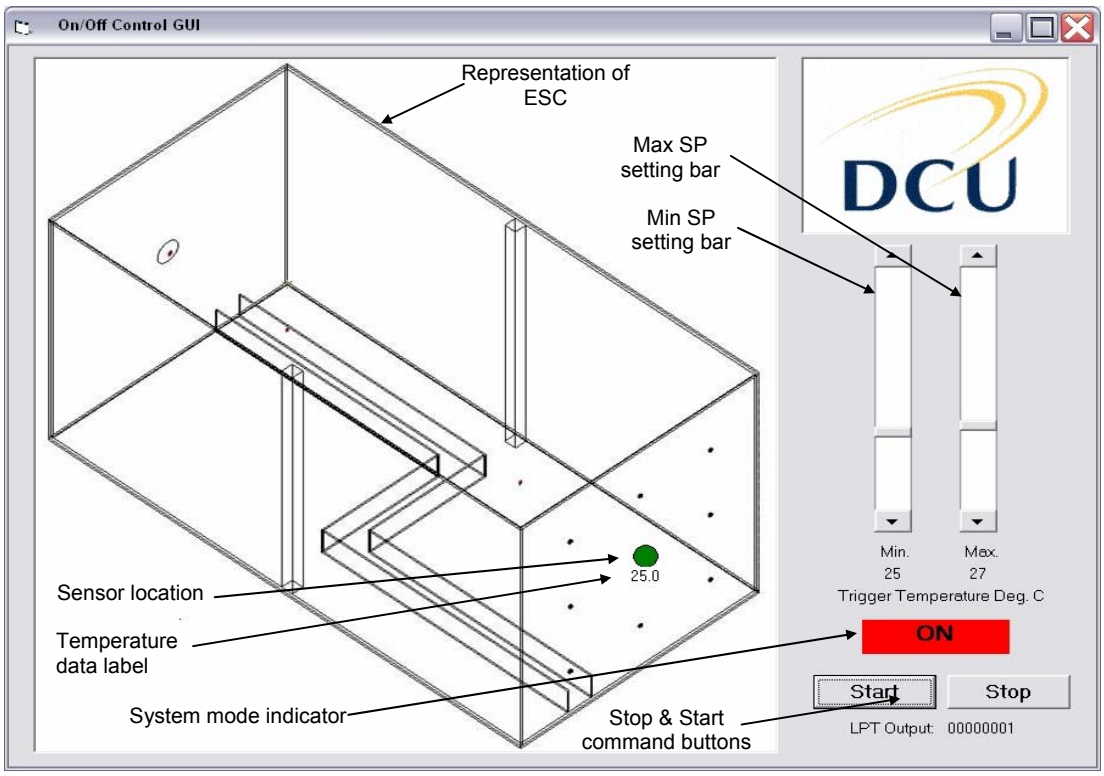

Fig. 3.20 On/Off control GUI

The location of the wireless sensor was identified in a CAD representation of the chamber by a coloured circular marker, whose colour was automatically changed based on the sensor's temperature value with respect to the higher and lower temperature limits. Desired operating limits were set using the vertical scroll bars on the right hand side of the interface. For a more in-depth analysis of the control code operation, please refer to Appendix 4.

A trial of the control program was conducted. The MoteGate program was started and the interface was briefly monitored to ensure time stamped temperature data were logged to a specified file. Then, the control interface was opened and the control limits were set with a maximum SP of 27 °C and a minimum SP of 26 °C. The initial value of the PV was observed to be steady at approximately 20 °C. The system was started and allowed to operate for a period of 200 s.

Fig. 3.21 shows the temperature response at the outlet of the ESC obtained during the described control test. The monitored variable was observed to increase rapidly in response to the activation of the heat source until the point where the maximum value was exceeded. Upon exceeding the maximum value, power to the heat source was set low and the power to the extractor fan was set high. This is shown by the prominent

decrease in temperature that begins at approximately 90 s of the test. The decreasing temperature breached the minimum SP limit value after a cooling period of 16 s. At this point, the extraction fan was set low and the heat source set high. This cycle continued as a regular waveform for the remaining duration of the trial, with the PV being maintained within a temperature band of approximately 2.0 °C. The PV, therefore, overshot the desired operating temperature band limit of 1.0 °C.

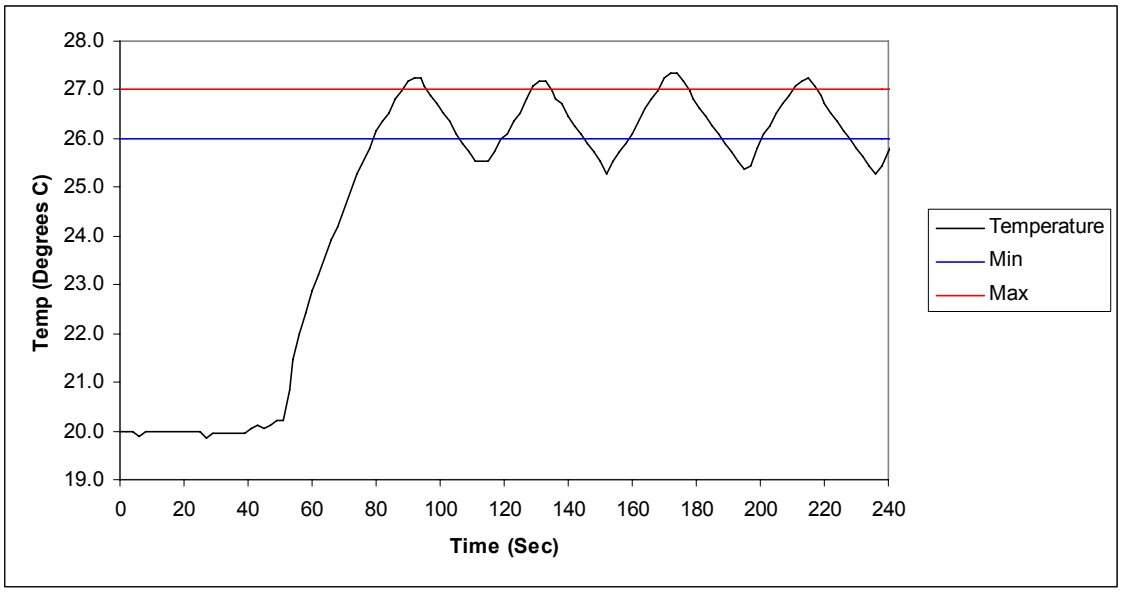

Fig. 3.21 On/Off control response graph

The PV overshoot levels observed at the maximum and minimum limiting points were relatively consistent throughout the test. A number of reasons have been ascribed to these observed effects. The overshoot of the higher SP is in part due to the slow start up speed of the extractor fan. The time taken between the output signal being switched on and the fan reaching operating speed was approximately 1 s. A similar effect was noticed at the lower SP limit. The heating coil of the heat source takes a period of time to reach operating temperature; therefore, the heating effect applied by the heat source was not instantaneous.

The location of the sensor relative to the heating and cooling devices also affects the overshoot at both operating limits. For example, when the sensor reaches the higher SP value, the heat source, a distance of 2 m from the sensor, is turned off. This distance induces an overshoot effect on the system response because when the heat source is turned off, it has already introduced too much hot air into the system.

The data acquisition software and output control software operated in conjunction with each other to achieve real-time reaction to a changing parameter with limited information from a single sensor node. Sensor location relative to the source had a bearing on the effectiveness of the response of a control system.

A logical step is experimentation with a network of wireless sensor nodes. This will lead to a better working knowledge of the sensing platforms when being used collectively and act as a bridging point before the integration of less established component based chemical sensors.

3.5.2 Wireless Sensor Actuator Network Implementation

Before proceeding to testing a WCSN, the operation of a WSAN using temperature sensing devices was evaluated to highlight problems and deficiencies when networking wireless sensor platforms. The three node sensor network was deployed along the central axis of the chamber as depicted in Fig. 3.22. The physical locations of the sensors were fixed during testing from the top of the chamber using support wires.

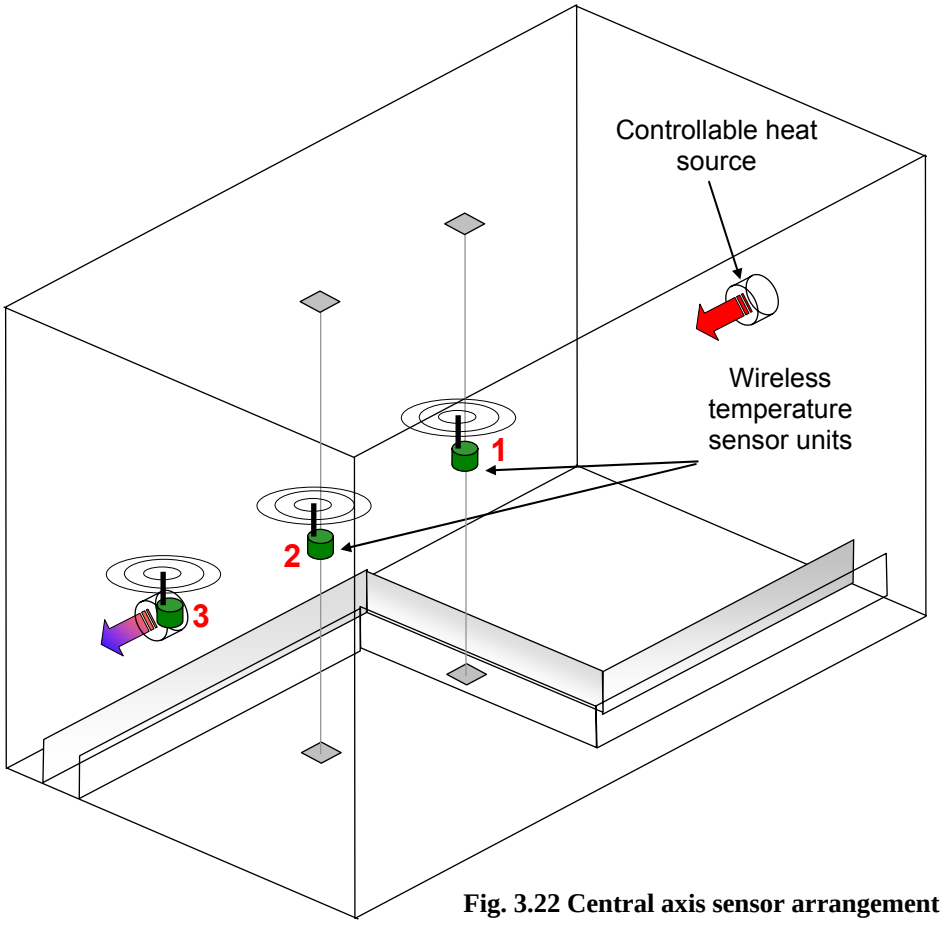

Fig. 3.22 Central axis sensor arrangement

The control method was changed to a proportional strategy. Implementation of this strategy allowed for more stable management of the temperature process variable (PV) and later examination of the reaction of a stable system to a disturbance event.

A proportionally controlled system is one in which the control output is proportional to the difference between the value of the PV and a desired set point (SP) [133]. Due to the internal wiring of the heat source it was not possible to vary the level of heat being generated by the heating coil and, so, an operating duty cycle was applied to the heat source. Proportional control was then applied to this cycle so that it consisted of two distinct time periods; the time period that the heat source was active and the time period that the heat source was inactive. This is also known as pulse width modulation.

The ultimate goal of a proportional controller is to reduce the error, e(t), in a system to zero, meaning that the system PV is equal to the desired SP. The block diagram shown in Fig. 3.23, effectively displays the flow pattern of the negative feedback proportional control system. It can be seen that the output from the control software, Control Output (CO), governed the duty cycle of the heat source. The control parameters were chosen to accommodate the time taken for the heat source to reach full operational speed and temperature.

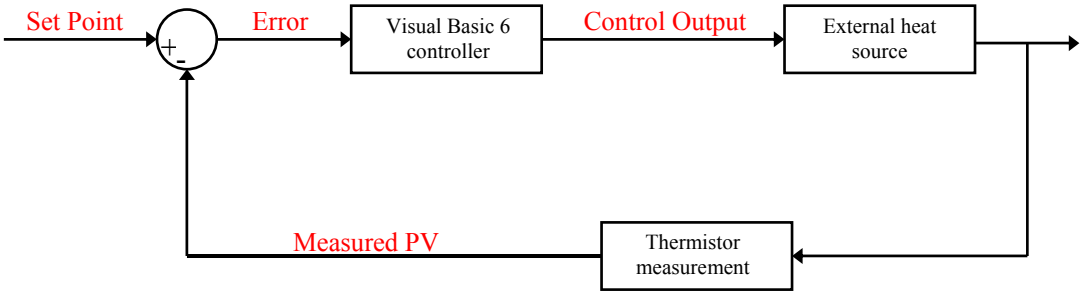

Fig. 3.23 Proportional control block diagram

$$CO = CO_{BIAS} + K * e(t) \tag{3.10}$$

The duration of the duty cycle was set to a period of 2 s. Within this duty cycle the heat source was active for a minimum of 1 s, to prevent cooling when the system reached stability. The minimum CO was, therefore, 50 % of the duty cycle. This minimum output value is referred to as the control output bias [134]. The remaining 50 %, or 1 s,

of the cycle was managed by the proportional control algorithm, described in Equation 3.10 [134, 135].

The value described by K in Equation 3.10 is the gain that is applied to the system by the controller. This value is a tuning parameter that can be adjusted to influence the control effect necessary for a particular system. As mentioned earlier, $e(t)$ is the error between the PV and SP at any given point in time. These two values will now be examined for the temperature control system under consideration.

It was first necessary to define the proportional band of the system. The proportional band is the temperature range within which control is required. The range chosen was from the SP to 5 ºC less than the SP. When the PV entered this temperature range the pulse length of the heat source was changed so that the SP was not exceeded.

The maximum error of concern was, therefore, 5 ºC. If the $e(t)$ was greater than this no control effort was necessary and the heat source was allowed to operate without any interruption. It has already been stated that the maximum value for the CO was 2 s, and that the output bias value was 1 s. Therefore, subtraction of the control output bias from the CO resulted in the maximum product of $K*e(t)$ being 1 s. As the maximum error value of concern was 5, the resultant K value was 0.2.

A control program to achieve proportional control with respect to an integer SP value was constructed within an additional VB user interface form integrated into the existing data acquisition code. The objective of this work did not require that the control equation be tuned to achieve specific temperature responses, as the principle interest was in displaying an operational real-time WSAN that would allow for easy adaptation to a wireless chemical sensor actuator network (WCSAN).

The proportional control user interface is detailed in Fig. 3.24. The desired SP was manipulated using the scrollbar on the right hand side of the interface. The control output relied on an internal countdown timer. The timer interval was specified as 10 ms. One complete duty cycle, 2 s, therefore, equalled a counter value of 200 units. For compatibility between data variable types, the PV and SP were scaled by a factor of ten, removing the possibility of fractional components in the resultant integer e(t) value.

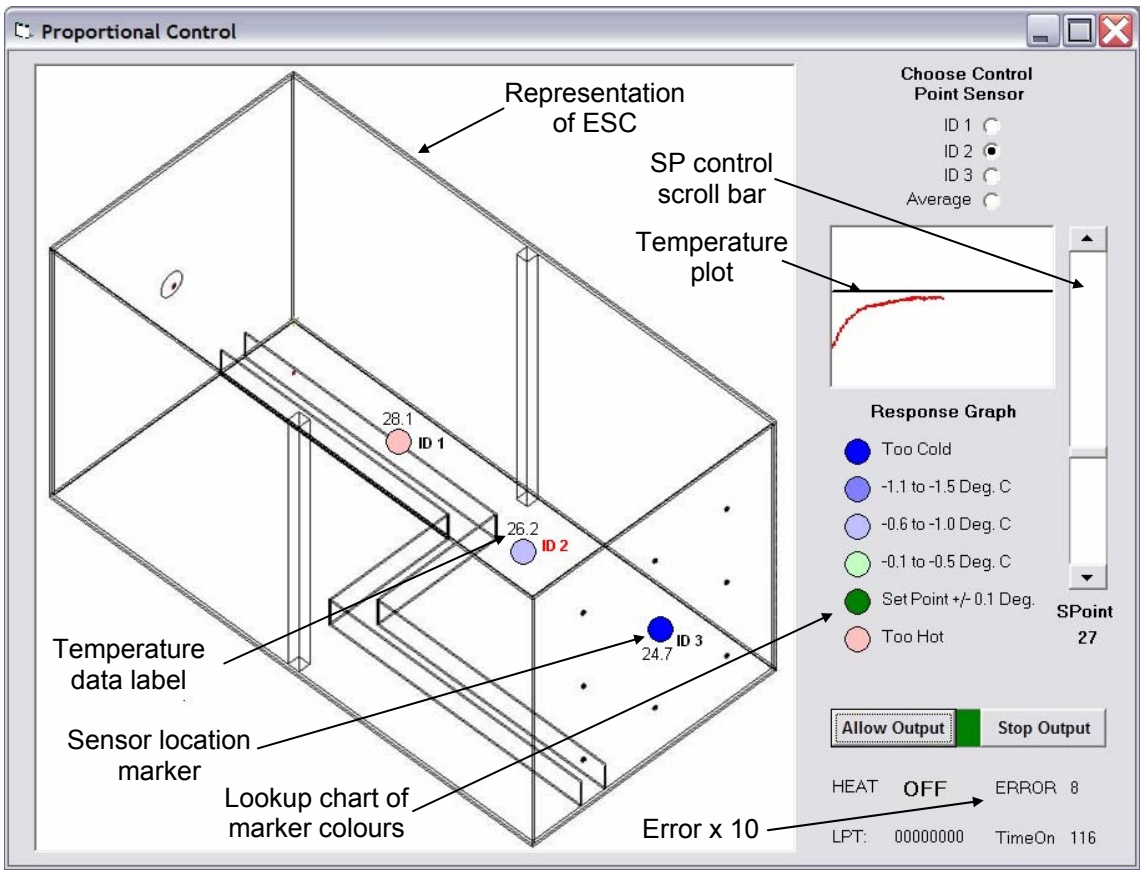

Fig. 3.24 Temperature sensing network proportional control interface

The CO was denoted within the control code as an integer variable, "TimeON". Based on changing error values, Equation 3.11 was used to calculate the quantity of timer counts that the external heat source would be in operation over. In Equation 3.11, the control bias value was included as 100 timer counts, corresponded to 1 s. The process gain value, discussed earlier in this section, was scaled by a factor of 10 to maintain continuity with the scaled PV and SP values.

$$TimeON = 100 + 2 * e(t) \tag{3.11}$$

The operation of the system was specified by the user to be governed by the response of an individual sensor or the collective response of the 3 sensor nodes. If the operation of the system was based on the collective response of the sensor network, the error value was calculated by subtracting the average temperature value recorded by the sensors from the system SP, by using Equation 3.12. The WSAN program, code with detailed commenting, can be referred to in Appendix 5.

$$ErrorValue = SP - \left(10 \times \left(\frac{T_{Motel} + T_{Mote2} + T_{Mote3}}{3}\right)\right) \quad (3.12)$$

3.5.3 Wireless Sensor Actuator Network Study

Trials were conducted using the collective response of the sensors as the controller input. The nodes were arranged at three locations along the central axis of the chamber at distances of 1 m, 1.5 m and 2 m from the heat source, as shown earlier in Fig. 3.22. The recorded temperature values are displayed in Fig. 3.25.

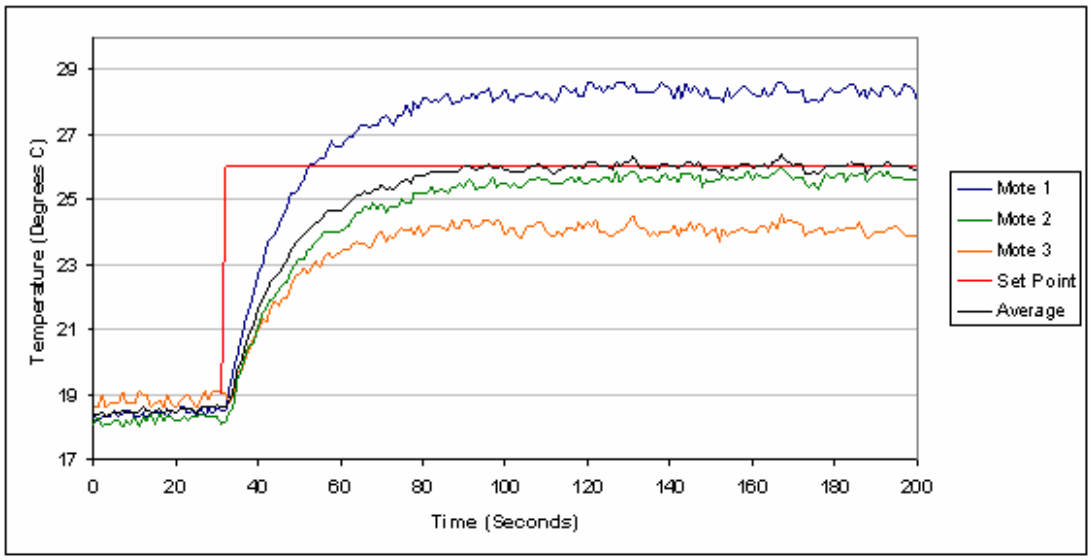

Fig. 3.25 Central axis test temperature results

The results of this study show that the PV, i.e., the average temperature of all three sensors, reached the SP level of 26 °C after approximately 55 s of system operation. At this point, the system stabilised with only small variations around the SP. As would be expected, mote 1, the device closest to the heat source, recorded the highest temperature. Mote 2, being equidistant from the other nodes, recorded a temperature comparable to that of the average. Mote 3, positioned furthest from the heat source, recorded the lowest stabilised temperature. Oscillations present in the temperature responses resulted from the pulse operation of the external heat source. The temperature variation between each of the sensors was a consequence of sensor location relative to the heat source.

The response of the stabilised system to a disturbance event was then examined. A pneumatic air line was introduced into the chamber, as shown in Fig. 3.26. The line was

positioned so that, when active, it would discharge air at approximately room temperature onto the thermistor sensor of mote 1, inducing a localised disturbance on that sensor. The temperature control system was then examined in two modes of operation. The first mode relied on the response of a single sensor to manage the operation of the heat source, while the second mode relied on the collective temperature measurements of the network.

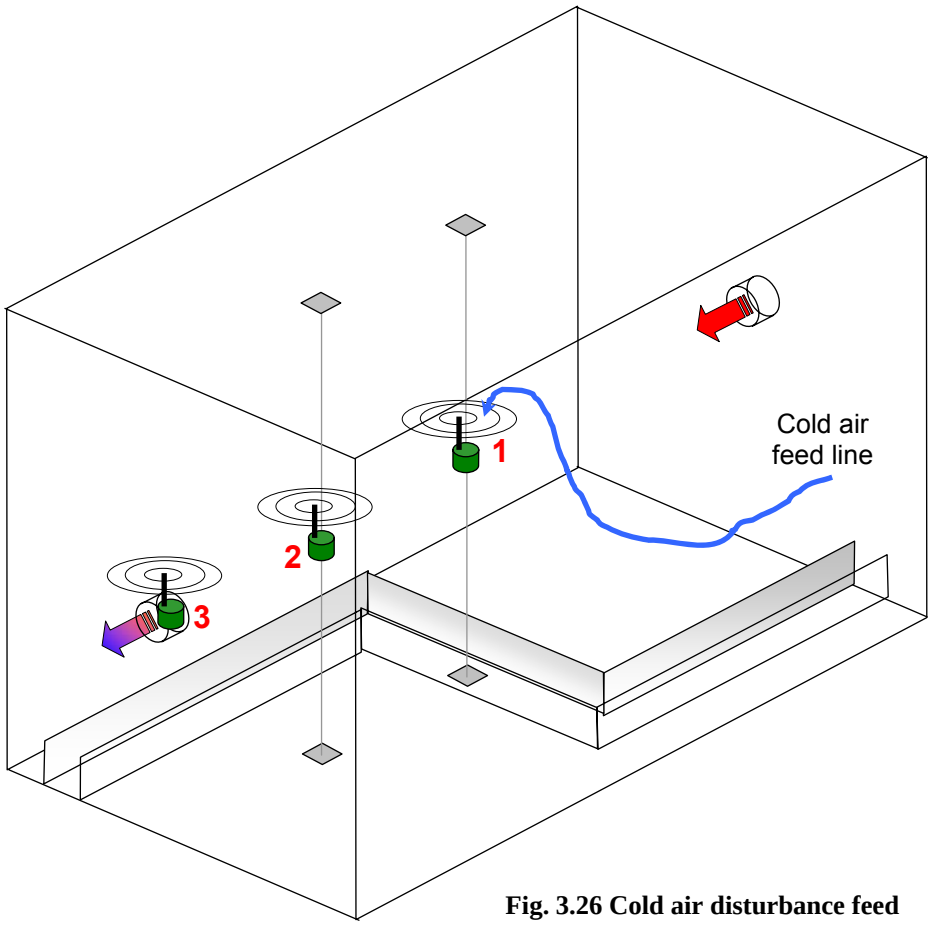

Fig. 3.26 Cold air disturbance feed

A set point of 27 °C was used for continuity between both conducted tests. In both test cases the system was started and allowed to run for 120 s after an initial settling period of 60 s. This activity period allowed the PV to reach and stabilise around the SP. When this time period had elapsed the cold air feed was activated for a time of 40 s. The system was then allowed to re-stabilise at the SP.

The temperature data recorded while the operation of the system was governed by a single sensor, mote 1 positioned centrally in the ESC, are presented in Fig. 3.27. The activation of the cold air feed is clearly visible at t = 180 s in the temperature data. The reduction of the temperature observed by the sensor forced the control system to

increase the active period within the heat source duty cycle. The proportional controller compensated for the temperature difference by adding heat to the system.

When the cold air feed was removed, at t = 220 s of the study, the sensor began to record the true temperature of the location. This can be seen by the rapid increase to a temperature level of 29 °C. As the SP had been exceeded, the response from the controller was to stop the heat source until the PV had returned to a value less than that of the SP. At this time, 140 s after the cold feed was stopped, the heat source was reactivated and operated within the fixed duty cycle to maintain the SP temperature.

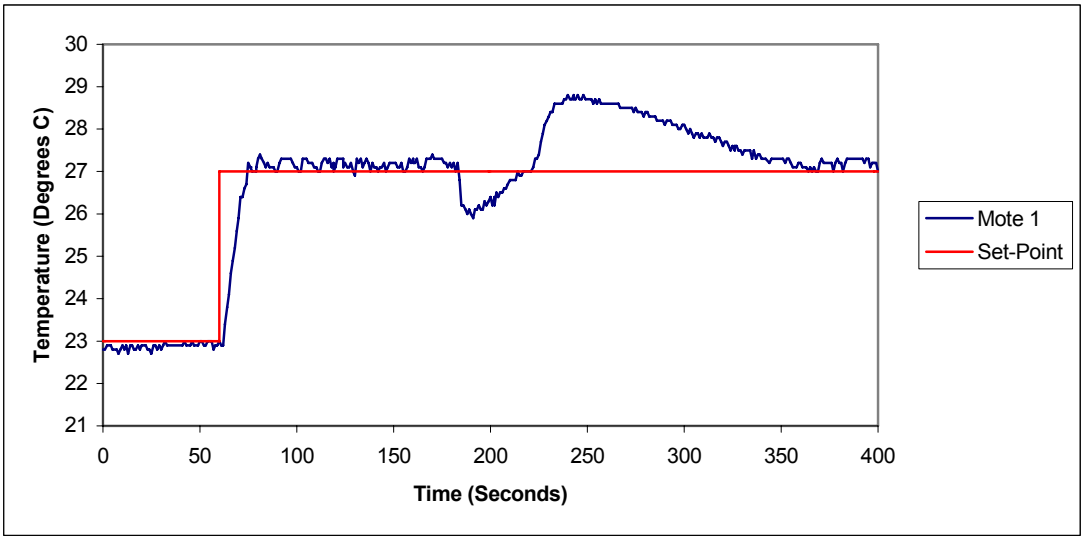

Fig. 3.27 Response of single node to temperature disturbance

The same test was repeated using the collective response of the three node sensor network. The response of the system to the disturbance is shown in Fig. 3.28. The activation of the disturbance caused the temperature value observed by mote 1 to decrease. The system responded to this, as in the previous study, by increasing the volume of hot air applied to the chamber. However, as the control output was dependent on the average response of the sensors, the system stabilised quickly, because of the increased temperature observed by motes 2 and 3 respectively.

The response of a network of sensors furnished the controller with a greater level of information regarding the temperature state of the air volume being monitored, preventing an unnecessarily dramatic increase in the control output, as seen in the previous study. A system which gathers a greater amount of information can, therefore,

be programmed to react in a more controlled manner to a disturbance than a control system that is based on the response of a single sensor device.

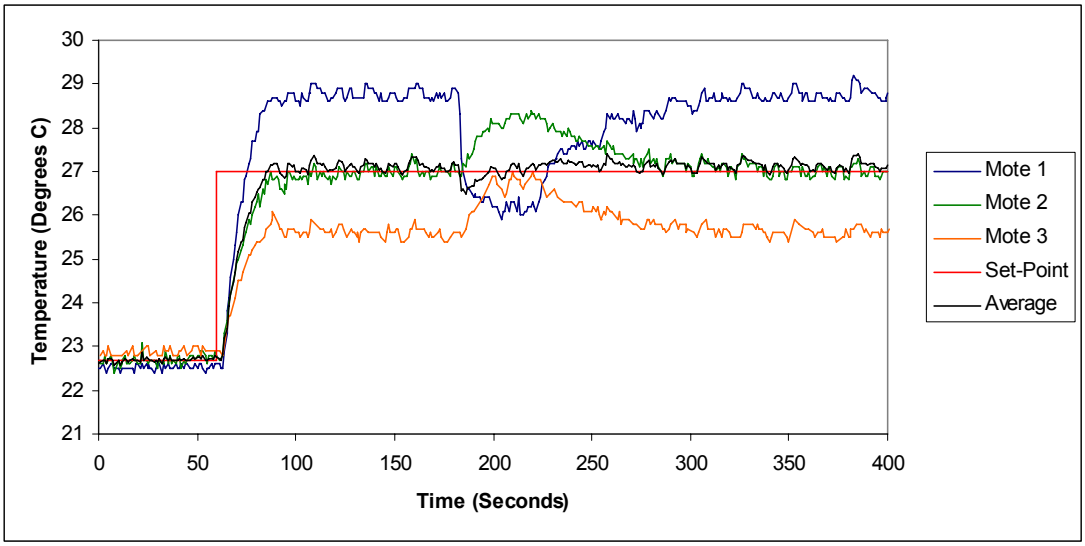

Fig. 3.28 Response of sensing network to temperature disturbance

This is significant in terms of a low cost wireless chemical sensing system. As will be explored in Chapter 5, one chemical sensor would provide a monitoring system with very limited data. Regardless of the quality of the sensed data, one would be limited to measurements from a single specified location. If an event were to occur, it is possible that a single sensor would not observe the event because the event may not affect the immediate environment surrounding the sensor. If the environment was being monitored by a number of spatially dispersed sensing nodes, it would be possible to gather more representative data concerning an event. Data obtained from a number of different locations would allow for a system to react appropriately to an event as it is occurring.

3.6 Chapter 3 - Summary and Conclusions

A commercial wireless sensing and communications platform was modified to the requirements of this specific research so that sensor data can be relayed to a host PC in real-time at a frequency of 1 Hz. A node power management scheme was implemented to facilitate an operation lifespan, approximately 4 weeks, which is adequate for laboratory sensor testing.

An initial target parameter of temperature was measured using a thermistor based potential divider circuit mounted on a prototyping sensor board available from the communications platform supplier. Analysis of the thermistor sensor in comparison to a validated t-type thermocouple when exposed to a hot air plume indicated a measurement error. The error was compensated for by using a linear approximation of the error over the measured temperature range incorporated into the Steinhart-Hart conversion equation for thermistors. In total, three wireless temperature sensor nodes were constructed, tested and normalised against a validated thermocouple. Comparison of the devices when positioned together and exposed to a hot air plume shows good correspondence between the measurements of the sensor nodes.

A developed data acquisition and processing interface was integrated with an output control routine to demonstrate On/Off control of electro-mechanical components using a single wireless temperature sensor. The controller was expanded to manage the temperature parameter based on sensed values at one of three specific points or the average value over a sensing area. Results obtained during system tests, with data being received at a rate of three packets per second, have shown that mote based wireless sensing devices can be used in real-time to supply a system with information so that it can react to changes in the measured parameter. The development and successful operation of this WSAN makes it possible to proceed towards the integration of a low power component based chemical sensor with the communications platform so that a reactive Wireless Chemical Sensor Actuator Network can be implemented.

4 Wireless Chemical Sensing Node

As discussed in the literature review, recent research has seen the use of LEDs as simple light detectors. The initial coupling of this light detection method with a colorimetric chemically responsive layer showed the potential use of reversed biased LEDs as chemical detectors, but was not fully realised.

With a point to point wireless sensor actuator network in place it is now possible to integrate this optical chemical sensing method with the developed sensing and communications platform to allow for wireless monitoring of chemical plumes introduced into the Environmental Sensing Chamber (ESC).

The initial objective of this chapter is to construct the low cost optical chemical sensor. The response of the sensor to an acidic stimulus will be confirmed before its integration with the wireless communications platform. The operation of the initial wireless chemical sensor is evaluated. The results of this evaluation lead to modifications of the device. The modifications to achieve a stable wireless chemical sensor node are discussed in detail.

Subsequently the operation of the modified wireless chemical sensor node is studied to ensure protection from ambient lighting changes in a laboratory test environment. Further studies investigate the response characteristics, such as, response time, response reproducibility and limit of detection of the developed device. These successful trials facilitate calibration of the wireless chemical sensor to known concentrations of the target contaminant over a contaminant range of 0 to 1 mg/l.

Finally, the data acquisition interface is modified to accommodate reception of data from a five node wireless chemical sensor network. The developed interface facilitates real-time processing and conversion of sensor data to concentration units, essential to the reactive wireless chemical sensor actuator network discussed in Chapter 5.

4.1 Low-cost Chemical Sensor Construction

A low cost optical chemical sensor was constructed using an opposing emitter and detector LED configuration, as investigated by Shepherd *et al*. [119]. This physical arrangement was adopted as it had been shown to be suitable to gas phase contaminant sensing. Surface mount LEDs (1206 format) soldered to a 2.54 mm pitch header pin formed the low-cost component parts of the sensor. The header pin acted both as a means of connecting the sensor to its control circuitry but also as a rigid mounting that maintains a fixed gap of approximately 2.5 mm between the LED surfaces, as shown in Fig. 4.1. The addition of a chemically sensitive surface coating between/on the LEDs was required so that the structure could function as a simple chemically sensitive optical sensor.

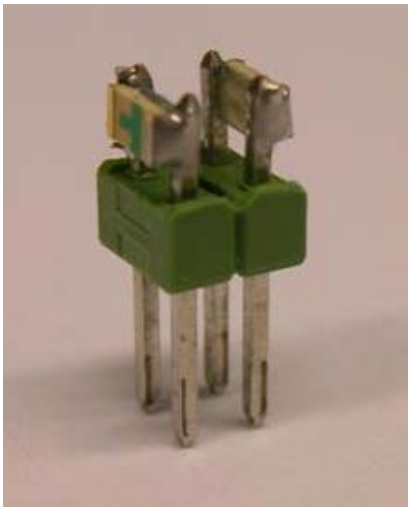

Fig. 4.1 Paired emitter and detector LED sensor structure

As discussed in Section A1.4.3, acetic acid (Fluka, Ireleand, no. 45727) was used as the model compound to generate the acidic stimulus vapour. Acetic acid is considered to be a mild acid and can be recognised by its strong vinegar like smell. The indicator, bromophenol blue (BPB), was chosen as a suitable indicator for the chemically sensitive LED surface coating because of its high sensitivity to acidic vapours.

Optimal sensitivity was achieved by matching the absorbance spectra of the dye, and the emission spectrum of the LED light source. The colour change gradient of this indicator dye is shown in Fig. 4.2. At the deprotonated (alkaline) state (pH > 5) the indicator dye is dark blue in colour. As the acidity of the environment increases, the indicator colour shifts towards yellow. The colour change process is reversed when the chemical stimulus is removed from the indicator's environment.

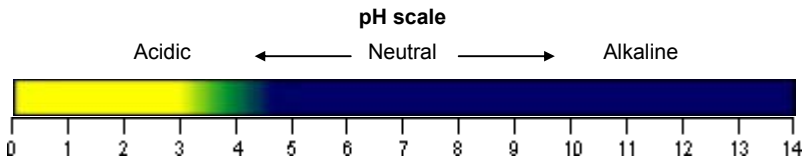

Fig. 4.2 Colour change gradient of bromophenol blue (BPB) induced by a change in pH in the environment [136]

The absorbance spectrum of the acid and alkaline forms of the BPB indicator dye, with respect to the emission spectrum of the super bright orange 610 nm emitter LED (Kingbright, KP-3216SEC, 3.2 x 1.6 mm) is shown in Fig. 4.3. When applied to the LED surface, the indicator acts as a filter that modulates the intensity of light passing from the emitter LED to the detector LED.

When the sensor is exposed to acidic vapour, the colour of the sensing film changes from blue to yellow, corresponding with the absorbance of the dye at 610 nm diminishing and a new absorbance peak appearing at 430 nm, as shown in Fig. 4.3. Consequently, the amount of light transmitted from the emitter LED through the sensing layer to the detector LED increases. Conversely, as the polymer sensing film recovers, switching back to the blue alkaline state, the strong absorbance band associated with this indicator reappears so that a significant portion of light from the emitter LED is filtered out.

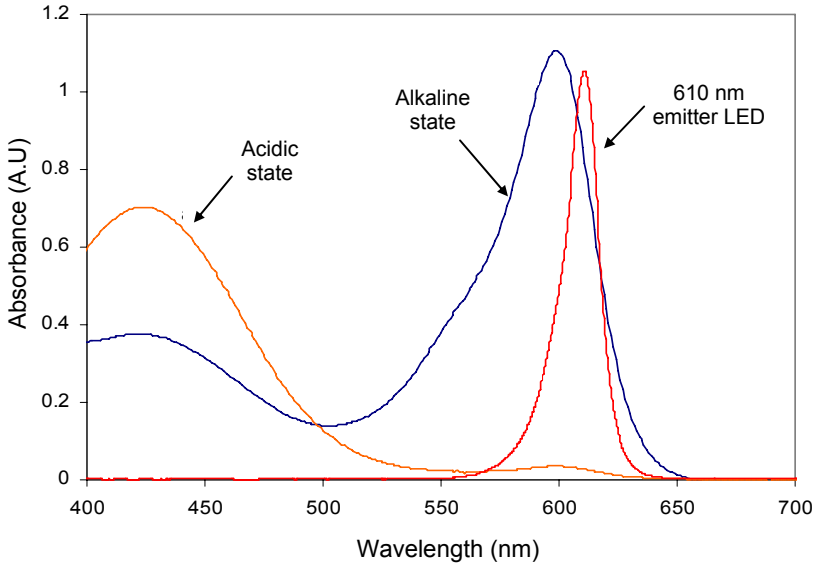

Fig. 4.3 Absorption spectrum of BPB in acidic and alkaline states with overlapping emission spectrum of emitter LED

4.1.1 Polymer Reagent Preparation and Coating

The chemically sensitive indicator was applied to the LED light sensor surface as a polymer layer. The colorimetric sensing polymer was prepared by dissolving the pH indicator BPB with a solution of ethyl cellulose in ethanol. In order to prepare a sensing polymer, which was responsive to acid, it was necessary to stabilise the BPB in the blue alkaline form. This was achieved by adding the salt tetrahexylammonium bromide (THABr), to the polymer formulation. The THABr salt acts as a solid-state pH buffer.

The research of Shepherd *et al*. [119], which used a similar sensor configuration, effected application of a polymer reagent layer to only the detector LED surface, by releasing a small volume of reagent from a pipette. Since the coating acts as a filter, its application to the surfaces of both LEDs would yield a greater change in response when exposed to an acidic chemical stimulus. Fig. 4.4 displays the filtering effect on light from the emitter LED when the sensor is exposed to an alkaline, Fig. 4.4(a), and acidic, Fig. 4.4(b), environment.

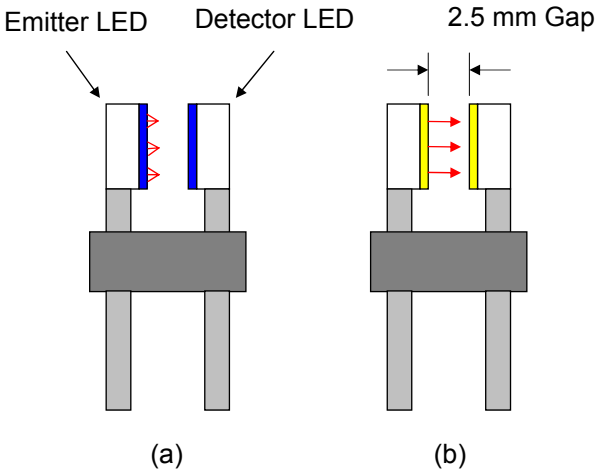

Fig. 4.4 Reactive coating configuration

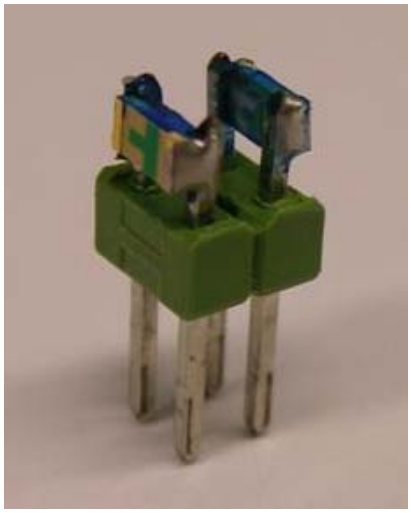

Fig. 4.5 Coated emitter and detector LED chemical sensor

A small volume of the polymer formulation was manually applied directly to the lens of both LEDs using a small crafts paint brush. A short drying period of ten minutes after the polymer application ensured the sensing layer had adhered to the surface of the LED. The coated sensor was then exposed to the head space of a small vial of ammonia solution. These alkali vapours dispersed residual solvents and stabilised the reagent in its blue alkaline form.

The sensor was then left to dry completely in air for 6 hours and stored in the dark before use. This resulted in a low cost, colorimetric, pH sensitive sensor responsive to acid, as presented in Fig. 4.5. The present fabrication process makes no provision for reproducible coating layer thickness. This issue was not addressed in this thesis but will be discussed as part of future work in Chapter 6. Chemical sensors constructed during the course of this research were, therefore, individually calibrated as the response characteristics of each sensor could not be assumed to be the same.

4.2 Study of Fundamental Sensor Response

The sensor was connected to a microcontroller test board, as shown in Fig. 4.6, so that its response to an acetic acid stimulus could be observed. The test board was coated in a PVC sealant to protect the sensitive electronic components from corrosion as a result of exposure to acidic vapours. The microcontroller was programmed to govern the operation of the developed sensor.

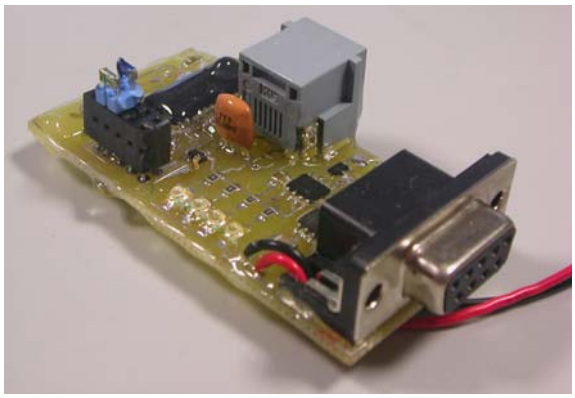

Fig. 4.6 Microcontroller sensor test board

To perform a measurement, the internal capacitance of the detector LED was first charged by setting the digital I/O pin connected to its cathode to logic high, i.e., reverse bias. The states of the digital I/O pins connected to the detector LED were then reversed, allowing the capacitance to discharge into the microcontroller at a rate dependent on the light falling on the LED [113]. Simultaneously, the emitter LED was activated to act as a consistent light source over repeated sample measurements.

The state of the discharging pin was checked for a fixed number of processor counts (4000). The sensor response is the quantity of processor counts within the fixed period for which the logical state of the detector voltage is high, i.e., an integer value ranging from 0 to 4000. The sensor's response to the presence of a chemical stimulus was a measured increase in light, represented by a reduction in the quantity of processor counts, over the detector LED discharge period, for which the voltage was in a logic high state. Recorded sample measurements were transferred to a PC interface over a standard RS232 serial connection. The sample frequency was set to 8 Hz so that high resolution response data could be obtained.

The study involved the exposure of the sensor unit to a static headspace of concentrated acetic acid (Fluka, Ireland, no. 45727). The lid of a plastic vial containing the stimulus chemical was opened and the LED sensor was placed above it for a period of approximately 30 s. The raw sensor data are presented in Fig. 4.7 and contain noise similar to that present in the signal response of the ammonia sensor developed by

Shepherd *et al*. [119]. This is a common feature of the responses of LED based chemical sensors. The obtained data, shown in Fig. 4.8, were smoothed for presentation purposes.

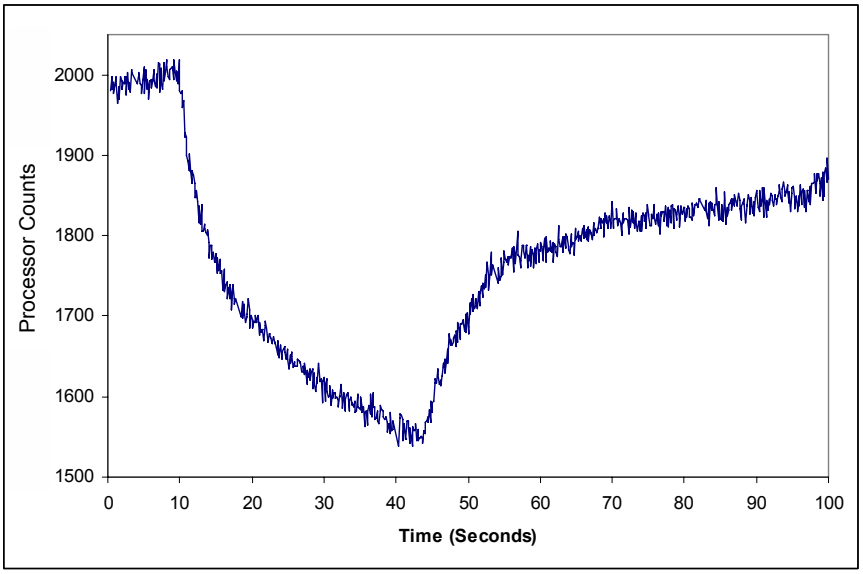

Fig. 4.7 Coated sensor response to acetic acid vapour

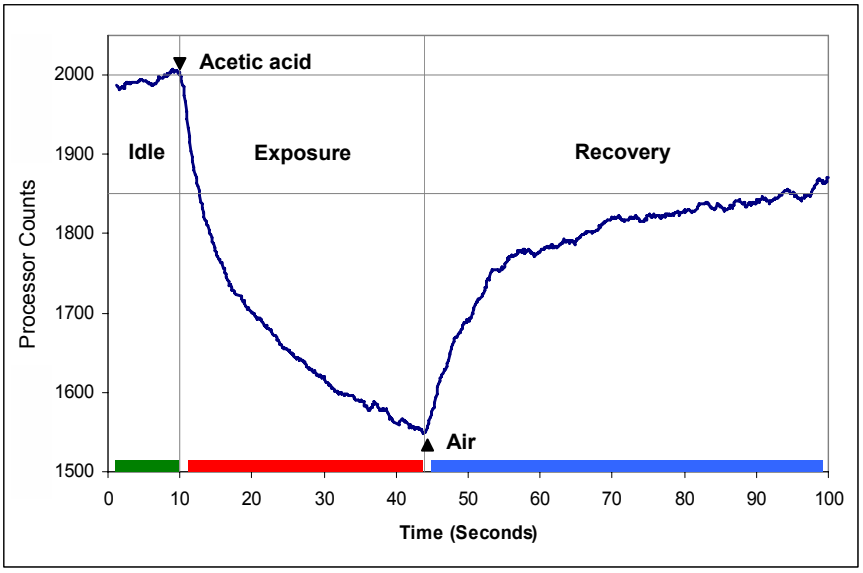

Fig. 4.8 Smoothed sensor response to acetic acid vapour

The data give an indication of the response characteristics of the sensor, showing a dramatic measured response (maxing at t = 43 s), which is distinguishable from any noise present in the signal as soon as the sensor is exposed to the acetic acid vapour.

The response of the sensor over the 34 s exposure period is a measured negative change in the logic high processor counts per sensor sample of approximately 450 units, as depicted in Fig. 4.8.

Removal of the concentrated chemical stimulus at t = 44 s, resulted in an increase in the quantity of logic high processor counts recorded from the discharging detector LED. The recorded increase is an indication that the chemically sensitive LED coating layers began to revert to their alkaline blue colour states. However, it can be seen that the recovery rate of the sensor in clean air does not match its reaction rate with the chemical stimulus.

After 34 s of recovery, the value being returned by the sensor is 61 % (274 processor counts) that of the change induced by the chemical stimulus. After 56 s of recovery, the measured detector value has not returned to the pre-exposure response level, giving a 130 unit offset. In this particular case, it is likely that the recovery rate of the sensor was restricted because the concentrated acetic acid vapours saturated the chemically sensitive polymer layer. No attempt was made to purge any contaminants from the sensor surface after the exposure period. The study was successful in showing a target specific change in sensor response. The issues of sensor purging, reuse and reproducibility are discussed in Section 4.4.2

The device's proven sensing ability allowed for the integration of this low cost device with a wireless sensing and communications platform, which will be discussed in the following section and undergo further refinement in Section 4.4.

4.3 Prototype Wireless Chemical Sensor Node

A prototype wireless chemical sensor node was developed with the objective of evaluating the node's operation when exposed to a chemical stimulus. The wireless sensing node was evaluated prior to and during the mote operating program refinement, detailed earlier in Section 3.2. The evaluated node, therefore, used the continuous operation control code and was powered using a CR2354 3 V coin cell battery.

The sensor was wired to a MTS510A sensor prototyping board and connected to a Mica2Dot mote via the 18-pin expansion connector. The forward biased emitter LED was driven in series with a 1 kΩ current limiting resistor to ensure that the detector LED was not saturated with light. The emitter LED anode was connected to the general purpose I/O pin INT1. The cathode of this LED was connected to the ground terminal via the current limiting resistor. The anode and cathode of the detector LED were connected to the terminals of I/O channels PW0 and PW1 respectively. An additional 3 mm LED, which acted as a sensor status indicator, was connected in series with the 1 kΩ resistor between INT0 and ground. A diagram of the arrangement is shown in Fig. 4.9.

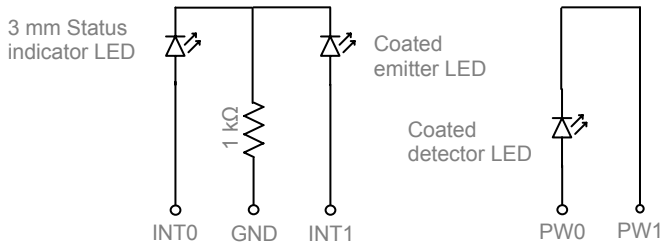

Fig. 4.9 Sensor and indicator connections to prototyping board

Exposure of the sensitive electronic components of the Mica2Dot wireless sensing platform to acetic acid vapour would cause corrosion which could possibly affect the electronic circuitry and cause a failure in operation of the device. A sensor node enclosure was developed to ensure that, although, the optical sensor was exposed to the environment, all other electronic components were isolated and protected from chemical vapours.

The enclosure consisted of a 35 mm film canister with a hexagonal nylon ¼" BSP threaded plug recessed into its surface and bonded into place. The disassembled

prototype wireless chemical sensor node is shown in Fig. 4.10. The centre of the threaded plug had been drilled out to a diameter of 7 mm, allowing for the opposing LED sensor and indicator LED to be mounted within the threaded section, as displayed in Fig. 4.11. Hot glue was used to form a seal between both the status indicator and sensing LEDs and the prototyping board that they were connected to. Final assembly of the node saw the Mica2Dot mote connected to the sensor board within the body of the film canister. The constructed node allowed for sensor readings to be repeatedly taken from fixed port points on the chamber's interior faces.

Fig. 4.10 Mica2Dot mote chemical sensing enclosure

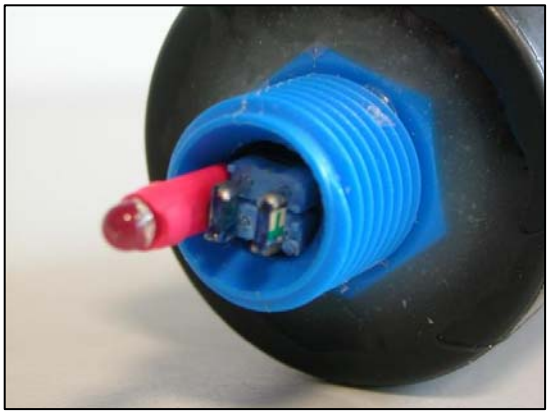

Fig. 4.11 Opposing LED chemical sensor and 3 mm indicator LED

The operation of the indicator LED was controlled by the onboard processor. Activation of this LED provides a visual indication of a change in the sensor's response, i.e., presence of a chemical vapour, independent of data relayed to the basestation. It was, therefore, necessary for the node to perform onboard processing of sensed data to determine a change in sensor response. To achieve this, sensed information was compared to a baseline reference point.

Upon node start-up, an initial settling phase of 25 s allowed the sensor to stabilise after handling. After the settling period, the node performed a baseline reference calculation routine that recorded the average of thirty two subsequent sensor measurement values. An indicator LED triggering threshold value was then set to a predefined value below that of the baseline reference. For example, if the baseline reference value was 1800 processor counts (out of 4000), the threshold value for the chemical sensor would be set at a value of 1600 processor counts. The 200 unit (~10 %) offset, which defined the

triggering point, was incorporated purely as an arbitrary switching level to activate the indicator and did not signify a specific chemical species concentration level.

The sample rate of 8 Hz used in the initial sensor test was maintained for the operation of the prototype wireless chemical sensor. Therefore, every 125 ms the detector LED was charged, after which time the emitter LED activated and the discharge of the detector LED was analysed. Data were assembled into data payloads of ten individual samples and transmitted. Concurrently, the measured sensor value was compared to that of the stored trigger point.

If the measured value was less than the trigger value there had been a significant measured change in the colour of the reactive layer, i.e., there had been an increase in the acidity of the air surrounding the sensor. The indicator LED was switched on by setting the I/O pin INT0 high. Removal of the chemical stimulus resulted in the sensor response increasing above the trigger value as the reagent layer recovered. The indicator LED was turned off by switching the I/O pin to a logic low state. The constructed wireless sensor node was tested within the chamber environment to examine its operation when exposed to a plume of acetic acid contaminated air.

4.3.1 Preliminary Trial Results for the Prototype Wireless Chemical Sensor

Acetic acid vapour has a density 2.07 times that of air [137]. It can, therefore, be assumed that a denser than air acetic acid plume entering the chamber at the inlet to the river channel would be largely confined to the vicinity of the channel by the vertical boundaries. Positioning the chemical sensing node on the base of the chamber within these boundaries, as shown in Fig. 4.12, would, therefore, ensure that the stimulus would interact with the chemically sensitive coating of the sensor and cause a response change.

Initial examination of the sensor was conducted without the indicator LED in place. The node was screwed into position and activated. Data logging of incoming packets was started within the Crossbow Scope interface. The CDA inlet feed to the bubbler unit containing acetic acid was manually activated using an in-line ball valve.

The stimulus chemical vapour was allowed to enter the chamber for a period of time, after which the stimulus was turned off and the extraction fan, in conjunction with the

air agitation lines, was turned on. The sensor response obtained over the thirty three minute duration of the test is presented in Fig. 4.13.

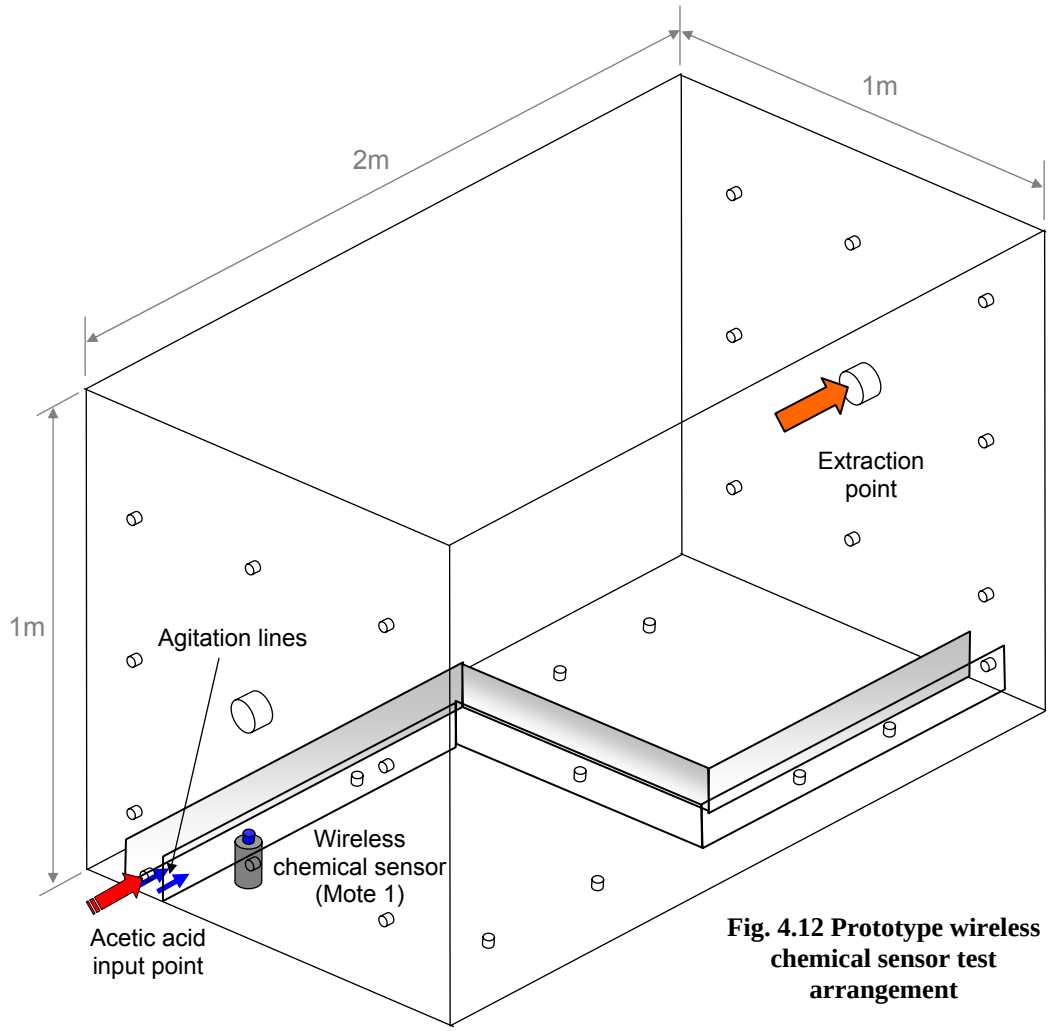

Fig. 4.12 Prototype wireless chemical sensor test arrangement

This sensor response raised concerns about the effectiveness of the device's operation. Distinct response to the chemical stimulus is present in the first 500 s of the test. When the stimulus was removed, the sensor began to recover, as expected. However, the sensor recovered beyond its initial baseline value and continued to drift from this level while exposed to uncontaminated air. Fluctuations in the response were also apparent. In a subsequent test, the status indicator LED was activated when the indicator trigger point, 200 units below the baseline response level of 1715 processor counts, was breached. This affected the sensor's response by increasing the amount of light falling on the detector LED, as detailed in Fig. 4.14. The effect of this was an artificially increased reduction on the detector LED's discharge rate.

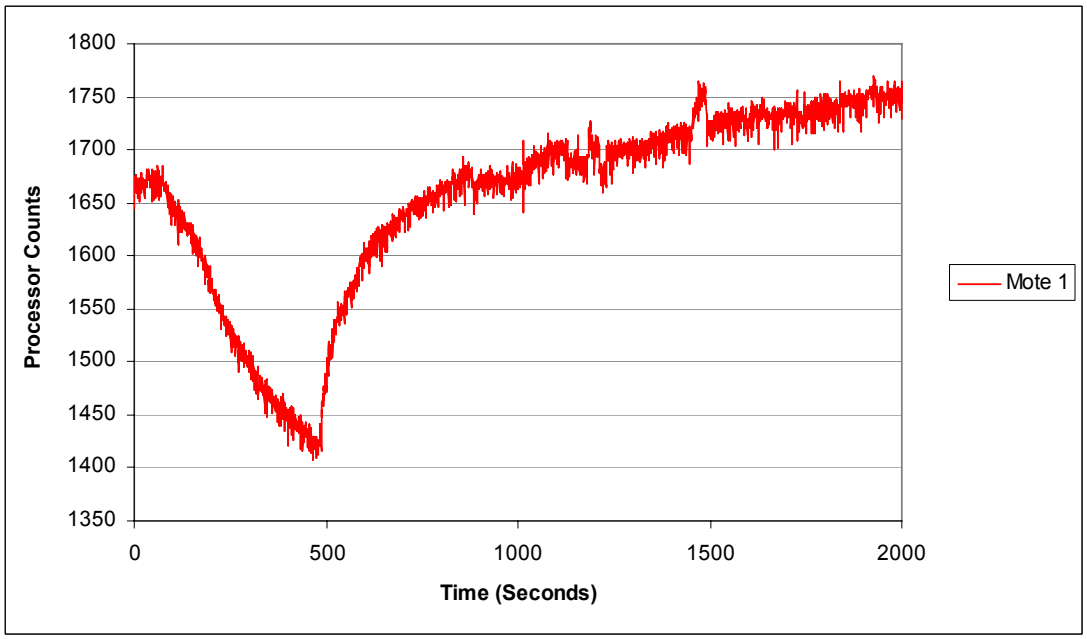

Fig. 4.13 The response of the prototype wireless chemical sensing node to the acetic acid stimulus within the chamber environment

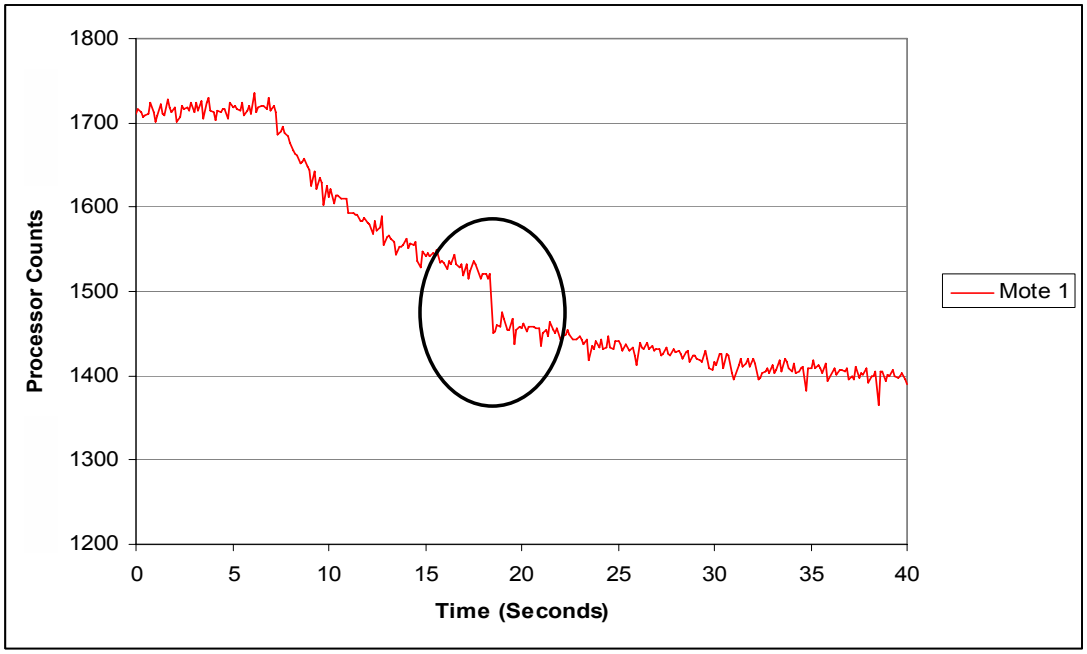

Fig. 4.14 The effect on the sensor response caused by the activation of the status indicator LED

Fig. 4.15 details the drift and response fluctuation effects between 800 s and 1800 s of the initial sensor test. The highlighted random fluctuations in the sensor's response are similar to those observed by the activation of the status LED. As the status LED was not in use during this experiment, recorded fluctuations were likely caused by changes in ambient light. Personnel movements in the vicinity of the test chamber during the

trial period possibly cast shadows over the sensor's location. This had the effect of reducing the level of ambient light, observed as sharp increases in the sensor's response.

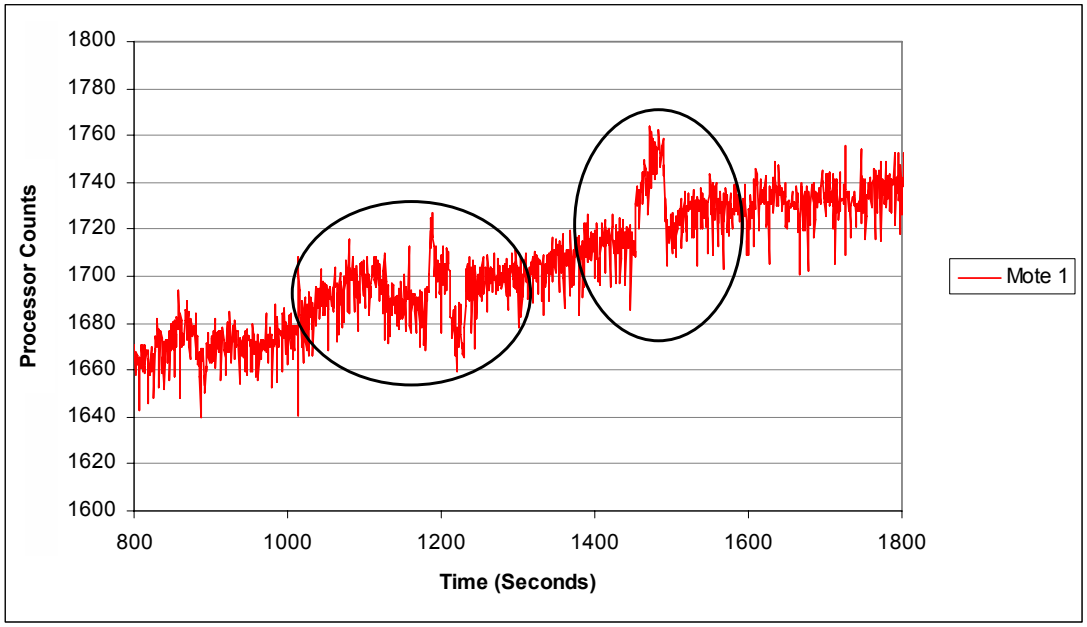

Fig. 4.15 Drift and response fluctuations of the prototype wireless chemical sensing node during operation in a clean air environment

The drift in response over the presented trial period was attributed to the power source. The power source in use during this test was a CR2354 coin cell battery with a rated capacity of 560 mAh. The peak current requirement of this device while in operation would be approximately 21.8 mA, as shown earlier in the power consumption study carried out on the temperature sensing node (Section 3.2.2).

The lifespan prediction, based on the capacity of this battery, would be in the order of 37 hrs. This is significantly longer than the actual continuous operating duration obtained during testing of 1 hr. This can be explained because the magnitude of the continuous current draw was approximately 15 mA. In the battery manufacturer's technical specifications the recommended maximum continuous draw level should not exceed 0.2 mA [37]. Low current draw levels allow coin cell batteries to operate successfully over long periods of time, e.g., in powering a wrist watch. Operating the coin cell battery in the manner that has been shown here, with such a high continuous output demand, greatly reduced the output capacity of the battery resulting in it discharging at a much higher rate than expected. The result of the accelerated drain on

the power supply was a reduction in the voltage applied to the emitter LED and, thus, a reduction in the intensity of light that it produced.

Following these observations, considerable modifications were required to stabilise the device. The required modifications and their implementation are discussed in the following section.

4.4 Wireless Chemical Sensor Node Refinement

The sensor enclosure and operation of the sensing routine were refined to improve the reliability of the chemical sensing node so that it could be used in a real-time reactive wireless chemical sensor actuator network. The requirements in achieving a reliable chemical sensing node, building from the prototype node, were,

- simplification of the node operation,
- reduction of ambient lighting effects, and,
- provision of a more suitable power source.

The operation of the prototype chemical sensor required that the baseline reference value would be calculated onboard, stored in memory and checked against each updated sample measurement. It was possible to perform this task within the custom data acquisition interface operating on the host PC. The node control program was modified so that its operation routine was restricted to performing a sample measurement and transmitting the sensed value.

This routine was integrated into the low power node operation code implemented in the previous chapter. This reduced the onboard processing requirements and also the necessity for averaging routines. When considering a larger group of sensors, (5 node network), by transferring responsibility for data processing to the host PC, it was possible to start any baseline calculation routine simultaneously for each node. This is opposed to the previous configuration where the routine was started upon activation of the node and which allowed the possibility of human movements around the chamber environment to impact on the calculated baseline value by affecting the light falling on the sensor.

It is, however, noted that this communication strategy would be ineffective in a large scale deployment due to the quantity of unnecessary data that would be passed through the network. A large scale deployment would require that a level of processing capability would be placed on the node itself so that data analysis could be performed at the node level. This would allow the node to determine if a change was occurring in the sensor's response and to decide whether this information should be transmitted. This approach is not yet feasible at this stage of the research, as it is necessary to analyse all data being generated by deployed sensing nodes.

The prototype chemical sensor was shown to be sensitive to changes in ambient and artificial lighting. It was possible to shroud the sides and bottom of the status indicator LED using shrink wrap so that its activation would not induce an additional light source that would affect the operation of the sensor. However, this LED component was no longer necessary in the node assembly as a threshold breach indication could be performed within the user interface. To reduce the effects of small changes in laboratory lighting conditions, the sensor would require partial isolation from the overhead lighting. This was achieved using a hood or cover that acts as a shroud over the sensor. Openings in the hood were required to allow moving chemical vapours pass over the sensor and interact with the chemically responsive layer.

The use of a coin cell battery was not sufficient in this application as the minimum current requirement for the sensing node, while in the implemented sleep mode, is 2 mA. This value exceeds the manufacturer's rated consumption level for the coin cell battery. Implementation of a more economical sleep routine would not have provided a solution because these laboratory experiments required relatively high node sensing rates, in the order of seconds rather than minutes or hours. It has been shown that 2 AA batteries can be employed to supply power to a node of this configuration; sensing and transmitting at a rate of 1 Hz for a period of 28 days. Replacement of the coin cell power supply with a 2600 mAh AA battery pack provided a stable power source capable of providing a more consistent operating voltage to the emitter of the sensing node.

The sensing node was operated using a similar sensing routine to that investigated in the wireless temperature sensing network. The sampling frequency (8 Hz) employed in the prototype chemical sensor was also considered excessive. Real-time data were collected and transmitted at a rate of 0.5 Hz. This sampling frequency would allow a data acquisition interface to receive data from a 5 node wireless chemical sensor network at a similar reception rate to that of the developed WSAN investigated in the previous chapter.

4.4.1 Modified Sensing Node and Enclosure

The sensor was interfaced with the modified Mica2Dot platform including the larger power supply battery pack and header pin. The chemical sensor interface board was adapted by removing the status indicator LED and adding a 4-pin plug connector to the

end of the sensor connection wires. The plug connector allows for the sensor to be easily removed from the node when necessary. The unprotected chemical sensing node is shown in Fig. 4.16. An enclosure was later developed to hold the LED sensor in position while accommodating the increased physical size of the node and protecting the electronic components from chemical vapours.

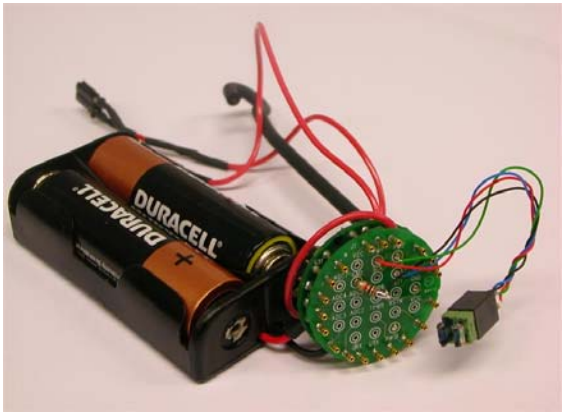

Fig. 4.16 Opposing LED chemical sensor integrated with modified Mica2Dot wireless sensing platform

The area of the enclosure where the sensor was to be mounted was re-designed to reduce the effects of ambient lighting changes. Connection of the sensor node to the chamber via a ¼" BSP connector was maintained. A mounting sleeve was inserted into a double ended connector which had been drilled out to a diameter of 9 mm. The sleeve has a rectangular internal cross section of 5.5 x 5.0 mm used to hold the 4-pin sensor connection plug in place. The sleeve was inserted into the connector to a depth of 13 mm, limited by an 11 mm diameter collar around the sleeve's circumference. The sensor hood, which includes two openings that allow free movement of vapours across the sensing surfaces, was pressed by hand over the exposed portion of the mounting sleeve and held in place by an interference fit. This portion of the node assembly is detailed in Fig. 4.17.

A lower casing was designed to hold the wireless platform, the sensor interface board and the power supply. The cylindrical casing has a tapered top, into which the double ended connector is screwed. This portion is tapered to allow access so that the unit can be easily tightened into position. The wireless platform and associated components were held inside the casing by an end cap. The end cap has openings to allow the mote antenna and the node power switch to protrude through. A semi-transparent view of the completed wireless sensor node enclosure assembly is presented in Fig. 4.18.

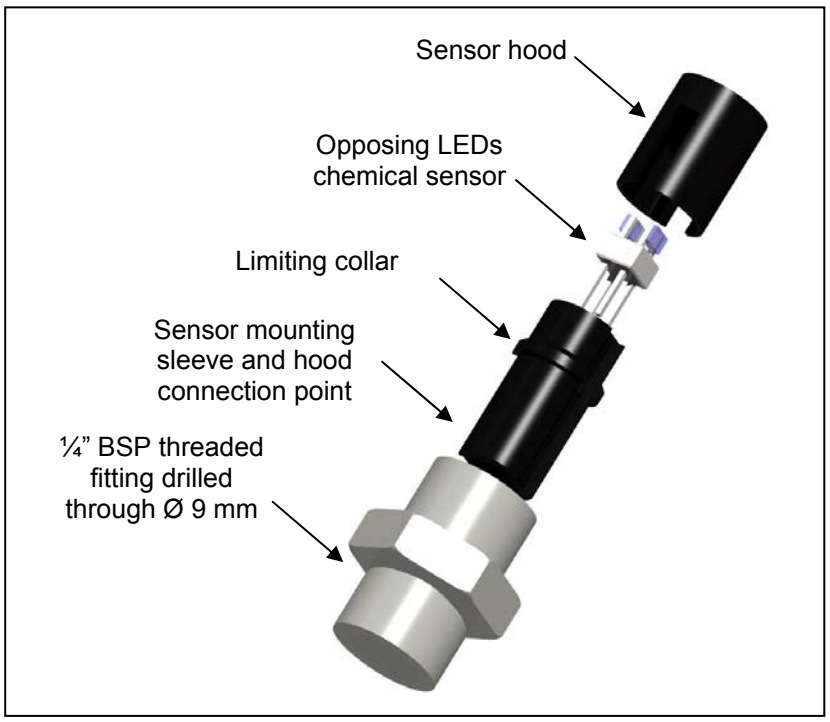

Fig. 4.17 Sensor mounting and protecting sub-assembly of the wireless chemical sensor node enclosure

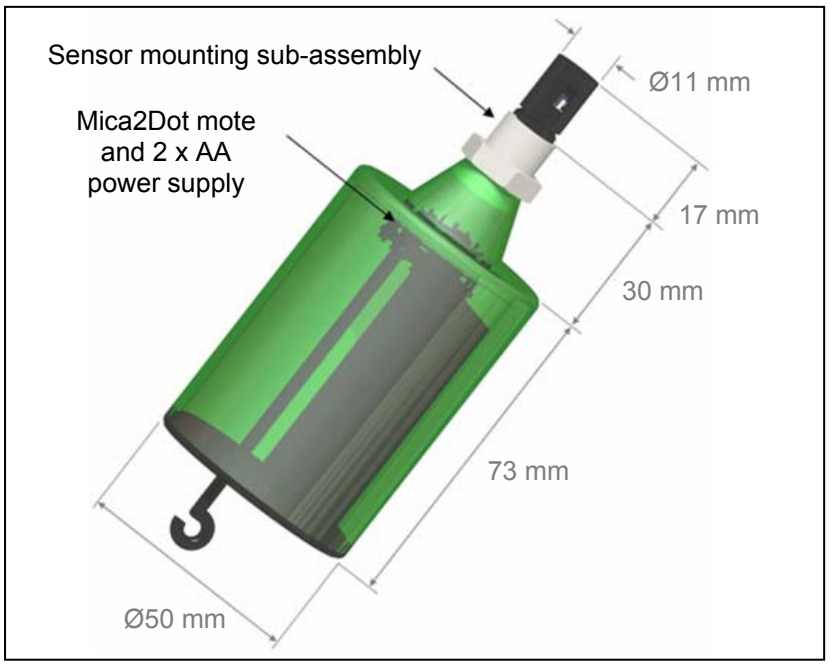

Fig. 4.18 Semi-transparent view of the wireless chemical sensor node enclosure assembly

The component parts of the enclosure, apart from the metallic threaded connector, were modelled using Pro-Engineer CAD software. This software package allowed the generation of .Stl files that represent a component part as layers of material built upon one another. Once saved in this format, the components can be exported to a rapid

prototyping hardware environment where the component can be built layer by layer. The available equipment, a Dimension SST 768 3D printer [138] allowed the production of the component parts using ABS materials with individual layer thicknesses of 0.254 mm. Black ABS material was chosen to form the thin walled hood and sensor mounting sleeve as it would be most effective in shielding the sensor from the overhead illumination.

4.4.2 Modified Chemical Sensor Node Evaluation and Calibration

The first assessment of the modified chemical sensing node focused on the effectiveness of the sensor hood in reducing the effects of ambient lighting changes. Using an uncoated sensor for this test eliminated the possibility of interference in the measuring of the ambient light parameter because of the presence of a chemical species. The node, minus the protective hood, was connected to the bottom surface of the chamber as described in previous tests. A bank of fluorescent lighting over the node location was turned off. The node was activated and data were collected for a period of 180 s. At t = 60 s of the test the overhead lighting was turned on for a period of 60 s. A further 60 s of data were collected with the overhead lighting in its original off state. This assessment was repeated with the shrouding hood in position. Both sets of collected sensor data are presented in Fig. 4.19.

The collected data clearly shows that the overhead lighting affected the response of the non-shrouded sensor for the 60 s period that it was active. This effect was not present in the response of the sensor when shrouded by the hood. This sensor arrangement was, therefore, less susceptible to ambient lighting changes than the prototype wireless chemical sensor node. Due to the increased protection from ambient lighting, the sensor response is only dependent on the light supplied by the emitter LED.

Following on from the trials of the modified node in an uncontaminated environment, the chemical sensor node was exposed to a plume of acidic air for a period of 30 s to ascertain whether it would respond in a similar manner to the prototype sensor. Directly after the chemical stimulus was stopped, the CDA inlet was activated to accelerate the response recovery. Smoothed response data for this test is shown in Fig. 4.20.

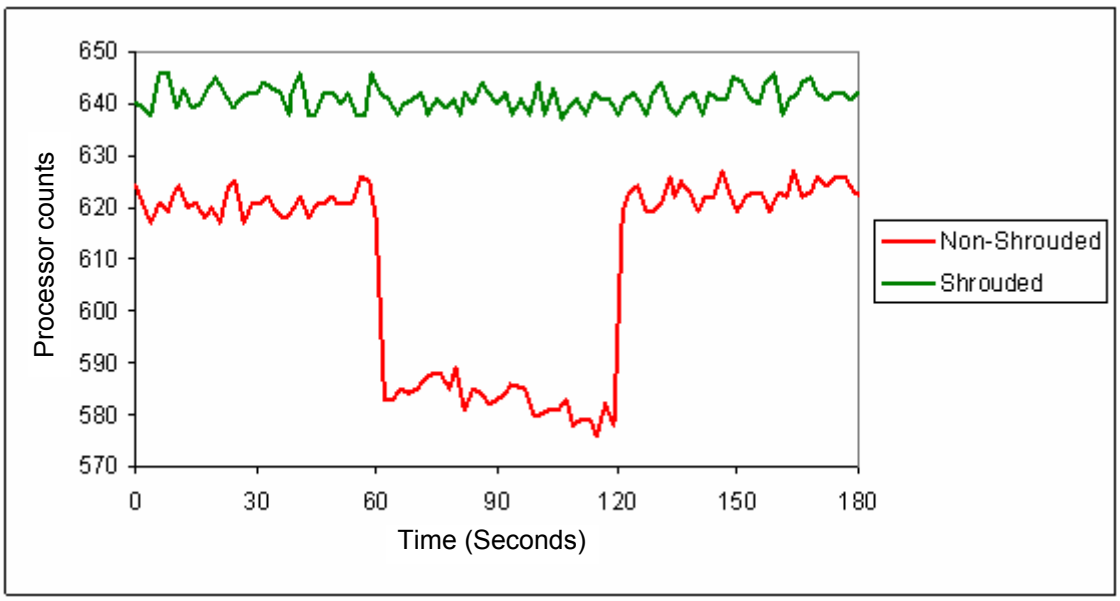

Fig. 4.19 Response of uncoated sensor to overhead lighting changes while non-shrouded and shrouded

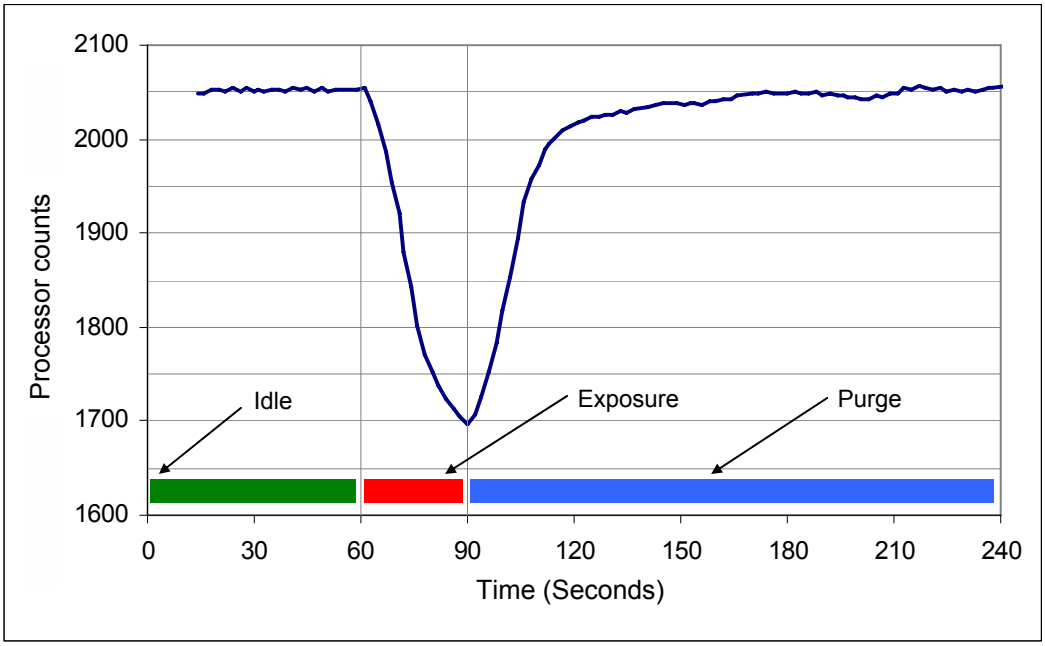

Fig. 4.20 Smoothed response data when the wireless chemical sensor node is exposed to a plume of acidic air for 30 s

The sensor response before application of the stimulus plume between t = 0 s and t = 60 s is stable. After the period of stimulus application, t = 60 s to t = 90 s, the sensor is observed to recover quickly to a level comparable to that of the initial sensor response level. The employed sensing rate of 0.5 Hz is 1/16 that of the prototype node, however, the response to the chemical stimulus remains clearly distinguishable. It was, therefore,

possible to use this sensing rate to gather data of an effective resolution in further monitoring of chemical plumes. This trial was repeated with the sensor exposed to three distinct periods of stimulus plume activity so that the response reproducibility could be examined and detailed in Fig. 4.21.

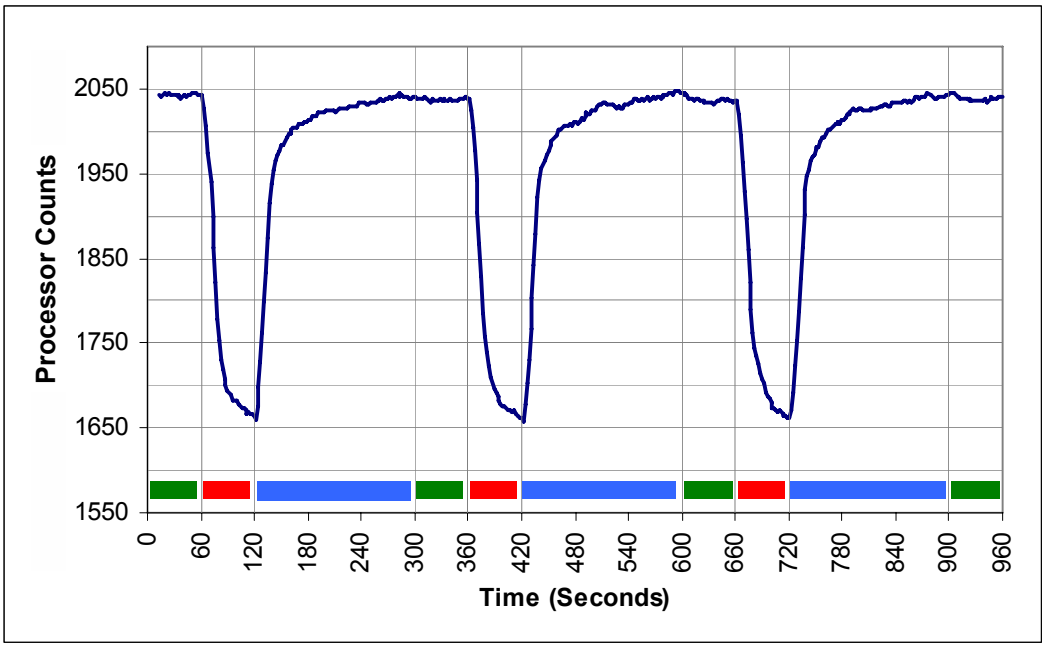

Fig. 4.21 Smoothed response data when the wireless chemical sensor node is exposed to three consecutive plumes of acidic air

The magnitude of the sensor response and its recovery when the chemical plume was removed are comparable over each of the consecutive exposure periods. The relative standard deviation (RSD) or percentage error observed for the three repeated exposures was calculated using Equation 4.1.

$$\%Error = \frac{StdDev}{AvgR} \times 100 \tag{4.1}$$

The average change in response (*AvgR*) over each 60 s exposure period was 378.33 processor counts with the standard deviation (*StdDev*) in response being 2.52 processor counts. The calculation results in a percentage error between the repeated exposures of 0.67 %. Repeating the calculation over the 180 s recovery period yields a comparable percentage error of 0.69 %.

The sensing node, therefore, displays excellent reproducibility. This study shows that the modified sensor is not a "single shot" device and is, therefore, appropriate for real world deployments where it would be necessary to monitor a number of distinct separate chemical events. These successful experiments have displayed reproducible responsiveness to a chemical contaminant and allow for a network of similar devices to be constructed and investigated in further detail.

A chamber with a small internal volume (13 litres), relative to the ESC, was assembled for the purpose of sensor data analysis when exposed to measured contaminant concentrations. The chamber shown in Fig. 4.22, allowed for node response time, reproducibility and limit of detection (LOD) to be tested while also providing an environment within which node calibration could be performed. Node location ports (¼" BSP) were located on the sides of the chamber. A 12 V fan that would disperse and mix the chemical contaminant evenly within the chamber space was located on the base of the unit. The acetic acid contaminant is introduced manually via a septum injection port. Purging of the environment was performed by applying a compressed air supply at a push-fit pneumatic port and opening a similar port at the rear of the small test chamber.

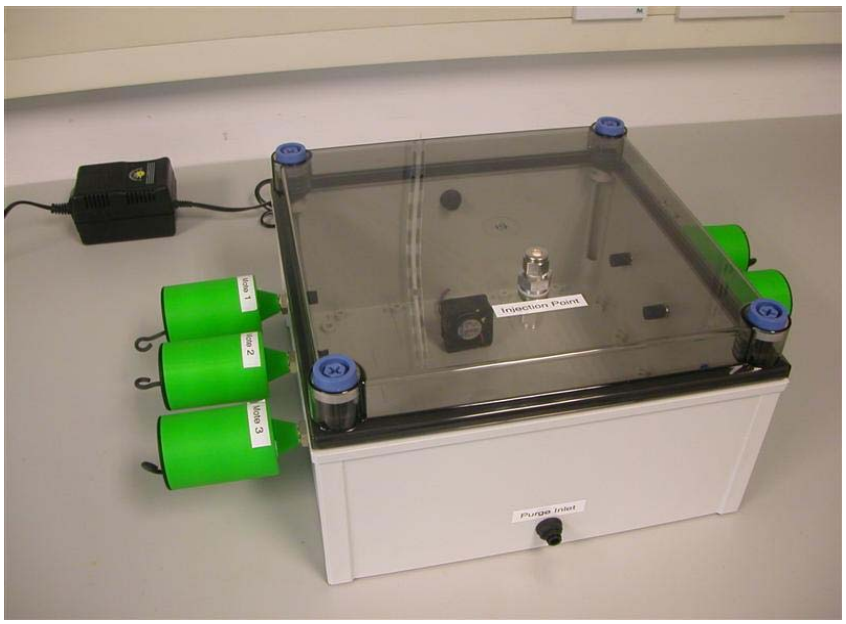

Fig. 4.22 Small volume sensor network test chamber for node response time, reproducibility, limit of detection analysis and node calibration

Sensor response time was examined initially, using two sensor nodes located in the test chamber. One sensor was used as an indicator to inform the operator when the

contaminant was evenly distributed within the chamber. The second sensor was the test device.

A protective hood was placed over the test sensor and sealed against the face of the chamber so that it would be isolated from the contaminated environment, as described in Fig. 4.23. Removal of the hood, by pulling on a wire connected to it, would expose the test node to the seeded volume. It was necessary to perform this test in such a manner because the time taken to disperse the contaminant throughout the chamber affected the response time measurement.

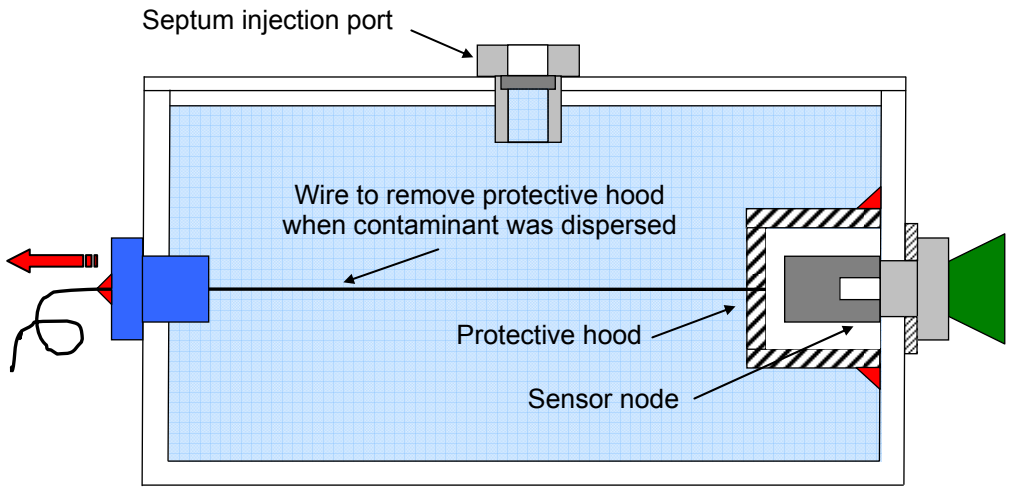

Fig. 4.23 Cross-section of wireless chemical sensor node test chamber with sensor response time test arrangement

A 13 µl volume of acetic acid, corresponding to 1 mg of liquid acetic acid per litre of air (from here on referred to as mg/l), was introduced into the chamber using a 50 µl syringe (World Precision Instruments, Inc. no. 500129) and allowed to disperse over a 300 s time period. At this point, the response of the un-shielded sensor to the contaminant had been at a steady state for a period of approximately 200 s. The hood was removed and the sensor was allowed to respond to the seeded environment. The response of the sensor, normalised over a range of full response (0 to 1), is presented in Fig. 4.24.

The data were processed by calculation of a baseline response value over the first eight transmitted sensor readings. Subsequent readings were then compared to the baseline reference to calculate the percentage deviation in the response. It is for this reason that the change in response is a positive value rather than the "processor count"

representation that resulted in a negative change in response in the presence of an acidic vapour. The response time was specified as the time taken for the sensor to respond to 95 % of full response. The recorded data, seen in Fig. 4.24, indicate this value to be 51 s.

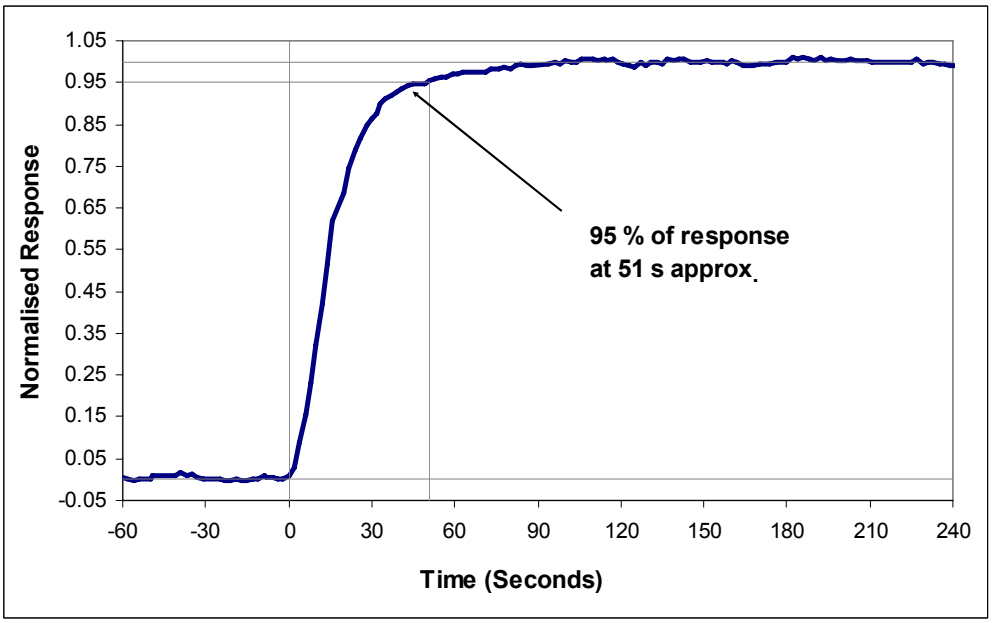

Fig. 4.24 Response time of the low cost wireless chemical sensor to an induced 1 mg/l concentration step change

The reproducibility trial was repeated within the low volume test chamber with a known contaminant concentration and over exposure periods where full sensor response would be observed. The contaminant was applied as described in the previous trial. Removal of the contaminant from the environment between applications was conducted using a compressed air purge supply at the purge inlet (regulated pressure of 1 bar) in conjunction with the opening of the purge outlet at the rear of the chamber. The results of the sensor response to three individual contaminant exposures are presented in Fig. 4.25. Collected data were processed in the same manner, with the percentage deviation in response for the sensor normalised over a scale of 0 to 1.

An initial idle period with no chemical activity is present between t = 0 s and t = 180 s. Three manual injections of the contaminant are clearly distinguishable at t = 180, 900 and 1620 s. Exposures occurred for a duration of 180 s. Purging of the environment took place over each subsequent nine minute period. The percentage error over the three exposures was calculated as 1.76 % (Equation 4.1). Performing this calculation over the first and final exposure yields a significantly reduced percentage error of 0.16

%. Although the initial calculated percentage error of 1.76 % is acceptable, it is likely that human error affected the correct measurement of the 13 µl acetic acid volume applied to the chamber for the second exposure period.

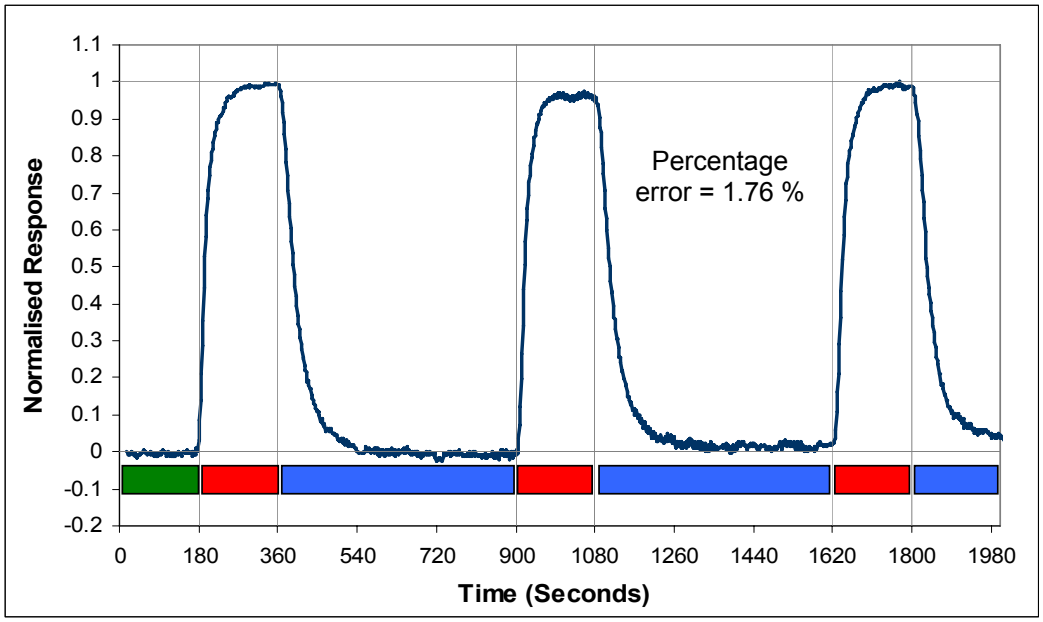

Fig. 4.25 Response data for the chemical sensor node with three consecutive 1 mg/l exposures to an acidic contaminant

In the two previous trials, introduction of 1 mg/l concentrations of acidic contaminant to the test chamber have resulted in significant and clearly distinguishable deviations in sensor response. Therefore, it is reasonable to assume that concentrations of less than 1 mg/l can be reliably detected with the developed wireless chemical sensor node. For this reason, calibration of developed nodes was carried out by means of a series of 0.1 mg/l step inputs to the test chamber.

A lower capacity (10 µl) precision syringe (World Precision Instruments Inc., no. SGE010RNS) was employed to measure the required 1.3 µl volume. Inputs were applied to the chamber at five minute intervals with the dispersion fan in constant operation. Unprocessed collected data are presented in Fig. 4.26. Step changes in response to contaminant introductions are clearly visible. The magnitude of the change in sensor response decreases at higher contaminant concentrations.

Collected data were processed as a percentage deviation from the initial baseline response. This allows for a common reference between constructed nodes, as

individually coated nodes will have differing response characteristics, such as initial baseline level and magnitude of change in response to specific contaminant concentration. The processed data are presented in Fig. 4.27.

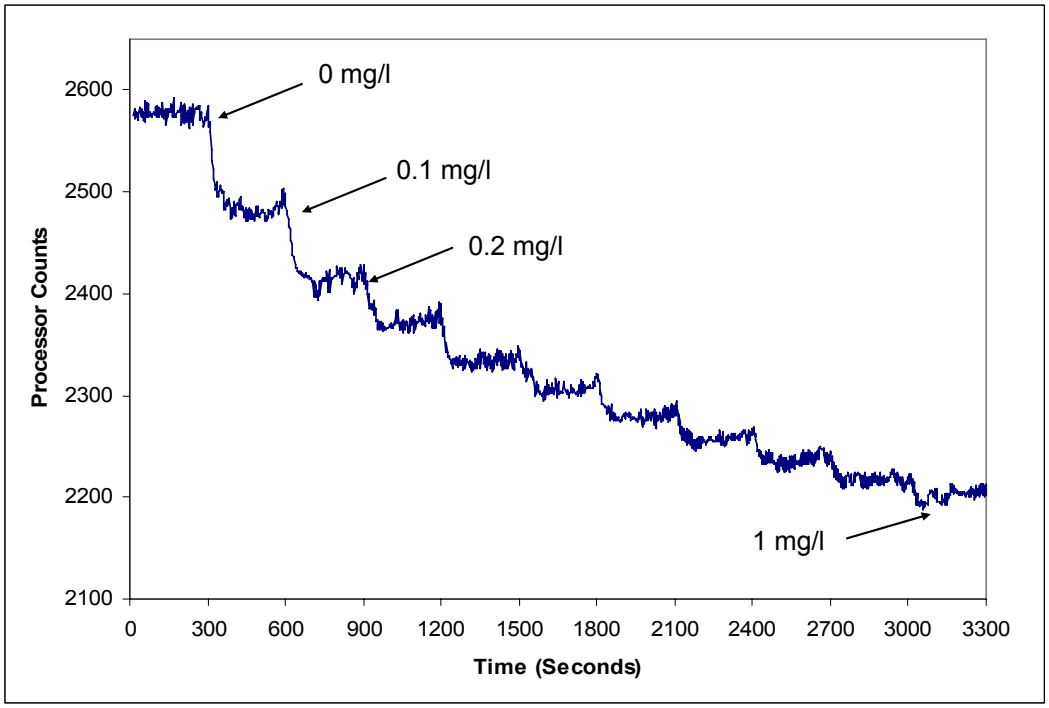

Fig. 4.26 Sensor response to incremental 0.1 mg/l contaminant injections over a 0 – 1 mg/l range

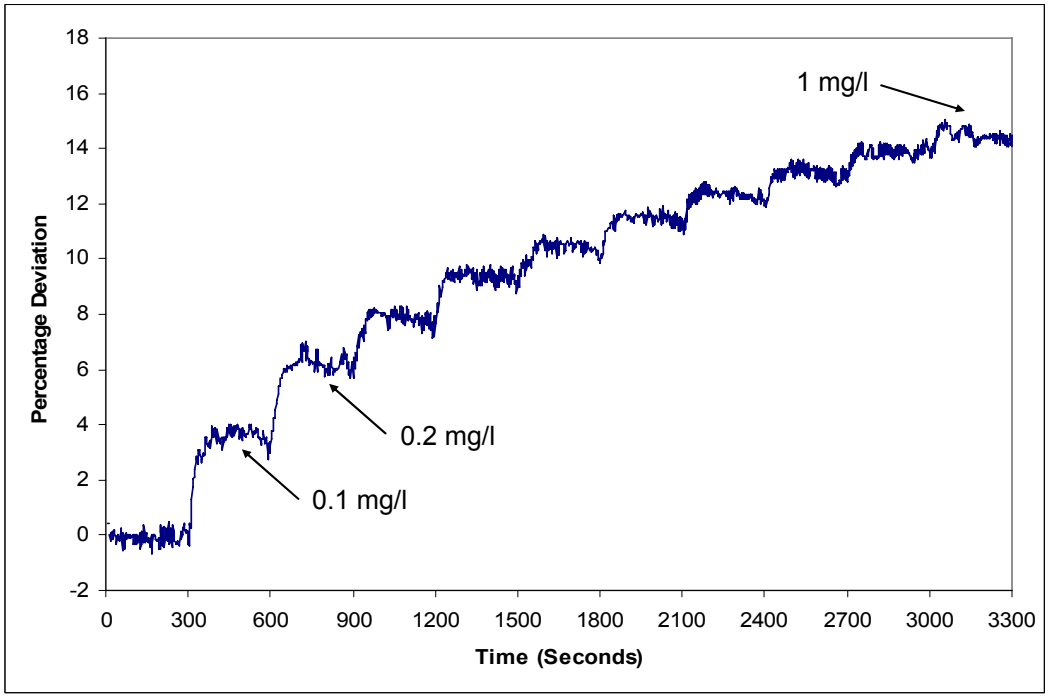

Fig. 4.27 Sensor response to incremental contaminant injections processed as a percentage deviation in sensor response with respect to baseline reference

Data were extracted from this graph to generate a multi-point calibration curve. Each data point was found by calculating the average response level between 200 s and 300 s of each 300 s exposure period. This results in an eleven point data set over the 0 – 1 mg/l range, as seen in Fig. 4.28. A third order polynomial trend line crossing both the X and Y axes at zero was applied to this data set, as also displayed in Fig. 4.28.

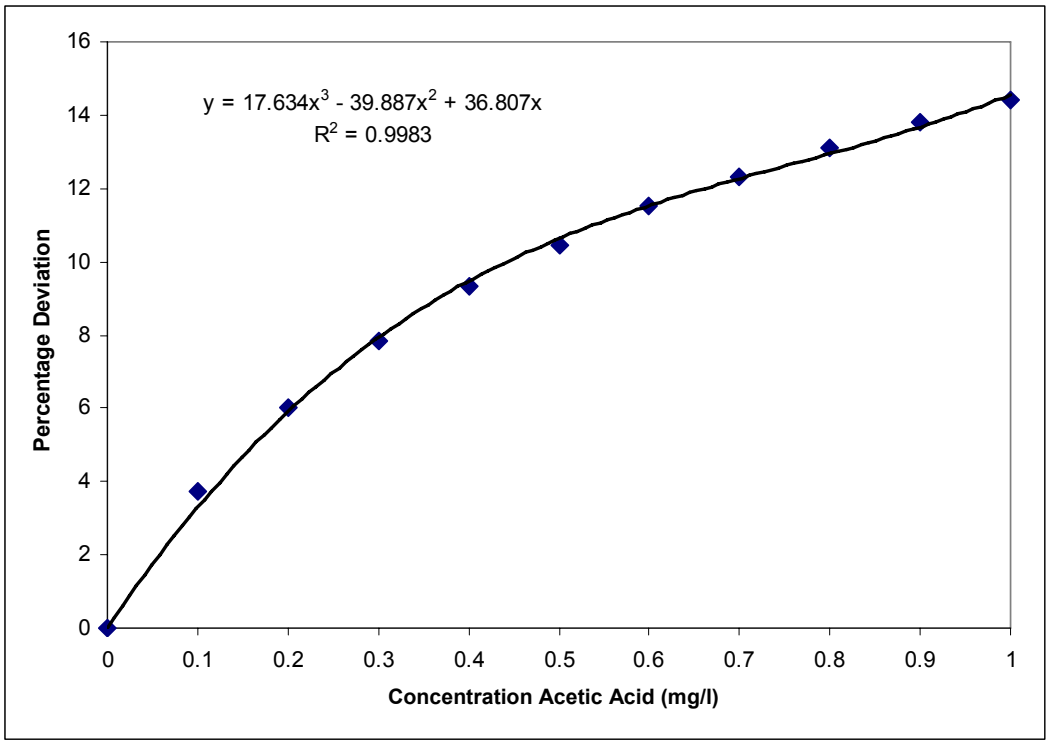

Fig. 4.28 Eleven point third order calibration curve over 0 – 1 mg/l range

The R^2 value of 0.9983 shows excellent correlation between the data and trend line. The equation of the line was later integrated into the data acquisition interface (detailed in Section 4.6) allowing for incoming data to be converted to calibrated concentration levels in real-time. The calibration was applied to the collected data to confirm the applied concentration levels. In order to extract a mg/l concentration level, it was necessary to calculate the real root of the third order polynomial with the constant component of the equation being formed by the recorded percentage deviation in response. The solving process was applied to the collected data resulting in the data set displayed in Fig. 4.29.

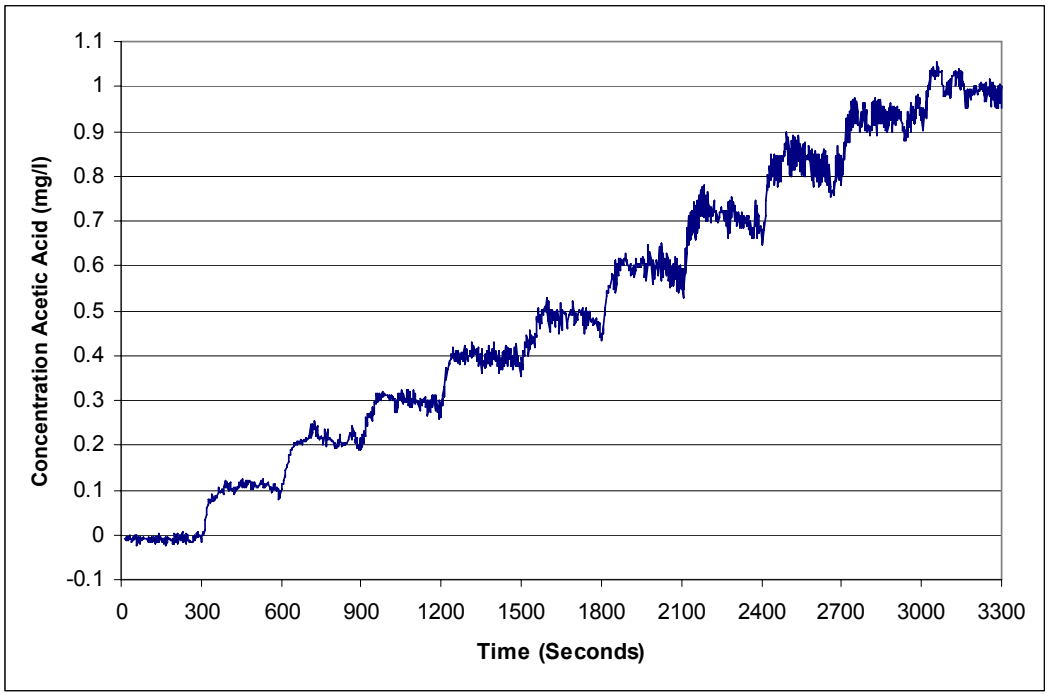

Fig. 4.29 Application of calibration equation to the collected data set

The 0.1 mg/l steps are clearly defined at sub 0.4 mg/l levels. The clarity of definition at specified concentrations is reduced above this level and is due to the non-linear response of the sensor to the contaminant as expressed by the third order polynomial calibration curve. Therefore, at higher concentration levels noise present in the sensor signal was amplified, leading to an unreliable concentration reading.

Four additional nodes were calibrated simultaneously to the same contaminant exposures. The outlined response extraction process was repeated for each set of data resulting in a unique calibration curve for each constructed node. Significant variation between individual nodes was evident because of the non-reproducible surface coating process employed. Their data sets are displayed in Fig. 4.30, and the equation corresponding to each calibration curve is presented in Table 4.1 along with the respective R^2 values.

The LOD of the collective group of developed nodes was investigated based on node response, when operating in an uncontaminated environment. This value was defined as the lowest concentration where the sensor has a signal to noise (s/n) ratio of three [139, 140]. Thus, the LOD is three times the standard deviation in response to an uncontaminated air sample. The standard deviation for each of the five nodes was extracted from collected data and presented in Table 4.2.

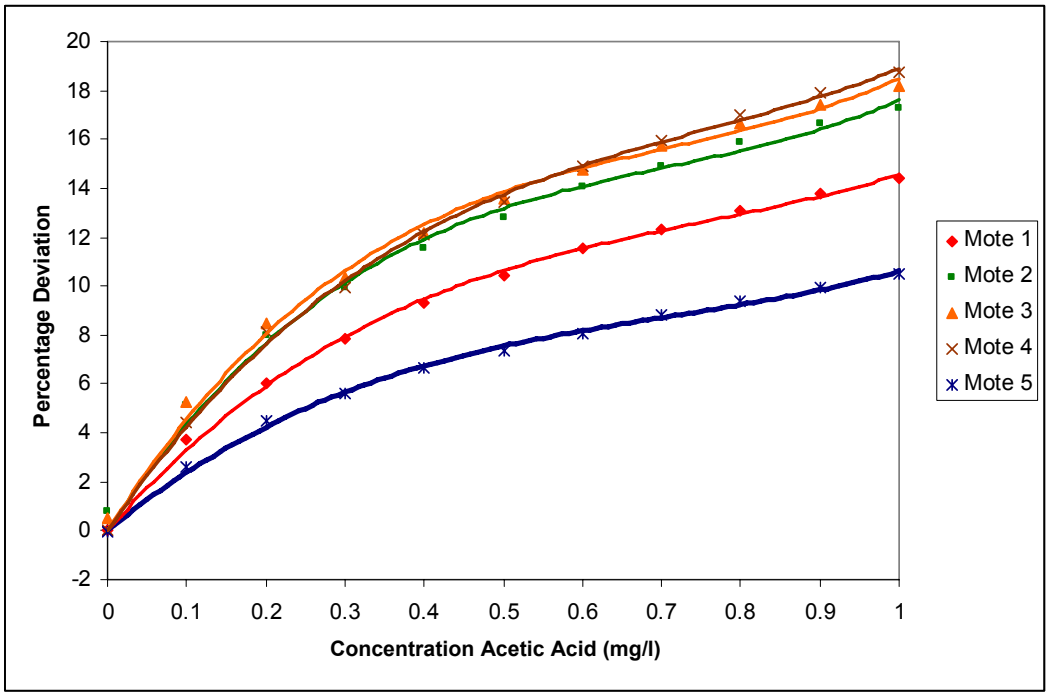

Fig. 4.30 Sensor responses of 5 node network to specific contaminant concentrations with respect to the percentage deviation from the reference baseline

Node ID	Equation	R^2
1	$y = 17.634x^3 - 39.887x^2 + 36.807x$	0.9983
2	$y = 27.889x^3 - 59.368x^2 + 49.070x$	0.9927
3	$y = 28.981x^3 - 61.904x^2 + 51.409x$	0.9956
4	$y = 22.399x^3 - 50.795x^2 + 47.289x$	0.9985
5	$y = 14.264x^3 - 30.376x^2 + 26.719x$	0.9978

Table 4.1 Third order polynomial expressions describing the percentage change in response to controlled concentration levels

Table 4.2 also presents the multiple of the standard deviation for each sensor which corresponds to the individual LOD. The developed nodes display different degrees of noise interference which affected the standard deviations in sensor response and thus individual LODs. Of the five developed nodes, the largest individual LOD is 0.03 mg/l, with the lowest calculated LOD being half this value (Node 3 LOD = 0.015 mg/l). The higher of these values was applied to each node. The percentage change in sensor response corresponding to the LOD concentration level (0.03 mg/l) for each of the constructed sensor nodes has been extracted from Fig. 4.30 and is displayed in Table

4.2. The different percentage deviation levels that correspond to the LOD for each of the sensors further highlights the large variances between constructed the sensors.

Node ID	Standard Deviation (mg/l)	LOD (mg/l)	% Change at 0.03 mg/l
1	0.006	0.018	1.07
2	0.010	0.030	1.42
3	0.005	0.015	1.49
4	0.007	0.021	1.37
5	0.009	0.027	0.77

Table 4.2 Standard deviation, LOD and percentage change values corresponding to 0.03 mg/l in individual sensor node measurements when exposed to uncontaminated air

These measurements show that optimisation of the reagent coating layer thickness and noise cancellation within the sensor signal could potentially, as part of further research, lead to an improvement in the developed sensors LOD. This will be further discussed in Chapter 6 of this thesis.

4.5 Contaminant Plume Concentration Study

For each of the conducted monitoring experiments presented in Chapter 5, acidic air was generated by applying CDA at a rate of 300 ml/min to a bubbler unit containing an 80 ml dilution of acetic acid in the ratio of two parts water to one part concentrated acetic acid. A single outlet was taken from the accumulating headspace of acidic air in the bubbler.

Applying the outlet of the bubbler to an inlet point on the chamber in the same way as that employed for the modified sensor testing allowed for the contaminated air to enter the chamber as a plume. By including a Y-piece connector on this inlet line it was possible to split the chemical vapour so that two distinct inlet points could be applied to the chamber.

The concentration of the contaminant plume entering the chamber was measured using a node integrated into the outlet line of the bubbler unit. A 4-way pneumatic distribution housing, shown in Fig. 4.31, with appropriate ¼" BSP ports, was used to achieve this. The unused port opposite the wireless chemical sensor node was sealed using a suitable blanking plug. The outlet of the bubbler unit was applied to the assembly using tubing connected via 6 mm push-fit fittings. Interaction of the contaminant with the sensor was ensured by orientation of the device so that the sensing surfaces were parallel to the plume flow, as indicated in Fig. 4.32. A schematic of this contaminant concentration test arrangement is provided in Fig. 4.33.

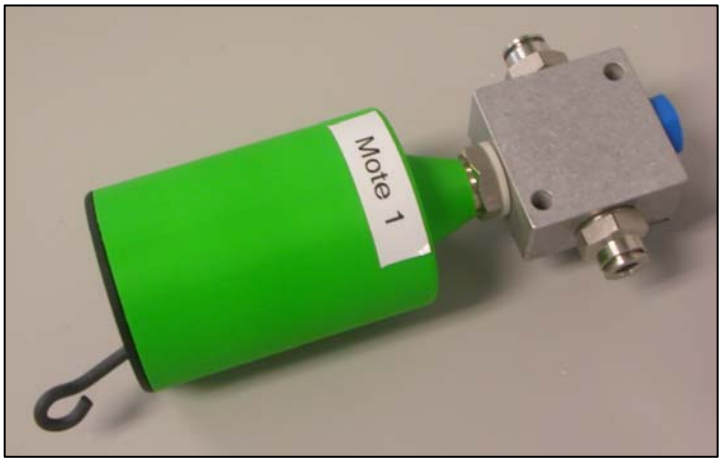

Fig. 4.31 Wireless chemical sensor node in 4-way inline flow housing with 6 mm pneumatic hose inlet and outlet

Fig. 4.32 Opposing LEDs sensor surfaces parallel to plume flow

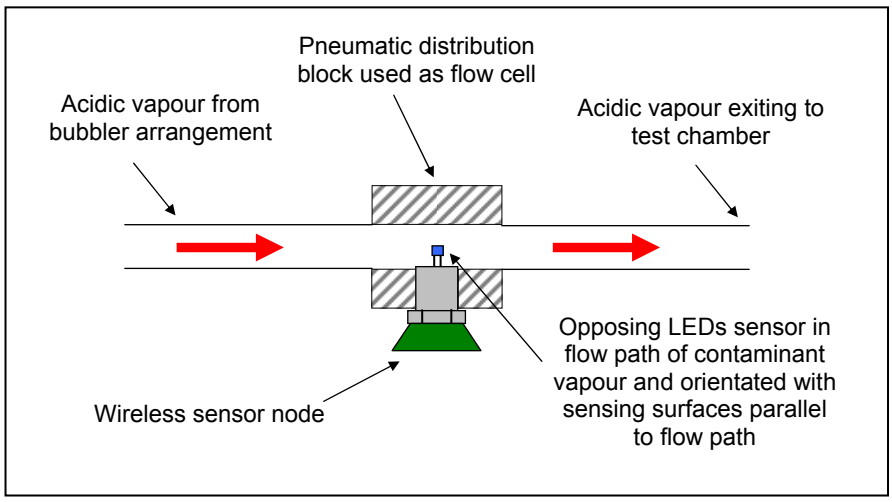

Fig. 4.33 Schematic of sensor in flow housing with flow direction of acidic vapour generated from bubbler unit

Data were recorded while the CDA inlet to the bubbler was active and are presented in Fig. 4.34. The trial yielded a stabilised percentage deviation in the sensor's response of 36.49 %, a value significantly greater than that observed in previous calibration trials. Based on this data, the response of the sensor node was re-examined within the concentration test chamber, used previously in Section 4.4.2, so that the bubbler outlet concentration level could be determined.

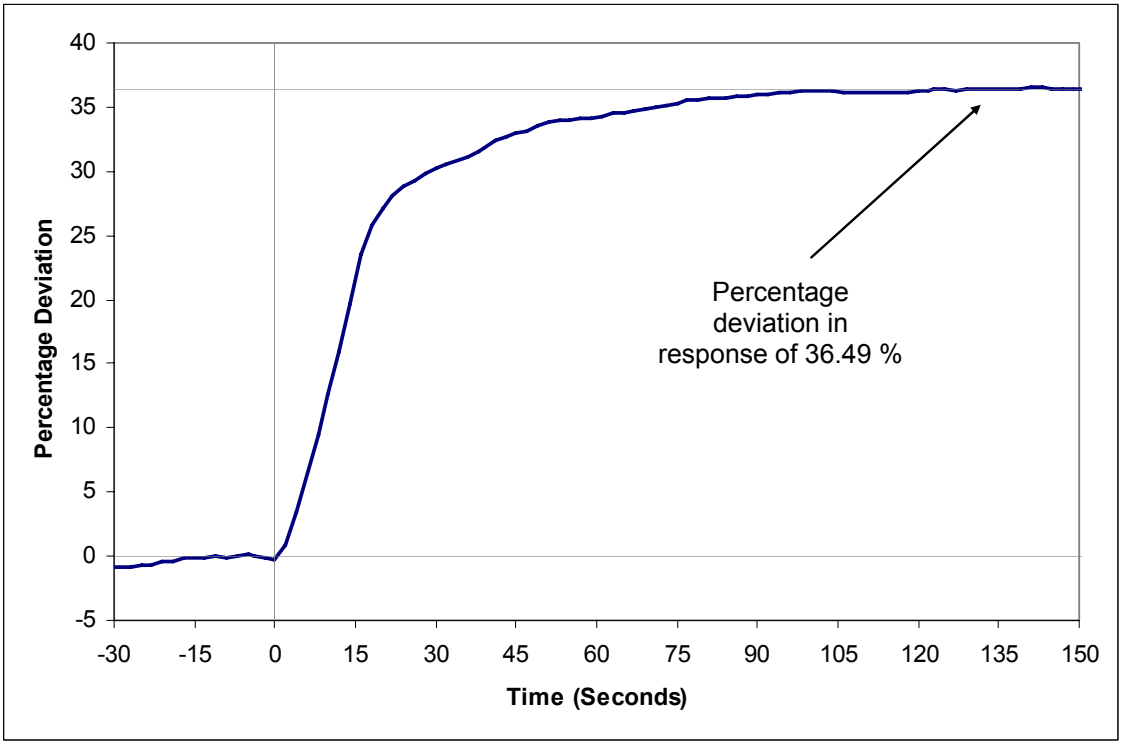

Fig. 4.34 Stabilised response of node directly exposed to generated acetic acid contaminated air contaminant.

The wireless chemical sensor node was exposed to 1 mg/l increments in concentration at five minute intervals over a concentration range of 2 - 7 mg/l. The response of the sensor with respect to the contaminant concentration level is presented in Fig. 4.35. The percentage deviation recorded in the inlet plume concentration test was found to correspond to 6.48 mg/l, as indicated in Fig. 4.35.

From this chemical concentration measurement it can be expected that contaminant concentration levels during monitoring trials, over relatively short exposure periods within the 2 m^3 chamber volume (discussed in Chapter 5), will be at a value less than the measured inlet concentration because of diffusion and dilution of the contaminant within uncontaminated air.

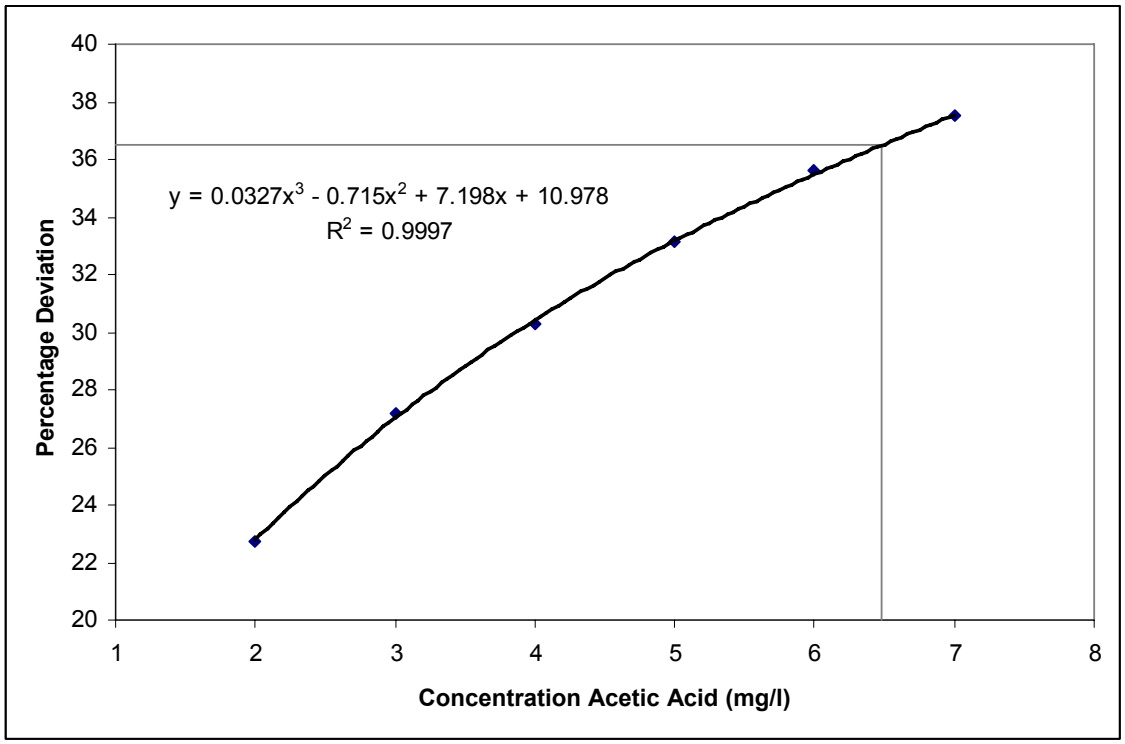

Fig. 4.35 Percentage deviation in sensor response vs. contaminant concentration over 2–7 mg/l range with contaminant concentration at inlet identified as 6.48 mg/l

The measured concentration of the produced acidic air was used to calculate the density of the applied contaminant within a computational fluid dynamics (CFD) prediction model. The construction of the computational model and its resultant predicted plume flow path through the chamber volume is discussed in Section 5.1.

4.6 Wireless Chemical Sensor Network Data Management

The final objective of this body of work is the development of a reactive wireless chemical sensor actuator network. In preparation for this, and to facilitate a means of collecting data from a deployed five node wireless chemical sensor monitoring network, discussed in Chapter 5, it was necessary to have real-time data acquisition and processing capabilities.

An interface was developed to process sensor information transmitted from a five node network operating at a sensing frequency of 0.5 Hz in real-time. The specific functions of this interface were to extract incoming data, log consecutive sensor readings for moving average filtering, calculation of baseline response levels, and in turn, conversion of percentage deviation in response values to chemical concentration levels, as per the calibration equations found through the studies conducted in Section 4.4.2 and presented in Table 4.1. The developed interface is shown in Fig. 4.36. Data extraction and initial processing from hexadecimal values were performed in the background of the user interface. Processed data were presented to the operator on screen and separated into rows based on node identification number.

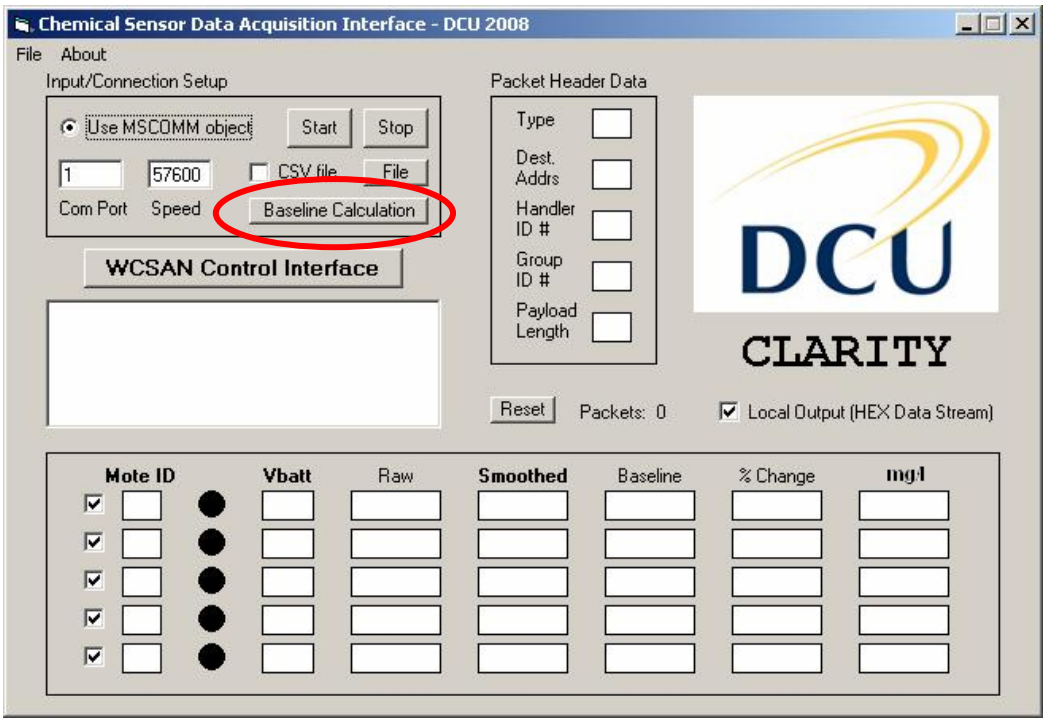

Fig. 4.36 Wireless chemical sensing network data processing interface

Raw sensor values were displayed to the right of the node's current battery voltage level. After eight data packets were received from a particular sensing node, the average of those sensed values was displayed to the right of the raw sensor value in the "Smoothed" column. This value, i.e., the moving average of the sensor data, was updated with the arrival of additional data packets from that sensing node.

Selection of the "Baseline Calculation" button (highlighted in Fig. 4.36) instructed the program to take the average of the next eight sensor readings from a node and store that value as the node's baseline response. Comparison of the filtered data from a node to the corresponding baseline resulted in a value giving percentage deviation in response. This value was then automatically converted to a mg/l concentration, level based on the individual conversion equations found through the study detailed in Section 4.4.2.

4.6.1 Communication Reliability Study

As a final assessment of the refined chemical sensor node, the operations of the constructed nodes were examined over a four hour period to ascertain the level of communications reliability that could be expected with five nodes operating simultaneously in close contact and at a sensing/transmission rate of 0.5 Hz. The four hour period corresponded to 14,400 s and therefore at a sensing rate of 0.5 Hz, a maximum of 7200 data points were expected from each individual node over the trial period. The numbers of successfully received data packets per node was less than this, as shown in Table 4.3. The corresponding percentage of successfully received transmissions from the maximum expected transmissions is also presented.

Node ID	Data Packets Received	Successful Transmissions (%)
1	6823	94.76
2	6828	94.83
3	6901	95.85
4	6831	94.87
5	6891	95.71

Table 4.3 Quantity of data packets received over an extended test period presented both in actual units and as a percentage of total transmitted packets

The average successful transmission rate over the five nodes was 95.2 %. This was considered acceptable as no routine to guarantee packet reception was employed in this laboratory scale wireless chemical sensor network. The quantity of unsuccessful packet receptions was consistent across the five individual nodes and was attributed to packet collisions, resulting from the relatively high data reception rate of 2.5 Hz.

4.7 Chapter 4 - Summary and Conclusions

This chapter has addressed the research objective of developing a stable and reproducibly responsive wireless chemical sensing node. A low-cost acid responsive chemical sensor was fabricated and integrated with the Mica2Dot wireless communications platform. The operation of the initial wireless chemical sensor node was examined through exposure to an acidic contaminant plume. Trials of the initial device highlighted interference and drift effects in the sensor's response. The results of these trials prompted development of a modified wireless chemical sensor node. The communications platform was provided with a suitable power source. The sensing frequency was reduced from 8 Hz to 0.5 Hz and facilitated implementation of the low power node operating program. A final refinement was the development of an enclosure to protect the optical chemical sensor from interference caused by fluctuations in ambient light.

Trials of the modified wireless chemical sensor node were conducted in a custom built low volume chamber. These trials resulted in measured values of sensor response time (51 s), sensor reproducibility (percentage error of 1.76 %) and LOD (0.03 mg/l). Sensor node calibration was also performed over a range of 0 – 1 mg/l. In total, five wireless chemical sensor nodes were fabricated. Due to the non-reproducible reagent coating process employed during fabrication, each node required a unique contaminant concentration conversion equation to convert the value of percentage deviation in sensor response to concentration units of mg/l.

Prior to the plume tracking studies presented in Chapter 5, the trial conducted to measure the concentration of acidic air generated by bubbling CDA through a solution of acetic acid in water was discussed and the concentration at the outlet of the bubbler was measured as 6.48 mg/l.

A user interface for real-time processing of contaminant concentration data was developed through modification of the three node temperature data acquisition interface discussed in Chapter 3. Chemical concentration data are received at the network basestation at a rate of 2.5 Hz. The communications reliability of the developed five node WCSN was examined over a four hour test period. The results of this study indicated that, on average, 95.2 % of transmitted packets are successfully received at the network basestation.

In conclusion, the work described in this chapter satisfactorily demonstrates that the integration of an optical chemical sensing method with a wireless communications platform has successfully resulted in a low cost wireless chemical sensor node. Through the studies discussed in Section 4.4.2, the resultant device has been shown to reproducibly respond to an acidic contaminant vapour. The device can, therefore, be used to detect multiple chemical events over the period of its deployment. The responses of five fabricated devices have been calibrated over a range of 0 – 1 mg/l, and so, it is now possible to gather synchronised contaminant concentration data from the immediate environment of a number of deployed sensor nodes. As the devices were simultaneously calibrated over the same contaminant concentration range, their resultant data sets, when deployed in a contaminated environment, can be examined and compared to data, in the same form, returned from neighbouring nodes.

The investigated wireless chemical sensor node facilitated the development of a Wireless Chemical Sensor Network (WCSN) to track a contaminant plume development within the ESC, which will be discussed in Section 5.2. Furthermore, the development of the wireless chemical sensor node permitted the collection of real-time contaminant concentration data which could then be integrated with the ESC control system to form a real-time Wireless Chemical Sensor Actuator Network (WCSAN). This, in turn, will be discussed in Section 5.3.

5 Wireless Chemical Sensor Network Studies

Current research into Wireless Sensor Networks (WSNs) is only really at the beginning of the journey towards the ultimate goal of global internet scale sensing. The literature reviewed within this thesis has shown that only a few examples of actual WSN deployments currently exist. The deployments that have been reported are small in scale and have focused on the areas of communications and power management [141]. Examples of chemical sensor deployments are extremely rare [142, 143].

The studies described in Chapter 4 have shown that the developed low-cost optical chemical sensor operating on a wireless sensing and communications platform displays responsiveness to a chemical stimulus, namely acetic acid vapour. The design and successful testing of this wireless chemical sensor node has made it possible to explore the monitoring capabilities of a network of these very low cost devices on exposure to multiple chemical plume scenarios. In this way, the fullest potential of the developed system for chemical plume monitoring can be investigated.

It is shown in this chapter that low cost Wireless Chemical Sensor Networks (WCSNs) have applications in chemical plume tracking and contaminant source identification. These applications, which require a high level of spatial and temporal chemical species concentration data, are possible because of the low cost nature of the devices. However, before the vision of distributed low-cost chemical monitoring systems can be achieved, it is first necessary to conduct laboratory scale testing of small scale WCSNs. These studies will prove the potential of WCSNs as a viable means of collecting high resolution chemical species concentration data over a deployment area.

In this chapter, the developed WCSN, constructed from a number of low-cost wireless chemical sensor nodes, is trialled. A computational model was used to inform the designation of monitoring node locations in an initial contaminant monitoring scenario. Two additional chemical plume scenarios will also be examined and discussed.

Subsequently, it is shown how data retrieved from a WCSN can be used to better inform a reactive response mechanism for the removal of a contaminant species from the environment being monitored. A trial to illustrate this further application of WCSNs is facilitated by adaptation of the wireless sensor actuator system, previously discussed in Chapter 3 of this thesis. The study will show the integration of the WCSN and

Environmental Sensing Chamber (ESC) control systems so that they operate together to form a real-time reactive Wireless Chemical Sensor Actuator Network (WCSAN).

A final comparison is made, based on the results of the three monitoring scenarios, between the low cost WCSN and current contaminant monitoring techniques. The comparison will show that the common time domain data retrieved from low cost wireless chemical sensor nodes, when examined collectively, provides a better representation of a contaminants distribution in a monitored area. The comparison also shows that the use of a WCSN eliminates the misinformation that can be inferred from data collected through conventional monitoring techniques.

5.1 Preliminary Modelling of a Contaminant Species Plume

Before mainstream testing of the WCSN could commence, a computational model of the chamber with a single point contaminant source was constructed. The results of the computational model gave an indication of the predicted contaminant plume path within the monitoring environment and were thus used to define an appropriate chemical sensor node layout scheme. This required that a time-dependent simulation be performed to approximate the dispersion of an applied chemical contaminant vapour within the chamber environment over a simulated time period.

A three dimensional mesh of the chamber's internal volume was constructed within Gambit 2.2.30, a mesh generation tool supplied with Fluent 6.1.22 modelling software. The mesh volume included the solid water channel wall features of the chamber and consisted of approximately 600,000 tet/hybrid elements (a mixture of structured hexahedral cells and unstructured tetrahedral cells). Boundary conditions were applied on the appropriate faces. The contaminant vapour inlet was specified as a velocity inlet with a uniform and constant inlet velocity of 0.4 m/s. The outlet of the volume was specified as an unrestricted outflow. Finally the exterior faces of the volume and the water channel partitions were specified as walls.

As a contaminant plume was being modelled, it was necessary to specify a species model. Two species were defined, one as air and, one as acidic air. As discussed in Section 4.5 and displayed in Fig. 4.35, the concentration of acetic acid applied at the inlet to the chamber had a volume of 6.48 mg/l. The extra component in the acidic air species (acetic acid vapour) marginally increased the density of this species when compared with the pure air species. Thus, the density of the acidic air was calculated as the density of air (1.225 kg/m^3) plus the density of the acetic acid present in the vapour (6.48×10^{-3} kg/m^3) resulting in a density of 1.231 kg/m^3.

At a flow rate of 0.4 m/s, turbulent flow was induced within the channel and, therefore, the k-epsilon model was applied. The inlet species was defined as acidic air with a mass fraction of 1. The initial condition of the air filled chamber volume was assigned an acidic air mass fraction of zero. The outlet from the chamber volume, which was open to atmosphere, was specified as an unrestricted outflow, preventing the modelling software from allowing an increase of pressure within the volume.

A period of 100 s of plume inlet activity was modelled with data saved at 2 s intervals. Fig. 5.1 charts the predicted movement of the contaminant plume, applied to the inlet of the river channel, at times of 2 s, 10 s, 20 s and 100 s respectively.

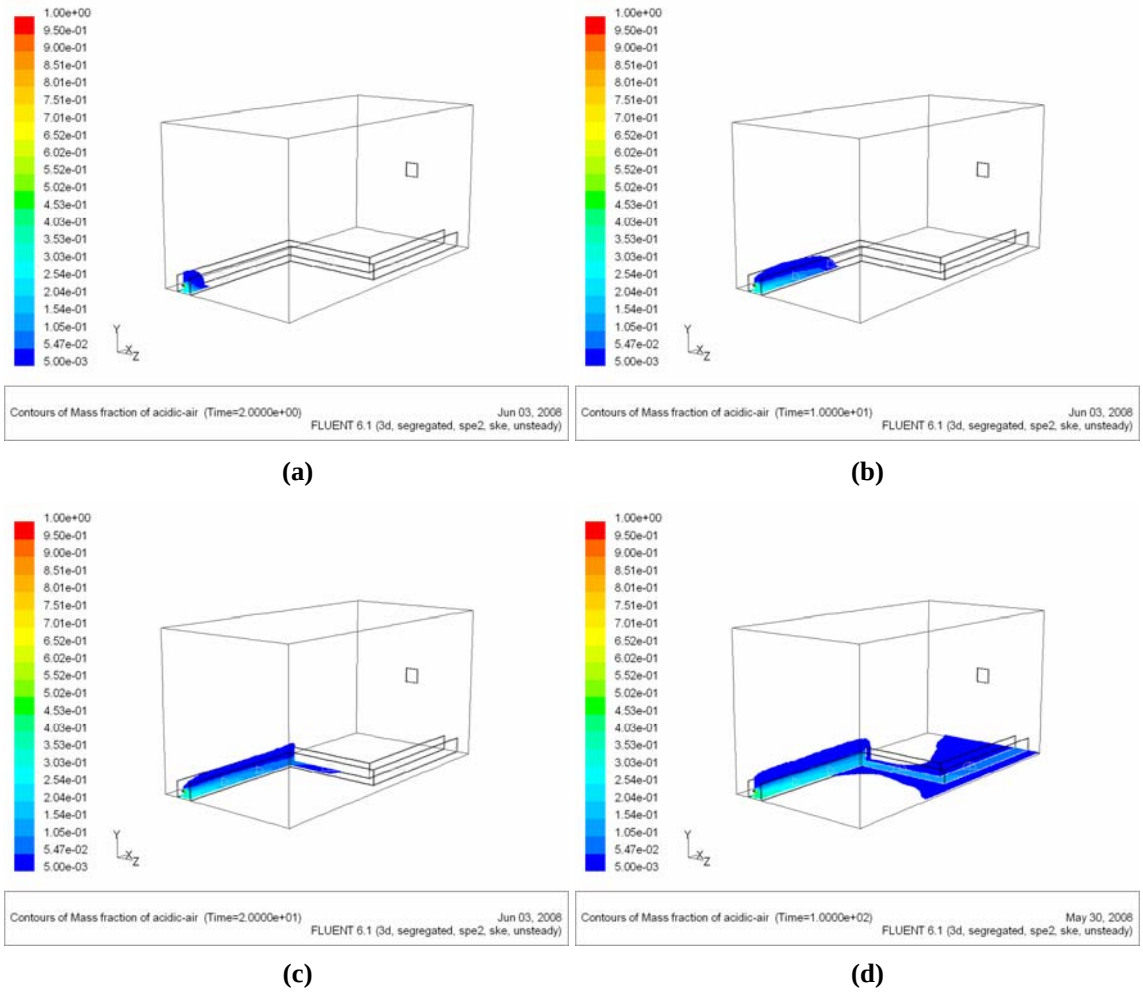

Fig. 5.1 Plume development within chamber over a simulated 100 s time period, (a) t = 2 s, (b) t = 10 s, (c) t = 20 s, (d) t = 100 s

For visual purposes, mass fraction contours are provided in two planes. The first plane is located on the base of the chamber. An additional plane, perpendicular to the base, was positioned through the centre of the inlet. After a period of 2 s (Fig. 5.1a), the initial development of a plume front can be observed at the inlet to the channel. At t = 10 s (Fig. 5.1b), it is evident that the plume front is moving through the channel and is constrained by the channel walls. Shortly after this, at t = 20 s (Fig. 5.1c), the plume front is observed to have travelled approximately half way along the length of the channel. At t = 100 s, the contaminant has travelled the distance of the channel and has

begun to disperse across the base of the chamber, while the concentration of the contaminant contained within the channel continues to increase.

An initial assumption, based on the fact that the contaminant gas was denser than air predicted that the channel walls would constrain the applied contaminant until the channel volume was reached. Fig. 5.1c and Fig. 5.1d indicate that this assumption was inaccurate. Mass fraction data were visually examined at the time step of t = 40 s and are displayed in Fig. 5.2. This representation indicates a breach of the channel wall by the contaminant vapour prior to the plume front reaching the end of the channel. The factors leading to this are twofold. Mixing of the contaminant with air above the channel would be induced by the inflow gas disturbing the air above the entry point. Also, the plume flow would be restricted because of the two 90° bends in the channel, which would lead to a build up of contaminant between the inlet and the first right angled bend in the channel. Once the contaminant built up to the top level of the channel it would inevitably "spill" over the wall because of its higher density relative to the air outside of the channel.

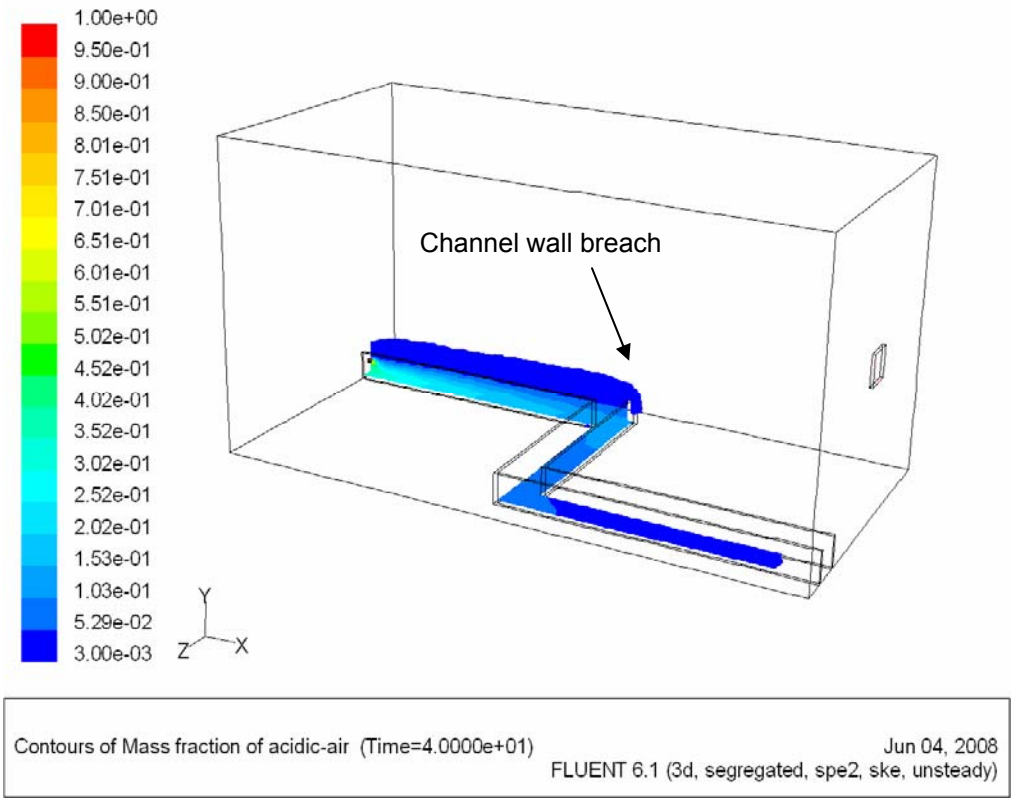

Fig. 5.2 Contaminant plume development at t = 40 s, indicating a breach of the channel wall by the acidic air

The model provided useful information for the positioning of a group of nodes within the ESC. This allowed for an actual contaminant plume scenario, where the contaminant vapour entered the ESC at the inlet to the river channel, to be monitored in real-time. Section 5.2.1 discusses this actual plume monitoring scenario. From the predicted plume path generated by the computational model, it was determined that the best monitoring capability for detection and tracking of the contaminant plume would be achieved by locating the majority of the deployable wireless chemical sensor nodes within the channel feature on the base of the ESC. The predicted breach of the channel wall would be monitored by one sensor node positioned on the base of the chamber outside of the channel path but in close proximity to the first turn in the channel.

5.2 Passive Plume Monitoring Studies

This section focuses on the monitoring of three separate chemical species plume scenarios within the ESC. The studies are conducted using a continuous plume application period followed by purging of the monitoring environment. The initial plume monitoring scenario was designed based on the predicted plume path gleaned from the computational model described in Section 5.1. A further two monitoring scenarios were explored to determine the plume tracking capabilities of the WCSN when exposed to the same contaminant but when applied to the chamber volume in differing arrangements and source locations.

Monitoring scenario 1 sees the response of a deployed WCSN to a contaminant plume in a single source arrangement as modelled in the previous section. The second monitoring scenario investigates the response of the WCSN to two separate contaminant sources. A third, and final, monitoring scenario explores the network's response to a centrally positioned contaminant source. For convenience, the three individual monitoring scenarios are attributed the abbreviations, S1, S2 and S3 respectively.

Data retrieved from the WCSN during each scenario are examined collectively and discussed in detail. In the case of S1, the data are analysed first in their unprocessed state, their percentage deviation in response state, and finally as processed chemical species concentration values. Contaminant plume paths, inferred from the five sensor data sets and, with knowledge of the contaminant source, are presented during each of the discussed monitoring scenarios.

The data gathered during the course of these studies are subsequently used in Section 5.4 where they are examined in comparison to data that could be gathered using conventional monitoring techniques. This examination highlights that during a chemical event, the collective data retrieved from a WCSN would provide a better representation of the contaminant concentration over the dispersion area when compared with the data retrieved using conventional, expensive techniques.

5.2.1 Plume Monitoring Scenario 1: Single Inlet

Based on the predicted plume development data, a network of five wireless chemical sensor nodes were deployed within the chamber and exposed to a single point source originating at the inlet of the channel. The physical layout of the sensor nodes with respect to the plume source, as displayed in Fig. 5.3, ensured a direct interaction of the contaminant vapour with the devices. Sensor nodes 1 to 4 were positioned in sequence on the base of the chamber to track plume development through the river channel. Sensor node 5 was positioned outside of the channel so that a breach of the channel wall by the contaminant plume, as indicated by the CFD model (Section 5.1), could be monitored.

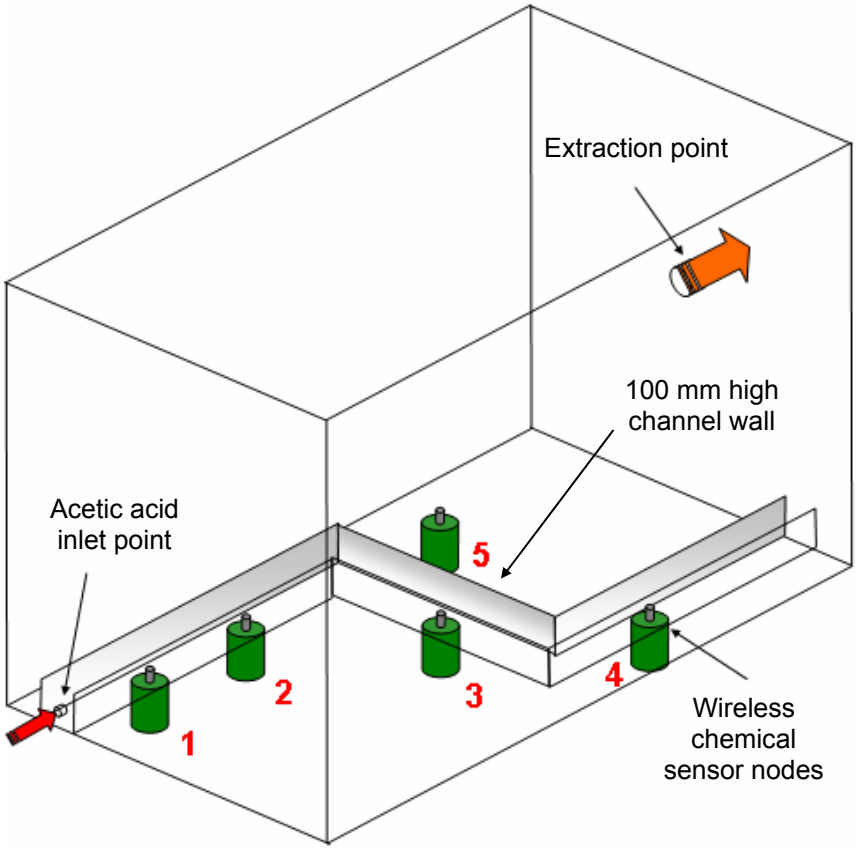

Fig. 5.3 Layout of five node WCSN within the ESC, relative to a point source contaminant inlet

As shown in Fig. 5.3 (not to scale), there was no physical obstruction between node 1 (positioned 330 mm from the plume source) and node 2 (positioned 660 mm from the plume source) that would restrict the movement of contaminated air between these two points. The distance between nodes 2 and 3 through the channel path was 580 mm and included a right-angled turn in the path of the channel. Node 4 was located a further 580 mm from node 3 and included an additional right-angled turn. The location of node

5 was 660 mm from node 2, but the path between these two nodes was separated by the 100 mm high channel wall, as also indicated in Fig. 5.3.

Sensor devices were allowed to operate in uncontaminated air for a period of 120 s. This idle period was employed to ensure stability of the sensors after handling and to determine a baseline response level for each sensor. At the end of this period, the chemical stimulus was activated so that a continuous plume of acidic air was applied to the chamber volume for 180 s. At this point (t = 180 s), the purge system was activated so that the contaminated air within the chamber was removed.

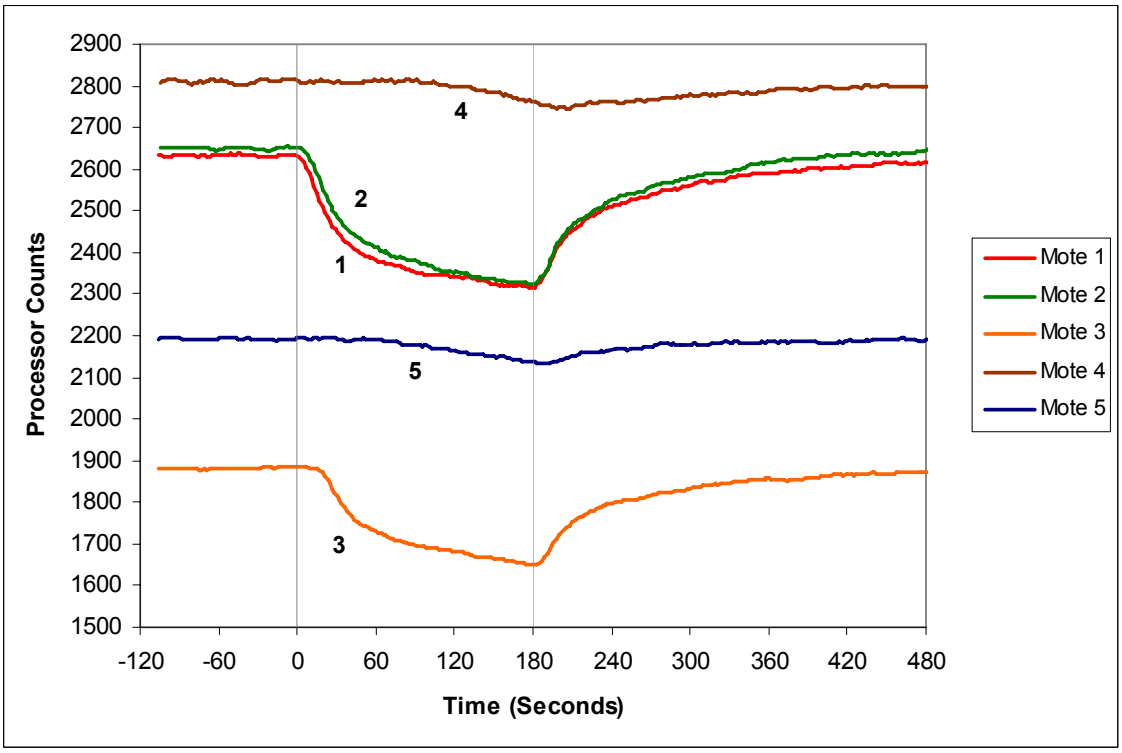

Fig. 5.4 Unprocessed 5 node sensor network response data to a 180 s contaminant exposure period and a subsequent 300 s purge period

Fig. 5.4 presents recorded sensor data from the five node network during the test conducted over a total time period of 600 s. The unprocessed sensor response, i.e., the value of processor counts where the detector LED was in logic high state, for each sample, is displayed on the y-axis of the graph. These data were smoothed using an 8-point moving average to eliminate most of the noise present in the individual responses.

The first observation from this data set is the significant differences in the response levels of individual nodes during the idle period (t = -120 s to t = 0 s). As noted earlier

(Section 4.4.2) the difference in baseline response resulted from the employed sensor coating process. The response levels were, however, stable and displayed no sign of significant interference.

From the point of plume activation (t = 0 s), the recorded response levels across the chemical sensor network were observed to change. Nodes 1 and 2 displayed a similar response characteristic, both in magnitude and rate of response. The response of node 3 was comparable to that of nodes 1 and 2, although, a delay in respect to the time of their responses was apparent. The response of nodes 4 and 5 did not display a distinct change during the plume activity period (t = 0 s to t = 180 s), unlike sensor nodes, 1-3.

Activation of the purge system at t = 180 s resulted in the recovery of all sensor responses towards their initial idle period values over the remaining 300 s duration of the trial. The significant difference in the baseline response values of the nodes masked the magnitude of their response in comparison to each other.

Baseline response values for individual sensors were calculated as an average sensor response during the idle period while exposed to uncontaminated air. Processing the data as a percentage deviation in response from the respective baseline response values yielded the data set presented in Fig. 5.5. This processing operation allowed for a clearer time domain picture of the collected data to emerge, as sensor nodes displayed a common negligible deviation in response prior to the plume activation.

Visual examination of the percentage deviation data after the plume activation point (t = 0 s) allowed trend data, such as the sequential response of sensor nodes 1, 2 and 3 to the chemical stimulus, to become apparent. The data also displayed that the response of node 5 began to change before that of node 4.

Interestingly, these data sets indicated that the response magnitudes of nodes 1, 2 and 3 were similar at the end of the contaminant activity period (t = 180 s). This was contrary to the simulated data, which visually indicated that the degree of concentration observed by the sensor nodes would decrease with increased distance from the plume source. Application of the individual node calibration conversions, detailed in Section 4.4.2, resulted in a plot of specific concentration data which provided a more accurate view of the contaminant monitoring data, as presented in Fig. 5.6.

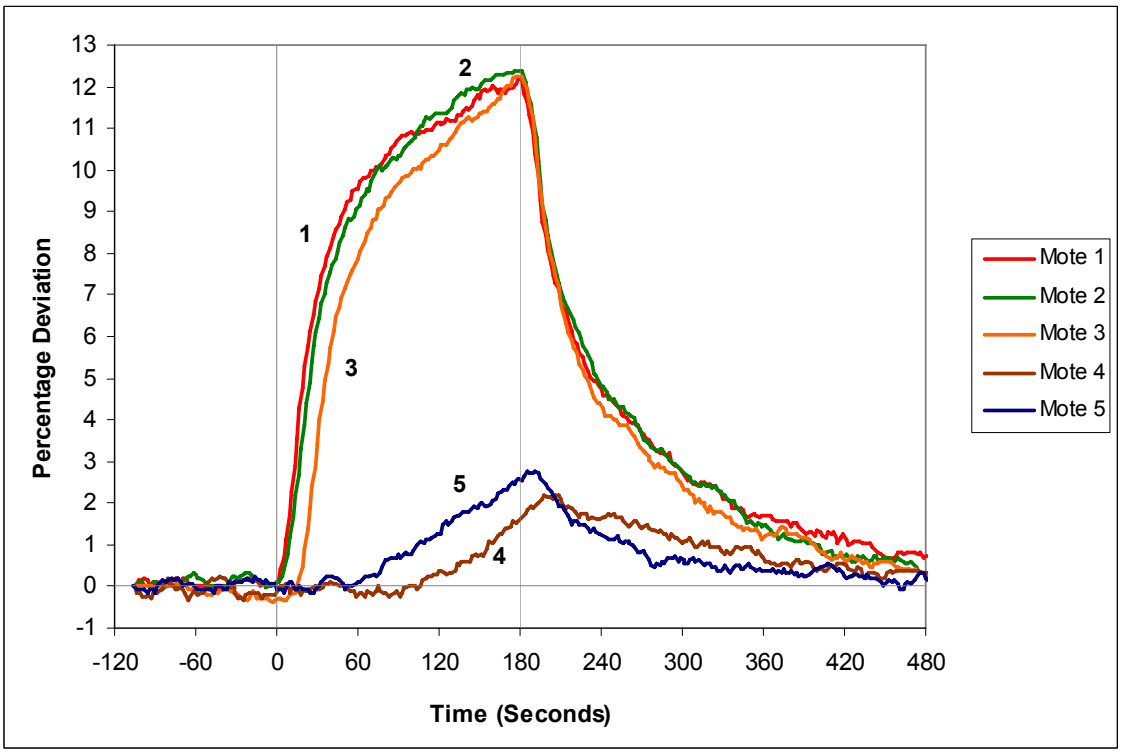

Fig. 5.5 Data from five node WCSN expressed as a percentage deviation from individual node baseline response levels

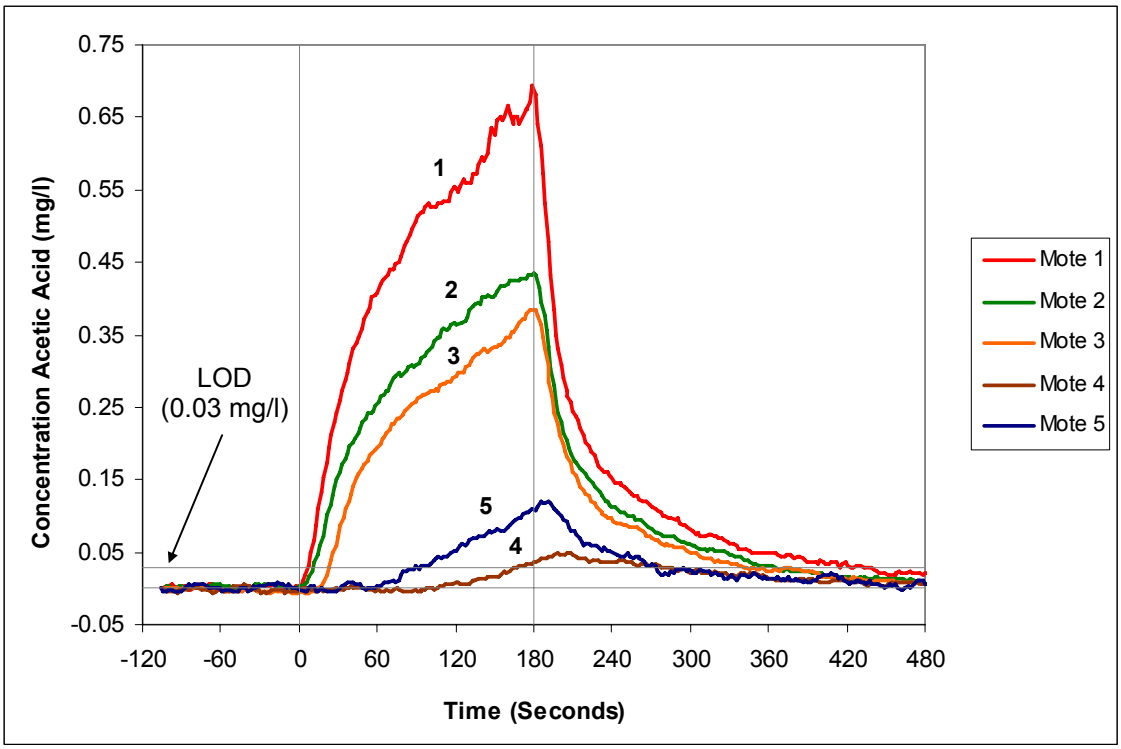

Fig. 5.6 Processed chemical concentration data obtained from a 5 node WCSN exposed to a point source contaminant plume

When analysing the chemical species concentration data, individual sensor activation times were classified as the time interval between activation of the contaminant source

and a sensor node's recorded contaminant concentration level exceeding the LOD (0.03 mg/l). This threshold level has been included in Fig. 5.6 for visual reference.

Sensor node 1 reacted to the chemical stimulus almost instantaneously because of its close proximity to the acidic air inlet. The intervening period between the activation of the chemical input and the resulting change in response of node 1 to a value exceeding the LOD was 7 s. Node 2 also responded quickly to the contaminant. It did, however, take an additional 5 s, with respect to node 1, to respond to the threshold level. Sensor 3 responded in turn, 25 s after the initiation of the chemical stimulus. At this point the sequential response of the sensors was interrupted by the reaction of node 5 to the chemical stimulus. Node 5 was observed to respond at a rate that was less than that of nodes 1, 2 and 3, and exceeded the LOD threshold after 90 s of plume activity. After an additional 79 s (t = 169 s) the contaminant concentration recorded by node 4 reached the activation threshold level.

Throughout the 180 s exposure period, the monitored concentration levels were observed to have constantly increased across each of the five nodes. Sensor responses did not stabilise over the exposure period because of the increasing contaminant concentration within the test chamber volume, resulting from the continually active supply port.

The sequential activation of nodes 1-3 was as expected. The time taken for each of these nodes to respond with respect to their distance from the plume source indicated a flow rate along the base of the channel of 0.04 m/s, one tenth of the inlet flow rate. The response characteristics further correlated with the results of the prediction model (Section 5.1) by displaying a decrease in the recorded magnitude of contaminant concentration with increased distance from the plume source. This is shown through the concentration observed at t = 180 s at node 1 (0.69 mg/l) being greater when compared to that concurrently observed by node 2 (0.43 mg/l). Moreover, at the same time interval, the concentration level at node 2 was higher than that at node 3 (0.38 mg/l).

A distinct characteristic of the presented data is the response of sensor node 5 prior to the response of node 4. This trend was in agreement with the time dependent CFD prediction model. From the response of node 5, it has been inferred that the contaminant breached the channel wall before it dispersed along the base of the channel

to the location of node 4. The rate of response of node 4 with respect to the earlier activation of node 3 also indicated that there was a significant reduction in the plume flow rate after the location of node 3.

This reduced flow rate has been accounted for by the plume flow restriction effect that would have resulted from the second right angled turn in the channel's path (Fig. 5.3). Also of note, is that the magnitude of response of node 4 was significantly less than that of nodes 1 - 3. This was due to dilution of the contaminant caused by mixing of the vapour with ambient air over the distance between the plume's source and the sensor node's location.

The time of individual sensor node activation along with chemical concentration data at t = 180 s extracted from Fig. 5.6 is summarised in Table 5.1.

Node	Sensor Activation Time (s)	Concentration at t = 180 s (mg/l)
1	7	0.69
2	12	0.43
3	25	0.38
4	169	0.04
5	90	0.11

Table 5.1 Sensor activation times with respect to plume activation time and node concentrations at t = 180 s of S1

The activation of the purging system in the ESC caused the chemical vapour to be disturbed. This was observed after t = 180 s as a dramatic reduction in the concentration levels recorded by the five wireless chemical sensor nodes. The rapid response to the purge command at the locations of nodes 1, 2 and 3 was caused by the high pressure CDA, applied via the air agitation lines positioned at the contaminant inlet, dispersing the acidic vapour from the immediate area surrounding these nodes. The delay present in the reduction of concentration levels observed by nodes 4 and 5 during the purge operation resulted from the contaminant vapour, monitored by nodes 1, 2 and 3, being forced through the channel toward these locations by the CDA whilst being removed from the environment. The maximum concentrations recorded by nodes 4 and 5 were 0.05 mg/l at t = 208 s and 0.12 mg/l at t = 191 s respectively.

A visual summary of the plume path, during the exposure period, inferred from the data collected from the WCSN is presented in Fig. 5.7. As the plume entered from the inlet port it began to move through the channel and was initially constrained from dispersing throughout the chamber by the channel walls. Upon reaching the first corner, the acidic plume came into contact with a vertical face of the channel wall. At this point, the constant input pressure at the inlet caused the chemical plume to split. This, in turn, caused a quantity of the plume volume to breach the channel wall, with the remaining volume continuing on through the channel at a lower speed. The breach of the channel was recorded by node 5 at t = 90 s. The slower moving acidic air within the channel eventually arrived at node 4. This occurred 79 s after node 5 responded to a level above the LOD.

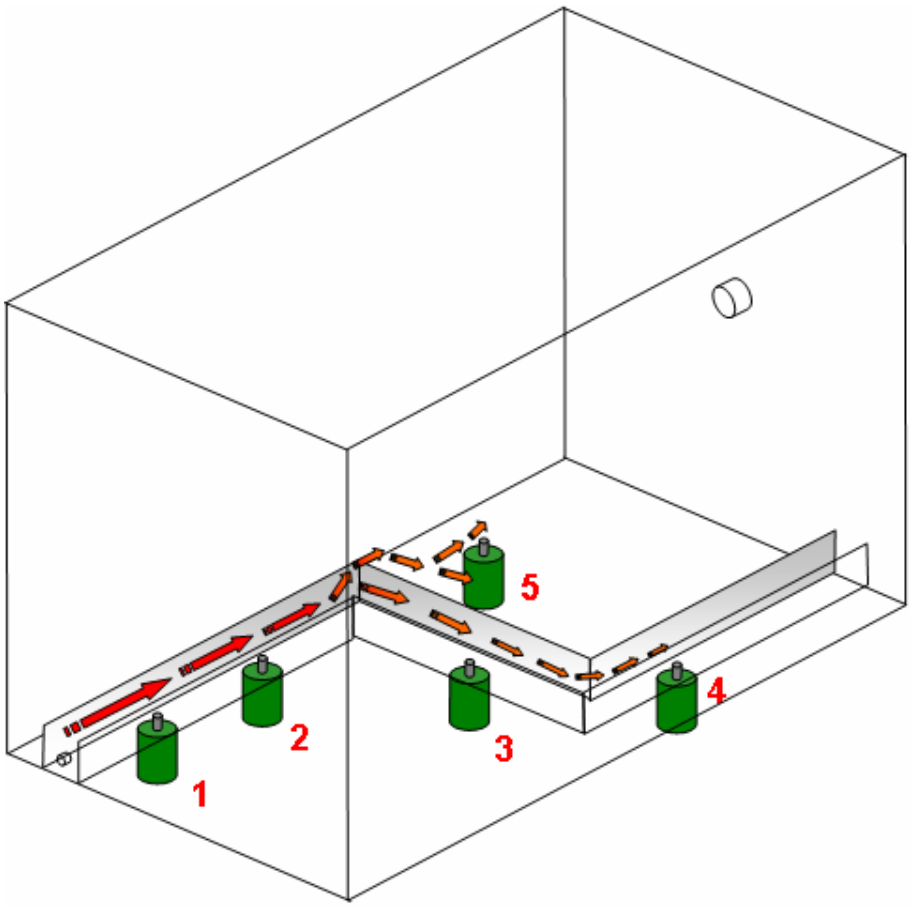

Fig. 5.7 The acidic vapour plume path inferred from data retrieved from the developed WCSN during S1

5.2.2 Chemical Plume Monitoring Scenario 2: Double Inlet

The second contamination scenario saw the chamber environment exposed to acidic plumes originating from two separate locations, which were arranged so that the contaminant would again interact directly with deployed monitoring nodes. Node 5 was relocated to a position within the channel as outlined along with the contaminant inlet points (A and B), in Fig. 5.8.

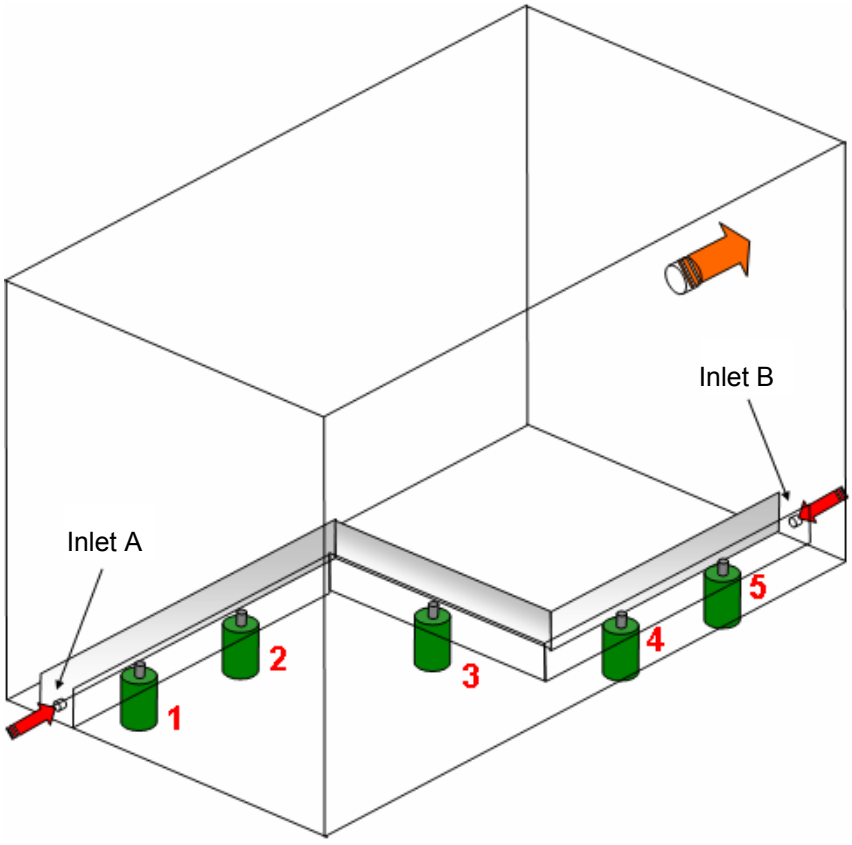

Fig. 5.8 Layout of five node WCSN within the ESC relative to two contaminant source inlets

From this sensor arrangement, it can be seen that nodes 1 and 5 as well as nodes 2 and 4 were equidistant from a contaminant source. As before, node 3 was centrally located in the channel path. It was expected that this arrangement would supply a similar volume of contaminant to both inlet locations during the 180 s exposure period.

For the purpose of continuity, the test routine, exposure period and volume of contaminant applied to the chamber in the previous scenario were maintained. Collected data were processed in the same manner as before and are presented in Fig. 5.9 as a graph of individual node concentrations with respect to time.

The response of nodes prior to the plume application (t = -120 s to t = 0 s) was again stable. Unlike data recorded in the previous trial (S1), where the reaction of node 4, in particular, was slow in comparison to nodes 1, 2 and 3, the data over the plume activity period (t = 0 s to t = 180 s) presented in Fig. 5.9 show that all five nodes reacted to the contaminant less than 30 s after the time of plume activation.

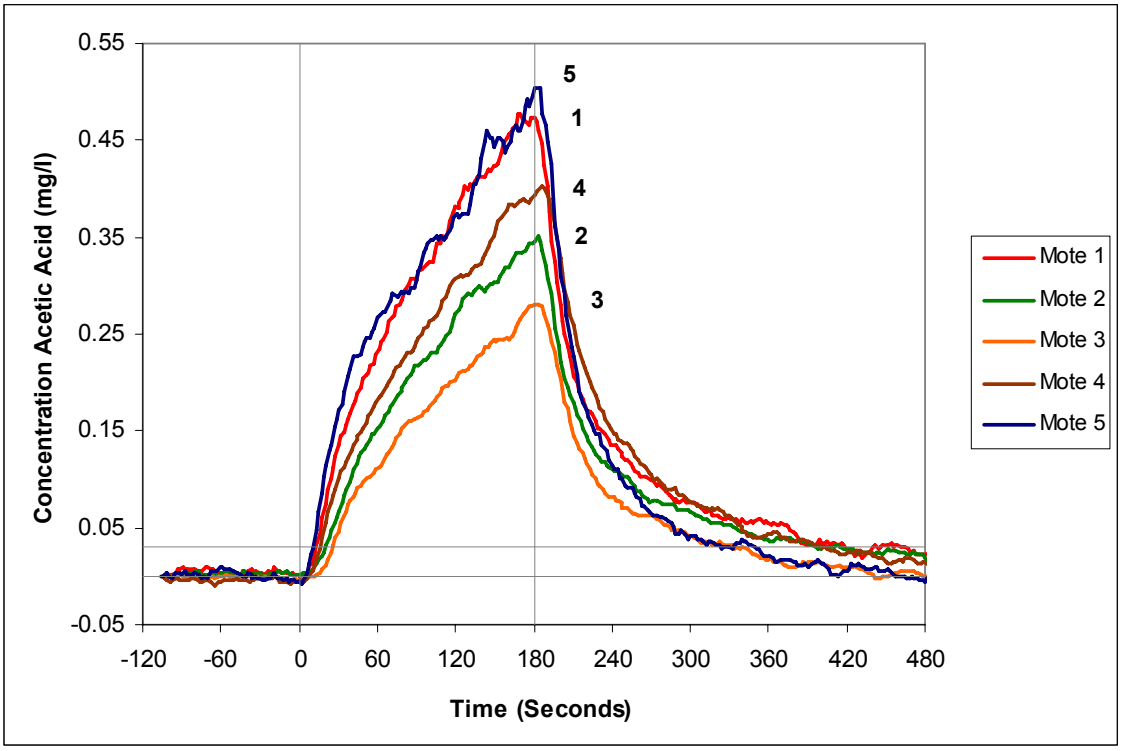

Fig. 5.9 Processed chemical concentration data obtained from a 5 node WCSN exposed to a dual source contaminant plume

The responses of nodes 1 and 5 positioned closest to inlets A and B respectively, were similar, as expected, because of their equidistant spacing from the contaminant source. Node 3, which was positioned furthest from either plume source, took the longest period of time to respond and also recorded the lowest contaminant concentration level.

The time taken for node 1 to exceed the LOD was marginally longer (1 s) than that of node 5. It was also noted that the contaminant concentration at the end of the exposure period (t = 180 s) was less than that recorded at node 5, by a minor value of 0.03 mg/l. Examination of the response of node 2 in comparison to node 4 displayed a similar trend. Node 2 exceeded the LOD at t = 21 s whilst the response of node 4 exceeded the same point after 18 s. The concentration recorded by node 2 after the exposure period was also less than the concentration observed by node 4 at the same time.

Comparison of the data between nodes 2 and 4 indicated that a larger volume of the contaminant was applied at inlet B. This was not as expected, and has been attributed to a restriction in the supply from the bubbler outlet to inlet A caused by a number of bends in the supply tubing. This is supported by the more rapid response to the contaminant of nodes 5 and 4 in contrast with nodes 1 and 2.

Node activation times and contaminant concentration levels at t = 180 s for scenario 2 are presented in Table 5.2 along with applicable data from scenario 1 for ease of comparison.

	Monitoring Scenario 1		Monitoring Scenario 2	
Node	Sensor Activation Time (s)	Concentration at t = 180 s (mg/l)	Sensor Activation Time (s)	Concentration at t = 180 s (mg/l)
1	7	0.69	14	0.47
2	12	0.43	21	0.35
3	25	0.38	26	0.28
4	169	0.04	18	0.39
5	n/a	n/a	13	0.50

Table 5.2 Sensor activation times and node concentrations at t = 180 s for monitoring scenarios 1 and 2

Examining the data of the dual contaminant source scenario with reference to the single source scenario showed that the time taken for nodes 1 and 2 to react had increased. In addition, the maximum concentration observed by these nodes was reduced. This was a result of the reduced flow rate at inlet A due to the split output of the bubbler. The activation time of the centrally positioned node (node 3) was very similar in both trials (activation at t = 25 s in S1 and at t = 26 s in S2).

No provision was made for examining concentration levels in the area outside of the channel walls, and for this reason data from node 5 during S1 has been omitted from Table 5.3. As the flow rate at the inlet points was reduced, the disturbance effect caused by the inflowing contaminant would have been lessened in comparison to S1. The lessened disturbance effect would have reduced the rate of contaminant mixing with air

above the inlets. Reduced mixing of the contaminant would have allowed the channel walls to constrain the contaminant's dispersion and delay a breach in the channel wall. To confirm this, the concentration levels recorded by the sensor nodes within the channel path at the end of the plume activity period for both monitoring scenarios were compared.

To compare the contaminant concentration levels within the channel path between S1 and S2 the recorded concentration levels at t = 180 s were summed. Examining the concentration level in the channel at the end of the exposure period of S1 showed that nodes 1-3 displayed a significant concentration level, while node 4 recorded a concentration level of 0.04 mg/l. If node 5 had been placed in the channel in the position after node 4 it would have recorded a concentration level similar to, or less than that of node 4. Therefore, the concentration level in the position after node 4 for S1 was taken as 0.04 mg/l.

Comparing the summed concentration values of 1.58 and 1.99 for scenario 1 and 2 respectively showed that a higher overall contaminant concentration was present within the channel during the second exposure period. As the same volume of contaminant was applied to the environment in both cases, this indicated that the lower inlet flow rate of scenario 2 resulted in a greater proportion of the contaminant being constrained by the channel walls during this trial.

A summarised plume flow path based on the data collected over the exposure period of S2 is presented in Fig. 5.10. Two separate contaminant sources induced a flow of acidic air towards the centre of the channel. Due to the geometry of the channel and the positioning of nodes relative to inlets A and B, similar response characteristics were displayed by nodes located the same distance from either inlet, e.g., node 1 and node 5.

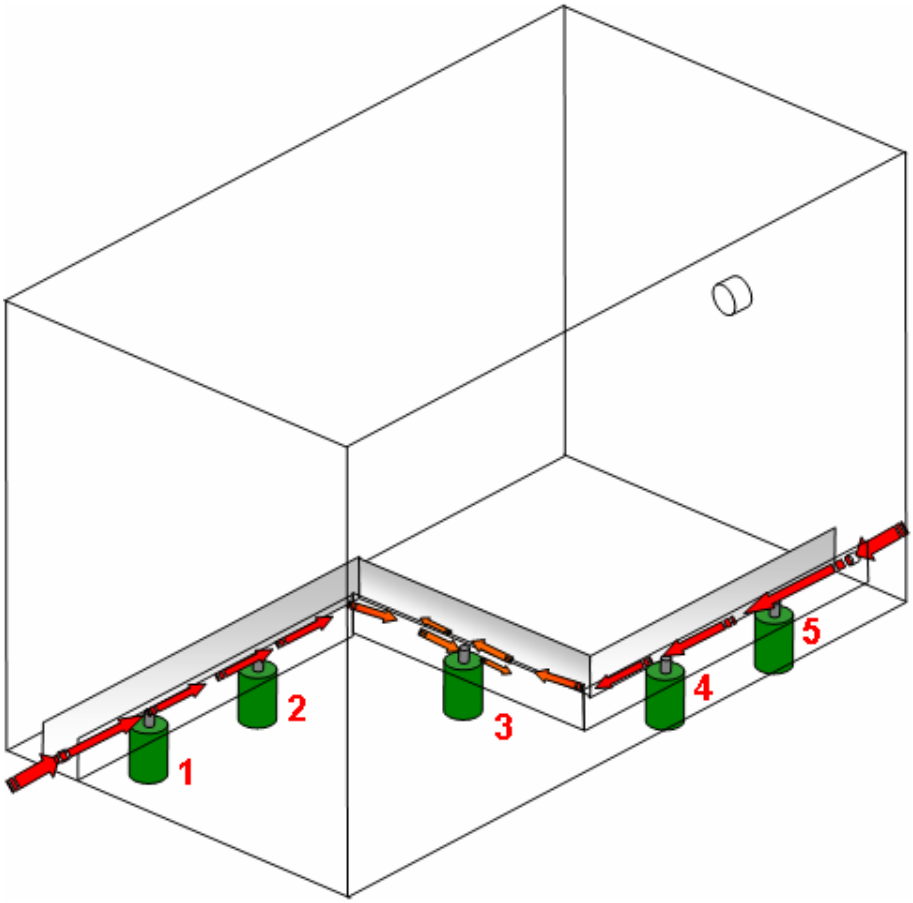

Fig. 5.10 Plume path inferred from data retrieved from the developed WCSN during monitoring scenario 2

5.2.3 Chemical Plume Monitoring Scenario 3: Central Inlet

The final passive plume monitoring scenario investigated the response of the chemical sensor network to a single inlet positioned centrally on the channel base with an initial vertical plume movement. Intuitively, it was felt that, as the velocity of the applied vapour decreased it would return to the base of the chamber because of gravity and disperse outwards from the plume source. A vertical cross-section of this expected plume dispersion pattern is depicted in Fig. 5.11.

In the case of the ESC, the channel walls located on the chamber base would certainly affect a radial dispersion pattern by acting as an obstacle to plume flow as a contaminant vapour returned towards the chamber base. However, it was anticipated that positioning nodes equidistant from the plume source, with the same geometric obstacles between them and the source, would result in similar concentration characteristics being monitored by nodes with a common distance from the source, as found in the previous monitoring trial, S2.

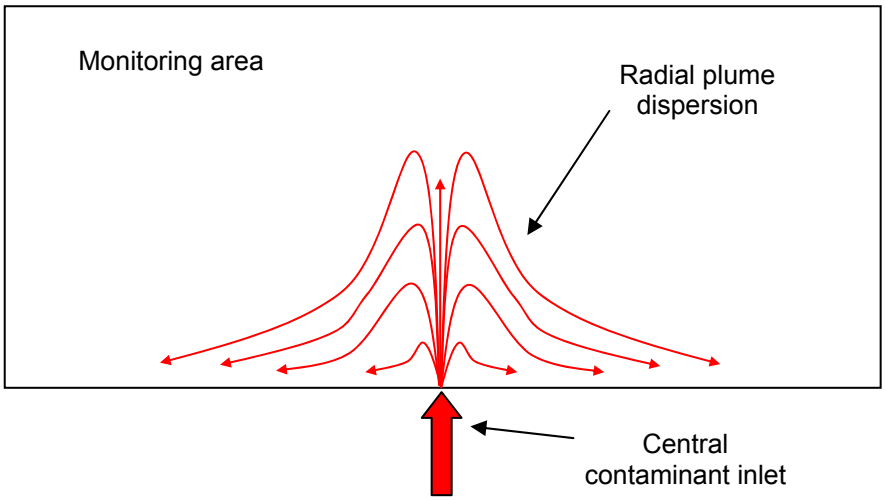

Fig. 5.11 Cross-section of expected plume dispersion resulting from central inlet contaminant application

Nodes were deployed along the chamber base, as identified in Fig. 5.12. Node 5 was located on the extraction face, 200 mm above sensor nodes 1-4 to detect a contaminant above the predominant monitoring plane of the chamber base. It was expected that forced mixing of the contaminant with air above the inlet location would result in a greater dilution of the acidic air in comparison to that seen in the two previous trials. For this reason, the exposure period was extended to 300 s; ensuring that the diluted contaminant would interact with the deployed nodes.

The collective responses of the network are displayed in Fig. 5.13. Unlike the previous trials, there was no distinct change in the sensor responses directly after activation of the chemical stimulus, i.e., in the first 30 s of plume activity. The expected dilution of the contaminant resulted in the general magnitude of responses across the network being significantly less than that observed in both of the previous trial scenarios.

The relatively stable response signal around 0 mg/l obtained from the deployed nodes was again observed during the 120 s idle period. The response characteristic obtained over the 300 s exposure period showed that uniform radial dispersion of the contaminant across the chamber base did not occur. The plume dynamic inferred from the response data was, therefore, not as expected and is discussed further.

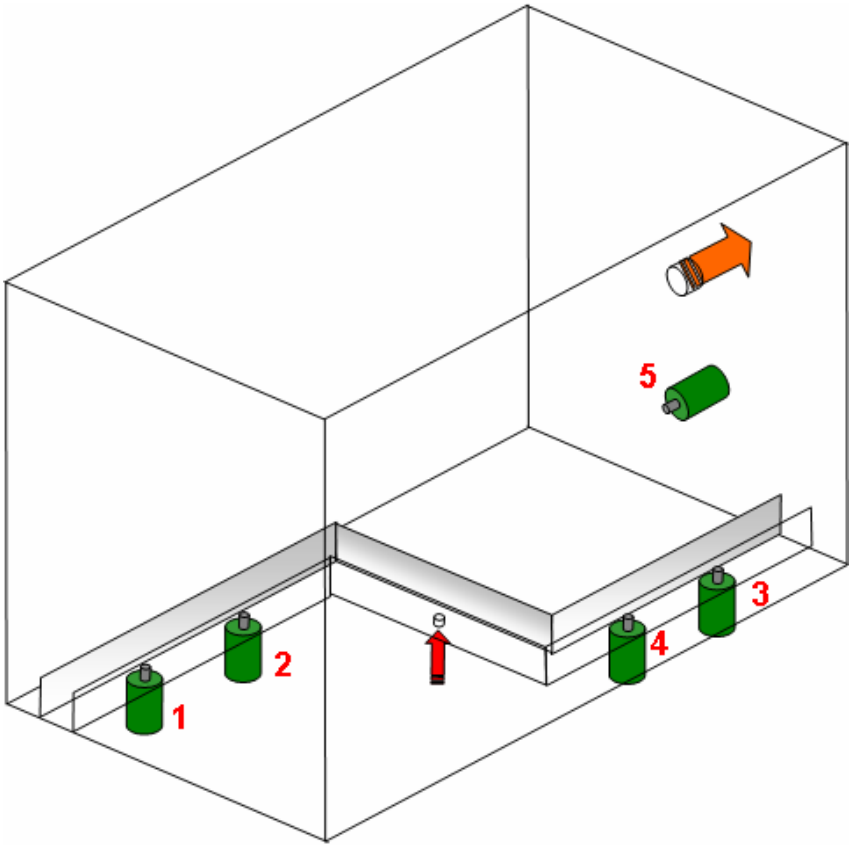

Fig. 5.12 Layout of five node WCSN within the ESC relative to a central point source contaminant inlet

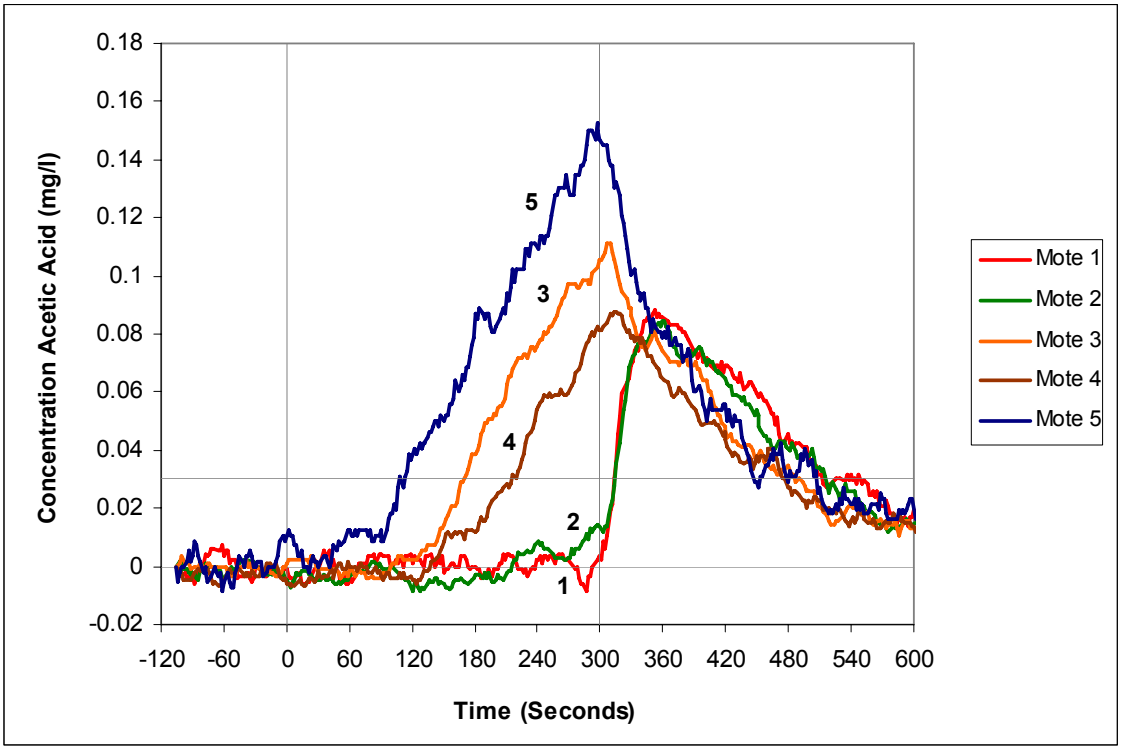

Fig. 5.13 Processed chemical concentration data obtained from a 5 node WCSN exposed to a central source contaminant plume

Node 5, positioned below the chamber outlet, recorded the first response to the contaminant after 109 s of plume activity. The response of this node, prior to a change in response of nodes closer to the source indicated that the contaminant descended across this node from a height above its location. This response, in itself, is not out of keeping with the anticipated radial dispersion, as the inlet velocity of the contaminant could have forced the vapour to interact with the top surface of the chamber. This would have, in turn, deflected the contaminant outwards along this face until it came into contact with the vertical faces of the chamber, as visualised in the cross-section presented in Fig. 5.14. Without additional data from the chamber face opposite to node 5, and indicated by "node x" in Fig. 5.14, it was not possible to verify this observation.

Examining the data provided by the other deployed nodes proved that the contaminant was not dispersed in the expected manner. Inspection of the data showed that nodes 3 and 4, which were closer in proximity to the plume source than node 5, did not respond to the contaminant until after 170 s and 217 s respectively, of the exposure period. The sequence of their responses was interesting, with node 3 responding before node 4. The direction of plume flow was, therefore, from node 3 towards node 4.

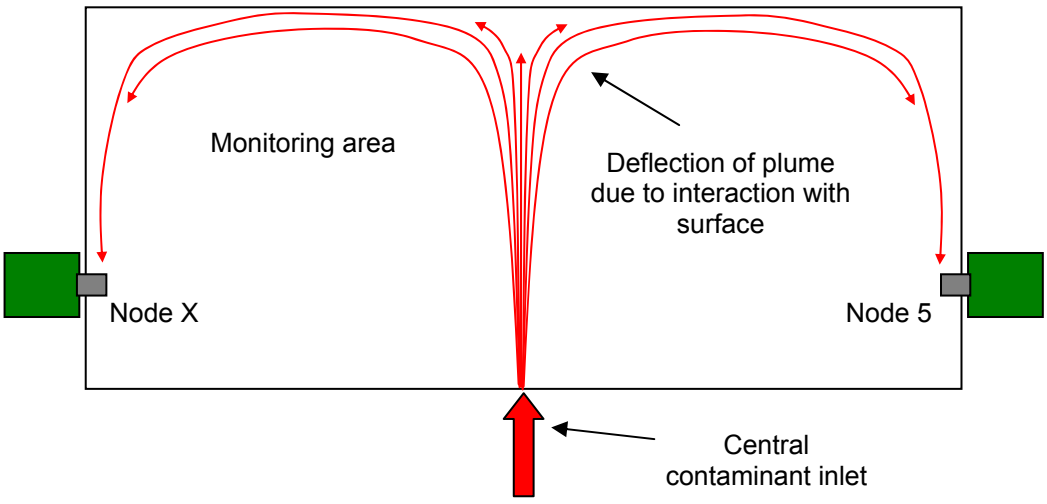

Fig. 5.14 Cross-section of dispersion pattern resulting from interaction with the chamber's top surface

The direction of flow between nodes 3 and 4 indicated recirculation of the contaminant plume towards the centre of the chamber. In keeping with the assumption that the contaminant would disperse evenly across the chamber base as it descended, it would be expected that the same pattern would be observed across nodes 1 and 2. This trend was

not visible in the data, as there was no significant deviation in the responses of nodes 1 and 2 during the course of the exposure period (t = 0 s to t = 300 s).

The arrangement of the chamber was examined, to account for the ambiguous nature of the sensor data. The limited size of the network did not provide data with respect to the free space above the chamber base, (apart from that recorded by node 5) and the symmetry of the chamber volume was interrupted by the outlet on the extraction face.

Although the extraction fan was inactive during the exposure period, its associated hosing allowed an open path to atmosphere. Due to external atmospheric conditions, a nominal draw would have been induced at the chamber outlet. The dispersion path of the contaminant plume introduced into the environment would have been affected by the atmospheric draw such that a greater proportion of the plume would be attracted towards the chamber outlet.

Whilst under the effect of the atmospheric draw, the contaminant would have returned towards the chamber base once it came into contact with the extraction face. The downward moving contaminant was then observed by node 5 before interacting in turn with nodes 3 and 4.

Activation of the extraction components at t = 300 s induced a rapid increase in the responses of nodes 1 and 2 with their peak recorded values of approximately 0.08 mg/l occurring at t = 350 s. The increase in contaminant at these locations was the result of the air agitation lines inducing recirculation in the environment, drawing contaminant in the zone above the sensors down across these nodes. A summary of the node activation times and recorded concentration levels at the end of the plume activity period for S3 are provided in Table 5.3.

The discussed plume path over the exposure period is graphically represented in Fig. 5.15. The split in the plume is unclear and could not be distinguished through the recorded data. The slow moving plume over the locations of nodes 1 and 2 has been included because of the reaction of these sensors in the initial period, post extraction activation.

Node	Sensor Activation Time (s)	Concentration at t = 300 s (mg/l)
1	313	0.00
2	316	0.01
3	170	0.11
4	217	0.08
5	109	0.15

Table 5.3 Sensor activation times with respect to time of plume activation and node concentrations at t = 300 s of S3

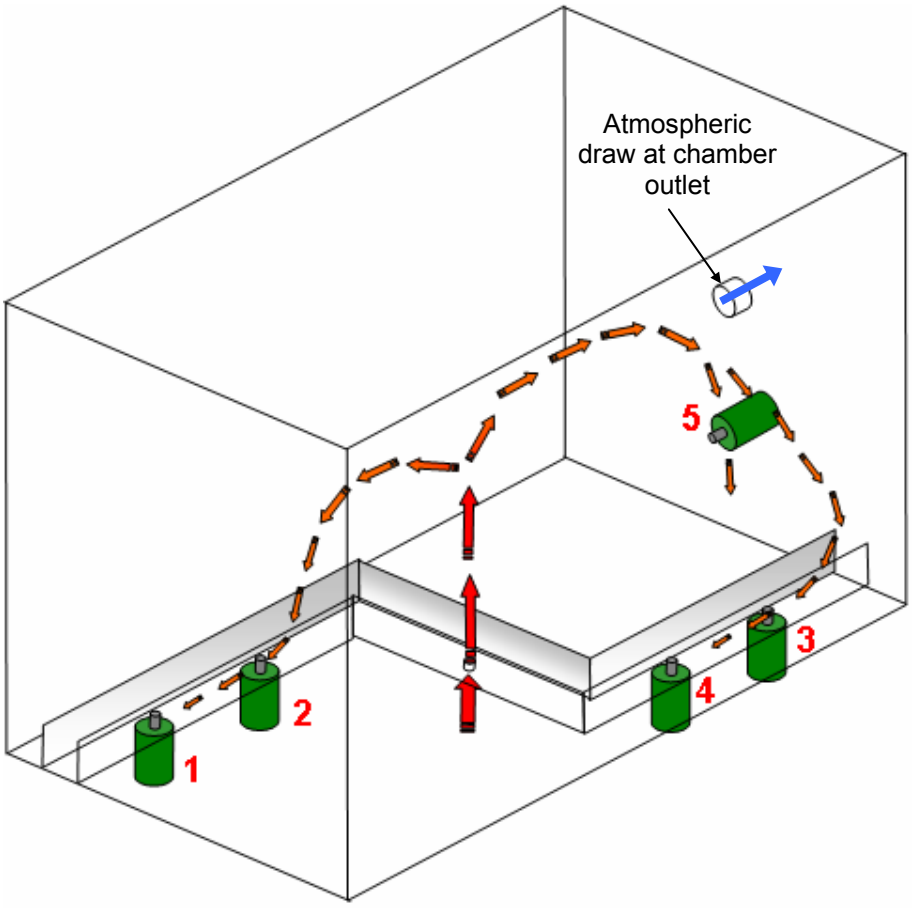

Fig. 5.15 Plume path inferred from data retrieved from the developed WCSN during monitoring scenario 3

5.2.4 Passive Plume Monitoring Summary

Three separate plume monitoring scenarios have been presented. Data from the deployed WCSN have indicated the chemical concentrations at distributed points within the monitored environment and thus facilitated plume tracking.

The development of an acidic contaminant plume originating from a single point source was investigated in S1. From the processed chemical concentration data it was possible to infer the movement of the plume within the ESC channel from the source towards the extraction face. A breach of the channel wall, because of a change in direction of the channel path and the constant input pressure of the contaminant vapour was recorded by a node positioned outside of the channel walls.

In the second scenario, S2, the contaminant concentration of the ESC was affected by exposure to two separate contaminant sources. The contaminant flow dynamic was again inferred from the WCSN data. These data were then compared to data obtained during S1. The comparison found that the dispersion of the contaminant vapour was constrained by the channel walls because of the reduced inlet flow rate caused by the splitting of the acidic air supply.

The third and final passive plume monitoring scenario displayed the importance of node positioning for accurately tracking a plume development. The plume dispersion results of S3 did not correlate with the expected radial plume dispersion pattern. The effect leading to this was an atmospheric draw on the system which affected the flow dynamic of the applied plume. The finding from this trial was that a better understanding of the contaminant distribution would be found through a higher node deployment density.

5.3 Reactive Plume Monitoring Study

As shown through the results of the passive monitoring scenarios, data from the deployed WCSN allowed a contaminant species to be detected by way of providing contaminant concentration data from a number of spatially distributed locations. In this section, the reaction to a detected contaminant based on the collective response of the WCSN, i.e., an event driven reaction, is shown. This provides a logical progression in system development.

The basis for using the collective data from a group of wireless chemical sensor nodes, as opposed to data from a single monitoring device in controlling a reactive response, is illustrated through re-examination of data collected during S1, where the WCSN was exposed to a chemical plume that dispersed across the length of the ESC base. A subset of data (nodes 1-4) obtained over the monitoring period of S1 are presented in Fig. 5.16. If a single node with responsibility for contaminant detection was positioned in the location of node 4, a contaminant would have been detected after 169 s of plume activity. Initiation of an extraction system in reaction to the detected contaminant would have resulted in the concentration level of the sensor decreasing below the LOD at t = 276 s.

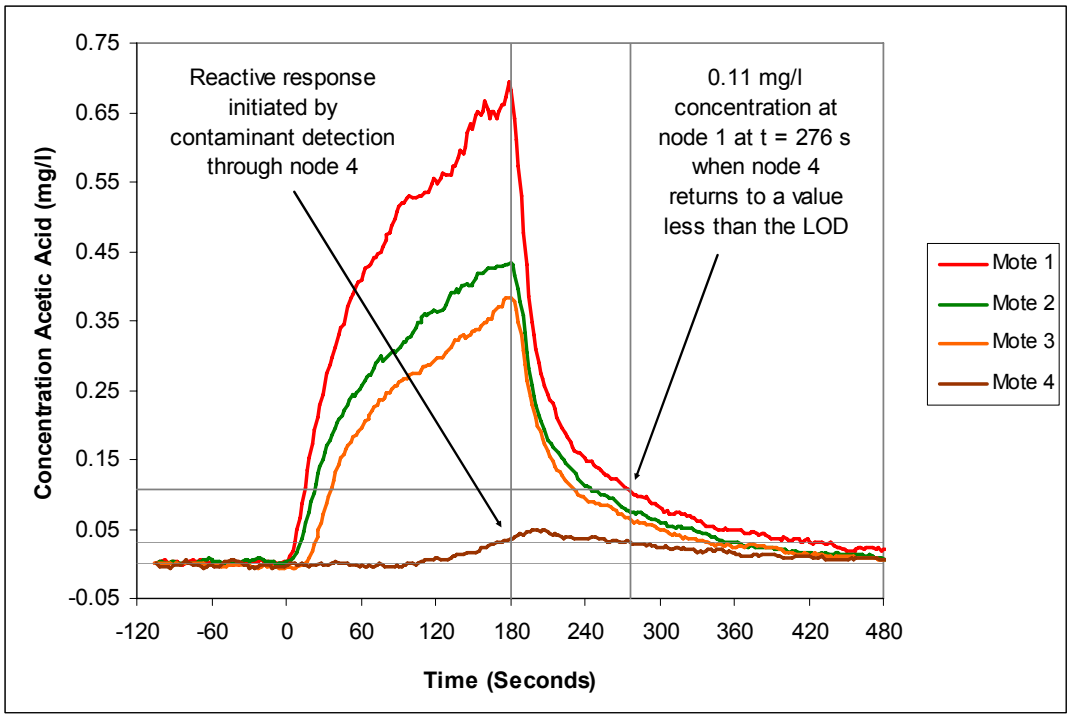

Fig. 5.16 Response data of nodes 1-4 extracted from monitoring results of S1

The LOD is the lowest sensor response value where it can be determined that a chemical stimulus is present. Recovery of the response of the sensor node to a value less than the LOD would result in the control system determining that the detected contaminant had been removed from the environment. However, as shown in Fig. 5.16, at this point in time (t = 276 s), additional sensors deployed in the environment display significant contaminant concentration levels, i.e., 0.11 mg/l at the location of node 1.

A cessation of the reactive response process at this point would result in contaminant remaining in the monitoring area. Thus, the data obtained from a single device do not provide a high enough level of spatial resolution from which an informed decision on when to stop a reactive response can be made. It is also evident from the data presented in Fig. 5.16, that the decision indicating when to initiate the reactive response could have been made earlier, based on the contaminant detections of nodes 1-3. For these reasons a WCSAN was developed, where reaction to a contaminant vapour was based on the collective responses of the WCSN. The following sections discuss the implementation of the WCSAN, the response criterion and the results obtained from a trial study.

5.3.1 WCSAN Reaction Criterion and System Management

The concept of the WSCAN is to examine the concentration state of a number of nodes within the WCSN to determine when an event is occurring. Confirmation of an event is achieved by a number of nodes simultaneously detecting a chemical contaminant. Therefore, the specific concentration of the contaminant is not of immediate concern. The first concern is whether or not a contaminant is present in a node's local environment. This was achieved by attributing a binary chemical contaminant state (No Event/Event) to the real-time data returned by deployed sensor nodes. The LOD (0.03 mg/l) was the logical choice for a point at which to define the state switching threshold. The binary states corresponded to no detected contaminant, i.e., a sensor response value less than the LOD, or a detected contaminant, i.e., a sensor response value greater than the LOD.

Upon detection of a contaminant, the event state of the affected sensor node was changed to "Event". To confirm the chemical species detection, the surrounding sensor nodes were examined to determine if they had also detected the contaminant. In this laboratory scale deployment, to demonstrate the operation of the developed system, the

collective responses from the network were examined until the event status of three separate nodes indicated a contaminant's presence. The criterion for the reactive response activation was, therefore, the event states of three nodes, within the five node network, simultaneously indicating the presence of a contaminant species.

The developed automated system was managed via a PC interface. Acquisition and processing of data from the WCSN has been addressed earlier, in Section 4.6. An additional interface called the "WCSAN Control Interface", accessed through the data acquisition interface, accommodated the control requirements of this system. This control interface, shown in Fig. 5.17, facilitated manual and automatic control of the electro-mechanical components of the test chamber. The manual control facility was necessary for ensuring the correct operation of the system components and allowed the operator to control the contaminant seeding and purge process components used in the plume monitoring trials discussed in Section 5.2.

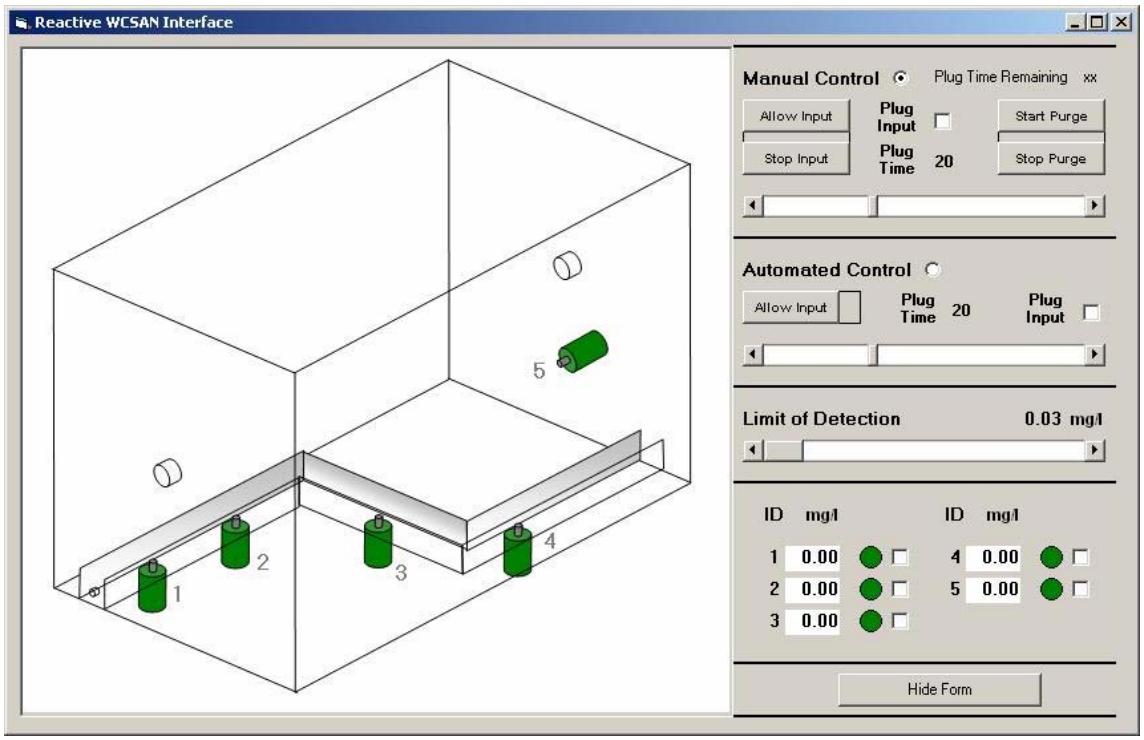

Fig. 5.17 WCSAN interface, with manual and automatic control functions

Automated control allowed for the operation of the components to be governed by the sensor states rather than the system operator. User adaptation of the threshold parameter for state switching was via a horizontal scroll bar. This value was maintained at the LOD (0.03 mg/l) for the WCSAN trial. The physical layout of the five sensor

nodes within the ESC was displayed on the left hand side of the interface, as shown in Fig. 5.17. A change in a sensor's state as a result of a contaminant's presence was symbolised in the interface through a change in that node's colour indicator from green to red.

Seeding of the environment commenced when the "Allow Input" button in the automated control section was selected. The event states of the individual nodes were continually examined. Fulfilment of the event criterion, i.e., three nodes reporting concentrations in excess of the LOD, resulted in an automatic reaction of the system that instructed the CDA supply to the bubbler to be stopped and activated the purge components of the ESC. Event states were reverted to "No Event" when the concentration observed by a node in an "Event" state decreased to its initial baseline response level. The purge operation remained active until all sensor nodes returned to a "No Event" state, ensuring that the detected contaminant was removed from the monitoring area.

5.3.2 WCSAN Trial Results

The sensor node arrangement during the WCSAN trial has been displayed in Fig. 5.17. There were two minor differences between this arrangement and that of S1. They were the relocation of node 5 to the extraction face, at a height of 200 mm above the chamber base, and adjustment of the contaminant inlet flow rate to 200 ml/min. Continuity between this trial and the monitoring trial of S1 was not necessary, as the objective of this study was to highlight the benefit of using the collective responses of a WCSN to make a reaction decision rather than basing a reaction decision on the response of a single monitoring device. However, as the node layout with respect to the contaminant source was similar to that of S1, a similar node activation sequence was expected.

The recorded data from the trial are presented in Fig. 5.18. The reduced contaminant inlet flow rate, resulted in a reduced response rate of sensors in comparison to the sensor activation times recorded in S1 and presented earlier in Table 5.1. The sequential response of nodes 1-3 to the contaminant vapour is also visible in the presented response data.

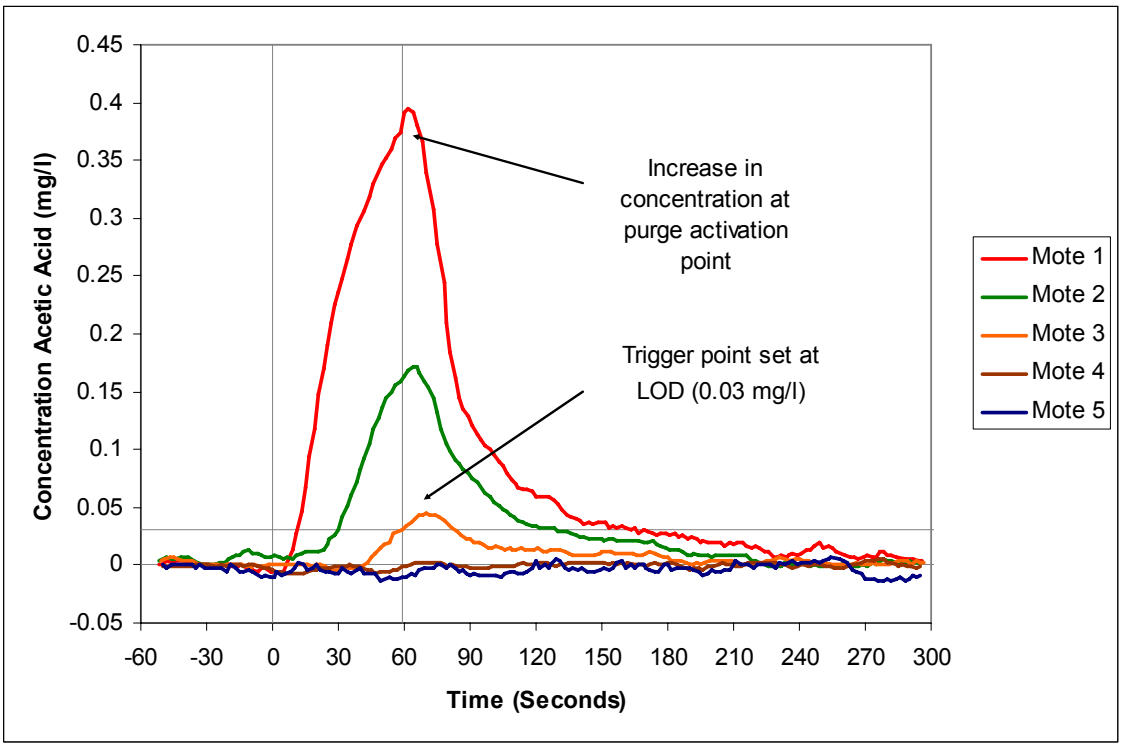

Fig. 5.18 Response data retrieved from five node WCSAN

From the response data presented in Fig. 5.18, it can be seen that the initial detection of the contaminant was recorded by node 1 and occurred at t = 13 s. At t = 30 s, node 2 reported the presence of a contaminant. Confirmation of an event, as per the event criterion outlined in Section 5.3.1, occurred at t = 59 s when three separate sensor nodes (nodes 1, 2, and 3) simultaneously reported a contaminant concentration at their locations in excess of the 0.03 mg/l LOD.

The automatic response to the detected chemical contaminant event was closure of the contaminant supply and activation of the purge system. Initiation of the reactive response is visible in Fig. 5.18 at t = 59 s, as a marginal increase in the concentration level recorded by node 1. The peak concentration recorded by node 1 occurred 3 s later at t = 62 s. The reason for the short delay in the recovery of this sensor node and the marginal contaminant concentration increase before beginning to recover towards a negligible contaminant concentration level was the activation of the CDA agitation inputs. The high pressure air supplied at the CDA inlet points dispersed the contaminant present in the channel path. At the start of this process, contaminant vapour in the section of the channel between the contaminant source and the location of node 1 was forced across the sensing surface of node 1. This induced the marginal

increase in the concentration level recorded by node 1 before the contaminant was purged from its immediate environment. The same contaminant removal process affected the responses of nodes 2 and 3, which were also positioned in the channel path. Maximum concentration levels were recorded by nodes 2 and 3 at t = 66 s and t = 72 s respectively. The sequence of recovery of nodes 1-3 shows that the denser than air contaminant vapour was forced across these sensor nodes by the applied CDA before it was purged from the environment.

Removal of the contaminant from the immediate environments of the sensor nodes is shown through the reduction in their recorded concentration levels. Sensor node 3, because of the minimal concentration to which it was exposed in comparison with nodes 1 and 2, was first to recover to a concentration level below the LOD. This occurred at t = 84 s. At t = 128 s the concentration recorded by node 2 had also been reduced to a value less than the LOD. After an additional 43 s, at t = 171 s, the concentration level of node 1, which had been exposed to the highest contaminant concentration level, as a result of its close proximity to the contaminant source, recovered to the 0.03 mg/l LOD. At t = 235 s all sensor nodes recorded a negligible contaminant concentration level and the purge response was stopped.

The developed WCSAN has shown the integration of real-time data from a group of low-cost wireless chemical sensors with a controlled response system. The developed system is capable of detecting an acidic contaminant vapour. Confirmation of the contaminant detection is achieved by a number of nodes simultaneously indicating a contaminant's presence. Once an event is confirmed, the reactive response is activated until the contaminant is removed from the environment. Removal of the contaminant is verified when all nodes deployed in the monitored area have returned to a negligible contaminant concentration level.

The following section will discuss the benefits that the developed Wireless Chemical Sensor Network (WCSN) and its further advancement that has resulted in a Wireless Chemical Sensor Actuator Network (WCSAN), present over conventional contaminant monitoring techniques.

5.4 Discussion of Results

This section will highlight the benefits of employing a distributed low-cost WCSN for the detection and monitoring of chemical species contaminant events in comparison with using conventional monitoring techniques. Examination of chemical species monitoring data collected by the developed WCSN, with knowledge of sensor node locations with data that could be collected through conventional monitoring techniques highlights the contribution provided by this low cost wireless network in the monitoring of chemical contaminant events.

Three possible monitoring techniques are presented. Data segments, extracted from the WCSN data sets generated during the monitoring studies are then presented to show possible chemical concentration data that would be obtained if these monitoring techniques were employed. The three possible conventional monitoring methods would use,

- a single sophisticated point monitoring device,
- a low density deployment of less sophisticated monitoring devices, or,
- a mobile/handheld monitoring device.

This examination will identify the shortfalls in current monitoring methods that can potentially lead to a misinterpretation of the state of the monitored environment. This analysis emphasises the advantage that a distributed WCSN would provide over conventional monitoring techniques for contaminant source localisation.

In addition, a discussion is provided relaying the benefits of a WCSN when implemented as part of a WCSAN for the removal of, or reactive response to, a detected contaminant, once it has been identified within a monitoring area and the probable location of the contaminant's source identified.

The first step in performing the analysis discussed in this section is the identification of sensor node locations so that contaminant concentration data can be viewed in the context of the WCSN deployment area.

5.4.1 Sample Measurement Location Coordinate System

For the purpose of accurate records in any monitoring routine, the locations of performed sensor measurements would be specified with reference to a coordinate system. For the analysis conducted in the following sections, the origin of the monitored environment coordinate system was specified as the centre of the ESC base. Node locations, in three dimensions (x, y, z), were identified with reference to this point, as shown in Fig. 5.19, and are presented for each of the examined monitoring scenarios in Table 5.4. Variation in node location between each of the monitoring scenarios has been highlighted in red.

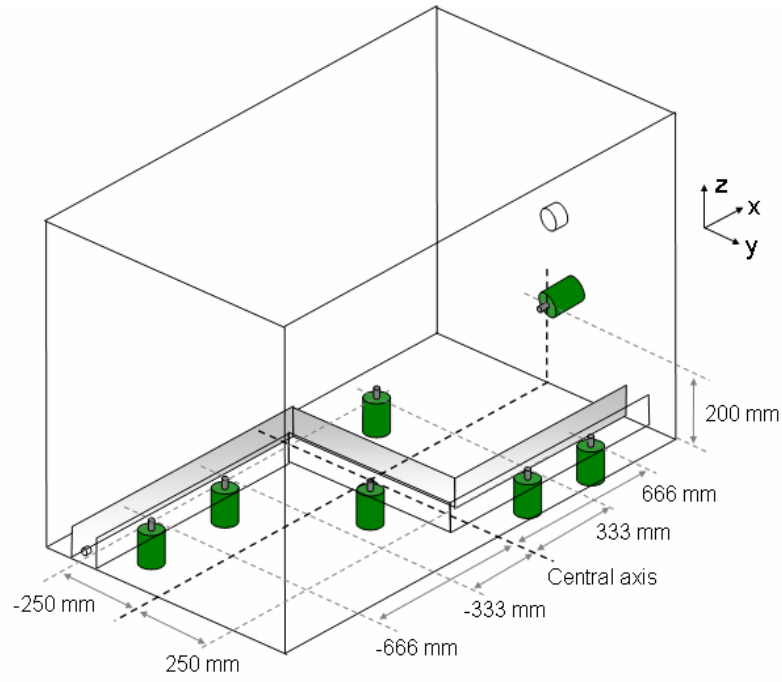

Fig. 5.19 Locations of deployed sensor nodes with reference to chamber origin

Node	Coordinates relative to origin (mm)								
	Scenario 1			Scenario 2			Scenario 3		
	x	y	z	x	y	z	x	y	Z
1	-666	-250	0	-666	-250	0	-666	-250	0
2	-333	-250	0	-333	-250	0	-333	-250	0
3	0	0	0	0	0	0	666	250	0
4	333	250	0	333	250	0	333	250	0
5	333	-250	0	666	250	0	1000	0	200

Table 5.4 Coordinates locations of sensor nodes in monitoring scenarios 1, 2 and 3

5.4.2 Data Set Collected Using Single Point Monitoring Device

In the occurrence of a hazardous chemical event, a single sophisticated piece of monitoring equipment, such as the portable GC/MS system [69], introduced in Section 2.5.1 of the literature review, could be deployed into the hazard area. The device would be introduced into the area by a suitably protected operator to perform chemical species measurements. As measurements would only be taken from one point in the area, it would be necessary to select an appropriate location in which to position the device. The obvious location that would be chosen from which to perform sensor measurements would be at, or as close as possible to, the central point of the area being monitored. Determination of this point would be difficult when the extent of the contaminant dispersion and thus, the extent of the monitoring area cannot be identified.

In the case of the ESC, the central point would be represented by the coordinate system origin, i.e., the centre of the chamber base. Concentration data obtained from node 3, during S1, are presented in Fig. 5.20 with reference to the node's location in the x-y plane of the chamber coordinate system. The concentration recorded by this node at 30 s time intervals is presented in the z-axis.

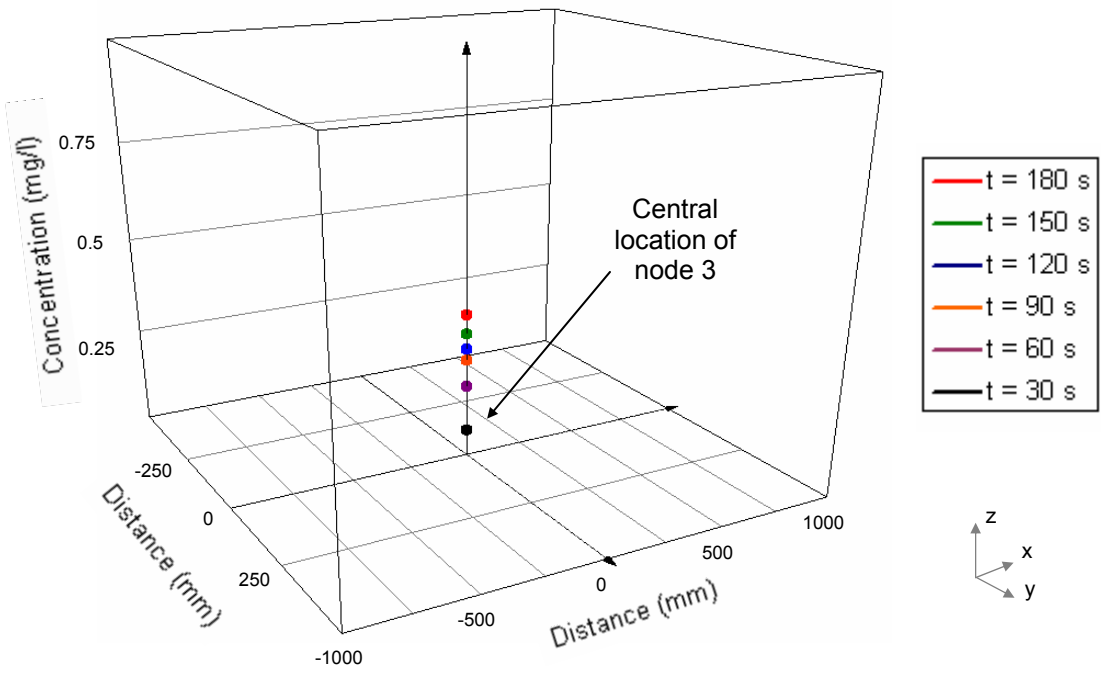

Fig. 5.20 Concentration data with reference to location obtained from node 3 during S1

While the presented data from a single node clearly indicate an increase in chemical concentration over time, it is impossible to ascertain what, if any, concentration change

is occurring at other points within the monitoring space. It is, therefore, not possible to determine how the chemical event is affecting the hazard zone. The result of using a single monitoring device is a distinct limitation to understanding the actual distribution and concentration of a chemical contaminant.

Application of this monitoring technique to any of the monitoring scenarios investigated in this body of work would result in a data set that would provide contaminant concentration information for only one specific point within the monitoring area. However, without a greater number of data sources it would be impossible to gauge the scale of contaminant dispersion and/or its development dynamics, other than whether or not it was increasing or decreasing at the monitoring device's location.

5.4.3 Data Sets Collected Using a Small Deployment of Monitoring Devices

As a single point measuring device would not provide representative data for the complete hazard zone, an alternate option would be to use a low density deployment of less sophisticated analytical gas monitoring devices. A small quantity of measurement systems, such as the TVA1000B [70], which incorporates both FID and PID chemical gas measurement techniques, could be deployed into the hazard zone. While perhaps not as accurate as a GC/MS system these devices would be able to simultaneously provide chemical concentration data from a number of separate locations. To mimic such a deployment, data were extracted from two devices within the ESC and examined to see if an adequate representation of the contaminant concentration within the monitoring environment would be provided.

Concentration data, at common time intervals, extracted from nodes 1 and 4 over the plume activity period of S1, are presented in Fig. 5.21. Concentration data from both nodes are again presented with reference to their individual locations in the x-y plane. The resultant concentration data (z-axis) highlights a high/low relationship between the two measurement devices. The negligible contaminant concentration at the location of node 4 compared to the continually increasing concentration at that location of node 1 indicates that the contaminant is present in the area of node 1. In this case, examining the data from two locations would correctly identify the area of node 1 as the probable contaminant source. However, utilisation of this sensing method would not have the same source identification results when applied to S2, as discussed in the following paragraph.

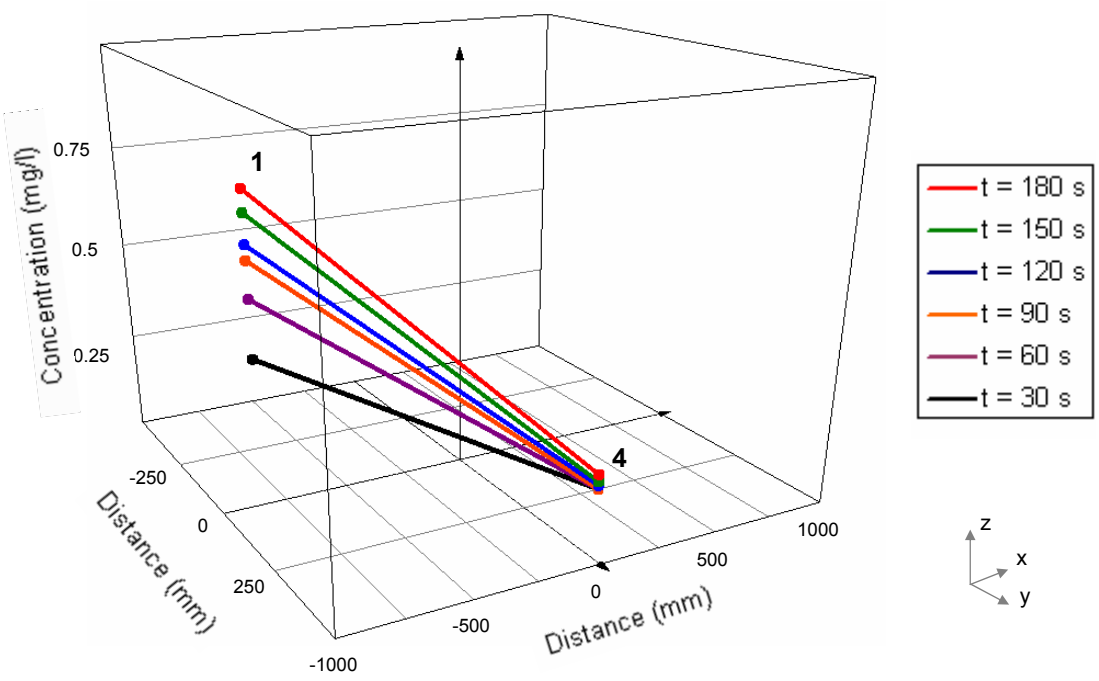

Fig. 5.21 Concentration data with reference to location obtained from nodes 1 and 4 during S1

Data have been extracted from the data sets obtained from nodes 1 and 5 during monitoring scenario 2 and are presented in Fig. 5.22. The resultant data indicate a uniform concentration level across the monitored area at each 30 s time interval. The data from two measurement devices, therefore, cannot be used in this case to determine the area of the contaminant source.

Presenting the data from the five node WCSN with respect to individual node locations, as shown in Fig. 5.23, provides a better representation of the environment's contamination level. These collective data show variation in concentration level across the monitored area that was not visible using data provided by a low density analytical gas measurement device deployment. The peaks in concentration at nodes 1 and 5 in comparison to the lesser concentrations observed by nodes 2-4 would alert the system operator to the possibility of two distinct contaminant sources existing in the monitored area.

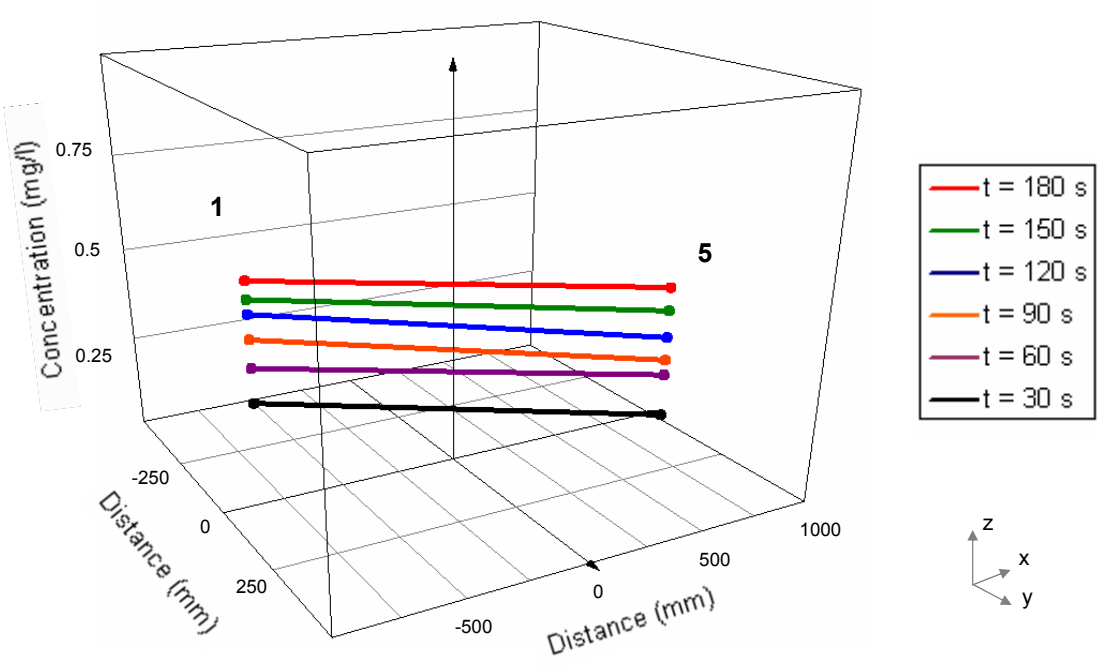

Fig. 5.22 Concentration data with reference to location obtained from nodes 1 and 5 during S2

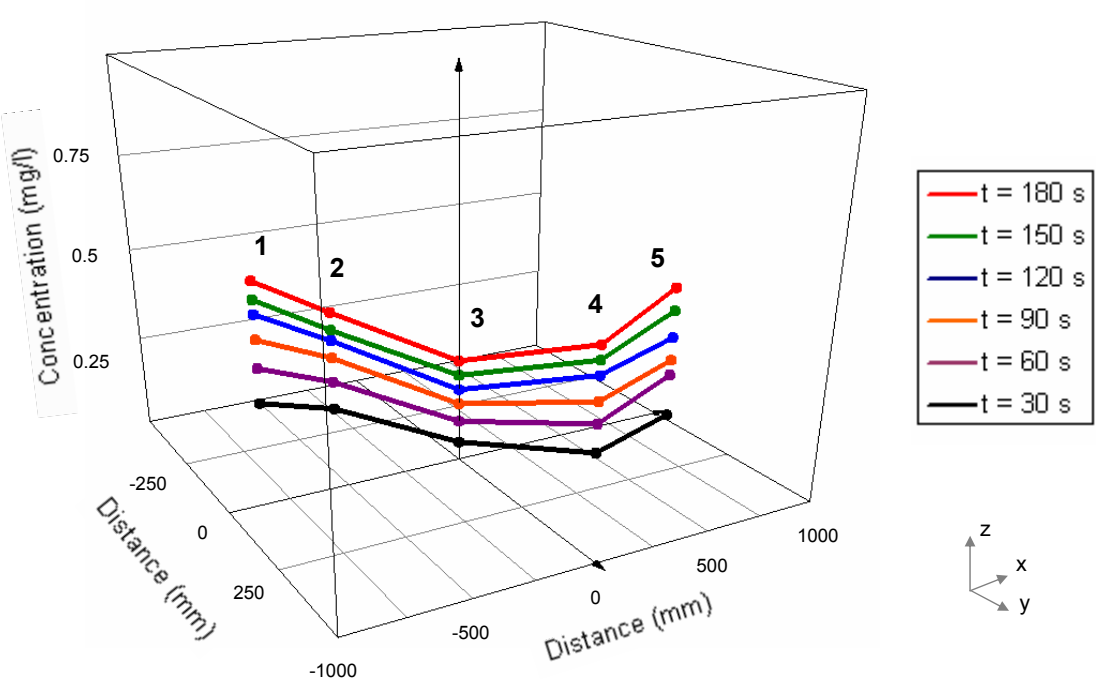

Fig. 5.23 Concentration data with reference to location obtained from 5 node WCSN during S2

In summation, the introduction of an additional monitoring device to increase the spatial resolution of a monitoring system in comparison to the use of a single sophisticated point measuring device does not alleviate the issue of limited reference data that is provided by a point measuring method. Although, this monitoring method would

provide two points of reference, the resultant data simply highlight a high/low relationship between the monitoring nodes in S1 and a misrepresentative consistent concentration measurement in S2. In either case, the operator would not have been furnished with a high enough level of data from which an accurate representation of the contaminant vapour dynamics could be determined. Although, it may have been possible to identify the contaminant's source using a low volume deployment in S1, this monitoring technique would have prevented a source being identified in S2. However, the data that would be obtained from a much lower cost high density deployment of wireless chemical sensors would provide a level of spatial information that would allow for the contaminant dispersion to be much more accurately mapped.

5.4.4 Data Sets Collected Using a Mobile Monitoring Device

A practical solution to the difficulty of limited data collection points would be the use of a mobile monitoring system, such as a handheld meter like the Photovac MicroFID [71]. To perform the sensing routine, an operator would move through the monitoring area, taking and recording concentration measurements at set intervals. This would allow data to be collected from a greater number of locations than achievable through the low density deployment discussed in the previous section. Data sets that could be obtained by monitoring an area in this way have been replicated by extracting data from the deployed WCSN, with an assumption that the time taken to travel between each sampling point would be 30 s. It is worth mentioning at this point that, in reality, it takes a number of minutes to perform a measurement using a handheld device. This would further extend the interval period between contaminant concentration samples by 2 to 3 minutes but has not been factored into this analysis. The path of the mobile monitor, in each case, was taken as being in the x-y plane and as starting from the coordinate (-666, -250) and moving towards the coordinate (666, 250) through the path of the channel.

For S1, the outlined mobile concentration measurement routine would have resulted in the data presented in Fig. 5.24. For comparison, the concentration levels of the sensor devices at the time that the handheld monitoring process would have been completed (t = 120 s) have also been included. As indicated in Fig. 5.24, the recorded mobile monitor data would show that there was a consistent concentration level over locations 1, 2 and 3, and a significantly lower measured concentration level at location 4.

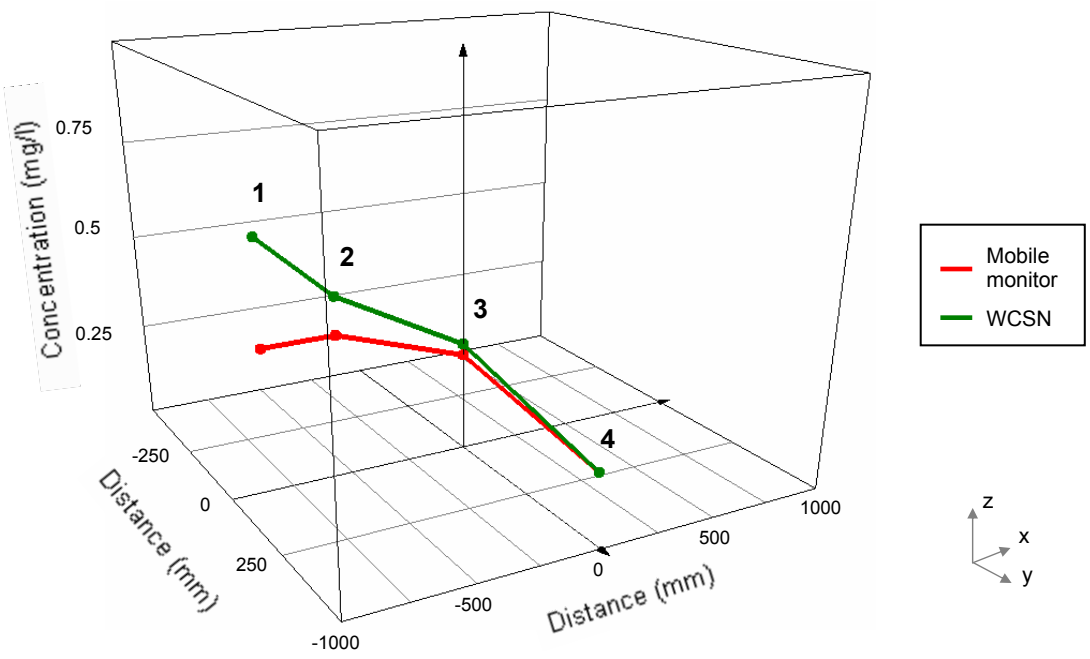

Fig. 5.24 Mobile monitor data taken over 120 s period in comparison to WCSN concentration data at t = 120 s extracted from S1

Data collected through the mobile monitoring method would not have indicated that the concentration level at location 1 had significantly increased by the time the mobile measurement was taken at location 3. In effect, the misinformation provided by this monitoring technique would result in the development of a contaminant plume originating in the area of node 1 being missed, when it is clearly visible from data collected by a number of low-cost fixed location nodes.

Data resulting from applying the same mobile monitoring methodology and sensing pattern to the data sets of S2 is presented in Fig. 5.25. Concentration data from the WCSN at the end of the monitoring routine (t = 150 s) is also presented for reference. The resultant data from the mobile monitoring method (highlighted in red) display a consistent contaminant concentration level over measurement locations 1-3. The concentration level increases at location 4 and peaks at the location of the fifth sample measurement (approximately 0.45 mg/l). Analysis of this data would lead to an interpretation that only one chemical source was present in the monitored environment, i.e., a contaminant entering the monitoring area with a source in the area of the fifth sample measurement and dispersing through the monitoring area towards the location of the first sample measurement. However, examination of common time domain data retrieved from the deployed WCSN would identify two possible contaminant sources.

This again highlights the misinformation that could result from a lack of common time domain data sets obtained from multiple locations.

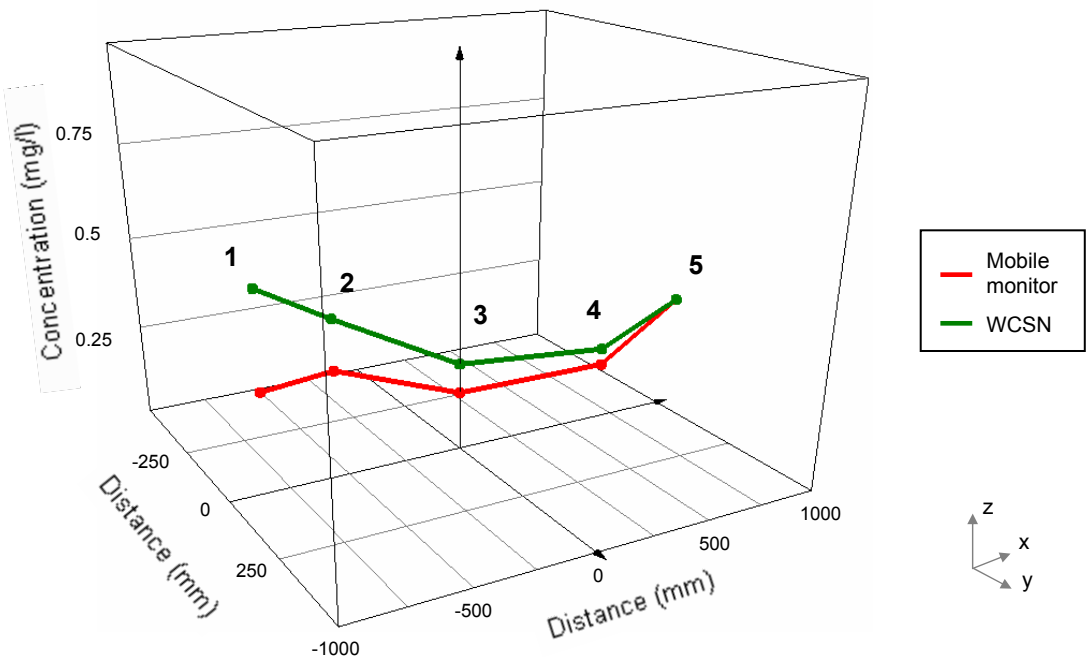

Fig. 5.25 Mobile monitor data taken over 150 s period in comparison to WCSN concentration data at t = 150 s extracted from S2

For the data sets of both S1 and S2 it has been shown that while it is possible to use a mobile monitoring method to increase the spatial resolution of contaminant monitoring data, the quality of these data are affected by data point measurements not being recorded at the same time. This leads to misinformation when examining collected data as they do not represent the same point in time. The WCSN, which provides data at common points in time from fixed sensing locations, provides data sets that concurrently measure the contaminant concentration level at various locations across a monitored area. These data sets provide an accurate representation of the contaminant distribution in the monitored area.

5.4.5 WCSN Limitations Resulting from Network Coverage

The third monitoring scenario, S3, highlights the importance of node deployment density and positioning. It has already been shown (Section 5.2.3) that the data retrieved from the WCSN did not identify the centre of the chamber base as the contaminant source due to the lack of a chemical sensing node in the vicinity of the plume source. Application of the mobile monitoring method to S3, with the assumption

of an obstruction that prevented a concentration measurement being taken at the origin of the monitoring area, results in the contaminant distribution presented in Fig. 5.26.

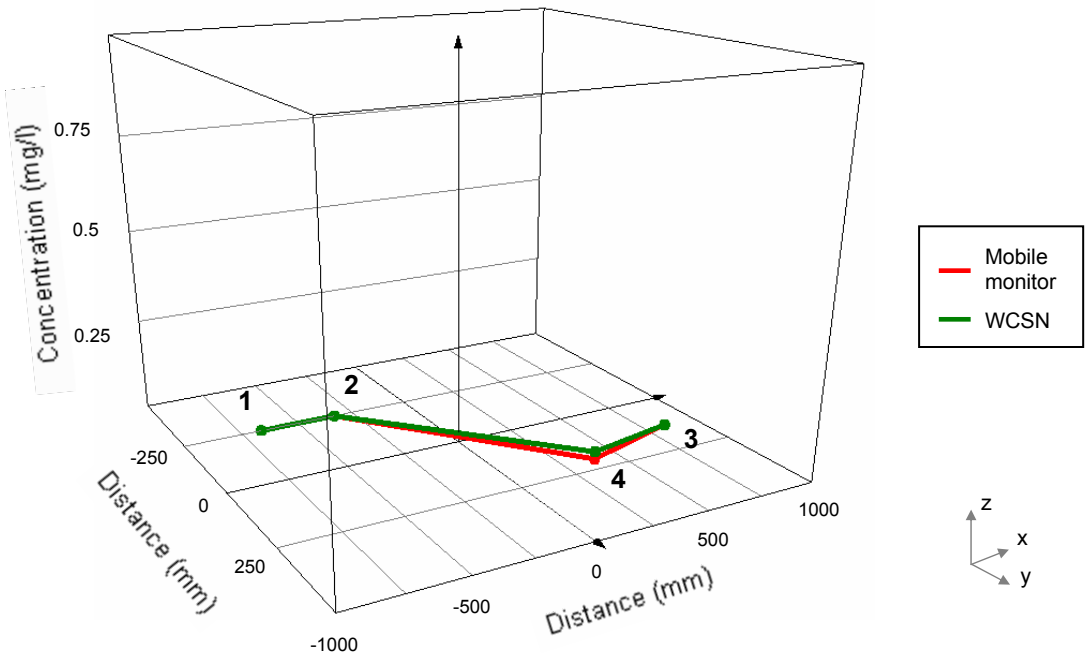

Fig. 5.26 Mobile monitor data taken over 150 s period in comparison to WCSN concentration data at t = 150 s extracted from S3

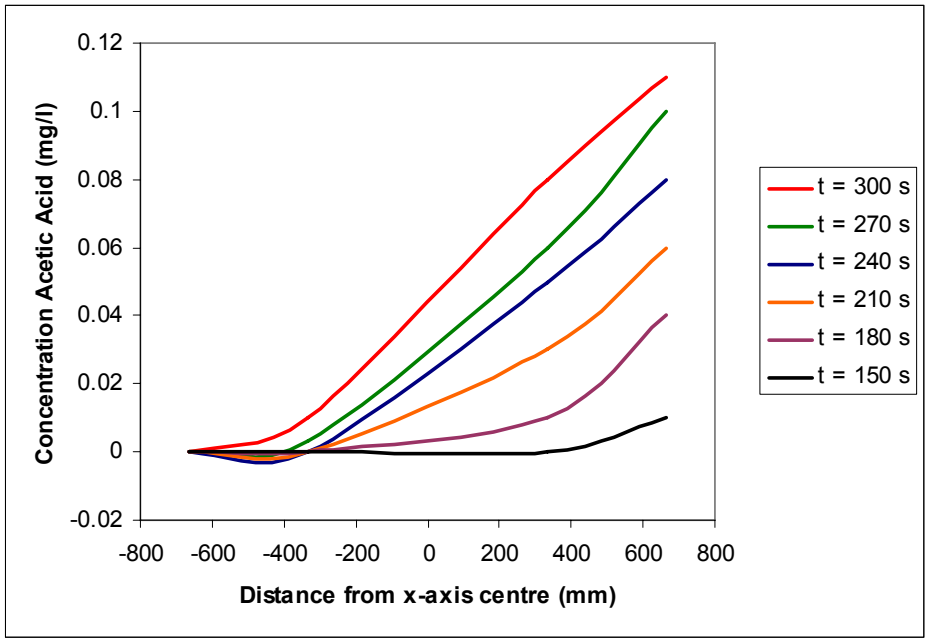

Fig. 5.27 Contaminant distribution along chamber x-axis between t = 150 s and t = 300 s of S3

A contaminant source is not clearly distinguishable from either data set. In actual fact, the data obtained from the WCSN over the 300 s plume activity period would identify

the extraction face of the chamber as the plume source. This can be seen from concentration trend data presented in a cross-section of the chamber's x-axis, as shown in Fig. 5.27. Inclusion of data from node 5, at a height of 200 mm above nodes 1-4 and located on the extraction face, would only tend to confirm the extraction face as the contaminant source, due to the higher concentration level recorded by this node in comparison to that of node 3, located 330 mm from the extraction face. While the WCSN did not accurately identify the contaminant plume source in this monitoring scenario it did supply common time domain data that were more informative than data measured using a mobile monitoring method.

The third monitoring scenario explored during the body of this work has highlighted the limitations of WCSNs. Determination of a contaminant source was not possible because of an insufficient quantity of data points from which the plume dynamic can be accurately ascertained. The solution to the challenge of mapping the plume dynamic and thus identifying the plume source for this monitoring scenario would be the introduction of additional sensor devices at height increments above the chamber base. Introduction of an additional sensor device above the source location would have supplied data indicating a distinct peak in concentration, which, when viewed in the context of the concentrations observed by other nodes would have indicated that the contaminant origin was located centrally in the monitored area.

The results of this monitoring scenario show that effective node positioning when monitoring a contaminant event is crucial. Arbitrary deployment patterns may not be sufficient for monitoring dispersion of a contaminant vapour within an environment. This would be most evident in a building environment where internal geometry would affect the dispersion dynamic. In an internal environment it would be essential to deploy sensor devices at regular intervals and at varying heights so that high quality representative data could be gathered. The monitoring of an outdoor environment would be somewhat different as dispersion of a contaminant would be predominantly affected by atmospheric conditions. In this case, concentration levels would be of most interest at ground level and thus nodes would be deployed in a structured manner on the surface of a hazard zone.

5.5 Chapter 5 - Summary and Conclusions

In the case of these experiments, by monitoring the environment using a single sensor device, the only credible information that can be gathered with regards to a chemical event is whether or not a contaminant was present. This would be further emphasised in real-world monitoring scenarios where the environments being monitored would certainly be on a much greater scale than that of the ESC. The response of a single node could not be considered as representative of the monitoring area as a whole.

During the course of these trials, a five node WCSN has been exposed to three separate contaminant plume scenarios. Individual nodes have successfully identified the presence of a contaminant and provided dynamic concentration measurements. The value in the deployed network has come from examining the retrieved data collectively and in context so that the condition of the environment, rather than the condition of a single location, can be understood.

In the case of each scenario, the response of a sensor node has indicated the presence of a contaminant, but it is the responses of sensor nodes in close proximity to the initial node that have confirmed the occurrence of a chemical event. Differences in the response of these sensors, i.e., because of reaction time and concentration level, have then been examined to deduce further information regarding the contaminant event, such as, potential source location, direction of contaminant movement and also the rate of contaminant movement. These three parameters would be vital in identifying a potentially hazardous contaminant and formulating an appropriate response or method of containment. Essentially, by knowing the location of deployed sensor nodes it is possible to gain an understanding of the dynamic changes that are occurring in their responses due to an event.

The studies described in this chapter have also highlighted the importance of node density versus monitoring resolution, which became particularly evident in the third monitoring scenario which saw an applied plume that did not interact directly with the deployed nodes. In this case, the path of the chemical plume was not easily determined using the collected data. Greater accuracy with regards to the actual plume pattern would only be achieved through a denser deployment of chemical sensors throughout the entire volume. Obviously, in a real-world environment, deploying a dense net of sensors throughout a monitored area would not be practical. It would be necessary to

cater the quantity of deployed nodes and their locations to the specific area being monitored.

The use of a WCSN to gather concentration data over a deployment area will also greatly benefit any reactive response to a detected contaminant. Examining the data reported by a WCSN collectively will allow for a contaminant detection to be confirmed before any response is taken; an important consideration when the response mechanism is either expensive or disruptive to the environment that it manages. The most suitable reaction method could also be determined with knowledge of the contaminant's location. The data from a WCSN would also inform the monitoring system on how the contaminant was being removed in terms of rate and direction. Therefore, if the contaminant was not being removed from the environment as anticipated the reactive response could adapt the operation of the reaction system accordingly. Once the contaminant's presence has been eradicated, as determined using the collective data from the WCSN, the control system would be able to stop the extraction process so that minimal expense and disruption is caused.

To conclude this section, the discussion of two recent events which highlight the potential application and the benefits of the low cost WCSAN outlined in this work is provided.

An explosion in the General Paint's Factory, Celbridge, Co. Kildare on March 29th, 2007, was caused by flammable chemical vapours collecting in an indoor environment. The fire resulting from the explosion was successfully and rapidly extinguished by a sprinkler system and limited the damage to one area of the facility. However, five employees were injured in the event [144].

Installation of a WCSN in this facility, with wireless chemical sensor nodes distributed at various heights would allow for concentration build ups to be mapped. An increase in the concentration of the target vapour to a hazardous level would be indicated by the network. The data from the network could be coupled with an early warning monitoring system that would have alerted staff to the hazardous condition. By examining the collective data and determining the location of the contaminant and possibly the source of the leak, the monitoring system would be able to inform employees of the best evacuation routes. The evacuation routes would be visually

indicated by means of a lighting system directing staff to emergency exits away from the affected area. The monitoring system would also govern the operation of a number of extraction fans. Again the location of the contaminant would be used to determine which fans should be activated to remove the contaminant from the facility while not inhibiting the staff evacuation.

A very recent chemical vapour incident occurred on July 3rd, 2008 at Goulding's Chemicals close to Cork city centre. A faulty valve allowed hydrochloric acid to escape from a holding tank and vaporise. Emergency services responded to the public health risk by evacuating the plant and all adjacent facilities. Employees were instructed to move upwind of the industrial area and traffic diversions were introduced on surrounding roads for a number of hours [145].

A pre-installed WCSN within the facility would have provided a means of mapping the contaminant dispersion within its confines. However, in an event such as this, the dispersion of the chemical vapour would also be of concern to the surrounding areas. To gather valuable data indicating the dispersion of the vapours, and thus inform the public to the extent of the affected area, it would be possible to strategically deploy sensor nodes in the area surrounding the facility. A remotely operated vehicle, which would include GPS location finding technology, would transport the sensor devices into the hazard area. The use of a remotely operated vehicle would remove the need for an operator to manually introduce the sensor devices, therefore, eliminating a potential risk to their health. The GPS unit would allow for deployment locations to be recorded and would be essential for accurate mapping of the extent of the contaminated area. These data would again be used to inform the public and neighbouring businesses, evacuated during the initial response, when it was save to return.

These events provide real-world applications for the work described in this thesis. The deployment of low-cost wireless chemical sensor nodes as part of early warning and reactive response systems in these environments would be cost effective compared to the loss of goods, delay in operations and most importantly, the loss of life, that could result from a chemical vapour event.

6 Conclusions and Future Work

At the outset of this thesis, the main objective of the development and validation of a Wireless Chemical Sensor Actuator Network (WCSAN) for the application of chemical contaminant plume tracking was outlined. Additional secondary objectives, necessary for the achievement of the primary objective, were also defined in Section 2.7. At this stage, it is clear that these objectives have been successfully achieved in the preceding chapters, culminating in the development and successful laboratory trialling of a WCSAN; proving the potential of dispersed wireless chemical sensor networks as applied to the monitoring of chemical contaminant events in real-time.

In arriving at this conclusion, it should be recalled that a number of developmental steps, i.e., the secondary objectives, have also been successfully realised. These critical developmental steps now warrant further mention before discussion of the future work in this research area; anticipated as an outcome of the presented research.

The first development step, upon which all subsequent simulations and studies depended, was the design and implementation of the Environmental Sensing Chamber (ESC), as detailed in Appendix 1. The controllable ESC, with an internal volume of 2 m^3, was designed and constructed to be airtight, easily accessible, optically transparent and capable of facilitating both gas and liquid monitoring devices. This satisfactorily fulfilled all current and future application demands made of the sensor test-bed. The additional proven capabilities to vary temperature of the environment and to efficiently remove any contaminant gas by use of an extraction fan, make this chamber an integral test component for small-scale simulation of real world Wireless Sensor Networks (WSNs) and, more specifically, Wireless Chemical Sensor Network (WCSN) deployments.

Another of the aforementioned developmental steps, crucial to WCSAN development, saw the configuration of a commercially available wireless sensing platform, i.e., a Mica2dot mote, to achieve a suitable continuous operation lifespan over a 4 week period. This facilitated reliable, high temporal resolution laboratory scale sensing. Without these modifications, it would not have been possible to achieve the stable wireless chemical sensing platform discussed in Chapter 4.

The integration of WSN data, processed using an in-house custom data acquisition interface, and coupled with output control signals, facilitated the progression of the WSN application to a Wireless Sensor Actuator Network (WSAN). The real-time management and control of a process variable, i.e., temperature, by the WSAN was only made possible using the data reported by a WSN, as presented in Chapter 3.

The proven real-time monitoring capabilities of the WSAN justified the further development of the system to include a chemical measurement component, resulting in the achievement of the primary objective of this body of work, i.e., development of a WCSAN.

Optimal sensitivity of the low-cost optical chemical sensor was achieved by matching the absorbance spectra of the bromophenol blue (BPB) indicator with the emission spectrum of the emitter LED at 610 nm. Laboratory trials using the finalised wireless chemical sensor node, operating at a sensing and transmission rate of 0.5 Hz, resulted in measured values of sensor response time (51 s), sensor reproducibility (percentage error of 1.76 %) and LOD (0.03 mg/l). Following on from these trials, a group of five wireless chemical sensing nodes were successfully calibrated, over an acidic contaminant concentration range of 0 – 1 mg/l. Resultant concentration conversion equations, integrated into the developed data acquisition interface, facilitated real-time processing of contaminant concentration data from the five node WCSN.

The confidence in the reliability of the node operation, as a result of the conducted studies, permitted three separate contaminant exposure studies of the WCSN to be conducted within the ESC, as discussed in Section 5.2. These studies displayed the plume tracking capabilities, i.e., direction and rate of movement, of a network of spatially deployed wireless chemical sensor nodes. The studies also successfully demonstrated the use of dynamic concentration data to provide a map of a contaminant's distribution over the network deployment area and predict the probable source of a contaminant release.

Prior to recommending this spatially distributed wireless monitoring method for real world deployment and application, it was vital to contrast its collective data acquisition capability with that of established conventional measurement techniques used to monitor the fallout of chemical vapour releases in real world environments, as

highlighted in Section 5.5. The favourable spatial resolution of data, provided by a WCSN, provides a more accurate representation of a contaminant's dispersion than is achievable through conventional monitoring techniques using sophisticated, and often restrictively expensive, laboratory grade equipment. Additionally, the WCSN is superior to any handheld monitoring device, in that it can collect concurrent data providing contaminant concentration information over the complete deployment area.

Coupling of the WCSN with the control functionality demonstrated through the WSAN achieved the first part of the primary research objective, i.e., development of a WCSAN. The preliminary validation of the WCSAN was shown through the successful detection, confirmation and automatic removal of an acidic contaminant vapour from the Environmental Sensing Chamber. The logical application, in light of the trial studies described in the previous chapters, is the use of a WCSN to provide an efficient and reliable method of gathering meaningful data to inform decisions on the most appropriate response to the constantly changing dynamics of a detected contaminant vapour.

The validation of the feasibility of a WCSAN for real world deployments encourages a progression of the research presented within this body of work in new directions and for additional applications. In achieving the primary objective of this thesis, a number of potential research avenues have made themselves evident but are, as yet, unexplored. A selection of these concepts will now be outlined.

- For the purposes of the proof of concept, described in this thesis with regard to WCSANs, acetic acid vapour was utilised as the target contaminant. However, the detection of this chemical species has limited real world applications. Therefore, additional chemical species of interest, capable of detection via colorimetric sensing means, as implemented in this research, will be identified and investigated. Research published by Mills *et al*. has described the development of colorimetric polymer coatings for the detection of carbon dioxide (CO_2) [112]. This target gas has various real world applications and it is, therefore, proposed that the opposing LEDs chemical sensor be modified for sensitivity to this chemical species, through matching of the emission spectrum of the emitter LED with the absorbance spectra of a polymer coating, sensitive to CO_2.

- During this research, it became evident that fluctuations in ambient lighting, of most consequence in real-world, open-air deployments, caused variations in the baseline measurements of the detector LED. Adaptation of the sensor configuration, to account for significant variations in ambient light, e.g., the change in light intensity over the course of a day, is therefore, a desirable avenue to explore in the next phase of this research. This development can be achieved through the introduction of a non-coated opposing LEDs sensor. Chemical species concentration values will result from the subtraction of an ambient light measurement from a chemical sensor measurement, taken at a similar point in time.

- Further to this, an investigation of the effect of temperature variation on sensor response will be conducted through the introduction of a thermistor sensor into the wireless chemical sensor node enclosure. Sensor responses, when exposed to a chemical species of constant concentration, will be analysed for deviation in response, resulting from variations of the temperature variable within the monitored environment. Both this and the previous recommendation for future research attention are considered essential before real-world deployments can commence.

- As a consequence of the non-reproducible coating layer thickness achieved during sensor fabrication, another essential avenue for further research has been highlighted. It is proposed that a drop-on-demand ink-jet printing process [146] be employed in the production of reproducible polymer coating layer thicknesses. This will allow for controlled fabrication, resulting in optical chemical sensors with more similar operating characteristics than those produced and examined as part of this research. Additionally, successful production of reproducible coating thicknesses will allow for characterisation and optimisation of colorimetric polymer layers. This will permit studies to investigate the effect that variation of coating thickness has on critical sensor parameters, such as, sensitivity, LOD and response time.

- Finally, it is believed that the operation of the sensor node hardware, i.e., the mote platform, should be adapted so that the conversion to units of concentration is performed onboard. This will allow for programming of the operating code so that only samples of data, which exceed the LOD, are transmitted, i.e., data transmission will be event-driven. This will reduce communications traffic in times when no

contaminant is detected, increasing energy efficiency. This will also allow for the implementation of an adaptive sensing rate that will facilitate the collection of high temporal resolution concentration data in the event of a contaminant's detection.

In this final chapter, the conclusions, drawn from the work presented in this thesis, have been detailed. As a consequence of these conclusions, some of the potential areas of further research have been highlighted. To facilitate practical real world deployments of future generations of wireless chemical sensor nodes, it will be necessary to address the outlined research topics while also appreciating that further research will inevitably raise additional, as yet, unforeseen challenges. It is hoped that the work described in this thesis and the resultant publications in peer reviewed journals will inspire further research into this innovative, emerging area.

References

[1] R. Kling, "Intel Mote: an enhanced sensor network node", In *Workshop on Advanced Sensors, Structural Health Monitoring, and Smart Structures*, Nov. 2003.

[2] P. Zhang, C. M. Sadler, S. A. Lyon, and M. Martonosi, "Hardware design experiences in zebranet," In *Proceedings of ACM SenSys 2004*, Nov. 2004.

[3] J. Wills, "Will HVAC control go wireless?", *ASHRAE Journal*, 2004, *46(7)*, 46-52

[4] M. Kintner-Meyer and M.R. Brambley "Pros and cons of wireless." *ASHRAE Journal*, 2004, *44(11)*, 54-59

[5] N. Wang, N. Zhang, and M. Wang, "Wireless sensors in agriculture and food industry - recent development and future perspective," *Computers and Electronics in Agriculture*, 2006, *50*, 1-14

[6] I.F. Akyildiz, W. Su, Y. Sankarasubramaniam and E. Cayirci, "Wireless sensor networks: a survey", *Computer Networks*, 2002, *38*, 393-422

[7] Y. Choi, M. G. Gouda, M. C. Kim, and A. Arora. "The mote connectivity protocol", *Technical Report TR-03-08, Department of Computer Sciences, The University of Texas at Austin,* 2003.

[8] J.M. Kahn, R.H. Katz, K.S.J. Pister, "Next century challenges: mobile networking for smart dust" In *Proceedings of the ACM MobiCom'99, Washington, USA,* 1999, 271-278

[9] R. Beckwith, D. Teibel and P. Bowen, "Unwired wine - sensor networks in vineyards", *In Proceedings IEEE Sensors 2004*, 2004, 561-564

[10] R. Cardell-Oliver, M. Kranz, K. Smettem and K. Mayer, "A reactive soil moisture sensor network: design and field evaluation", *Distributed Sensor Networks*, 2005, *1*, 149-162

[11] D. Doolin and N. Sitar, "Wireless sensors for wildfire monitoring", In *Proceedings SPIE Symposium on Smart Structures & Materials*, San Diego, CA, March 2005.

[12] G. Werner-Allen, J. Johnson, M. Ruiz, J. Lees, and M. Welsh, "Monitoring volcanic eruptions with a wireless sensor network" In *Proceedings Second European Workshop on Wireless Sensor Networks (EWSN'05),* 2005

[13] A. Mainwaring, J. Polastre, R. Szewczyk, D. Culler, and J. Anderson, “Wireless sensor networks for habitat monitoring”, In *Proceedings of the ACM International Workshop on Wireless Sensor Networks and Applications*, 2000

[14] J. S. Sandhu, A. M. Agogino, A. K. Agogino, “Wireless sensor networks for commercial lighting control: decision making with multi-agent systems,” In *Proceedings AAAI-04 Workshop on Sensor Networks*, 2004

[15] A.M. Agogino, “MEMS ‘Smart Dust Motes’ for designing, monitoring and enabling efficient lighting”, Final report to UC Project MICRO, 2003

[16] D. Diamond, “Internet scale sensing – analytical science and the next communications revolution”, *Anal. Chem.*, 2004, *76*, 279A-286A.

[17] W. M. Dalton, "Wireless - Telegraphy", in W. M. Dalton, ed., "The story of radio, pt.1 How radio began", Hilger, 1975, pp. 71-115.

[18] L. Coe, "They Called it Wireless", in L.Coe, ed., "Wireless Radio, A brief history", McFarland, 1996, pp. 3-15

[19] K Feher, "Introducation to Wireless, Cellular, Digital, PCD-Mobile Radio", in K Feher, ed., "Wireless digital communications : modulation and spread spectrum applications", Prentice-Hall PTR, 1995, pp. 1-29

[20] L. Coe, "Military Radio", in L.Coe, ed., "Wireless Radio, A brief history", McFarland, 1996, pp. 90-102

[21] Bardeen, J., and Brattain, W. H. "The transistor, a semiconductor triode," Phys. Rev. 74 (1948), 230.

[22] The chip that Jack built, [online], (Accessed 10-6-2006) http://www.ti.com/corp/docs/kilbyctr/jackbuilt.shtml

[23] Crossbow Product Details, [online], (Accessed 10-6-2005) http://www.xbow.com/Products/productsdetails.aspx?sid=3

[24] Tyndall 25 mm Mote Information Sheet, [online], (Accessed 24-6-2008) http://www.tyndall.ie/mai/25mm.htm

[25] MoteIV Webpage, [online], (Accessed 4-10-2007) http://www.moteiv.com

[26] Art of Technology Webpage, [online], (Accessed 4-10-2007) http://www.art-of-technology.ch/english/

[27] TecO Webpage, [online], (Accessed 24-6-2008) http://particle.teco.edu/upart/

[28] Ambient Systems Webpage, [online], (Accessed 4-10-2007) http://www.ambient-systems.net/

[29] S. Madden, M. J. Franklin, J. M. Hellerstein, and W. Hong., "The design of an acquisitional query processor for sensor networks." In *Proceedings ACM SIGMOD*, 2003

[30] A. D. Marbini and L. E. Sacks, "Adaptive sampling mechanisms in sensor networks," In *Proceedings of London Communications Symposium*, London, UK, 2003

[31] A. Jain and E.Y. Chang, "Adaptive sampling for sensor networks." In *Proceedings DMSN '04,* Toronto, Canada, June 2004

[32] Duracell AA Datasheet, [online], (Accessed 2-2-2007) http://www.duracell.com/oem/Pdf/MN1500.pdf

[33] Mica2 Pricelist, [online], (Accessed 28-8-2007) http://www.xbow.com/Products/SelectCountry.aspx?sid=174

[34] D. Gay, P. Levis, R. von Behren, W. Welsh, E. Brewer, and D. Culler, "The nesC language: A holistic approach to network embedded systems", In *Proceedings of the ACM SIGPLAN 2003,* June 2003

[35] Brian W. Kernighan, D.M.R., The C Programming Language (Second Edition). 1988: Prentice Hall, Inc.

[36] J. Deng, R. Han and S. Mishra, "Efficiently authenticating code images in dynamically reprogrammed wireless sensor networks," In Proceedings Fourth IEEE International Conference on Pervasive Computing and Communications Workshops (PERCOMW'06), 272-276

[37] Panasonic Coin Cell Specifications, [online], (Accessed 8-9-2006) http://industrial.panasonic.com/www-data/pdf2/AAA4000/AAA4000CE54.pdf

[38] J. Polastre, R. Szewczyk, and D. Culler, "Telos: Enabling ultra-low power wireless research", In *Proceedings of The Fourth International Conference on Information Processing in Sensor Networks: Special track on Platform Tools and Design Methods for Network Embedded Sensors (IPSN/SPOTS)*, 2005

[39] TelosB Datasheet, [online], (Accessed 8-11-2006) http://www.xbow.com/Products/Product_pdf_files/Wireless_pdf/TelosB_Datasheet.pdf

[40] Texas Instruments MSP430 Datasheet, [online], (Accessed 8-11-2006) http://focus.ti.com/lit/ds/symlink/msp430f1101a.pdf

[41] J. Barton, J. Buckley, B. O'Flynn, S.C O'Mathuna, J.P. Benson, T. O'Donovan, U. Roedig, C. Sreenan, "The D-systems project - wireless sensor networks for car-park management," In *Proceedings IEEE 65th Vehicular Technology Conference, VTC2007-Sprin.*, 2007, 170-173

[42] S.J. Bellis, K. Delaney, B. O'Flynn, J. Barton, K.M. Razeeb, C. O'Mathuna, "Development of field programmable modular wireless sensor network nodes for ambient systems", *Computer Communications*, 2005, 28(13), 1531-1544.

[43] J. Barton, B. O'Flynn, S. Bellis, A. Lynch, M. Morris, S.C. O'Mathuna, "A miniaturised modular platform for wireless sensor networks", In *Procceedings 2005 European Conference on Circuit Theory and Design*, 2005, 35-38.

[44] B. O'Flynn, S. Bellis, K. Delaney, J. Barton, S. O'Mathuna, A. Barroso, J. Benson, U. Roedig, and C. Sreenan, "The development of a novel minaturized modular platform for wireless sensor networks." In *Proceedings Fourth Int. Symp. Information Processing in Sensor Networks*, Los Angeles, CA, USA, April 2005, 370–375

[45] Crossbow Users Manual, [online], (Accessed 2-2-2007) http://www.xbow.com/Support/Support_pdf_files/MPRMIB_Series_Users_Manual.pdf

[46] Maxell Coin Cell Specifications, [online], (Accessed 8-9-2006) http://www.maxell.co.jp/e/products/industrial/battery/cr/index.html

[47] TecO uPart Specifications, [online], (Accessed 8-11-2006) http://particle.teco.edu/upart/datasheets/upart014xilmt.pdf

[48] J.L. Hill, M. Horton, R. Kling, and L. Krishnamurthy, "Wireless sensor networks: The platforms enabling wireless sensor networks", *Communications of the ACM*, 2004, *47(6)*, 41–46

[49] R. Szewczyk, E. Osterweil, J. Polastre, M. Hamilton, A. Mainwaring, and D. Estrin. "Habitat monitoring with sensor networks", *Communications of the ACM*, 2004, *47(6)*, 34–40

[50] R. Govindan, E. Kohler, D. Estrin, F. Bian, K. Chintalapudi, O. Gnawali, S. Rangwala, R. Gummadi, and T. Stathopoulos, "Tenet: an architecture for tiered embedded networks" *CENS Technical Report 56*, 2005

[51] J. Burrell, T. Brooke and R. Beckwith, "Vineyard computing: sensor networks in agricultural production", *IEEE Pervasive Computing*, 2004, *3(1)*, 38–45

[52] P. Buonadonna, D. Gay, J. M. Hellerstein, W. Hong, and S. Madden, “TASK: sensor network in a box”, In *Proceedings of the Second IEEE European Workshop on Wireless Sensor Networks and Applications*, 2005

[53] T. Schmid, H. Dubois-Ferrire, and M. Vetterli, “SensorScope: Experiences with a wireless building monitoring sensor network”, In *Workshop on Real-World Wireless Sensor Networks (REALWSN’05)*, June 2005, 13–17

[54] J.N. Al-Karaki and A.E. Kamal, “Routing techniques in wireless sensor networks: a survey”, *IEEE Wireless Communications*, 2004, *11(6)*, 6–28

[55] C. O’Mathuna, T. O'Donnell, R. V. Martinez-Catala, J. Rohan, B. O'Flynn, “Energy scavenging for long-term deployable wireless sensor networks”, *Talanta*, 2008, *75(3)*, 613-623.

[56] J.A. Paradiso and T. Starner, "Energy scavenging for mobile and wireless electronics," *IEEE Pervasive Computing*, 2005, *4(1)*, 18-27

[57] M. A. M. Vieira, C. N. Coelho Jr., D. C. da Silva Jr., and J. M. da Mata, “Survey on wireless sensor network devices”, *In Proceedings. IEEE Conference on Emerging Technologies and Factory Automation*, 2003, *1*, 537-544

[58] A. Hande, T. Polk, W. Walker, D. Bhatia, “Indoor solar energy harvesting for sensor network router nodes,” *Microprocessors and Microsystems,* 2007, *31(6)*, 420-432

[59] E. Cantatore and M. Ouwerkerk, “Energy scavenging and power management in networks of autonomous microsensors”, *Microelectronics Journal*, 2006, *37(12)*, 1584-1590

[60] V. Leonov, P. Fiorini, S. Sedky, T. Torfs, C. Van Hoof, “Thermoelectric MEMS generators as a power supply for a body area network” In *Proceedings of the 13th International Conference on Solid-State Sensors, Actuators and Microsystems (Transducers’05)*, 2005, 291–294

[61] K. Baert, B. Gyselinckx, T. Torfs, V. Leonov, F. Yazicioglu, S. Brebels, S. Donnay, J. Vanfleteren, E. Beyne, C. Van Hoof, “Technologies for highly miniaturized autonomous sensor networks”, *Microelectronics Journal*, 2006, *37(12)*, 1563-1568

[62] M. Kintner-Meyer, M. Brambley, T. Carlon, and N. Bauman, “Wireless sensors: Technology and cost-savings for commercial buildings.” In *Proceedings 2002 ACEEE Summer Study on Energy Efficiency in Buildings*. 7.121-7.134

[63] J. Janata and A. Bezegh, “Chemical sensors” *Anal. Chem.*, 1988, *60*, 62R-74R.

[64] R. Bogue, “Optical chemical sensors for industrial applications.” *Sensor Review*, 2007, *27(2)*, 86–90

[65] “Collins English Dictionary”, 6th Edition, HarperCollins Publishers, 2003.

[66] R. D. Simoni, R. L. Hill, M. Vaughan, and H. Tabor, “A classic instrument: The Beckman DU spectrophotometer and its inventor, Arnold O. Beckman”, *The Journal of Biological Chemistry*, 2003, *278(49)*, 79-81

[67] H.M. McNair & J.M. Miller, “Special Topics”, in H.M. McNair & J.M. Miller, eds., “Basic Gas Chromatography”, Wiley Interscience, New York, 1997, pp. 153-166.

[68] E. de Hoffmann and V. Stoobant, “Mass Spectrometry/Chromatography Coupling”, in E. de Hoffmann & V. Stoobant, eds., “Mass Spectrometry-Principles and Applications”, Wiley, Chichester, 2001, 2nd edition, pp. 157-180.

[69] HAPSITE Smart Chemical Identification System, [online], (Accessed 10-6-08) http://www.inficonchemicalidentificationsystems.com/en/hapsitechemicalidentification.html

[70] Thermo Scientific TVA1000B datasheet, [online], (Accessed 10-6-2008) http://www.thermo.com/eThermo/CMA/PDFs/Product/productPDF_5619.pdf

[71] Photovac MicroFID gas analyser, [online], (Accessed 10-6-2008) http://www.photovac.com/MicroFID.aspx

[72] GasAlertMicro portable gas detector, [online], (Accessed 10-6-2008) http://www.envirotechonline.com/proddetail.asp?prod=BW%2DGasAlert5

[73] Rae Systems MiniRAE 3000 datasheet, [online], (Accessed 10-6-2008) http://www.raesystems.com/~raedocs/Data_Sheets/MiniRAE-3000-DS_US.pdf

[74] Rae Systems AreaRAE Steel datasheet, [online], (Accessed 10-6-2008) http://www.raesystems.com/~raedocs/Data_Sheets/AreaRAE_Steel_Z1_11-12-07.pdf

[75] MiniRAE 3000 price guide, [online], (Accessed 10-6-2008) http://www.envirotechonline.com/proddetail.asp?prod=RAE%2D059%2DB110%2D000

[76] Geotech GA2000, [online], (Accessed 10-6-2008) http://www.geotech.co.uk/product_detail.php?prod_code=GA2K1-E001

[77] B. Kiernan, W. Guo, C. Slater, J. Hayes and, D. Diamond**, "**Autonomous monitoring of landfill gas migration at borehole wells on landfill sites using wireless technology" In *Proceedings of the 10th International Conference on Environmental Science and Technology*, 2007, A, 679-685

[78] B. Kiernan, C. Slater, J. Hayes and, D. Diamond, "Wireless monitoring of landfill gas emissions" In *Proceedings of The 22nd International Conference on Solid Waste Technology and Management,* 2007

[79] D. Diamond, "Chapter 1 Overview", in D. Diamond, ed., "Principles of Chemical and Biological Sensors", Wiley Interscience, 1998, pp. 1-18.

[80] K. Ihokura, "The Stannic Oxide Gas Sensor: Principles and Applications", Boca Raton, FL: CRC, 1994.

[81] P. Mitra, A. P. Chatterjee, and H. S. Maiti, "ZnO thin film sensor," *Mater. Lett.*, 1998, *35*, 33–38

[82] D. M. Wilson, S. Hoyt, J. Janata, K. Booksh and L. Obando, "Chemical sensors for portable, handheld field instruments", *IEEE Sens. J.*, 2001, *1(4)*, 256–274

[83] Y. Shimizu and M. Egashira, "Basic aspects and challenges of semiconductor gas sensors", *MRS Bull.*, 1999, *24(6)*, 18-24

[84] Y. Takao, K. Miyazaki, Y. Shimizu and M. Egashira, "High amonia sensitive semiconductor gas sensors with double-layer structure and interface electrodes", *J. Electrochem. Soc.,* 1994, *141(4)*, 1028-1034

[85] M.K. Ram, O. Yavuz, V. Lahsangah, M. Aldissi, "CO gas sensing from ultrathin nano-composite conducting polymer film", *Sensors and Actuators B: Chemical,* 2005, *106*, 750-57

[86] P. Sjöberg-Eerola, J. Bobacka, A. Lewenstam and A. Ivaska, "All-solid-state chloride sensors based on electronically conducting, semiconducting and insulating polymer membranes", *Sensors and Actuators B: Chemical*, 2007, *127(2)*, 545-553

[87] S. Radhakrishnan and Santhosh Paul, "Conducting polypyrrole modified with ferrocene for applications in carbon monoxide sensors", *Sensors and Actuators B: Chemical*, 2007, *125(1)*, 60-65

[88] J. J. Miasik, A. Hooper and B. C. Tofield, "Conducting polymer gas sensors", *J. Chem. Soc., Faraday Trans.*, 1986, *82*, 1117-1126

[89] M.C. Lonergan, E.J. Severin, B.J. Doleman, S.A. Beaber, R.H. Grubbs, N.S. Lewis, "Array-based vapor sensing using chemically sensitive, carbon black-polymer resistors", *Chem. Mater*., 1996, *8*, 2298

[90] M. M. Chehimi, M-L. Abel, C. Perruchot, M. Delamar, S. F. Lascelles and S. P. Armes, "The determination of the surface energy of conducting polymers by inverse gas chromatography at infinite dilution", *Synthetic Metals*, 1999, *104(1)*, 51-59

[91] M. Chavali, T-H. Lin, R-J. Wu, H-N. Luk and S-L. Hung, "Active 433 MHz-W UHF RF-powered chip integrated with a nanocomposite m-MWCNT/polypyrrole sensor for wireless monitoring of volatile anesthetic agent sevoflurane", *Sensors and Actuators A: Physical*, 2008, *141(1)*, 109-119

[92] J. Kong NR. Franklin, CW. Zhou, MG. Chapline, S. Peng, KJ. Cho, and HJ. Dai, "Nanotube molecular wires as chemical sensors", *Science,* 2000, *287(5453)*, 622-625

[93] K. Domansky, D. L. Baldwin, J.W. Grate, T. B. Hall, J. Li, M. Josowicz, and J. Janata, "Development and calibration of field-effect transistor based sensor array for measurement of hydrogen and ammonia gas mixtures in humid air," *Anal. Chem.*, 1998, *70*, 473-481

[94] J. Hendrikse,W. Olthuis, and P. Bergveld, "The EMOSFET as an oxygen sensor: Constant current potentiometry," *Sensors and Actuators B: Chemical*, 1999, *59*, 35-41

[95] H.-K. Liao, J.-C. Chou, W.-Y. Chung, T.-P. Sun, and S.-K. Hsiung, "Study of amorphous tin oxide thin films for ISFET applications," *Sensors and Actuators B: Chemical*, 1998, *50*, 104–109

[96] F. Shitthelm, K.-S. Rover, and R. Ferreti, "Electronic characterization of thin diamond like carbon films for pH sensor applications," *Proc. SPIE*, 1998, *3539*, 139-146

[97] J.-C. Cho and J.-L. Chiang, "Ion sensitive field effect transistor with amorphous tungsten trioxide gate for pH sensing," *Sensors and Actuators B: Chemical*, 2000, *2*, 81–87

[98] J. Bausells, J. Carrabina, A. Errachid, and A. Merlos, "Ion-sensitive field-effect transistors fabricated in a commercial CMOS technology," *Sensors and Actuators B: Chemical*, 1999, *57*, 56-62

[99] H.-K. Liao, E.-S. Yang, J.-C. Chou, W.-Y. Chung, T.-P. Sun, and S.-K. Hsiung, "Temperature and optical characteristics of tin oxide membrane gate ISFET," *IEEE Trans. Electron. Devices*, 1999, *46*, 2278-2281

[100] L.-L. Chi, J.-C. Chou,W.-Y. Chung, T.-P. Sun, and S.-K. Hsiung, “Study on extended gate field effect transistor with tin oxide sensing membrane,” *Mater. Chem. Phys.*, 2000, *63*, 19-23

[101] K. Länge, S. Grimm and M. Rapp, “Chemical modification of parylene C coating for SAW biosensors”, *Sensors and Actuators B: Chemical*, 2007, *125(2)*, 441-446

[102] C.A. Flory and R.L. Baer, “Surface transverse wave mode analysis and coupling to interdigital transducers”, *IEEE Ultrason. Symp. Proc.* 1987, 313–318

[103] M. Weiss, W. Welsch, M. von Schickfus and S. Hunklinger, “Viscoelastic behavior of antibody films on a shear horizontal acoustic wave sensor”, *Anal. Chem.* 1998, *70*, 2881–2887

[104] N. Barié, H. Sigrist and M. Rapp, “Development of immunosensors based on commercially available surface acoustic wave (SAW) devices”, *Analusis*,1999, *27*, 622–629.

[105] K. Länge, F. Bender, A. Voigt, H. Gao and M. Rapp, “A surface acoustic wave biosensor concept with low flow cell volumes for label-free detection”, *Anal. Chem.* 2003, *75*, 5561-5566

[106] Qi Han, A.P. Jayasumana, T. Illangaskare, T. Sakaki,, "A wireless sensor network based closed-loop system for subsurface contaminant plume monitoring," In *Proceedings IEEE International Symposium on Parallel and Distributed Processing, 2008. IPDPS 2008*, 2008, 1-5

[107] X. Yang, K.G. Ong, W.R. Dreschel, K. Zeng, C.S. Mungle, and C.A. Grimes, “Design of a wireless sensor network for long-term, in-situ monitoring of an aqueous environment”, *Sensors 2*, 2002, 455–472.

[108] N. Nakamura, Y. Amao, “An optical sensor for CO2 using thymol blue and europium(III) complex composite film” *Sensors and Actuators B: Chemical*, 2003, *92(1-2)*, 98-101

[109] A. Mills and Q. Chang, “Colorimetric polymer film sensors for dissolved carbon dioxide”, *Sensors and Actuators B: Chemical*, 1994, *21(2)*, 83-89

[110] K. Eaton, “A novel colorimetric oxygen sensor: dye redox chemistry in a thin polymer film”, *Sensors and Actuators B: Chemical*, 2002, *85(1-2)*, 42-51

[111] H. Dacres and R. Narayanaswamy, “A new optical sensing reaction for nitric oxide” *Sensors and Actuators B: Chemical*, 2003, *90(1-3)*, 222-229

[112] A. Mills, A. Lepre and L. Wild, "Breath-by-breath measurement of carbon dioxide using a plastic film optical sensor" *Sensors and Actuators B: Chemical*, 1997, *39(1-3)*, 419-425

[113] P. Dietz, W. Yerazunis, D. Leigh, "Very low-cost sensing and communication using bidirectional LEDs" *In Proceedings UbiComp 2003*, 2003, 2864, 175-191

[114] F. M. Mims III, "Siliconnections: Coming of Age in the Electronic Era", McGraw-Hill, New York, NY, 1986.

[115] F. M. Mims III, "LED Circuits and Projects", Howard W. Sams and Co., Inc., New York, NY, pp. 60-61, 76-77, 122-123.

[116] K. T. Lau, S. Edwards and D. Diamond, "Solid-state ammonia sensor based on Berthelot's reaction", *Sensors and Actuators B: Chemical*, 2004, *98*, 12-17

[117] L. Byrne, K.T. Lau and D. Diamond, "Monitoring of headspace total volatile basic nitrogen from selected fish species using reflectance spectroscopic measurements of pH sensitive films", *The Analyst*, 2002, *127*, 1338-1341

[118] K. T. Lau, S. Baldwin, R. L. Shepherd, P. H. Dietz, W. S. Yerzunis and D. Diamond, "Novel fused-LED's devices as optical sensors for colorimetric analysis", *Talanta*, 2004, *63*, 167-173

[119] R. L. Shepherd, W. S. Yerazunis, K. T. Lau and D. Diamond, "Novel surface mount LED ammonia sensors", *In Proceedings IEEE Sensors 2004*, 2004, 951-954

[120] G. Rosengarten, J. Cooper-White and G. Metcalfe, "Design and experimental issues with heat exchangers for microfluidics", In *Proceedings 15th Australasian Fluid Mechanics Conference, The University of Sydney*, 2004

[121] A Guide to Polycarbonate in General, [online], (Accessed 5-10-2007) http://www.ptsllc.com/polcarb_intro.htm

[122] C. M. McGraw, S. E. Stitzel, J. Cleary, C. Slater and D. Diamond, "Autonomous microfluidic system for phosphate detection", *Talanta*, 2007, *71(3)*, 1180-1185

[123] S-K Cheng and C-Y Chen, **"**Mechanical properties and strain-rate effect of EVA/PMMA in situ polymerization blends", *European Polymer Journal*, 2004, *40(6)*, 1239-1248

[124] Martin Magnum 800 Datasheet, [Online], (Accessed 5-8-2005) http://www.martin.com/service/downloadfile.asp?name=UM_Magnum800_EN_A.pdf&cat=65

[125] A. Ledeczi, G. Kiss, B. Feher, P. Volgyesi, G. Balogh, "Acoustic source localization fusing sparse direction of arrival estimates," In *Workshop on Intelligent Solutions in Embedded Systems, 2006* , 2006, 1-13

[126] Type DK thermistor Datasheet, [online], (Accessed 5-8-2005) http://www.thermometrics.com/assets/images/dk.pdf

[127] Steinhart-Hart thermistor conversion equation, [online], (Accessed 5-8-2005) http://www.thermometrics.com/assets/images/3.pdf

[128] CH Instruments Product Brochure, [online], (Accessed 8-4-2008) http://www.chinstruments.com/

[129] TC-08 Datasheet, [online], (Accessed 5-9-2007) http://www.picotech.com/document/pdf/tc08.pdf

[130] VBMotegate Webpage, [online], (Accessed 20-8-2006) http://sourceforge.net/projects/vbmotegate

[131] Parallel port output DLL, [online], (Accessed 25-8-2006) http://www.logix4u.net/inpout32_source_and_bins.zip

[132] C. P. Underwood, “HVAC Control Systems”, in C. P. Underwood, ed., “HVAC Control Systems, Modelling, Analysis and Design”, E & FN Spon, 1999, pp. 1-31

[133] C. P. Underwood, “Device Technology”, in C. P. Underwood, ed., “HVAC Control Systems, Modelling, Analysis and Design”, E & FN Spon, 1999, pp. 34-76

[134] P. Faurre and M. Depeyrot, “Elementary PID control and process control”, in P. Faurre, M. Depeyrot, ed., “Elements of system theory”, North-Holland, 1977, pp. 17-34

[135] M. S. Mahmoud, “Systems Control Modelling and Representation”, in M. S. Mahmoud, ed., “Computer-operated Systems Control”, Marcel Dekker, 1991, pp. 21-70

[136] pH Indicator Dyes, [online], (Accessed 4-11-2005) http://antoine.frostburg.edu/chem/senese/101/acidbase/indicators.shtml

[137] Acetic Acid Properties, [online], (Accessed 24-7-2008) http://www.sigmaaldrich.com/catalog/search/ProductDetail/FLUKA/45727

[138] Dimension 768 SST 3D Printer, [online], (Accessed 24-7-2008) http://www.dimensionprinting.com/3d-printers/printing-productspecs768series.aspx

[139] B.J. Doleman and N.S. Lewis, "Comparison of odor detection thresholds and odor discriminablities of a conducting polymer composite electronic nose versus mammalian olfaction" *Sensors and Actuators B: Chemical.* 2001, *76*, 41–50

[140] J. Nicolas and A-C Romain, "Establishing the limit of detection and the resolution limits of odorous sources in the environment for an array of metal oxide gas sensors", *Sensors and Actuators B: Chemical*, 2004, *99(2-3)*, 384-392

[141] J. Yick, B. Mukherjee, D. Ghosal, "Wireless sensor network survey", *Computer Networks*, 2008, *52(12)*, 2292-2330.

[142] R. Byrne and D. Diamond, "Chemo/bio-sensor networks" *Nature Materials*, 2006, *5(6)*, p. 421

[143] D. Diamond, K. T. Lau, S. Brady, J. Cleary, "Integration of analytical measurements and wireless communications--Current issues and future strategies", *Talanta*, 2008, *75(3)*, 606-612

[144] N. Donnelly, "Explosion injures five" Liffey Champion, Number 685, Apr 7th 2007

[145] R. Riegel, "Hundreds of plant staff evacuated after acid gas leak" Irish Independent, July 4th 2008

[146] J. C. Carter, R. M. Alvis, S. B. Brown, K. C. Langry, T. S. Wilson, M. T. McBride, *et al.*, "Fabricating optical fiber imaging sensors using inkjet printing technology: A pH sensor proof-of-concept", *Biosensors and Bioelectronics*, 2006, *21(7)*, 1359-1364.

Appendices

Appendix 1

A1 Development of a Controllable Environmental Chamber

Before the studies described in Chapters 3, 4 and 5 could be carried out, a number of development steps were required in order to move from a hard-wired LED based chemical sensor to an independent wireless chemical sensing node and further towards a reactive wireless chemical sensing system. The initial development step towards this goal has been the design and construction of a controllable Environmental Sensing Chamber (ESC). The chamber provides a laboratory test environment where developed nodes can be deployed and evaluated through exposure to varying parameters, such as, temperature and chemical species concentration.

In this chapter, the design requirements for the chamber structure and concept solutions will be discussed. Following selection of a suitable construction method the design of the chamber is refined to ensure that it meets the outlined requirements. The final chamber design is then presented. The constructed chamber is tested to clarify that the employed methods for achieving an airtight test environment have been successful. Modifications, to improve the operation of the chamber, resulting from observations during the seal testing of the environment are then discussed and implemented.

Control of electro-mechanical components, which are employed during wireless sensor network studies to influence parameters of interest, is addressed. Provision is made for automated control of these components via output signals generated by a PC. An associated intermediary relay control board is described along with additional components required for the operation of devices requiring power supplies of 24 VDC and 240 VAC, respectively. The two specific parameters of interest which can be managed through the developed control arrangement are temperature and acetic acid vapour concentration.

The outcome from this chapter is the development of a controllable test-bed for the testing of laboratory scale wireless sensor networks and specifically wireless chemical sensor networks. The testing of two developed networks will be described in Chapter 3 and Chapter 5.

A1.1 Environmental Test Chamber Concepts and Design

Following a critical design evaluation of the chamber structure requirements a number of design criteria were specified. The chamber environment must,

- be airtight,
- be easy to access,
- be transparent, and,
- facilitate sensors in both gas and liquid environments.

It is important to state at this point that the use of chemical sensing devices in liquid environments has not been examined by the author during the research period described in this thesis. However, liquid based sensing is being undertaken by others in the research group, with a view to using the ESC in their studies.

The first and most crucial requirement for the enclosure was that it be airtight. This was critical, as potentially hazardous chemicals, such as dilute ammonia, were initially proposed as gas targets for use in seeding the environment within the chamber. From a health and safety point of view it would be unacceptable to have chemical substances such as this escaping into a room where an operator was carrying out a testing programme. Also, because of the nature of the substances that could be introduced into the chamber regular cleaning and maintenance of the unit would be necessary. A second design requirement would, therefore, have to allow for all-round, unobstructed access to the internal surfaces.

The third requirement was that the chamber would have to provide all-round optical transparency. This was necessary in order to allow for video capture equipment and to give multiple viewing angles for demonstration purposes. This requirement allowed a number of choices for the main construction material. Perspex®, polycarbonate and glass are readily available transparent materials used in a wide range of industrial applications, and offered in sheet form with varying thicknesses and size. However, they have different properties.

Glass was quickly removed from the option list due to its weight and because of safety concerns over its ease of breakage. Perspex® is a trade name for the synthetic polymer polymethyl methacrylate (PMMA) [120]. PMMA is about half the weight of

glass with a density of 1190 kg/m^3. It does not shatter and is easily formed by heating but, as it is softer than glass it can be easily scratched. Although, shallow scratch marks can be removed from the surface of the material using polishing compounds. Polycarbonate displays higher impact strength than PMMA [121], but is a more expensive material. It was deemed that both Perspex® and polycarbonate would perform well as the structural material for this application, but as Perspex® provided the more cost effective option, it was selected as the main construction material.

Finally, the proposed applications for environmental sensors were not restricted to gas phase monitoring of environments. Therefore, the chamber needed to be capable of detecting other media in the environment. Chemical sensing within fluids, i.e., detection of chemical contaminants in outdoor watercourse environments, is another area of ongoing research within the Adaptive Information Cluster [122]. To give the test chamber multifunctional testing capabilities, it was proposed that a water channel be incorporated to run along the base of the unit. This would facilitate other researchers to conduct trials using sensors designed specifically for fluidic environments. An overview schematic of the proposed multifunctional chamber is presented in Fig. A1.1.

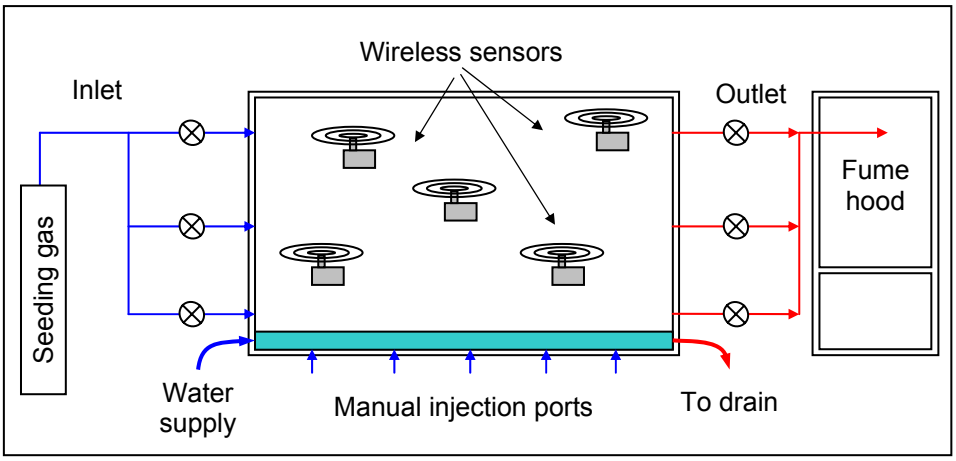

Fig. A1.1 Schematic of Environmental Sensing Chamber

A number of concept solutions were examined with emphasis on the design requirements detailed above. Initial concepts were developed around a unit with an internal volume of one cubic metre and two of these concepts are discussed in the following sections.

A1.1.1 Concept 1: Aluminium Frame Method

The first design proposal for the construction of the test chamber can be seen in the accompanying CAD representation, shown in Fig. A1.2. This design was based on using extruded aluminium profile lengths as a rigid frame that would hold clear panels of Perspex®. The Perspex® panels would fit into a rubber seal placed in the grooves of the extruded profile, giving an airtight environment.

The advantage of this concept was that the unit could be easily assembled and if necessary disassembled on-site from prefabricated components cut to specified sizes, satisfying the second requirement of easy access. However, there were a number of problems with this approach.

Firstly, it would be difficult to ensure an airtight seal around the unit. This was due to the fixing method employed in attaching the extruded lengths to each other, resulting in the corners of the frame not having a recess to hold the rubber seal. There was also concern that if the test-bed was required to be of a larger scale, additional supports would be required, possibly obstructing the view into the unit. The installation of a channel would be possible, although, it would complicate the design, as it would need to be bonded into place after assembly to ensure a watertight seal between the panel faces. The height difference between the bottom panel and the support frame into which the channel walls would sit would also require sealing. These concerns would have detracted from the ease of assembly and also added difficulty to any disassembly process. This concept fully satisfied none of the requirements, unlike the next design which used an alternative construction method.

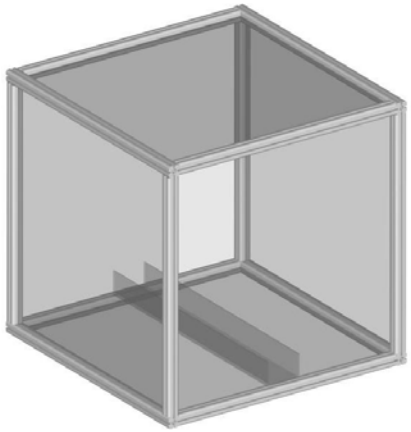

Fig. A1.2 Aluminium frame concept, including channel

A1.1.2 Concept 2: Bonded Panel Method

In this second possible method, instead of using rubber seals, the panels would be bonded together to form their own support. The strongest factor in favour of using this approach was that it would be relatively simple to ensure an airtight seal between the panels, because of the bonding process that would be employed during fabrication.

However, the design would have to cater for the fact that Perspex® (PMMA) is a brittle material [123] that can be easily cracked when stressed. The occurrence of a significant crack in a bonded unit such as this, would compromise the airtight integrity of the chamber. Sealing of a crack might be possible in a panel, however if the crack were through a structural joint complicated repairs would have to be undertaken. One foreseen problem with this approach was that it would be impossible to completely disassemble the unit once fabricated. Because of this, it became obvious that the final dimensions of the test chamber would have to be of manageable size so that heavy lifting equipment would not be required for moving the unit.

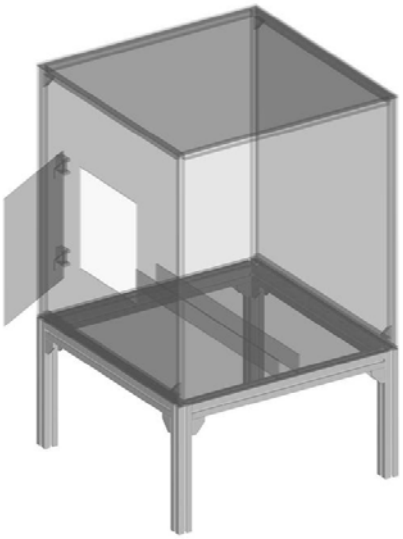

Fig. A1.3 Access hatch concept

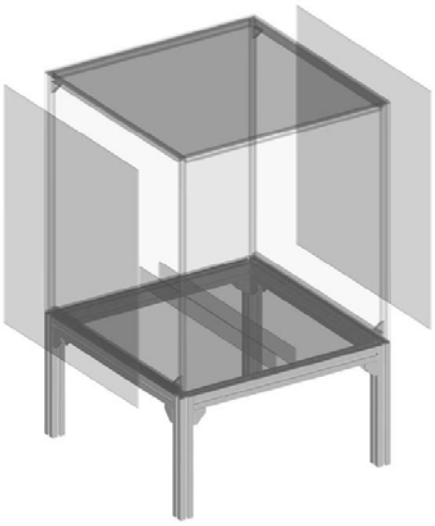

Fig. A1.4 Removable panel concept

Access to the unit was also essential and a requirement of the design demanded that the panels be removed easily by one person using a suitable and safe method. There were a range of methods which could be used to incorporate these criteria into the design. Two possible solutions are described here. The first, displayed in Fig. A1.3, is an access hatch. Depending on the requirements of the planned studies, a number of hatches could be placed around the unit. The drawback to this, however, was that the structure would be weakened by each additional hole and depending on the size of the holes, the operator may have found that access to some areas within the unit would be restricted. The operator would have unrestricted access if two of the side panels were removable, as shown in Fig. A1.4. As earlier stated, this would ultimately weaken the structure; however a method of reinforcement could be developed. An approach for holding the

panels securely in place would also need to be designed and in both of these cases sealing of the units at either the hatch or the removable panel would be required.

The incorporation and sealing of a water channel would be less complicated in this case as the outer panels would meet at right angles. It would therefore, be possible to permanently bond panels of appropriate height, to act as channel walls, directly into place.

During the concept design phase it became apparent that floor space availability within the research building would also become a critical factor. Initially, it had been proposed to have a test environment with an internal volume of twenty cubic metres. This was reduced to two cubic metres so that the test bed could fit into the available room space. It was however, decided that the design should allow for expansion in the future.

A combination of the bonded panel method with removable side panels satisfied all the key structural design requirements and was thus chosen as a basis for the final design. Refinement of the final concept design, shown in Fig. A1.5, was necessary to overcome and accommodate the seal, strength and potential future expansion problems outlined above.

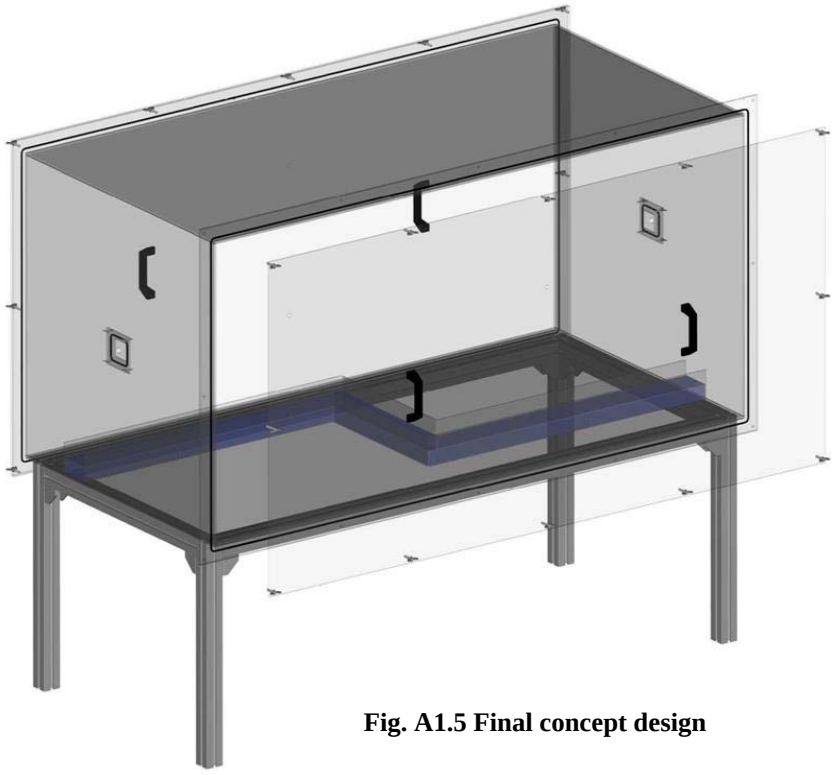

Fig. A1.5 Final concept design

A1.2 Refinement of Final Design

With the concept design accepted, the first area to address was the method of fixing the removable panels to the chamber test-bed so that they could be easily removed by the operator when required. This area of the design was critical to the strength of the unit and so it was important that the method used would increase the overall strength of the structure.

It would be impractical to tap boltholes into the sides of the top, bottom and end panels as shown in Fig. A1.6, as this would certainly induce stress in the panels and result in their weakening and cracking. At this point, the fact that the test-bed should allow for easy expansion was also taken into consideration. The simplest way of expanding the test-bed was to bolt two similar units together. The solution to this was to use a flange, to which the side panels could be attached, but could also be mated to a similar unit once the side panels had been removed.

The flange would be constructed from strips of Perspex®, bonded to the panel faces. Initially, the flange design was a continuous ring of material but this would not have been practical from a fabrication standpoint and also because of the large amount of wasted material. There were two options available to mount the flange. The flange could be fixed either inside or outside the panels as shown in Fig. A1.7 and Fig. A1.8, respectively. The bonding surfaces are highlighted in both diagrams in red.

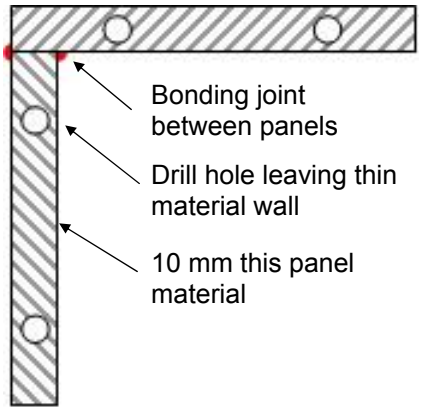

Fig. A1.6 Weak panel bond

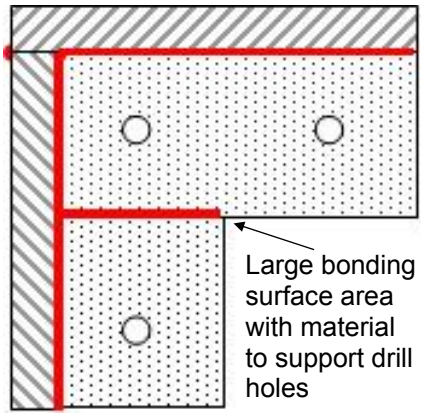

Fig. A1.7 Internal mounting flange

Mounting the flange inside the panels would provide the greater structural rigidity of the two options. However, if this method was used it could lead to complications if the

chamber volume was expanded through connection of multiple units. It would be complicated and awkward to connect two constructed units together from inside the test-bed. Also, the resultant joint between two connected units would act as an obstacle that would affect movement of gases within the volume. The preferred option, and the option used in the final design, was to bond the flange to the exterior of the panels, as this would not impede any airflow. This does not add the same degree of strength and rigidity to the unit, but it is still sufficient. The quality of the bonding is very important in this design as the joint between the flange strips is stressed by the weight of the top panel. Both an elevation and end-view of this bonded flange arrangement are detailed in Fig. A1.8.

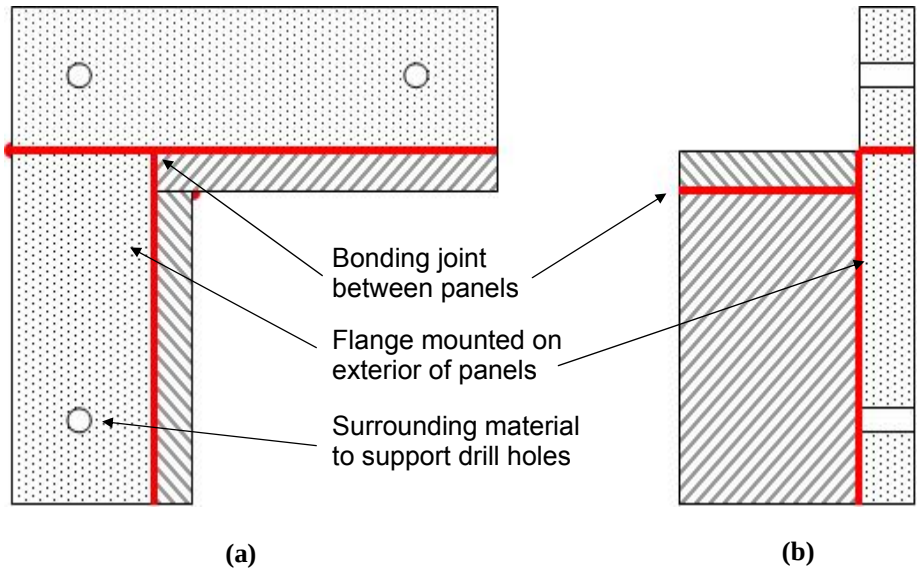

Fig. A1.8 External mounting flange (a) elevation (b) end-view

With the method of attaching the side panels chosen, the next stage was to develop a method of achieving an airtight seal at the joint. The initial concept solution for this challenge was the use of a continuous length of rubber with a circular cross section and diameter of 5 mm as an o-ring. This would achieve a seal between the side panel and flange, as shown in Fig. A1.9. The o-ring would be recessed 2.5 mm into the flange and held in position using an adhesive. It would therefore, have been necessary to machine the groove in the flange, before final assembly of the test-bed. Members of the in-house engineering workshop staff were consulted on the feasibility of this sealing method. Serious concerns were expressed on the suitability of this method, as it was thought that the side panel would be under stress when tightened to achieve an adequate seal. The viability of the fabrication process was also called into question, as there were no

facilities available on-site to carry out machining operations on material with a length in excess of two metres.

A simpler approach was developed where the seal would be made from expanded foam (Radionics no.205-0906) that forms an airtight seal when compressed. This can be seen in Fig. A1.10. The foam is available in 25 mm wide strips and has an uncompressed thickness of 10 mm. This sealing approach accommodated the possibility that the side panel and flange surfaces may not be perfectly matched. There was no need for additional machining as the seal could be easily cut to length and applied by hand directly to the flange face. The seal is held in place by an adhesive backing that was exposed when a protective strip of paper was removed.

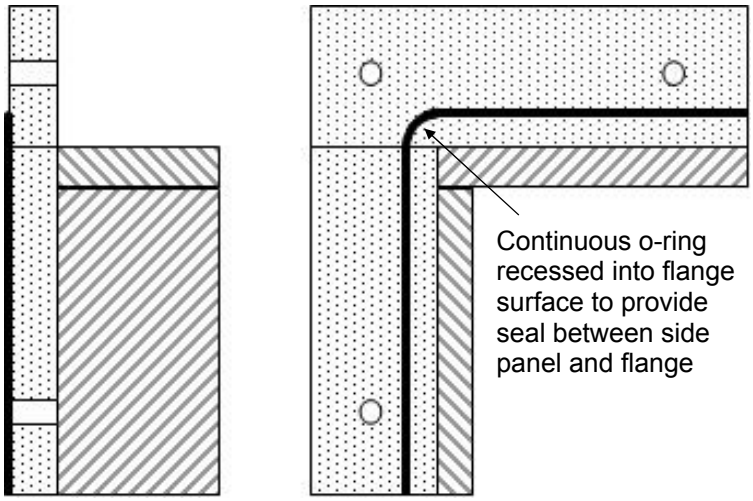

Fig. A1.9 O-ring panel seal

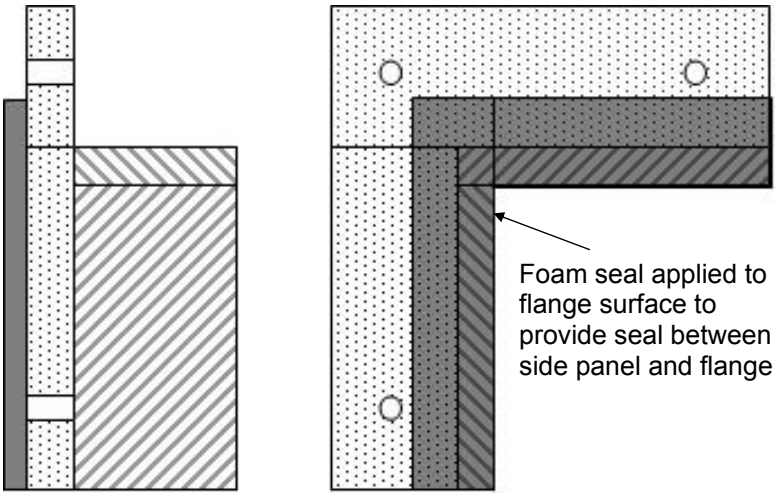

Fig. A1.10 Foam panel seal

Bolts (M8, 40 mm long) threaded into the flanges would act as guides for the positioning of the side panels, as shown in Fig. A1.11. The corresponding holes in the side panel would be slightly larger, with a diameter of 9 mm, giving a good clearance to account for any fabrication errors. Tightening the side panel against the expanded foam using M8 wing nuts would make the seal. The advantage in using wing nuts was that they could be loosened and tightened quickly and easily by hand.

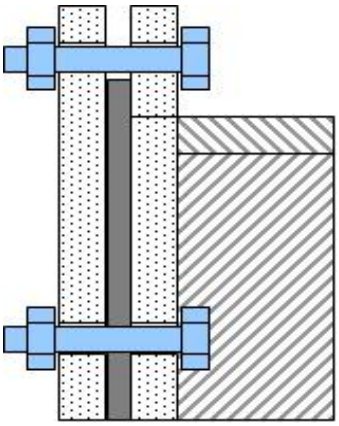

Fig. A1.11 Panel guide bolts

Threaded inlet and outlet ports distributed along the base and end faces of the chamber were added to the design to allow for the introduction and removal of gases and liquids. British Standard Pipe (BSP) fittings of ½" and ¼" were chosen due to the anticipated use of compressed air and water inlets seeded with mild acids and alkalis. Unused ports could be blocked using threaded plug fittings of suitable size. Port fittings were specified to be made from either stainless steel or nylon, because of their chemical resistance properties. The inlet and outlet points of the water channel were assigned ½" ports. All other port locations were specified as ¼" BSP. Ports incorporated into the base of the channel could be used to act as manual injection points at which contaminants could be introduced into a water flow.

The final design included the discussed provisions. The chamber and its component parts were drawn and assembled within a CAD package called Mechanical Desktop V5. Detailed part drawings of the chamber components are provided in Appendix 2. Appropriate material thicknesses for the wall, flange and side panels were chosen and specified on the component drawings. The precise location of port holes and their sizes were also addressed in detail. A rendered representation of the final design is shown in Fig. A1.12.

The frame shown in Fig 3.13 was designed to allow the chamber to be easily moved, carrying it at a working level so that the operator can comfortably access the unit. It also provides an area where the control and chemical handling components of the system can be safely mounted. The trolley frame was constructed from rigidly connected, pre-cut lengths of extruded aluminium with a square cross-section of 45 mm. Individually lockable wheels bolted to the end of each leg allow mobility.

With the chamber constructed as per the final design specifications and all requirements described at the outset satisfied, the next logical step was testing of the chamber.

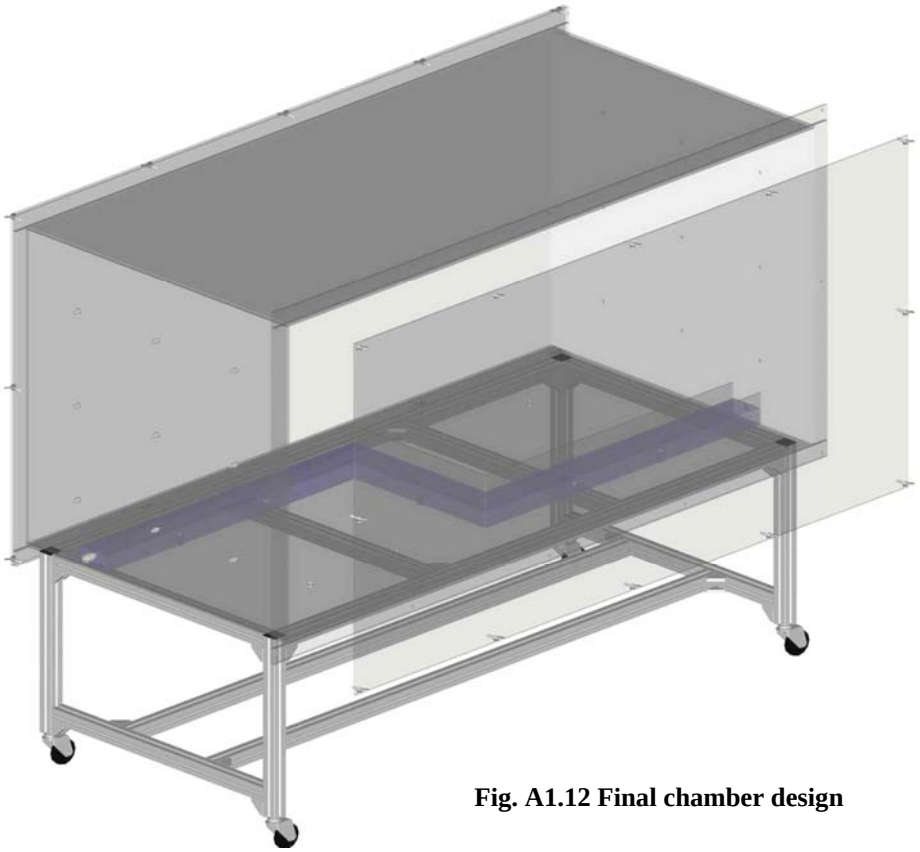

Fig. A1.12 Final chamber design

Fig. A1.13 Test-bed support frame

A1.3 Seal Evaluation & Smoke Testing

After construction, it was necessary to ensure that the chamber unit was correctly sealed, due to the expected use of potentially hazardous chemicals within it. A readily used medium for leak detection is artificial smoke. The smoke generator used for the test was a Martin Magnum 800, shown in Fig. A1.14. "Smoke" is produced by passing a fluid containing food grade glycols, polyglycols and de-mineralised water from a refillable plastic container through a 750 W copper and aluminium heat exchanger operating at a maximum temperature of 300 °C. When active an internal pump forces the liquid into the heat exchanger where the glycols are atomised and exit the heat exchanger under pressure as "smoke" [124].

Fig. A1.14 Martin Magnum 800 smoke generator

A method for directing the "smoke" output from the nozzle to the inlet ports of the chamber was developed. A protective guard around the nozzle was used as a sealing point. A Ø 40 mm union plumbing fitting was placed over the guard. Additional lengths and bends of 40 mm tubing were added so that the flow of "smoke" could be manipulated. A double ended ½" tapered nylon connector with an internal diameter of 12 mm connected the tubing outlet to an inlet port of the chamber. The "smoke" generator was positioned on the shelf of the test-bed frame, as shown in Fig. A1.15. The arrangement was tested to ensure that the "smoke" flow was satisfactory. It was found that the "smoke" flow through the pipe work was unobstructed and at a comparable rate to that when no additional pipe work was connected to the generator.

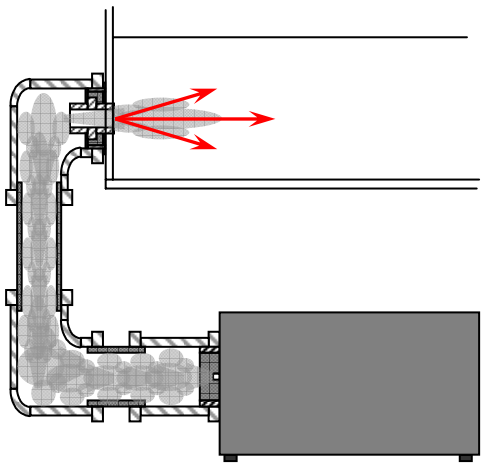

Fig. A1.15 Smoke application assembly

A1.3.1 Smoke Test Results and Required Chamber Modifications

To identify any leaks in the chamber's structure it was essential to pressurise the chambers internal volume using "smoke" as a leak indicator. The side panels were attached and tightened into place. The "smoke" generator was started with one port on the opposite face of the chamber left open to prevent an increase in the chamber's internal air pressure, as described in Fig. A1.16. When the volume was approximately 75 % full, the port was closed. "Smoke" continued to build up within the chamber. The side panel sealing and inlet/outlet ports were monitored for any sign of leakage. None was observed, as shown in Fig. A1.17.

However, leakage was observed at the connection point between the piping and the smoke generator. The reason for this leak was the positive pressure build-up within the chamber escaping at the point of least resistance. From this, it was deemed that the sealing of the side panels and ports was sufficient to contain a small positive internal pressure. It was not envisaged that there would be a need to apply chemical inputs at large pressures, so the sealing would be adequate. One significant observation was made during the process of removing the "smoke" from the chamber. It was found that the "smoke" did not disperse easily. Over time, the "smoke" condensed back into a liquid residue on the base of the chamber. The seal test concluded that there was a need for an extraction system to remove applied contaminants from the chamber.

Fig. A1.16 Initial smoke application

Fig. A1.17 Smoke filled chamber

Provision for an extraction system had been overlooked during the chamber design phase. An evacuation method which could remove a similar volume of gas or air to that entering the chamber was developed. Initially the use of a vacuum pump was suggested. However, the internal volume of the chamber (2 m^3) and an acceptable time period to perform the evacuation process were far in excess of the capabilities of such pumps. Instead a small extraction fan was used.

A square opening was made at one end of the unit. A connecting plate, bolted to the extraction end of the unit, to allow attachment of a hose with a diameter of 100 mm was designed, as shown in Fig. A1.18.

The next phase of development introduced a means of managing the parameters of interest which would be monitored within the chamber environment throughout later wireless sensor network studies.

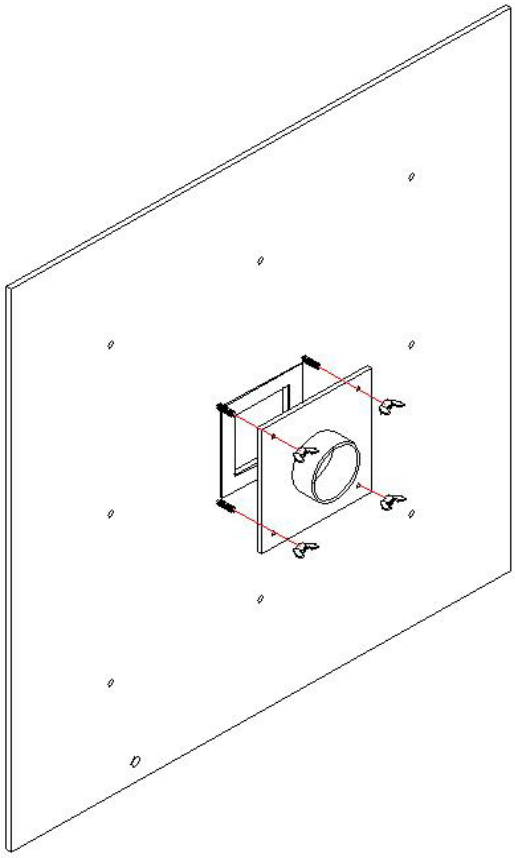

Fig. A1.18 Extraction hose connection plate

A1.4 Environmental Chamber Control

Control of equipment to vary parameters of interest within the chamber environment was vital. Manual control of the equipment was sufficient for basic sensor testing. However, the objective of a reactive real-time system required that provisions for automated control of electro-mechanical components be addressed. Control of the components was governed by 5 V output signals generated via a PC based graphical user interface, which is discussed in Section 3.5. The components that required automated control included,

- an external heat source,
- an extraction fan, and,
- multiple compressed air supplies.

The operating voltages of the systems electro-mechanical components differed from the signal voltage available from the PC. It was, therefore, necessary to develop an indirect power switching method. This was achieved through the use of an intermediate relay board that switched 240 VAC or 24 VDC power supplies to the appropriate component when the correct signal line was activated.

After the development of output signals to control electro-mechanical components it became necessary to integrate the components into the chamber arrangement so that two separate target parameters, temperature and an acetic acid/air mixture, could be varied for separate sensor network studies.

A1.4.1 Relay Signal Board

A relay board was designed around the relay control circuit shown in Fig. A1.19. This circuit was employed to indirectly operate the 24 V relay to ensure protection of the control PC from any stray voltages or signals. When the signal line from the PC was activated, i.e., set to logic high (5 V), the transistor was turned on. This allowed a current to flow through the solenoid of the 24 V relay switching its contacts. In the presence of an active power supply, a device connected across the switched contacts was activated.

Returning the PC signal line to a state of logic zero (0 V) turned the transistor off, preventing a current flow through the relay coil. The coil was no longer energised and

so the contacts reverted to their initial open position. This, in turn, broke the connection between the controlled device and its power supply. When controlling mains powered devices or devices that draw a significant current, an additional double pole change over (DPCO) relay such as that shown in Fig. A1.20 (Radionics no. 348-784) was used.

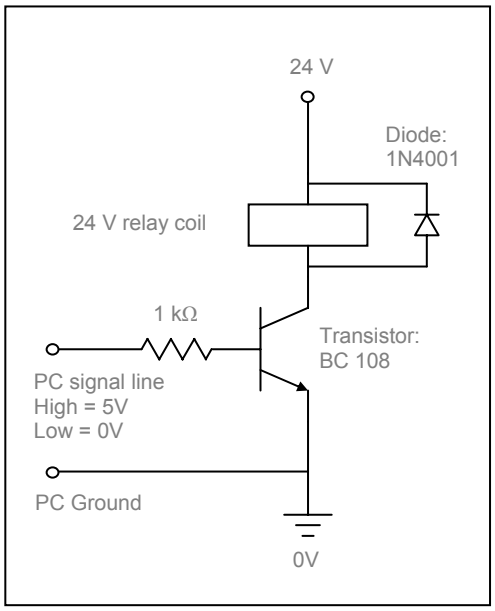

Fig. A1.19 Relay control circuit

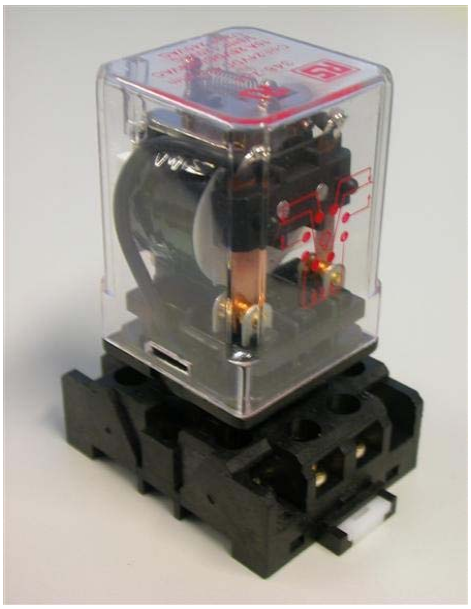

Fig. A1.20 Industrial DPCO relay

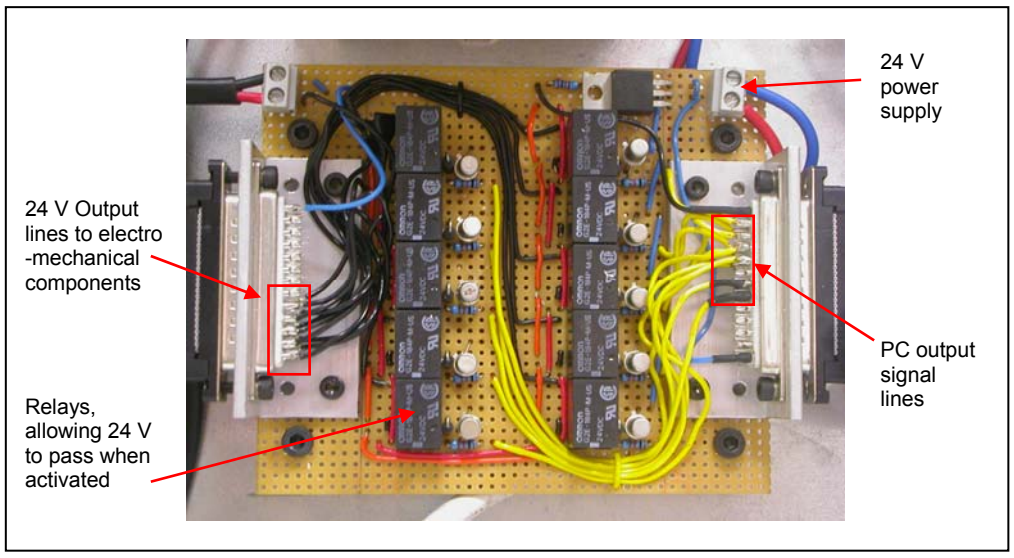

Fig. A1.21 Custom relay board

The circuit was replicated and assembled, as shown in Fig. A1.21, using Omron 24 VDC miniature PCB relays (G2E-184P-M-US-24VDC, Radionics no. 369-539) and standard electronics components, as identified in Fig. A1.19. The constructed relay control board allowed for up to ten output signal lines. Power for the relay coils and the

switching contacts was provided by a regulated 24 VDC power supply unit. This power supply was also used to provide power to the DPCO relay coils. Connections to the board were standard 25-pin male and female D-sub connectors. This allowed for easy disassembly of the board for maintenance or modification.

A1.4.2 Temperature Control

Initial sensor platform testing was based on temperature change within the chamber volume. Monitoring of a known physical parameter allowed for node communications and system output signalling to be tested (Section 3.5) before the incorporation of a less established optical chemical sensor (Chapter 4). A domestic 2000 W hairdryer (Braun FuturePro) was obtained to act as an external heat source which, when active, would apply heated air to the chamber inducing a temperature change at various sensor locations.

Additional modifications to the chamber were required to facilitate the attachment of the heat source. An opening of similar size to that made in Section A1.3.1 was incorporated on the inlet face of the chamber. A removable mount was constructed to hold the external heat source in a fixed position. The position of the heat source nozzle was fixed in the centre of the inlet, perpendicular to the inlet face, using a reduction ring within a connection plate.

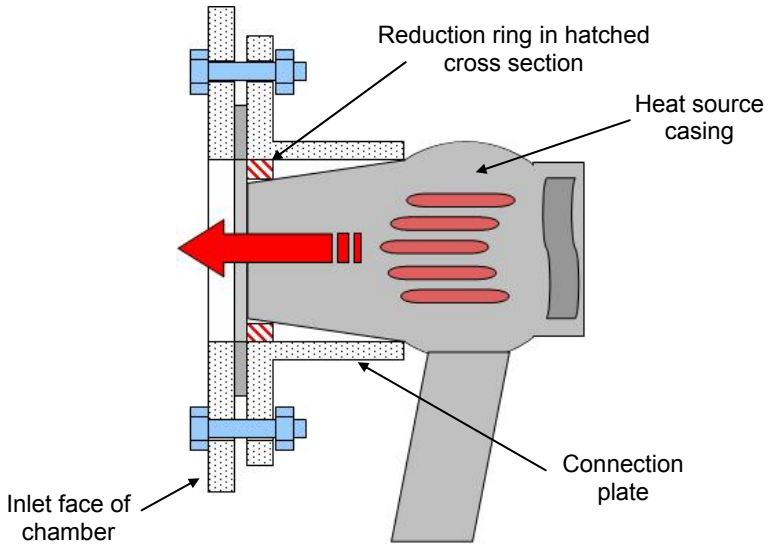

Fig. A1.22 Heat source mounting

A schematic of the housing (not to scale), is shown in Fig. A1.22. The joining edge between the connection plate and the casing of the heat source was sealed using industrial tape, thus securing the heat source to the mount, which was then bolted in place on the chamber face. Cooling of the environment, if necessary, would be achieved using an extraction fan mounted at the opposite end of the chamber to the heat source. When active, the fan would cause a reduction of the internal temperature by drawing room temperature air through the chamber volume.

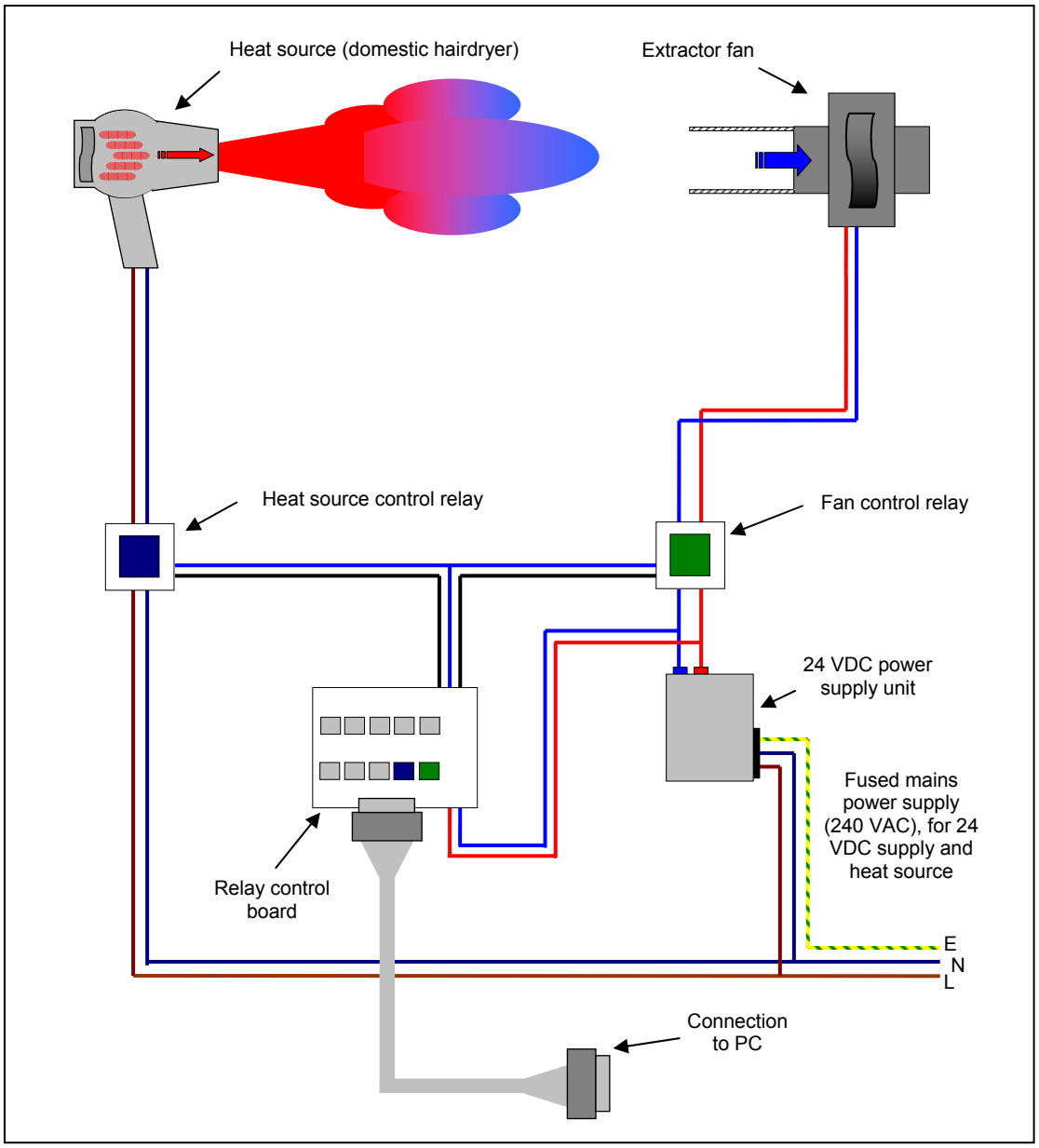

Fig. A1.23 Heat source and extraction fan control arrangement

The arrangement of the devices used to manage the air temperature within the chamber environment is presented in Fig. A1.23. Two separate signal lines were required for

control of the two devices. Signals from the connected PC controlled the switching of the two highlighted control board relays. These relays, in turn, governed the switching of two DPCO relays. Power for the heat source and extraction fan was connected across the respective DPCO relay terminals, as also shown in Fig. A1.23.

A1.4.3 Chemical Contaminant Control

A key objective of this research was to develop a reactive wireless chemical sensor actuator network. It was, therefore, essential to have a method of seeding the chamber environment with a chemical stimulus. The chemical proposed for use in the seeding of the environment was acetic acid.

The acid is available in liquid form but for the air based sensor tests undertaken in Chapters 4 and 5 it was necessary for the chemical to be dispersed through the chamber as a gas. This was achieved by bubbling compressed clean dry air (CDA) through the liquid acid in a sealed glass container.

This sealed container is referred to as a bubbler. The acetic acid vapour, known as the acidic air, collected in the headspace above the liquid. The acidic air was forced out of the bubbler as a plume, as shown in Fig. A1.24, by the constant pressure of compressed air on the inlet side. The volume of CDA applied to the bubbler governed the rate of acidic air production. Therefore, by increasing the volume of air entering the bubbler, the volume of acidic air exiting from the outlet in turn increased. The acidic air was applied to the chamber by connecting the outlet line of the bubbler unit to one or more of the available inlet ports on the chamber face. The contaminant concentration of the produced acidic air is investigated in Section 4.5.

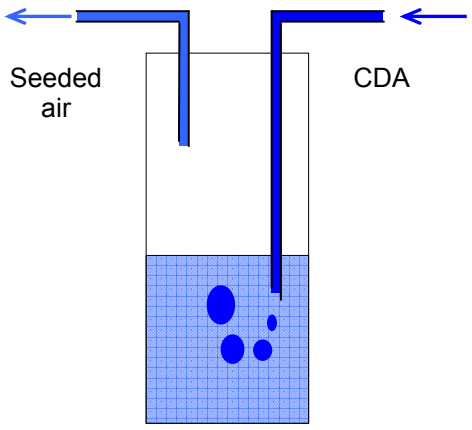

Fig. A1.24 Bubbler arrangement

Upon the completion of sensor studies, purging of the acetic acid/air mixture from the system was accomplished using the extraction fan in conjunction with auxiliary CDA inlets, as described in Fig. A1.25. The purpose of the auxiliary inlets was to agitate any

stationary contaminated air. It was found during initial testing, that the chamber volume was difficult to purge and so the inlet face was modified to include a vent. The vent, shown in Fig. A1.26, made use of the opening and bolt fittings that had been put in place for the heat source inlet. The vent consisted of a slide plate mounted between a backing and top plate. Two guides attached to the backing plate at either side of the slide plate restricted the slide plate to linear movement. Actuation of the slide plate into the open position aligned holes cut into each of the three assembled plates, providing an opening through which additional air could enter the chamber. An o-ring, with a radius of 53 mm located between the backing and slide plates, provided a seal that prevented escape of the seeding contaminant when the vent was closed.

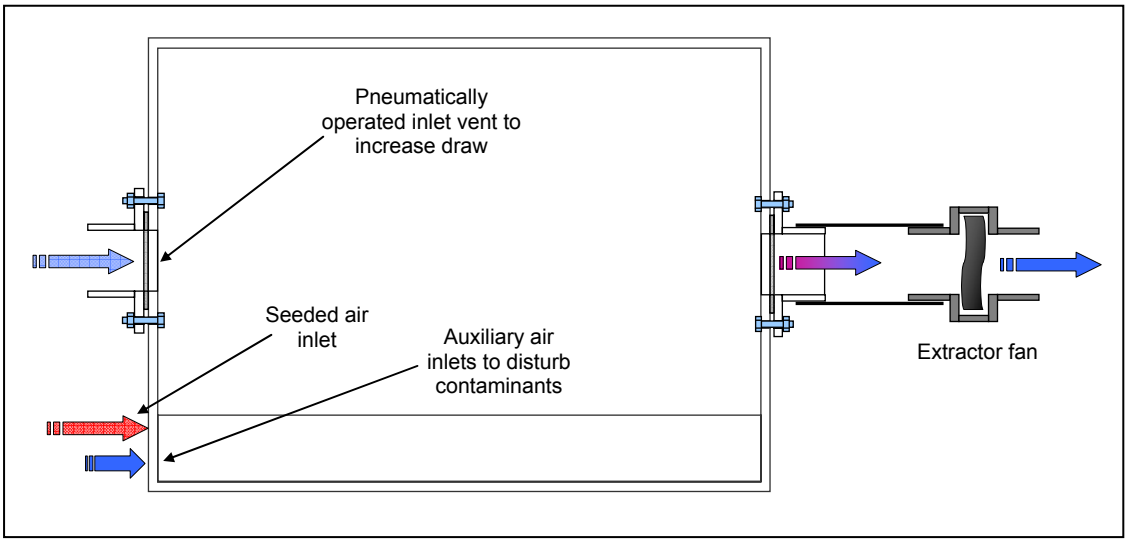

Fig. A1.25 Contaminated air purge components layout

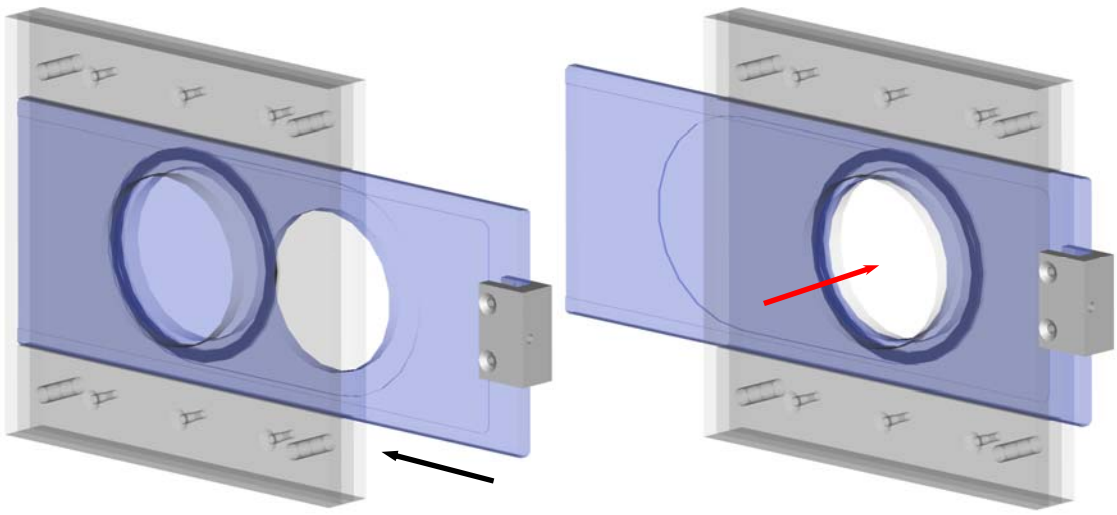

Fig. A1.26 Slide vent operated by a pneumatic cylinder

Opening of the vent ensured that there was a sufficient draw of air through the chamber volume, assisting the purge operation. Movement of the slide plate was achieved using a standard double acting pneumatic cylinder with a stroke length of 100 mm. The threaded end of the cylinder rod was connected to the slide plate via an aluminium connection block and held in place on the slide plate using two M5 countersunk screws. The pneumatic cylinder (not shown) was fixed to the chamber face and mounted so that its central axis was parallel to the direction of movement of the slide plate and that the vent was closed when the cylinder was in its rest position.

Movement of the pneumatic cylinder, and in turn the vent, was controlled by a standard 5/2-way solenoid operated pneumatic valve. This valve was also responsible for the application of purge air to the chamber volume. It was possible to use a single valve in achieving this, as both operations were called at the same time to purge the chamber of any chemical contaminants.

A 2-way solenoid operated valve governed the supply of CDA to the bubbler unit for application of acidic air to the chamber. A stainless steel bodied valve was specified for the role because of its resistance to corrosion (Bürkert Type 6213, supplied by Flomax). A manually operated flow controller with a visual flow rate indicator was included on the bubbler supply line to give an indication of the volume of seeded air entering the chamber and to facilitate flow rate changes when necessary.

The arrangement of the control devices used for the seeding and evacuation of chemical contaminants is displayed in Fig. A1.27. In normal operation, the air supply lines to the chamber were inactive, the fan was off and the chamber opening was closed unless an appropriate control signal was received at the relay board.

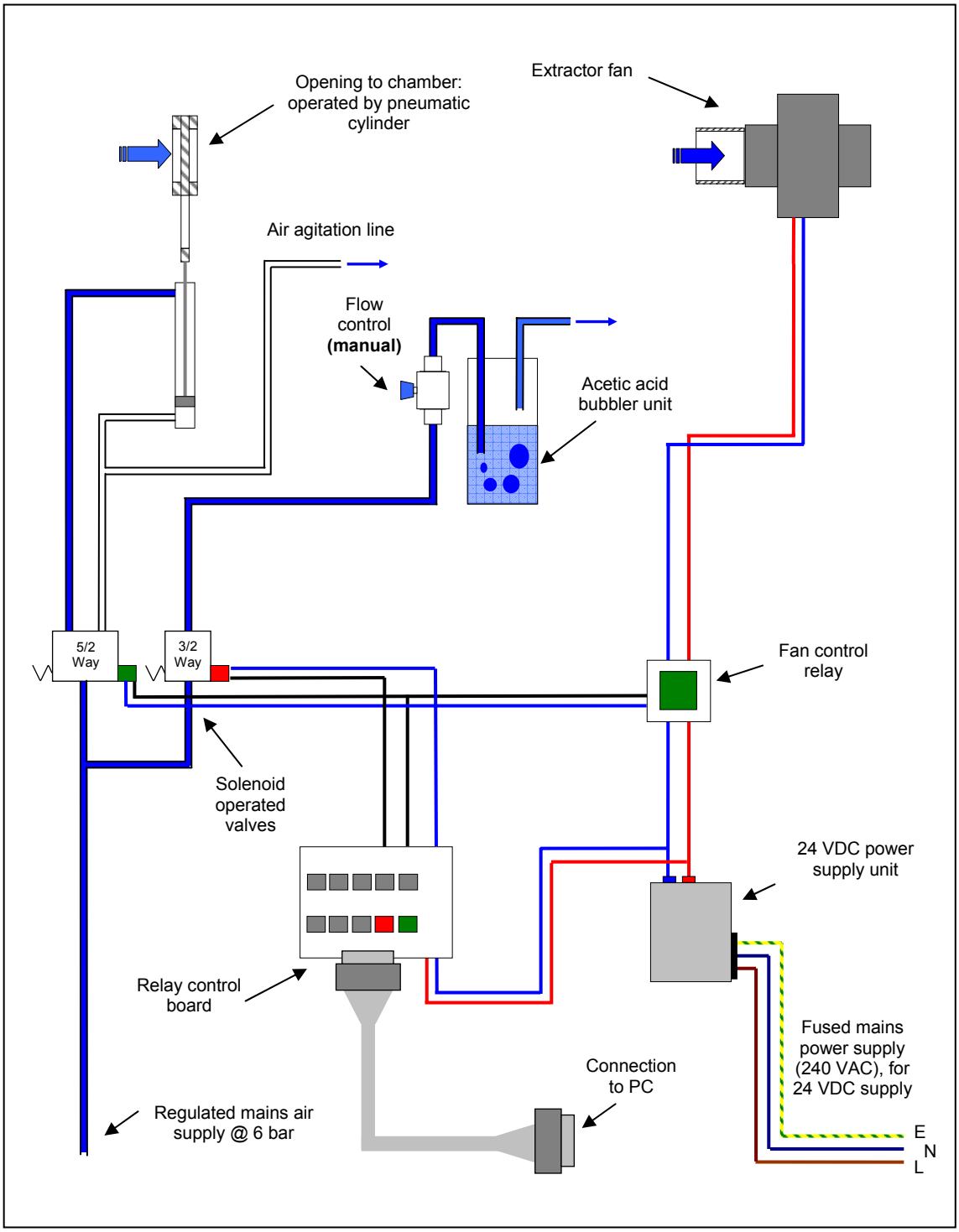

Fig. A1.27 Chemical contaminant generation and purge control arrangement

A1.5 Appendix 1 - Summary and Conclusions

In this chapter, concept designs for an environmental sensing chamber were evaluated. The final design successfully satisfied the four main criteria outlined for the chamber at the beginning of the chapter. The developed 2 m^3 ESC has been designed to be airtight, easily accessible, optically transparent, and to facilitate both gas and liquid monitoring devices. The integrity of the access panel sealing method was successfully verified through the application of "smoke" as a leak detection medium.

Provision for control via a PC interface was also implemented in this chapter. Operation of 24 VDC and 240 VAC electro-mechanical components, for the purpose of target parameter management was achieved through an intermediary relay board.

A method to vary the temperature parameter within the chamber environment has been designed through the incorporation of an external heat source. Forced cooling has been made possible by inclusion of an extraction fan to draw room temperature air into, and remove heated air from, the developed test environment. Adjustment of this parameter is utilised during the evaluation of developed wireless sensor platforms, detailed in Chapter 3.

A method for reproducible acidic air plume generation was developed, through application of compressed dry air, at a controlled flow rate, to a bubbler unit containing a dilute solution of acetic acid in water. The resultant contaminant vapour acts as the target chemical species for a developed wireless chemical sensor, and later for wireless chemical sensor network studies. A developed process for contaminated air removal, also provided for the possibility of stagnant contaminant on the chamber base, through inclusion of air agitation lines for the purpose of dispersing the denser than air target. The use of contaminant plume generation and removal methods are detailed in Chapters 4 and 5.

Appendix 2

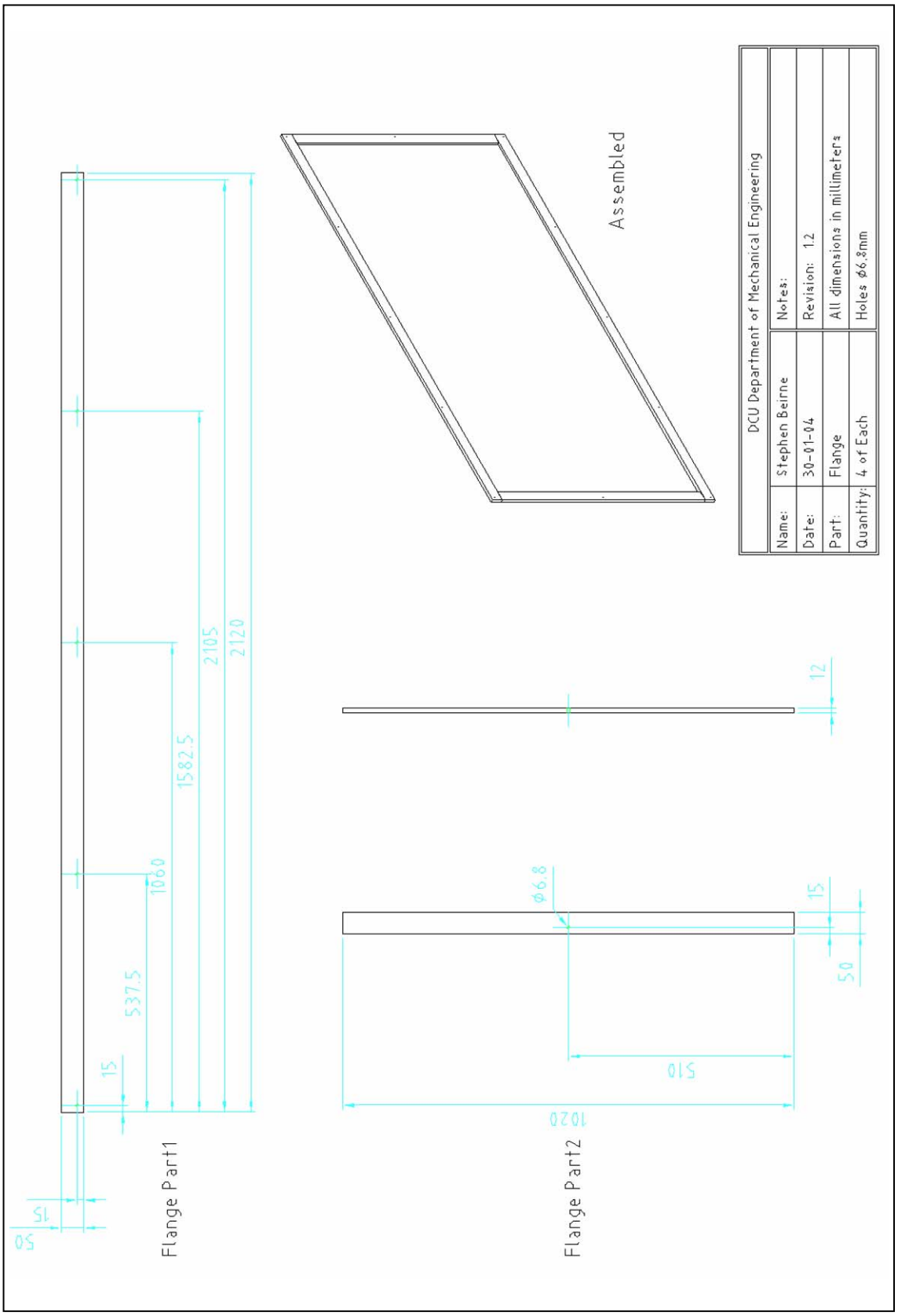
DCU Department of Mechanical Engineering
Name: Stephen Beirne
Date: 30-01-04
Part: Flange
Quantity: 4 of Each
Notes:
Revision: 1.2
All dimensions in millimeters
Holes ø6.8mm
Assembled
Flange Part1
Flange Part2
2120
2105
1582.5
1060
537.5
15
50
12
ø6.8
510
1020

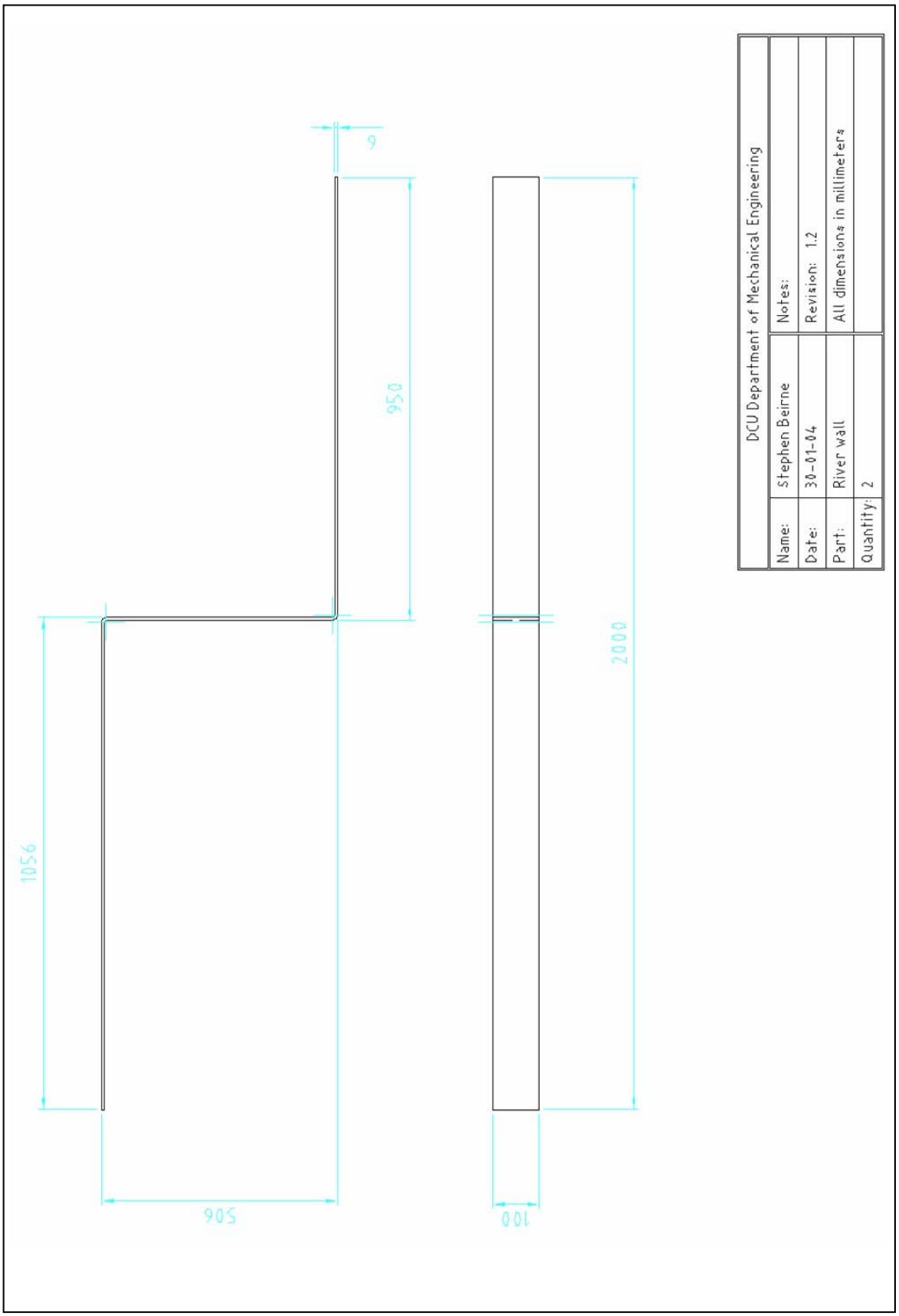
9
950
2000
1056
905
100
DCU Department of Mechanical Engineering
Name: Stephen Beirne
Date: 30-01-04
Part: River wall
Quantity: 2
Notes:
Revision: 1.2
All dimensions in millimeters

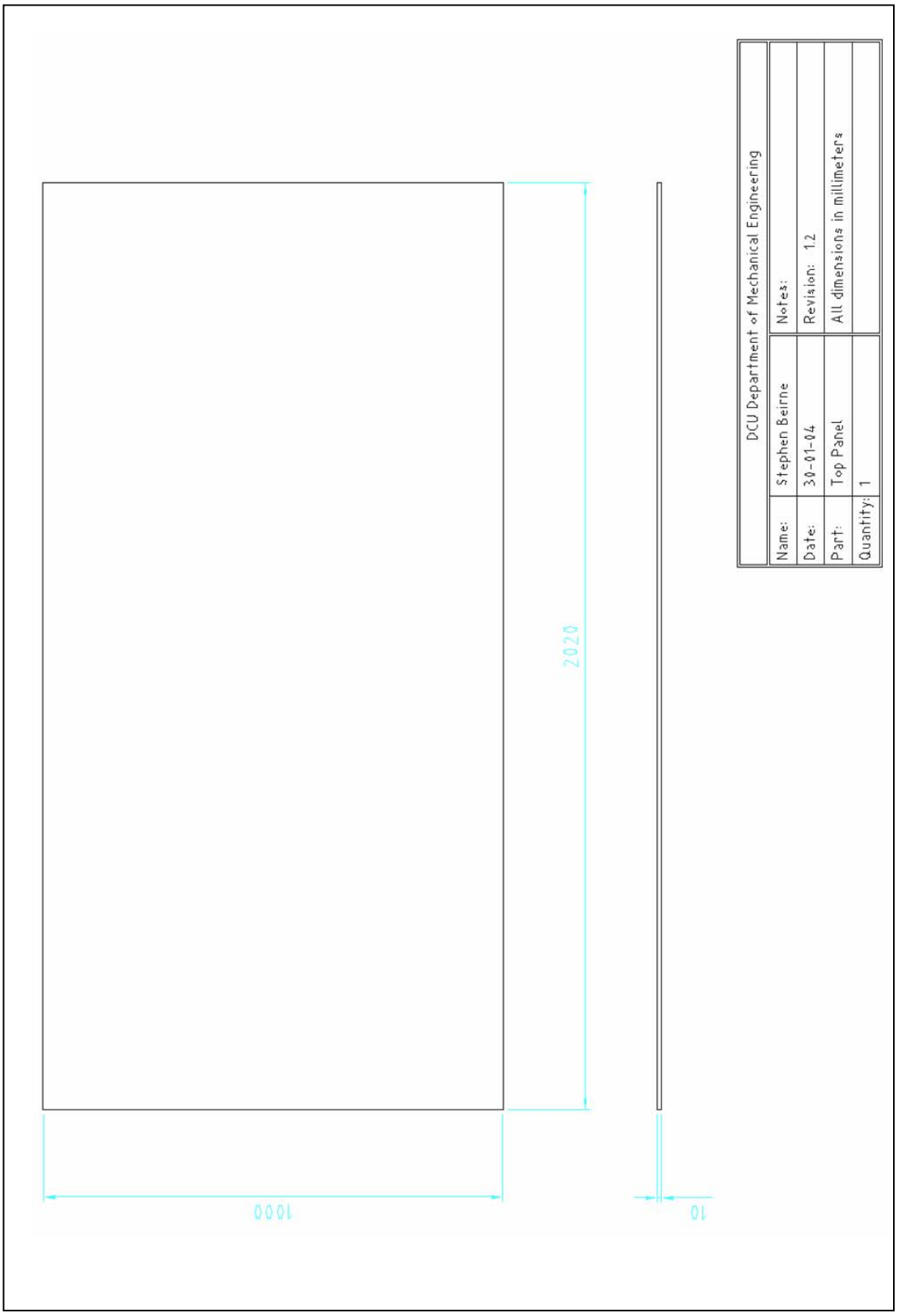
DCU Department of Mechanical Engineering
Name: Stephen Beirne
Date: 30-01-04
Part: Top Panel
Quantity: 1
Notes:
Revision: 1.2
All dimensions in millimeters
2020
1000
10

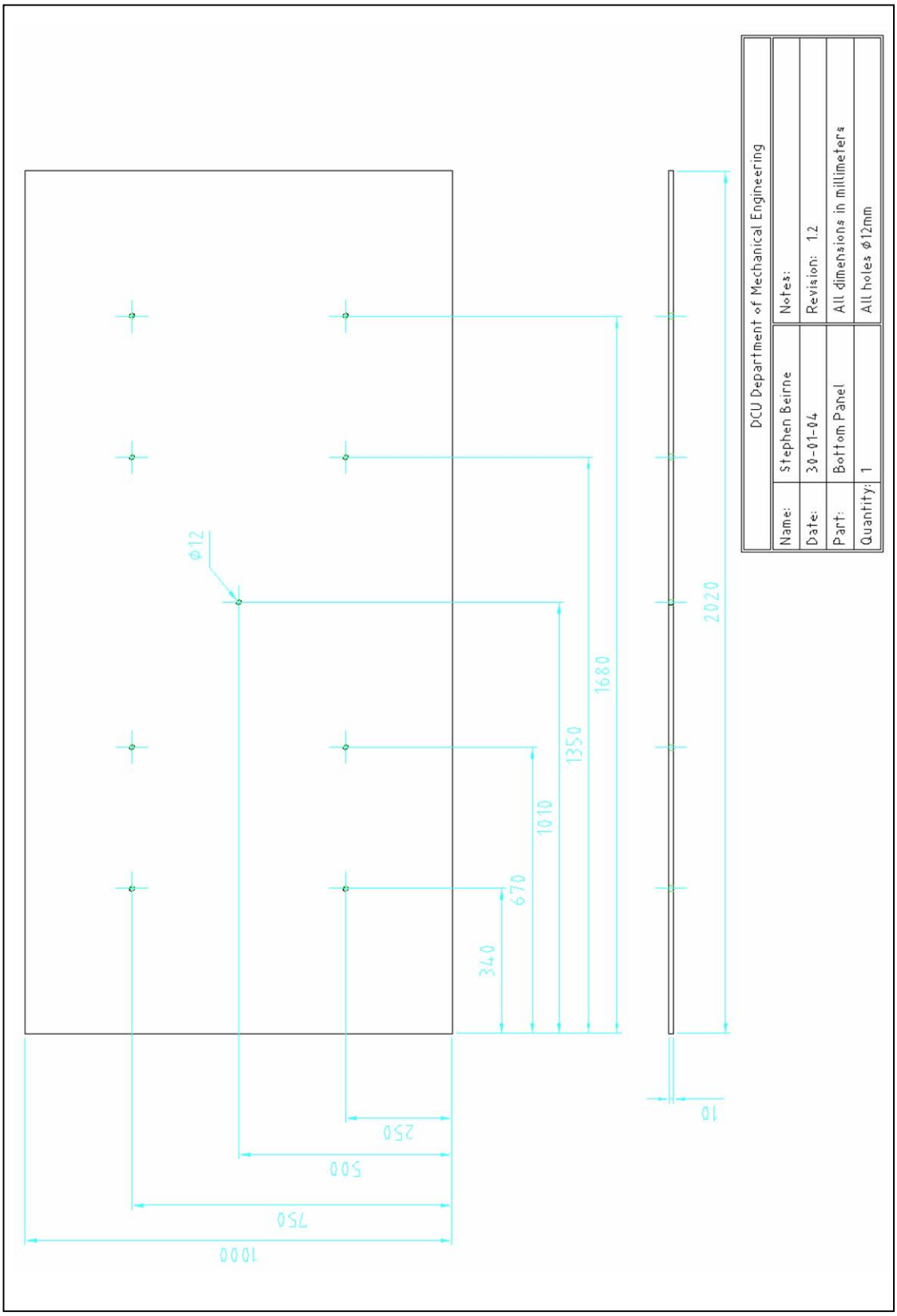
DCU Department of Mechanical Engineering
Name: Stephen Beirne
Date: 30-01-04
Part: Bottom Panel
Quantity: 1
Notes:
Revision: 1.2
All dimensions in millimeters
All holes ϕ12mm
ϕ12
340
670
1010
1350
1680
2020
250
500
750
1000
18

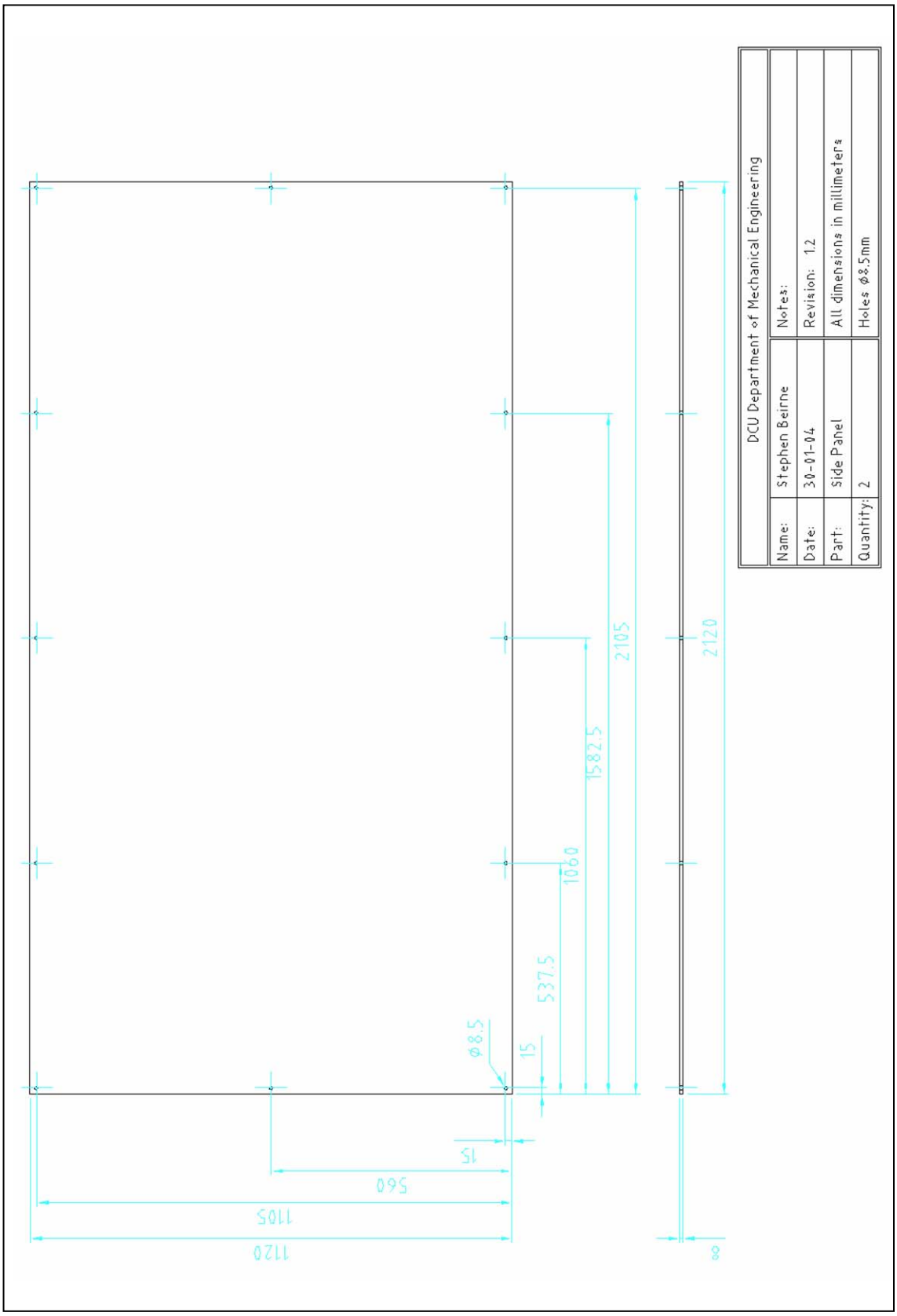
DCU Department of Mechanical Engineering
Name: Stephen Beirne
Date: 30-01-04
Part: Side Panel
Quantity: 2
Notes:
Revision: 1.2
All dimensions in millimeters
Holes ø8.5mm
2120
2105
1582.5
1060
537.5
15
ø8.5
15
560
1105
1120
8

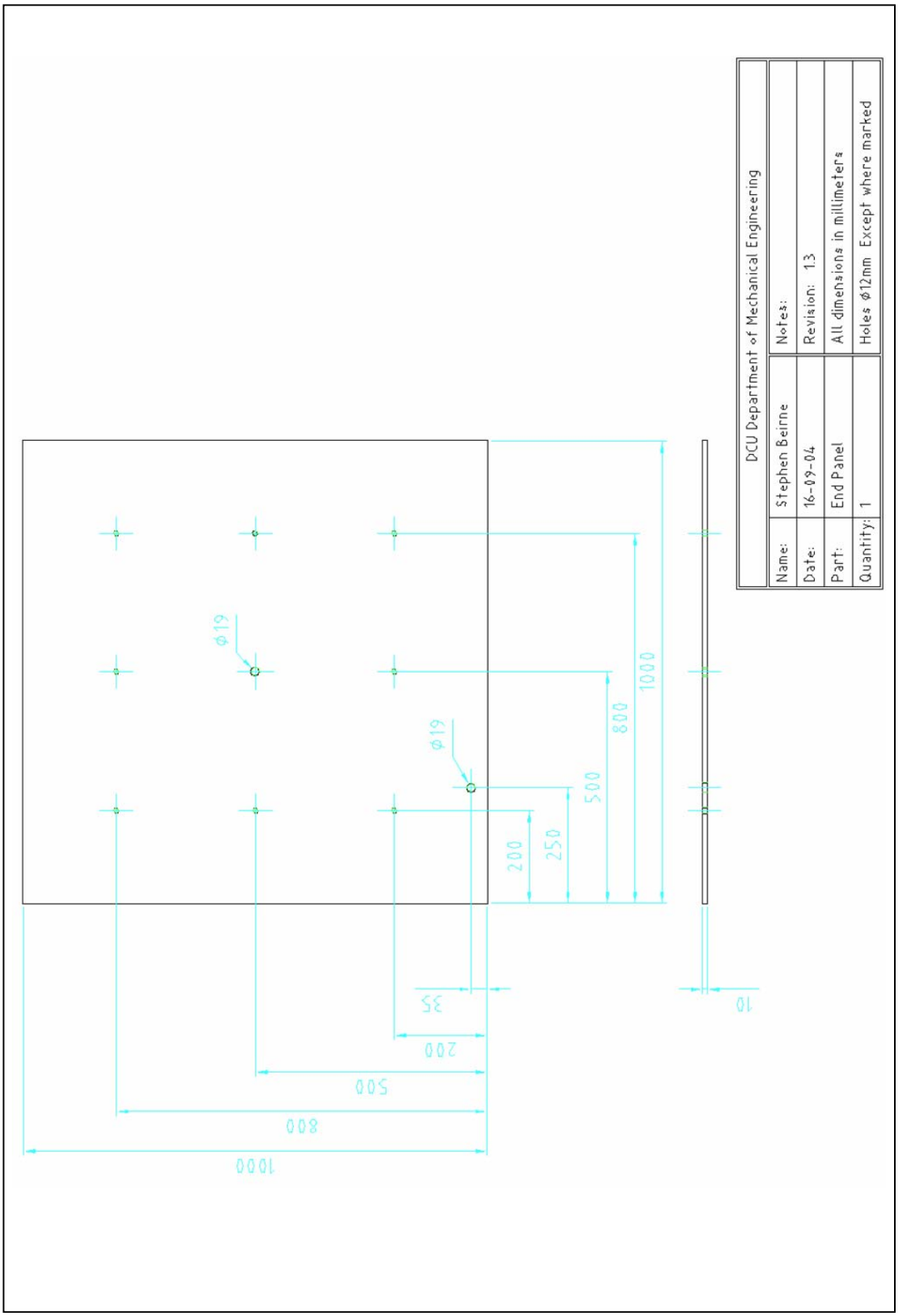
DCU Department of Mechanical Engineering
Name: Stephen Beirne
Date: 16-09-04
Part: End Panel
Quantity: 1
Notes:
Revision: 1.3
All dimensions in millimeters
Holes ø12mm Except where marked
ø19
ø19
1000
800
500
250
200
35
200
500
800
1000
10

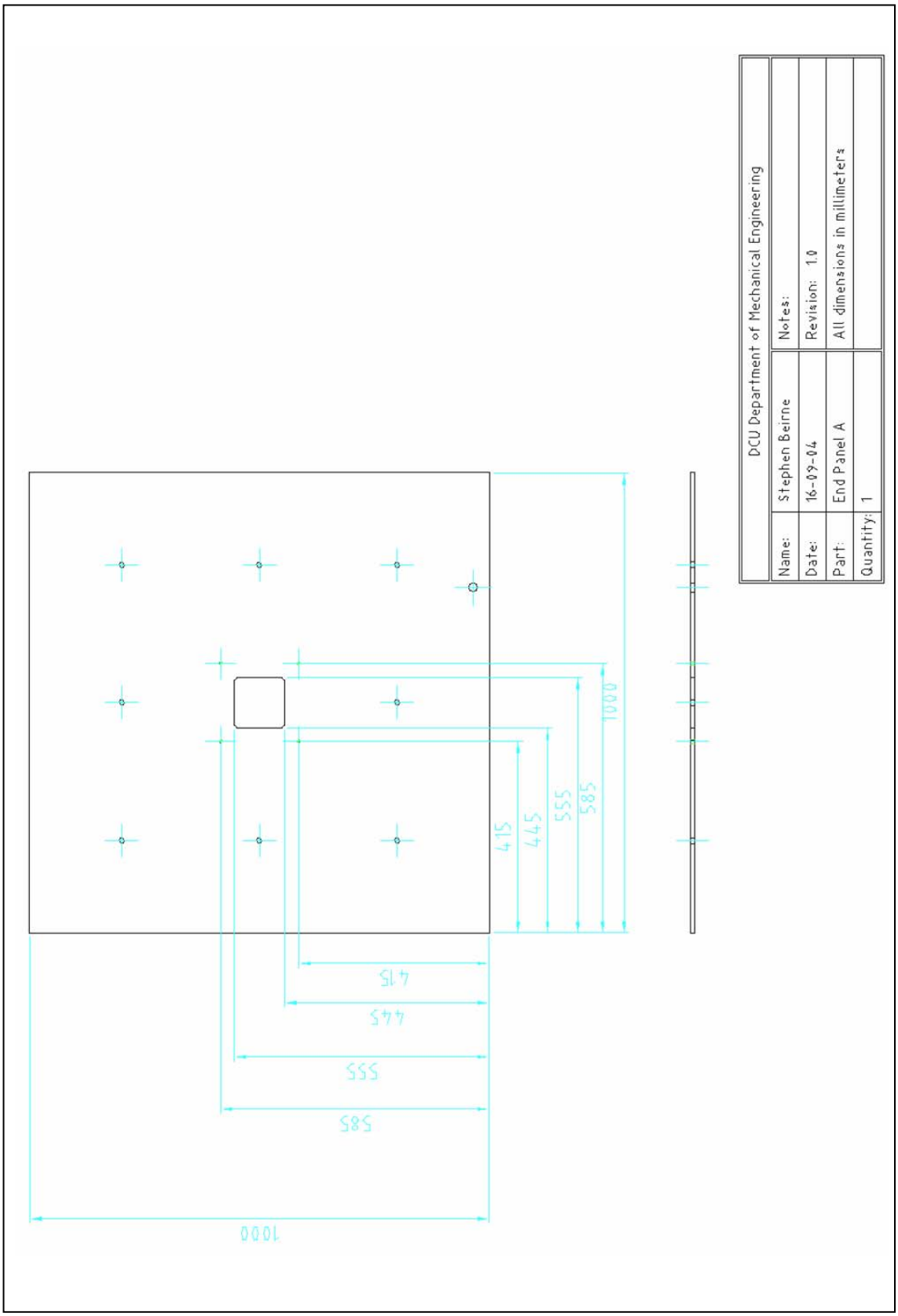
DCU Department of Mechanical Engineering
Name: Stephen Beirne
Date: 16-09-04
Part: End Panel A
Quantity: 1
Notes:
Revision: 1.0
All dimensions in millimeters
1000
585
555
445
415

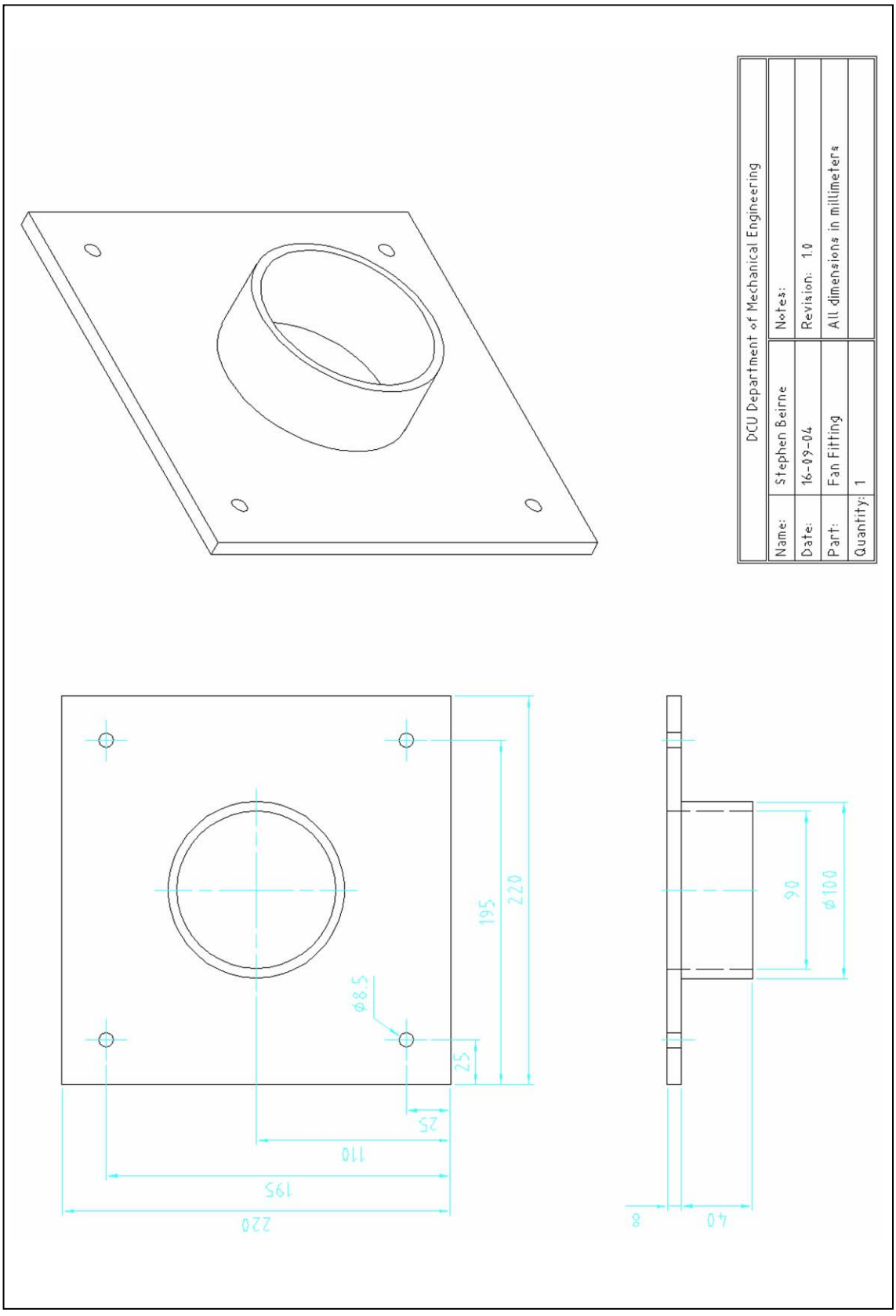
DCU Department of Mechanical Engineering
Name: Stephen Beirne
Date: 16-09-04
Part: Fan Fitting
Quantity: 1
Notes:
Revision: 1.0
All dimensions in millimeters
ø8.5
25
195
220
110
90
ø100
8
40

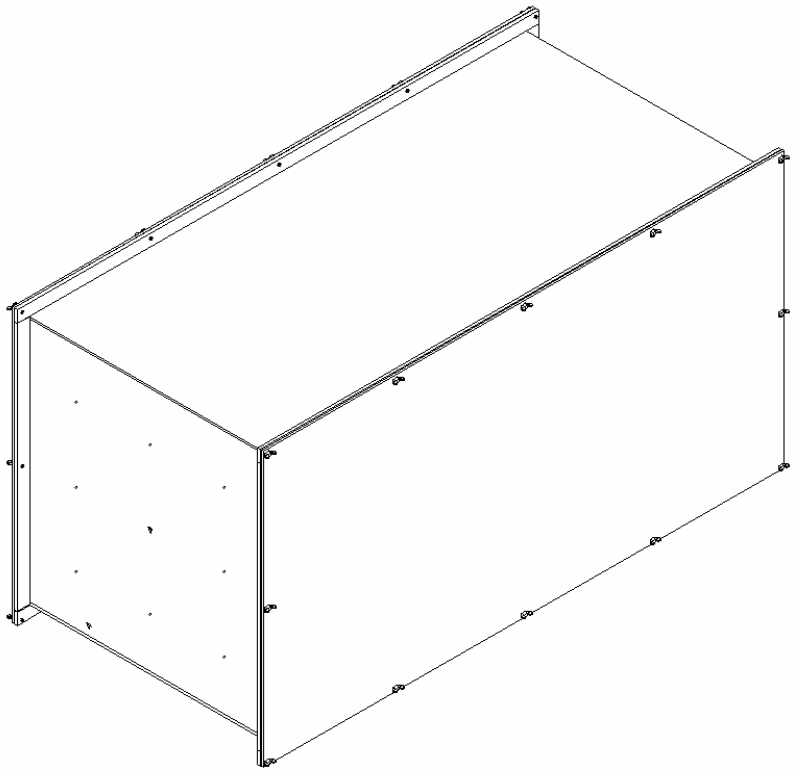

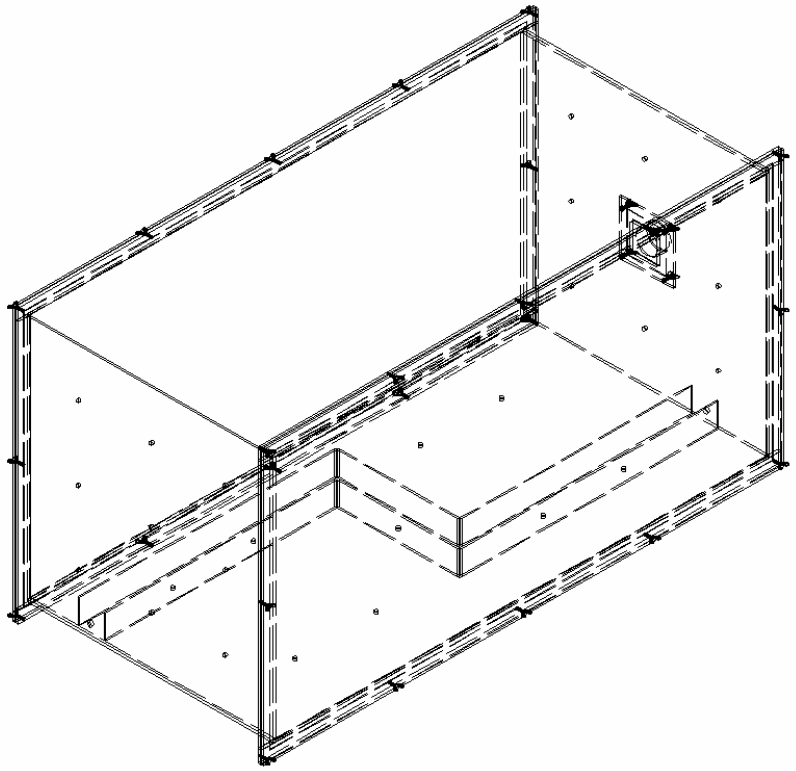

Bill of Materials			
Part Name:	Quantity:	Part Name:	Quantity:
Flange Part1	4	Top Panel	1
Flange Part2	4	Bottom Panel	1
Side Panel	2	River Wall	2
End Panel	2		

DCU Department of Mechanical Engineering		
Name:	Stephen Beirne	Notes:
Date:	16-09-04	Revision: 1.3
Part:	Assembly	All dimensions in millimeters
Quantity:	1	

Appendix 3

Example of ADC value conversion to temperature

V_{ADC} and R_T are found using Equations A3.1 and A3.2 respectively as described in Section 3.1.1. The calculated thermistor resistance, R_T, is then used in the Steinhart-Hart thermistor conversion equation along with the variables provided by Thermometrics, Equation A3.3. The temperature value arrived at using the conversion formula is in degrees Kelvin, Equation A3.4. To convert this value to degrees Celsius the value of 273.15 is subtracted. The resultant temperature value is rounded to 1 decimal point of accuracy giving a temperature reading of 21.6°C, Equation A3.5.

$$V_{ADC} = \frac{550 \times 2.9296875}{1000} = 1.611328V \tag{A3.1}$$

$$R_T = \left(\frac{10}{3} \times 1.611328\right) \Big/ \left(1 - \frac{1.611328}{3}\right) = 11.603376k\Omega \tag{A3.2}$$

$$\frac{1}{T} = \mathrm{a} + b\left(Ln\left(\frac{11.603376}{10}\right)\right) + c\left(Ln\left(\frac{11.603376}{10}\right)\right)^2 + d\left(Ln\left(\frac{11.603376}{10}\right)\right)^3 \tag{A3.3}$$

$$T = \frac{1}{0.003392398} = 294.7768\text{Kelvin} \tag{A3.4}$$

$$T = 294.7768 - 273.15 = 21.6^{\circ}\mathrm{C} \tag{A3.5}$$

Appendix 4

```
'Program code for the operation of the On/Off temperature controller
-----------------------------------------------------------------------
Dim TempMin As Integer
Dim TempMax As Integer
Dim LPT_Address As String
Dim HeatOff As Boolean
Dim MaxTemp As Boolean
Dim Outputallowed As Boolean
-----------------------------------------------------------------------
Private Sub Form_Load()
    LPT_Address = 378
    TempMin = 25
    TempMax = 27
    Outputallowed = False
    Out Val("&H" + LPT_Address), Val(0)
    Call VScroll1_Change
    Call VScroll2_Change
    Call Command1_Click
    Call Command2_Click
    Call Processing
End Sub
-----------------------------------------------------------------------
Private Sub VScroll1_Change()                   'Min Limit Bar changed
  TempMin = (80 - VScroll1.Value)
    Label8.Caption = TempMin
End Sub
-----------------------------------------------------------------------
Private Sub VScroll2_Change()                   'Max Limit Bar changed
    TempMax = (80 - VScroll2.Value)
    Label9.Caption = TempMax
End Sub
'VScroll bar goes from top to bottom.   Scroll range is 0 to 80.
'Subtract location of scroll bar from 80 to get 'actual temp
-----------------------------------------------------------------------
Private Sub Command1_Click()                    'Start Button pressed
    Outputallowed = True
    Call Processing
End Sub
-----------------------------------------------------------------------
Private Sub Command2_Click()                    'Stop Button pressed
    Outputallowed = False
    Out Val("&H" + LPT_Address), Val(0)
    Label10.Caption = "Stopped"
    Label12.Caption = "00000000"
    Call Processing
End Sub
'When the Stop button is pressed, System Mode indicator is set to
'display “Stopped”. Output signals are not allowed and all pins are
'set to be in logic low state
-----------------------------------------------------------------------
Sub Processing()

    If (Label1.Caption >= TempMin) Then
        If (Label1.Caption <= TempMax) Then
        Shape5.FillColor = &H8000&              'Green Fill
        End If
    End If
    If (Label1.Caption > TempMax) Then
        Shape5.FillColor = &HFF&                'Red Fill
    End If
```

```
    If (Label1.Caption < TempMin) Then
        Shape5.FillColor = &HFFFF80             'Blue Fill
    End If
'The colour of the Dot indicating the sensor temperature state is
'altered depending on the temperatures position within the user set
'Max and Min Limits

If Outputallowed = True Then
If (MaxTemp = False) Then
    If (Label1.Caption <= TempMax) Then
        Out Val("&H" + LPT_Address), Val(1)
        Label10.Caption = "ON"
        HeatOff = False
        Label10.BackColor = &HFF&
        Label12.Caption = "00000001"
        End If
    End If
'If temperature is not cooling after hitting the max limit heat is
'applied until the max limit is exceeded

If (Label1.Caption > TempMax) Then
    Out Val("&H" + LPT_Address), Val(2)
    Label12.Caption = "00000010"
    HeatOff = True
    MaxTemp = True
    Label10.Caption = "OFF"
    Label10.BackColor = &HFFFF80
End If
'If Maximum temperature has been exceeded MaxTemp marker set to true
'so that cooling cycle will be maintained until below Minimum Limit

If (Label1.Caption < TempMin) Then
    If HeatOff = False Then
        Out Val("&H" + LPT_Address), Val(1)
    End If
    MaxTemp = False
End If
'If Temperature is too low, all cooling complete, MaxTemp marker is
'reset, heat source turned on to bring back up to max limit

If (Label1.Caption >= TempMin) Then
    If MaxTemp = False Then
        Out Val("&H" + LPT_Address), Val(1)
    Else
        Out Val("&H" + LPT_Address), Val(2)
    End If
End If
'Temp within limits, cool or heat dependent on MaxTemp marker being
'true or false
End If
End Sub
--------------------------------------------------------------------------
```

Appendix 5

```
'Program code for the operation of a Proportional Controller
-----------------------------------------------------------------------
Dim Temp10 As Integer                'Temp from MoteGate form * 10
Dim SP As Integer                    'Set point value set by scrollbar
Dim SP10 As Integer
Dim ErrorValue As Integer            'Error between Temp10 & SP10
Dim TimeON As Integer                'Count value for output
Dim TimeOFF As Integer
Dim DutyCycle As Integer
Public t1_count As Integer           'Counter to manage Duty Cycle
Public xcord As Integer              'Coordinate variable for temp plot
Dim HeatsourceON As Boolean
Dim Outputallowed As Boolean         'Set true by pressing Allow Output
Dim LPT_Address As String
-----------------------------------------------------------------------
Private Sub Form_Load()

    LPT_Address = 378            'Parallel Port Address
    Outputallowed = False
    Shape13.FillColor = &HFF&    'Output allowed indicator filled red
    Out Val("&H" + LPT_Address), Val(0)
    SP = 28                      'Corresponds to initial position of
    SP10 = 280                   'scrollbar. Multiplied by 10 to avoid
                                 'incompatibility of variables
    DutyCycle = 200
    Timer1.Interval = 10
    t1_count = 0                 'Counter initialised at zero

    xcord = 0                    '1st x co-ord of temp plot set at 0

    Picture3.Cls                 '¦
    Picture3.ScaleMode = 3       '¦
    Picture3.ScaleHeight = 20    '¦Settings defining the size and
    Picture3.ScaleWidth = 200    '¦drawing style used for the updating
    Picture3.AutoRedraw = True   '¦onscreen temperature plot
    Picture3.ForeColor = vbCyan  '¦
    Picture3.DrawStyle = 0       '¦
    Picture3.DrawWidth = 2       '¦

    Call VScroll1_Change         '¦
    Call Command1_Click          '¦Individual sub-routines called
    Call Command2_Click          '¦
    Call Tempresponse            '¦

End Sub
-----------------------------------------------------------------------
Private Sub VScroll1_Change()    'SP Scrollbar changed by user

SP = (80 - VScroll1.Value)
Label8.Caption = SP              'New SP value stored, temp plot
SetPoint10 = SP * 10             'cleared and redrawn with line
Picture3.Cls                     'representing new SP value
Picture3.Line (0, 20 - (SP - 15))-(200, 20 - (SP - 15)), vbBlack
Call Tempresponse

End Sub
-----------------------------------------------------------------------
Private Sub Command1_Click()     '"Allow Output" Button pressed
    Outputallowed = True
    Shape13.FillColor = &H8000&
```

```
End Sub
-------------------------------------------------------------------------
Private Sub Command2_Click()     '"Stop Output" Button pressed
    Outputallowed = False
    Shape13.FillColor = &HFF&
    Out Val("&H" + LPT_Address), Val(0)
    Label10.Caption = "OFF"
    Label10.BackColor = &HE0E0E0 'Output set to zero and indicated to
    Label12.Caption = "00000000" 'the user
    Timer1.Enabled = False       'Timer routine cannot be entered
End Sub
-------------------------------------------------------------------------
Sub Tempresponse()               'Required control output calculated

    Temp10 = Label1.Caption * 10

        If (Temp10 < (SP10 - 15)) Then
            Shape5.FillColor = &HFF0000     'Dark Blue, Too Cold
        End If
        If (Temp10 >= (SP10 - 15)) Then
            If (Temp10 < (SP10 - 10)) Then
                Shape5.FillColor = &HFF8080 'Light Blue, -1.1 to -1.5
            End If
        End If
        If (Temp10 >= (SP10 - 10)) Then
            If (Temp10 < (SP10 - 5)) Then
                Shape5.FillColor = &HFFC0C0 'Lighter Blue, -.5 to -1.0
            End If
        End If
        If (Temp10 >= (SP10 - 5)) Then
            If (Temp10 < (SP10 - 1)) Then
                Shape5.FillColor = &HC0FFC0 'Light Green, -0.2 to -0.5
            End If
        End If
        If (Temp10 >= (SP10 - 1)) Then
            If (Temp10 <= (SP10 + 1)) Then
                Shape5.FillColor = &H8000&  'Green, 0.0 to -0.2
            End If
        End If
        If (Temp10 > (SP10 + 1)) Then
            Shape5.FillColor = &HC0C0FF     'Light Red, Too Hot
        End If

    'The colour of the sensor marker is changed dependent on the
    'relationship between current temperature and the system set point

    ErrorValue = SP10 - Temp10           'Process Error found

    If (ErrorValue > 50) Then            'If error is greater than 5°C
        ErrorValue = 50                  'no control effect will be
    End If                               'applied to the heat source

    TimeON = 100 + (2 * ErrorValue)      'Output Equation 5.13

    If (Errorvalue < 0) Then             'If error value is negative
        TimeON = 0                       'heat source is turned off
    End If

    Label26.Caption = ErrorValue         'Current variable values
    Label19.Caption = TimeON             'printed onscreen & plotted
    Picture3.PSet (xcord, 20 - (Label1.Caption - 15)), vbRed

    If Outputallowed = True Then
        Timer1.Enabled = True            'If "Allow Output" has been
```

```
    End If                                  'selected Timer routine will
End Sub                                     'be entered
-------------------------------------------------------------------------
Private Sub Timer1_Timer()
    TimeOFF = DutyCycle - TimeON
    If (t1_count >= TimeOFF) Then
        HeatsourceON = True
    End If
    If t1_count = 0 And TimeOFF <> 0 Then
        HeatsourceON = False
    End If

'The HeatsourceON variable will be true for the number of counts
'greater than the TimeOFF period and less than the total duty cycle
'length of 200 counts. When the count is reset to zero the routine
'will be exited so that a new temperature measurement can be taken.

    If (t1_count = DutyCycle) Then      'counter is reset after 200
        t1_count = -1                   'counts have elapsed
        xcord = xcord + 2               'x coordinate incremented 2s
        If xcord > 200 Then
            xcord = 0                   'Temp plot is cleared when full
            Picture3.Cls                'SP line is redrawn
            Picture3.Line (0, 20 - (SP-15))-(200, 20 - (SP-15)),
vbBlack
        End If
    End If

    If HeatsourceON = True Then
        Out Val("&H" + LPT_Address), Val(1)
        Label10.Caption = "ON"          'Onscreen indication of Heat on
        Label10.BackColor = &HFF&       'while output to heat source is
        Label12.Caption = "00000001"    'in logic high state
    End If

    If HeatsourceON = False Then
        Out Val("&H" + LPT_Address), Val(0)
        Label10.Caption = "OFF"         'Onscreen indication of Heat
        Label10.BackColor = &HE0E0E0    'off while output to heat
        Label12.Caption = "00000000"    'source in logic low state
    End If

    t1_count = t1_count + 1             'Counter incremented & routine
End Sub                                 'restarted until count = 0
-------------------------------------------------------------------------
```